Madelyn Lew
Judy Pang
Liron Pantanowitz
Editors

Normal Cytology

An Illustrated, Practical Guide

Springer

Normal Cytology

Madelyn Lew • Judy Pang • Liron Pantanowitz
Editors

Normal Cytology

An Illustrated, Practical Guide

Springer

Editors
Madelyn Lew
Department of Pathology
Michigan Medicine
Ann Arbor, MI, USA

Judy Pang
Department of Pathology
Michigan Medicine
Ann Arbor, MI, USA

Liron Pantanowitz
Department of Pathology
Michigan Medicine
Ann Arbor, MI, USA

ISBN 978-3-031-20335-0 ISBN 978-3-031-20336-7 (eBook)
https://doi.org/10.1007/978-3-031-20336-7

This Springer imprint is published by the registered company Springer Nature Switzerland AG
The registered company address is: Gewerbestrasse 11, 6330 Cham, Switzerland

To Raymond & Yee Lew and Dan Boyer, for their constant support and love.

– Madelyn Lew

To my wonderful kids, Brandon and Ashley Kim, who remind me every day of what's truly important in life.

– Judy Pang

To all those inquisitive pathology trainees who joined me during my cytology sign-out sessions.

– Liron Pantanowitz

Foreword

I vividly remember my first day of Histology class as a first-year medical student. The instructors provided each of us with a microscope and a wooden box filled with glass slides, each slide illustrating normal microscopic anatomy stained with hematoxylin and eosin. There was a slide for every organ (for some organs, more than one), and I remember discovering the diversity and, yes, the beauty, of the cells that make up our body: squamous cells, goblet cells, ciliated cells, hepatocytes, neurons, smooth muscle, and cardiac muscle, just to name a very few. I can see now, looking back over so many years, that it was that class and those slides that hooked me on the microscope, that I was destined to become a pathologist, someone constantly searching to distinguish the normal from the abnormal.

Without an understanding of normal microscopic anatomy, of course, one can't begin to understand and correctly identify disease. This was made clear to us as budding physicians during my first year. In fact, we didn't even begin to examine diseased tissues—abscesses, granulomas, tumors—until our second year, after we had mastered normal anatomy.

With this book, Drs. Lew, Pang, and Pantanowitz provide us with a comprehensive overview of normal cytology. As with histology, an understanding of normal cytology is the foundation of the practice of diagnostic cytology. It's only when we appreciate what an aspirate of a benign lymph node looks like can we begin to recognize a lymphoma. The same applies for all cytologic specimens. This book, with its beautiful illustrations and succinct text, can provide immeasurable help to both the trainee learning their craft and the practicing cytologist struggling with a challenging case. The ultimate beneficiary, of course, is the patient, whose caregiver will know what to do next.

Brigham and Women's Hospital
Harvard Medical School
Boston, MA, USA
June 17, 2022

Edmund S. Cibas

Preface

It is sometimes difficult to appreciate when something is abnormal without first knowing what is normal. This is definitely the case when trying to interpret cytomorphology, especially for diagnostic purposes in clinical practice. Given the wide spectrum of anatomical sites that can be sampled for cytologic evaluation, the variation of normal findings that may be encountered in such human cytology samples, and the alteration of cytomorphology that may result from specimen procurement and processing, we felt that it was important to share our experience by means of this practical and illustrative textbook to assist other pathologists, cytologists, and other learners with recognizing normal cytology. We hope that this reference will serve you well, optimize your diagnostic accuracy, and help you avoid potential interpretative pitfalls.

Ann Arbor, MI, USA

Madelyn Lew
Judy Pang
Liron Pantanowitz

Acknowledgments

We would like to extend our thanks and appreciation to: Our cytoprep technologists, Lana Jajko, Douglas Mullen, and Kimberly Meekins, whose efforts were instrumental in acquiring images for this atlas and Dr. Michael Caplan for his contributions to specimen acquisition of eye cytology specimens.

Contents

Introduction

1

Liron Pantanowitz, Xin Jing, and Madelyn Lew

Given the wide variety of anatomical sites that can be sampled by cytologic methods, it is important for cytopathologists and cytologists to be acquainted with the array of normal tissues that can be observed in various cytological specimens. Normal cytology is important to recognize as it also allows one to ascertain what is abnormal. Moreover, normal cytomorphology can sometimes be mistaken for abnormal findings. On occasion, normal findings may even mimic neoplasia, especially when there are associated specimen procurement and/or preparation artifacts (e.g., air drying, crushed cells, cautery, exposure to saline). The presence of only normal cellular material may at times render a sample unsatisfactory, and thus will need to be interpreted as nondiagnostic if the targeted lesion being sampled was missed. Furthermore, in some situations, the presence of normal cellular material may be the result of contamination. This may occur when normal anatomical structures are inadvertently sampled or traversed during a fine needle aspiration (FNA) procedure (e.g., passing through the gastric wall while trying to aspirate a pancreatic tail mass).

Each chapter in this textbook covers the normal cytology in humans from various anatomical sites, reviewing the spectrum of cell types that may be encountered and their appearance in different cytologic preparations. It is important to be aware that given the vast diversity of cells that exists and that such cells may normally undergo changes related to physiological function and aging, the prototypical findings described herein may differ from those encountered in routine human samples. Practical diagnostic pitfalls associated with normal cytology that are likely to be seen in clinical practice are also addressed.

L. Pantanowitz (✉)
Department of Pathology, Michigan Medicine,
Ann Arbor, MI, USA
e-mail: lironp@med.umich.edu

X. Jing · M. Lew
Department of Pathology, University of Michigan,
Ann Arbor, MI, USA
e-mail: xinjing@med.umich.edu; lewm@med.umich.edu

Cytology Preparation

Normal cytology may differ based on various cytology preparations. Therefore, it is important to briefly review these different methods. Cytology material can be collected by exfoliation (e.g., Pap smear of the cervix), scraping (e.g., Tzanck test), fine needle aspiration of a superficial or deep-seated mass, draining cysts, or tapping body fluid collections (e.g., effusions). Air drying of cells on slides, even if minimal, can distort cells, potentially impairing interpretation. Fixation of samples (e.g., spray fixation, 95% ethyl alcohol solution), intended to preserve cellular material, may also alter normal cytological findings (e.g., cause cell shrinkage). Conventional (direct) smears are prepared by expunging exfoliated or aspirated material onto a glass slide and then spreading this material across the slide as a thin layer using another clean slide. Touch preparations are made when cells are transferred from a core needle biopsy, or imprinted from larger tissue specimens, onto a clean slide. Liquid-based cytology (LBC) preparations include cytology samples collected into a liquid fixative, which may facilitate the removal of excess blood or obscuring mucus in these samples. Such liquid-based suspensions are subsequently vortexed or centrifuged to create a concentrated cellular deposit, usually as a monolayer placed within a defined (often circular) region on the slide. Routinely utilized liquid-based preparations include cytospins as well as ThinPrep (Hologic) and SurePath (BD) methods. Adequately procured cellular material obtained by any means can be further processed into sediment to create a paraffin-embedded cell block. Like small tissue biopsy samples, cell blocks can be sectioned by microtomy and stained with hematoxylin & eosin (H & E). Cell block material is also an excellent source for ancillary testing including histochemical stains, immunohistochemistry (IHC), in situ hybridization (ISH), and molecular studies.

Cytology glass slides may be stained with a Diff-Quik stain (DQ stain) where the slides can be air-dried, or with the Papanicolaou stain (Pap stain), where slides are usually first

M. Lew et al. (eds.), *Normal Cytology*, https://doi.org/10.1007/978-3-031-20336-7_1

fixed in alcohol or methanol. The DQ stain is a commercial Romanowsky stain based on a modification of the Wright-Giemsa stain. This stain permits visualization of slide preparations in a short amount of time, which is ideal for rapid on-site evaluation (ROSE) of air-dried smear or touch preparations. With the DQ stain, nuclei are purple and cytoplasm ranges from light blue to purple. This stain also effectively highlights extracellular substance material (e.g., mucin, colloid, myxoid matrix), as well as certain cytoplasmic details such as mucin, fat vacuoles, and various granules [1]. The Pap stain is a polychromatic stain developed by George Papanicolaou that leverages the use of five different basic and acidic dyes (hematoxylin, orange green 6, eosin Y, light green SF, and Bismarck brown Y) to differentially stain various cell components [2, 3]. The Papanicolaou stain particularly highlights nuclear detail. Nuclei are stained light to dark blue and cytoplasm ranges from pink to blue-green. When there is keratinization present, the cytoplasm is often intensely orange (orangeophilic). Some laboratories employ a modified ultrafast Pap stain to reduce processing times for ROSE [4]. H & E is the principal stain utilized for histology and staining cell block material, which stains nuclei dark blue-purple and cytoplasm pink.

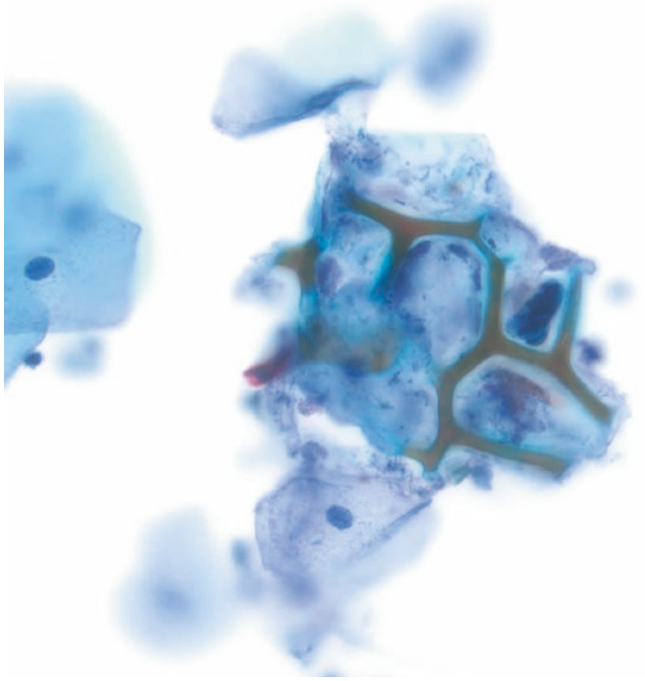

Fig. 1.1 Plant cells in this cytology specimen are characterized by thick rigid cell walls. Urine, ThinPrep preparation, Papanicolaou stain, 40× magnification

Cell Structure

All tissues are composed of cells. These cells vary in size, structure, and function. Many of the cytological features of these cells are discernable with a light microscope [5]. Unlike plant cells which have thick cell walls (Fig. 1.1), human cells are bound by a thin outer plasma membrane that is best visualized with an electron microscope. Nevertheless, some cells, such as squamous cells, display distinct cell membranes. The eukaryotic cell can be subdivided into a nucleus and cytoplasm. The nuclear to cytoplasmic (N:C) ratio is an important parameter in cytology, as a high N:C ratio may be seen in malignancy. However, basally located cells in some epithelium normally have a high N:C ratio, such as reserve cells seen in the uterine cervix or lung (Fig. 1.2). These reserve cells play an important role in tissue regeneration. However, they lack other features seen in malignancy such as nuclear irregularity, hyperchromasia, and coarse chromatin distribution.

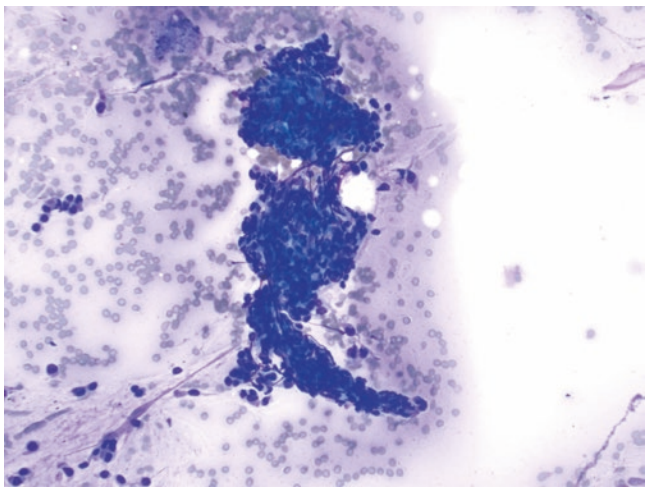

Fig. 1.2 Cohesive clusters of respiratory reserve cells. These small cells have minimal cytoplasm and bland nuclei with dense chromatin. Lung, air-dried smear preparation, Diff-Quik, 20× magnification

The nucleus of the cell is usually the largest organelle and is often round or ovoid. Hyperlobation may be observed in certain cells (e.g., neutrophils, megakaryocytes). Some cells may normally exhibit multinucleation such as urothelial umbrella cells, regenerating hepatocytes, syncytiotrophoblasts, macrophages (e.g., Langerhans cells), as well as reactive mesothelial (Fig. 1.3a), bronchial (Fig. 1.3b), and endocervical cells. The nucleus is surrounded by a nuclear membrane, which is usually smooth and without irregularity [6]. The center of the nucleus typically contains a nucleolus made up of ribonucleic acid (RNA) that helps makes ribosomes. Cells undergoing rapid cell growth may have large and even multiple nucleoli. Nucleoli usually stain red or blue with a Pap stain and blue to purple with a DQ stain. Chromatin within the nucleus contains a mixture of deoxyribonucleic acid (DNA) and histones which includes heterochromatin (dense, dark areas comprised of inactive DNA) and euchro-

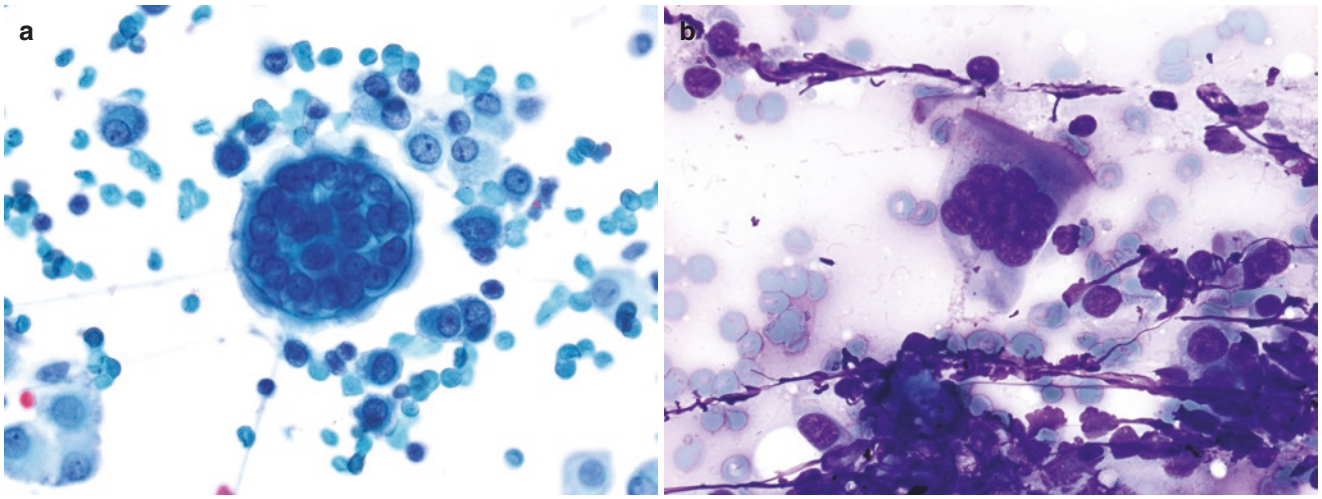

Fig. 1.3 (**a**, **b**) Multinucleation featured in different cell types. (**a**) A large reactive multinucleated mesothelial cell is shown in a peritoneal fluid sample taken from a patient with cirrhosis. (**b**) Multinucleated reactive bronchial epithelial cell. Note the apical and detached cilia in the background. Peritoneal fluid, cytospin preparation, Papanicolaou stain, 60x magnification (**a**). Lymph node, air-dried smear preparation, Diff-Quik, 60× magnification (**b**)

matin (light areas comprised of DNA that is active in RNA synthesis).

The cytoplasm of cells consists of cytosol and organelles. Most organelles are not readily visible with a light microscope. However, they do account for some morphologic findings commonly seen in cytology specimens. Despite the fact that the endoplasmic reticulum (ER) is one of the largest organelles, it is best seen with electron microscopy. The Golgi apparatus (body), which resides near the nucleus, is responsible for the pale stained perinuclear hof (halo) often seen in plasma cells. Mitochondria are usually only visible with light microscopy when they accumulate in abnormal conditions, such as those that result in oncocytic cells. Cells may also contain vesicles, vacuoles, and assorted granules. These contain a variety of substances such as enzymes, glycogen, mucin, and fat droplets. Secretory granules are often seen in endocrine cells, neuroendocrine cells, and certain gastrointestinal cells. Mucin and fat usually appear as clear cytoplasmic spaces with routine stains. Cells such as macrophages found floating in body fluids often develop clear vacuoles due to hydropic degeneration (Fig. 1.4). The cytosol also contains a cytoskeleton scaffold made up of thin microfilaments (e.g., actin), microtubules, and intermediate filaments (keratins, desmin, vimentin, glial fibrillary acidic protein, neurofilaments) [7]. Within epithelial cells, different cytokeratins (CK) can be highlighted by using various IHC stains. For example, low molecular weight (LMW) keratins stain with antibodies such as CAM5.2, CK7, CK8, CK18, CK19, and CK20 whereas high molecular weight (HMW) keratins stain with antibodies such as 34 beta E12 (CK903), CK1 to CK6, and CK9 to CK17.

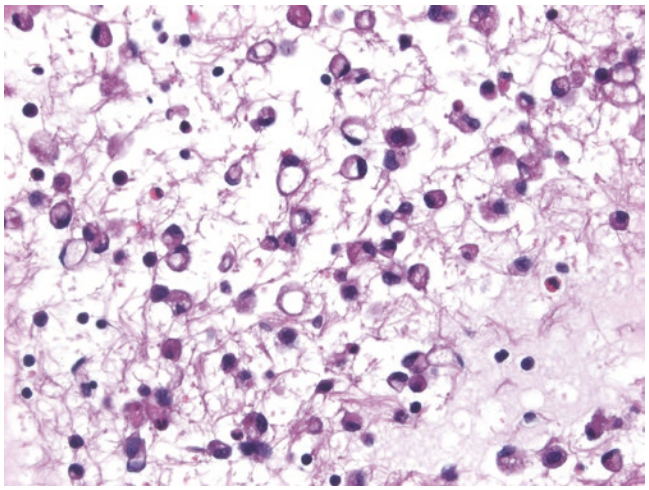

Fig. 1.4 Many of the macrophages shown in this pleural fluid have clear cytoplasmic vacuoles. The background contains haphazard fibrin material. Pleural fluid, cell block, hematoxylin & eosin, 40× magnification

Human cells typically contain 46 chromosomes, except for mature sex cells which are haploid ($n = 23$). This includes 22 pairs of autosomes and a pair of sex (XX/XY) chromosomes. In normal female somatic cells, one may identify a Barr body (sex chromatin) in interphase nuclei with routine stains (e.g., Pap stain (Fig. 1.5a)) or using specialized stains (e.g., aceto-orcein (Fig. 1.5b), Feulgen, Guard, cresyl violet, carbol fuchsin, fluorescent methods). The Barr body is an inactivated X chromosome formed due to lyonization. This intensely staining body measures about 1 μm in diameter, is usually triangular or dome-shaped, and is commonly situated

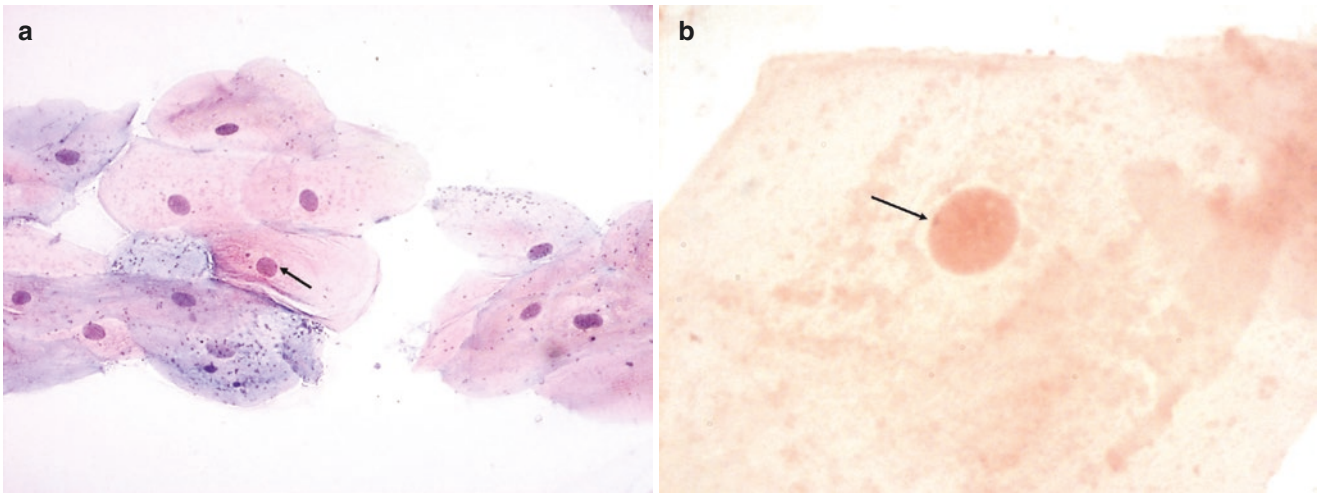

Fig. 1.5 (**a**) Buccal squamous cells showing a Barr body (arrow) juxtaposed against the nuclear membrane. (**b**) Buccal squamous cell showing a single dense Barr body (arrow). Buccal smear preparations, Papanicolaou (**a**) and aceto-orcein (**b**) stains, intermediate (**a**) and high (**b**) magnification. (Images provided courtesy of Punnya V. Angadi, KLE VK Institute of Dental Sciences, Belagavi, India)

on the inside of the nuclear membrane. Buccal epithelial cells found in saliva or mucosal scrapings can be used for sex determination by identification of these Barr bodies in the nucleus [8]. The proportion of Barr bodies detected may vary with ethnicity, age, menstrual cycle, as well as in premalignant and malignant lesions.

Most cells divide and replicate. Somatic cells divide by mitosis and germ cells divide by meiosis. Mitotic figures may be seen in cytology samples, and they signify that this cell is in the process of dividing. While they can be observed in normal cells, they are often not numerous as in malignant processes. Normal mitosis occurs in four stages: prophase (condensed chromosomes), metaphase (linear alignment of chromosomes at the equator), anaphase (chromosomes pull apart towards opposite ends of the cell), and telophase (cleavage with separation into two daughter cells, each with its own nucleus). The finding of an abnormal mitotic figure is suggestive of malignancy (Fig. 1.6).

Apoptosis (programmed single cell death) can occur with normal cell turnover and for physiological reasons (e.g., thymus involution), but this may also be observed in many cells within high-grade malignancies (e.g., Burkitt lymphoma). When apoptosis occurs, the dying cell shrinks while the cell membrane remains intact, and the nucleus undergoes pyknosis (shrinkage with chromatin condensation) and karyorrhexis (nuclear fragmentation with irregular chromatin distribution throughout the cytoplasm). Dying cells may release apoptotic bodies that are subsequently phagocytized by macrophages [9]. Macrophages that engulf and digest apoptotic cells are called tingible body macrophages (TBMs).

Depending on their function, certain cells can undergo specialization. For example, cilia are slender, flexible, hair-like protuberances present on the surface of certain cells.

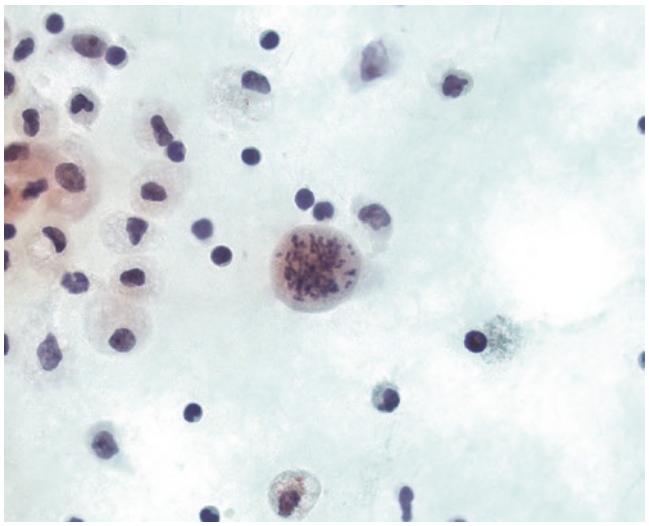

Fig. 1.6 A dividing malignant ovarian carcinoma cell is shown with chromosomes randomly scattered throughout the cell. Peritoneal fluid, cytospin preparation, Papanicolaou stain, 60× magnification

Motile cilia are found in upper and lower respiratory tracts (Fig. 1.7a), fallopian tube, and ependymal epithelial cells. Cilia are anchored perpendicularly to cells at their luminal end via a dense terminal plate (terminal bar) (Fig. 1.7b). With both Papanicolaou and DQ stains, cilia are usually pink-red to lavender in color. Their identification usually signifies benignancy. Ciliocytophthoria (CCP) is a degenerative process of ciliated cells, that is often caused by a viral infection (e.g., adenovirus) and is characterized by the presence of detached ciliary tufts.

The term euplasia has been used to describe cells that are in normal health and physiologic state [10]. However, cells

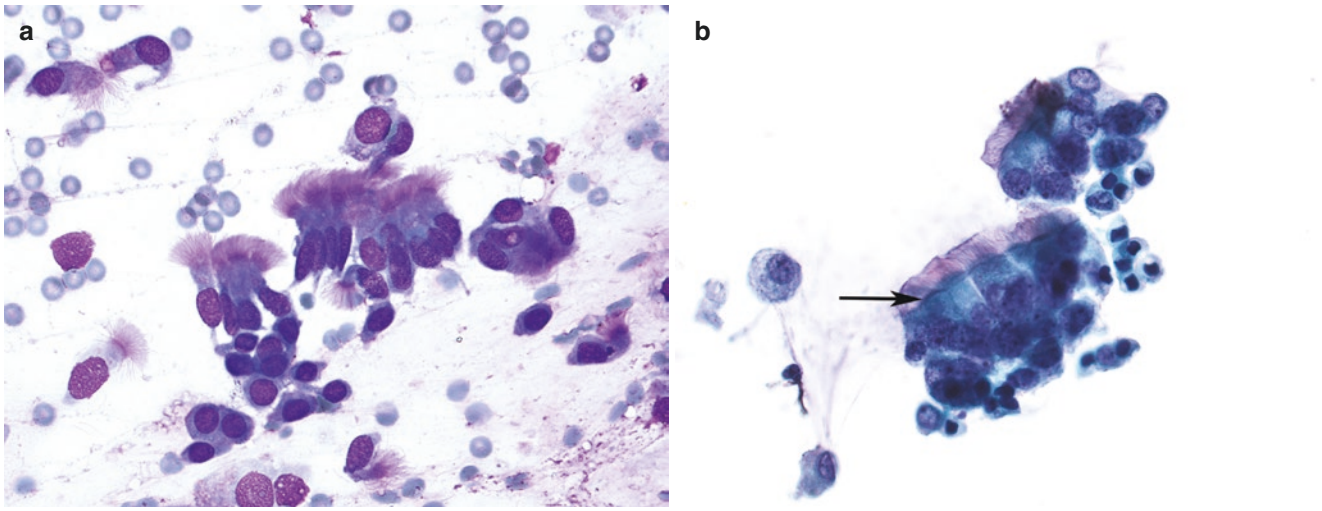

Fig. 1.7 (**a**) Benign bronchial cells are shown with pink apical tufts of cilia. (**b**) The cilia seen in these bronchial cells are attached apically to a dense terminal bar (arrow). Air-dried smear preparation, Diff-Quik, 40x magnification (**a**). ThinPrep preparation, Papanicolaou stain, 40× magnification (**b**)

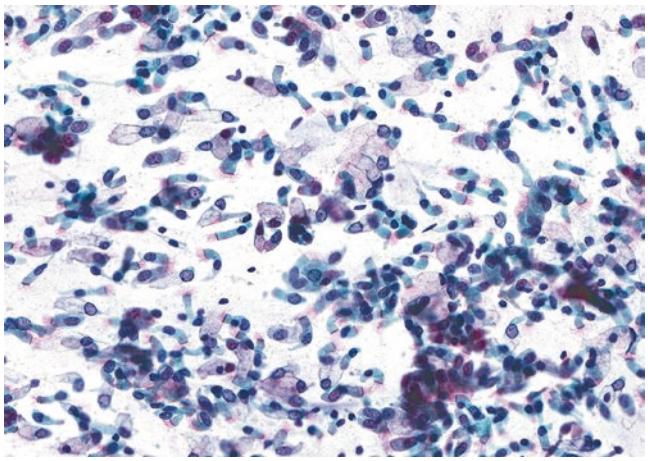

Fig. 1.8 Goblet cell hyperplasia in the lung is characterized by abundant cells containing clear intracytoplasmic mucus that are shown scattered among normal ciliated bronchial cells. Alcohol-fixed smear preparation, Papanicolaou stain, 20× magnification

may change due to physiological (e.g., growth, pregnancy) or pathological reasons (e.g., reactive stimulation, degeneration, neoplasia). Such changes may also include:

- **Hypertrophy**: Increased cell size that may result in organ enlargement (e.g., increased muscle cell size in body builders, enlarged myometrium in pregnancy, cardiomyopathy due to hypertension).
- **Hyperplasia**: Increased cell number due to rapid division that may result in organ enlargement (e.g., increased breast epithelial cells during pregnancy, benign prostatic hyperplasia, goblet cell hyperplasia in respiratory airways (Fig. 1.8)).
- **Atrophy**: Decreased cell size that may lead to a decrease in tissue or organ size (e.g., thymic involution, postmenopausal cervical mucosa).
- **Metaplasia**: Change or replacement of one cell type for another, usually in response to chronic irritation (e.g., squamous metaplasia of the uterine endocervix at the transformation zone).
- **Dysplasia**: Abnormal arrangement and maturation of cells which is a pre-neoplastic condition.

Cell Type and Arrangement

Tissues are comprised of different cell types. These tissues can be classified into four subtypes: epithelium, connective tissue, muscle, and nervous tissue. Different combinations of these tissues are present in various organs.

Epithelium refers to the protective sheet of contiguous cells that cover the skin (epidermis), lines internal cavities and lumina (mucosa), or invaginates to form exocrine and endocrine glands. Epithelial cell shape may be squamous (flat, polygonal, or spindled), cuboidal, columnar, or transitional. Mesothelium refers to epithelium that lines the serosal body cavities (pleura, pericardium, peritoneum). Epithelial cells may form a single layer (simple layer) or can be stratified or pseudostratified. In cytology samples, epithelial cells can be arranged singly, in sheets (Fig. 1.9), or form three-dimensional aggregates (cell clusters).

Squamous epithelial cells line the skin, as well as oral cavity, upper esophageal (Fig. 1.10), and rectal mucosa. Cytoplasmic coloration of squamous cells may differ depending on stain preparation and keratinization. Mature

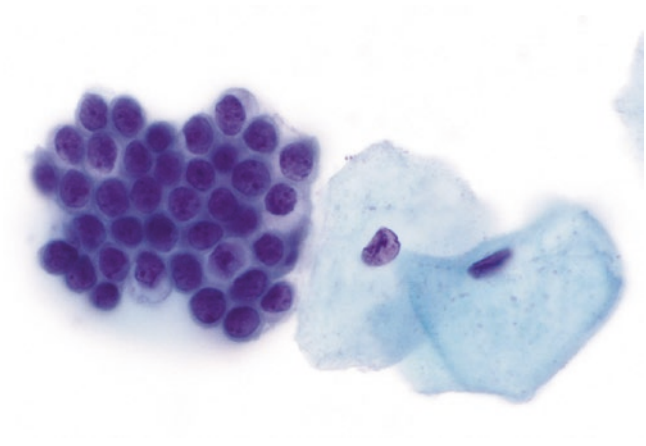

Fig. 1.9 Endocervical cells (left cell cluster) organized in a flat sheet. Cervical Pap, ThinPrep preparation, Papanicolaou stain, 60× magnification

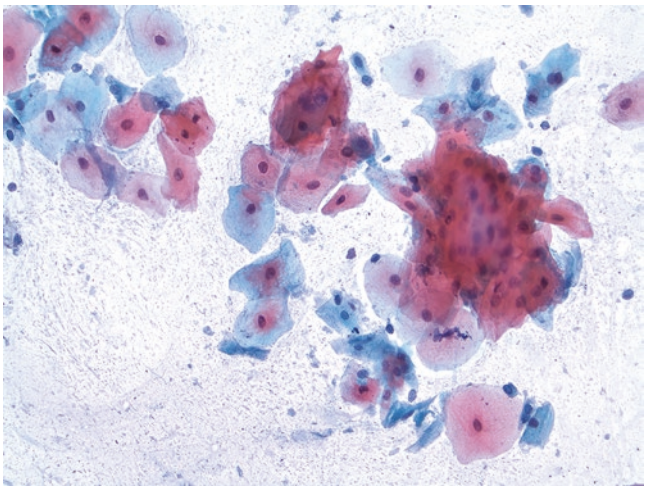

Fig. 1.10 Benign nucleated squamous cells of the esophagus. Alcohol-fixed smear preparation, Papanicolaou stain, 40× magnification

squamous cells have blue-purple cytoplasm on DQ staining. On Papanicolaou stain, they can be blue-green, or pink, and with increased keratinization, their cytoplasm becomes orangeophilic. Squamous cells have deep pink cytoplasm on H & E. In general, epithelial cells characteristically make contact with neighboring cells via cell junctions (intercellular bridges), such as desmosomes (macula adherens). Such intercellular bridges are notable with benign and neoplastic squamous epithelium (Fig. 1.11) [11].

Glands are comprised of epithelial cells that produce and release secretory products. Exocrine glands release their secretions into ducts that open onto a surface (e.g., skin, gut lumen). Ductal epithelium is formed by cuboidal to columnar cells with basally oriented nuclei and moderate to abundant amounts of apical granular to clear cytoplasm (Fig.

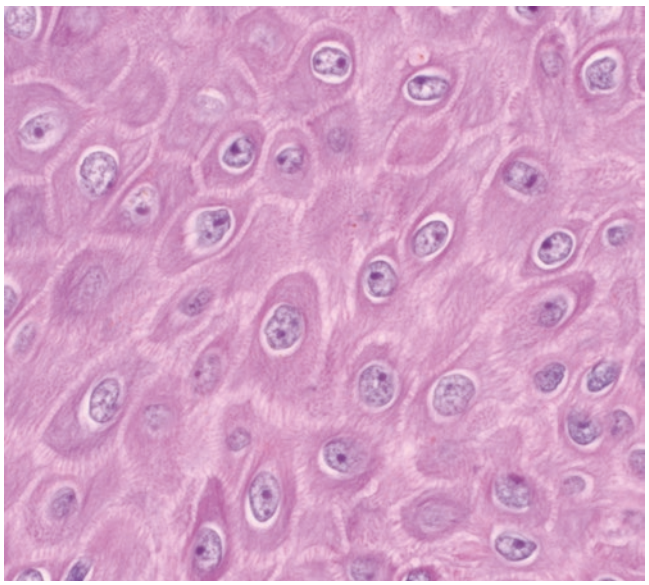

Fig. 1.11 Squamous epithelium in skin excision highlighting intercellular bridges. Skin, hematoxylin & eosin, 60× magnification

1.12a, b). In some organs, ductal epithelium as well as some acini can be surrounded by contractile myoepithelial cells. In FNA specimens, myoepithelial cells can be identified in a different focal plane to the underlying ductal epithelium (Fig. 1.13). Myoepithelial cells have small, bland hyperchromatic nuclei and indistinct cytoplasm [12]. Glandular epithelial cells appear differently when viewed in different orientations. When viewed from above (en face aspect), the epithelial cells are organized into honeycomb-like structures (Fig. 1.14a). When viewed from the side (longitudinal aspect), the cells demonstrate polarity with nuclei located basally beneath the apical cytoplasm resembling a picket fence (Fig. 1.14b). The secretory units of exocrine glands form an acinus that typically contains a central lumen that communicates with the duct system. In cytology preparations, acinar epithelium is frequently characterized by compact grape-like clusters (Fig. 1.15).

Endocrine glands have no ducts and instead release their secretions (hormones) directly into the bloodstream. Endocrine cells have round nuclei with smooth nuclear contours and granular chromatin, as well as variable amounts of cytoplasm. Some endocrine cells may have minimal amounts of granular cytoplasm (such as follicular cells of the thyroid), while others may have abundant granular or vacuolated cytoplasm (such as adrenal cortical and medullary cells). Benign thyroid follicular cells often contain intracytoplasmic "paravacuolar granules" (Fig. 1.16). They tend to be associated with increased metabolic activity, as well as degeneration within the thyroid gland. These granules consist of lysosomes containing hemosiderin (iron) or lipofuscin pigments [13].

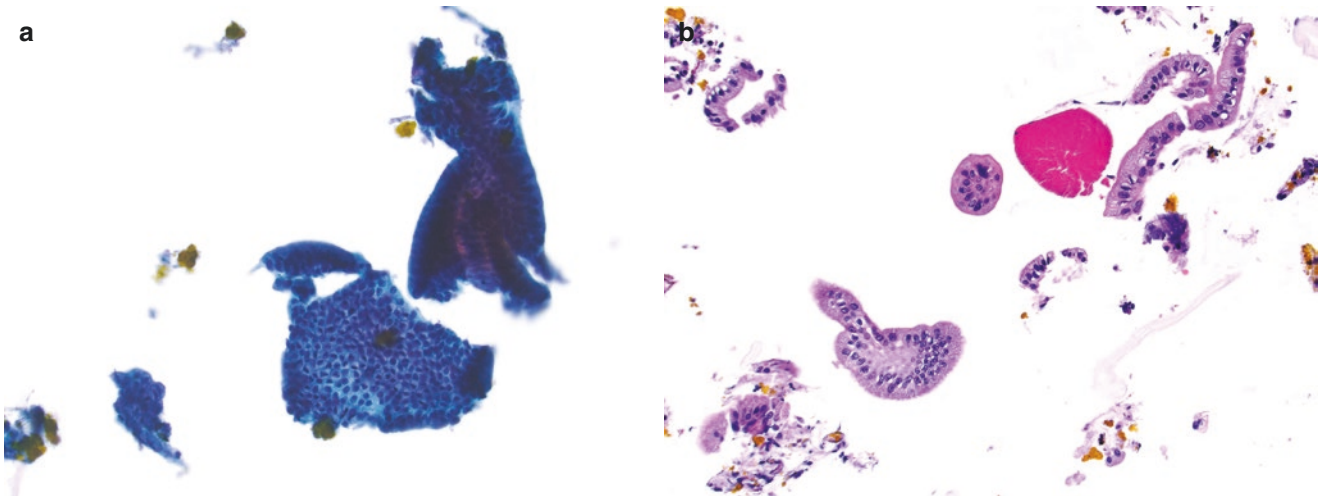

Fig. 1.12 (**a**) Sheets of benign bile duct epithelium are shown to be comprised of cuboidal cells. Note the associated yellow bile pigment in this specimen. (**b**) On cell block preparation, simple cuboidal to columnar bile duct epithelium is shown displaying basally located nuclei. ThinPrep preparation, Papanicolaou stain, 20x magnification (**a**). Cell block, hematoxylin & eosin, 20× magnification (**b**)

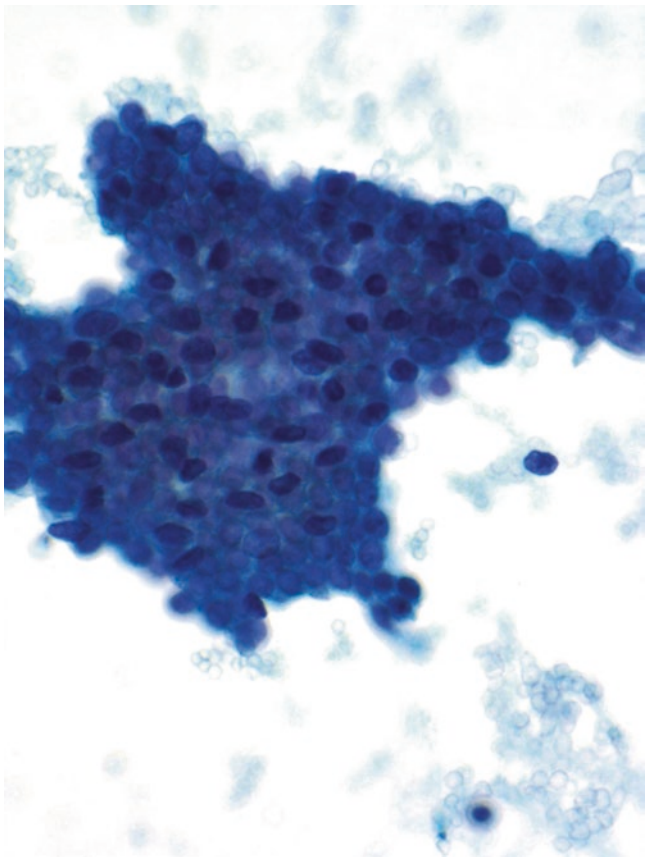

Fig. 1.13 Benign duct showing a mixture of pale ductal epithelial cells and, in a different focal plane, darker myoepithelial cell nuclei. Breast, Papanicolaou stain, 60× magnification. (Image courtesy of Charles D. Sturgis, Mayo Clinic, Rochester, MN, USA)

Mesenchymal tissue derived from mesoderm can be classified into bone and cartilage, vessels, and connective tissue (loose, dense, reticular, adipose). Apart from mesenchymal cells (e.g., fibroblasts, adipocytes (Fig. 1.17), pericytes along capillary walls), connective tissue also contains intermingled fibers (collagen, reticulin, and elastin) and amorphous extracellular matrix (ground substance). In cytology samples, connective tissue is often referred to as "stroma" or "stromal matrix." Normal resting fibroblasts tend to be spindle-shaped with tapered edges, have pale wispy cytoplasm, and contain a central oval, vesicular nucleus with an indistinct nucleolus. Reactive fibroblasts may have an enlarged nucleus, coarse chromatin, prominent nucleolus, and can be binucleated. Myofibroblasts, derived from fibroblasts, can be seen in reactive states (e.g., granulation tissue) [14] and within the stroma of neoplasms (e.g., desmoplasia) [15]. They contain contractile filaments, have a rounder nucleus (Fig. 1.18), and, like smooth muscle fibers, express smooth muscle actin (SMA) and desmin. Collagen fibers, which may be arranged in parallel bundles or haphazardly, stains light green with a Pap stain, pink-purple with a DQ stain, and pink with H & E stain. Elastic and reticulin fibers are usually much thinner than collagen fibers, and hence are best identified with special histochemical stains (Fig. 1.19). Connective tissue also forms membranes that may encapsulate organs (e.g., liver capsule) and line joints (e.g., synovial membrane). The cytological appearance of these different connective tissues as well as other specialized tissues of mesodermal origin such as muscle, nerve, and blood is described within dedicated chapters on these topics in this textbook.

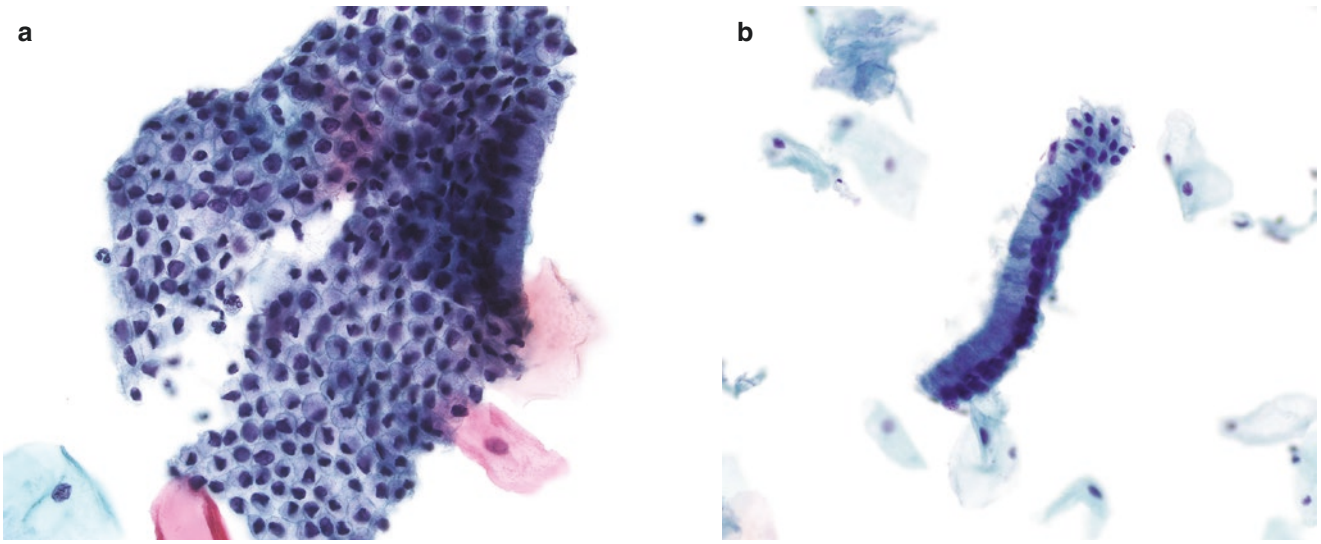

Fig. 1.14 Different orientation of ductal cells. (**a**) Benign endocervical cells in a Pap test showing a honeycomb arrangement. The cuboidal glandular cells towards the right edge of this glandular fragment show a picket fence arrangement. (**b**) A strip of endocervical cells showing cuboidal to columnar epithelium viewed longitudinally. The nuclei are all located towards the basal end of these cells. Cervical Pap, ThinPrep preparation, Papanicolaou stain, 20× (**b**) and 40 (**a**) magnification

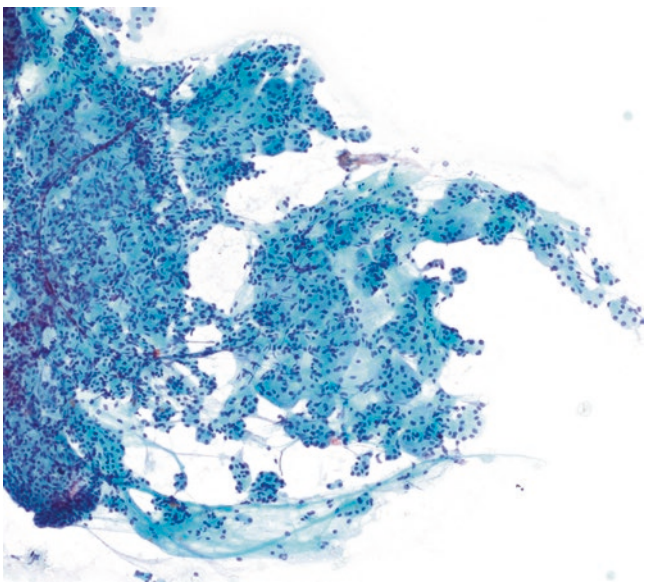

Fig. 1.15 Normal acinar epithelium of the pancreas. Pancreas, alcohol-fixed smear preparation, Papanicolaou stain, 10× magnification

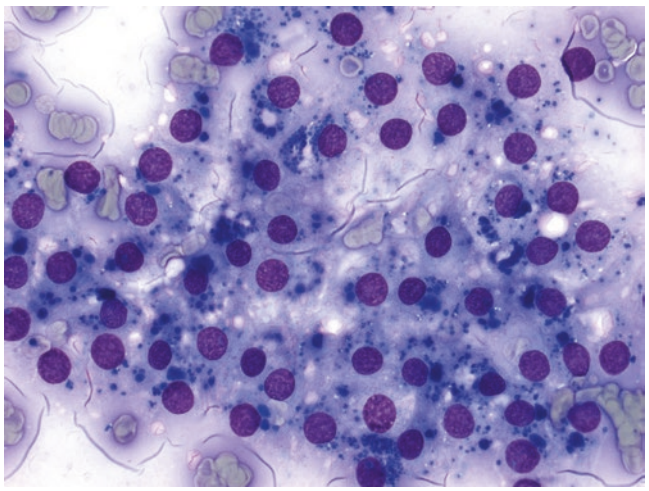

Fig. 1.16 Benign thyroid follicular cells are shown with similar-sized round nuclei, indistinct cell borders, and dense blue intracytoplasmic "paravacuolar" granules. Thyroid, air-dried smear preparation, Diff-Quik, 60× magnification

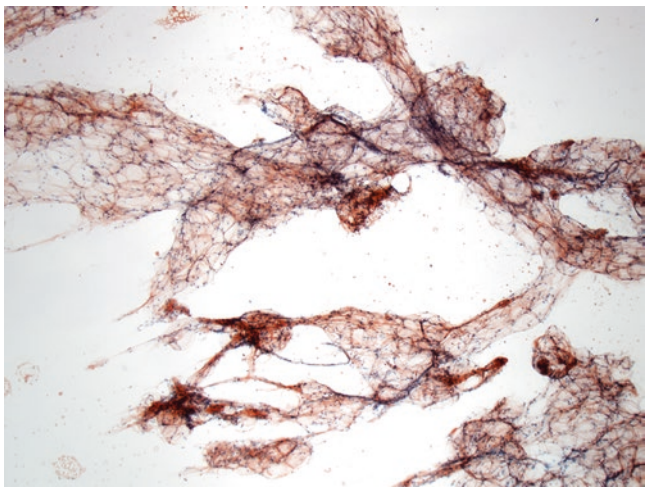

Fig. 1.17 Fragments of mature white fat are shown containing abundant univacuolated adipocytes. Apart from the rich fine vasculature, there is little intervening stroma in these fat lobules. This specimen has no amyloid deposition. Fat pad, air-dried smear preparation, Congo Red special stain, 4× magnification

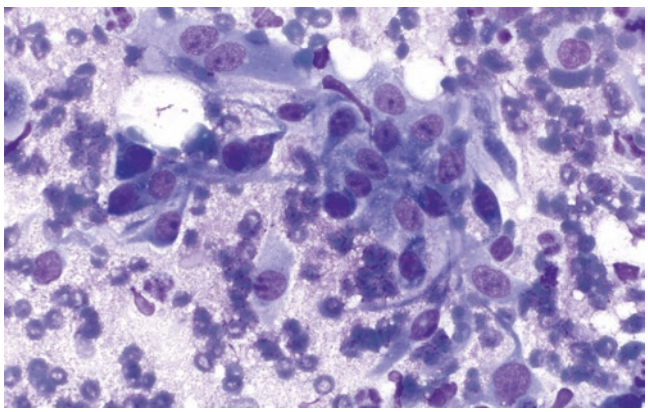

Fig. 1.18 Reactive myofibroblasts are shown, which have a spindled shape and increased amounts of cytoplasm and nuclear size compared to fibroblasts. Distinct nucleoli can also be seen. Air-dried smear preparation, Diff-Quik, 60× magnification

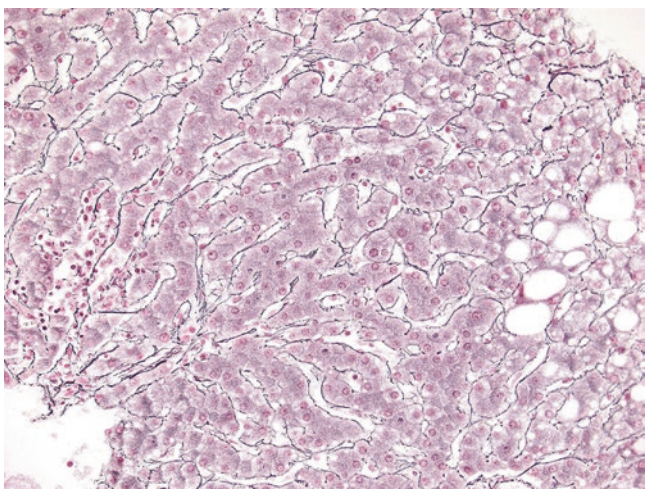

Fig. 1.19 Normal liver architecture showing one to two-cell thick plates of hepatocytes delineated by black stained reticulin fibers. Liver, cell block, reticulin stain, 20× magnification

Extracellular Material

Glandular differentiation can be appreciated not only by cellular features such as the formation of a lumen or intracellular mucous vacuoles, but also by extracellular findings such as background mucus. Background mucus composed of mucins and inorganic salts may appear as amorphous dense material (Fig. 1.20a), wispy strands (Fig. 1.20b), as well as inspissated globules.

Most cytology samples contain background blood comprised mostly of normal erythrocytes. Accompanying these contaminating red blood cells may be circulating white blood cells and even platelet aggregates. An increase in peripheral circulating neutrophils seen with blood dilution of cytology samples should not be misinterpreted as acute inflammation. Cytology samples may on occasion also contain pigmented material. Endogenous pigments that may be encountered include melanin, hemosiderin, hematoidin, and lipofuscin. Exogenous pigment may also be observed, such as anthracotic material.

Melanin is a natural pigment produced by melanogenesis in melanocytes that involves oxidation of the amino acid tyrosine. Melanosomes are increased in people with darker skin tone. Melanin is normally found in the skin (Fig. 1.21), hair, eye, adrenal gland (medulla, zona reticularis), inner ear, and regions of the brain (e.g., medulla, substantia nigra, locus coeruleus). Melanin pigment is usually finer than the coarse granules of hemosiderin. Melanin stains brown (Fig. 1.22) or sometimes green with Pap stain, blue-black with DQ stain, and brown with H & E stain. The presence of melanin can be confirmed via an argentaffin reaction with a Fontana-Masson histochemical stain, which stains this pigment black.

Hemosiderin is an iron-storage complex that results from the breakdown of blood [16], but may also occur via abnormal ferritin metabolism. This granular brown pigment can be seen within various cells, including macrophages following hemorrhage or trauma (Fig. 1.23a). Hemosiderin-laden macrophages in the lung (siderophages) may resemble smoker's macrophages (dust cells) (Fig. 1.23b). With Pap staining, hemosiderin deposits stain a faint yellow-brown color. However, hemosiderin appears as gray to blue granular material in DQ-stained preparations and is a golden-brown pigment with H & E stain. Hemosiderin can be confirmed with Perl's Prussian blue stain for iron which stains blue to black.

Hematoidin crystals are a bilirubin-like pigment that may be seen in samples where extravasated red blood cells have undergone degradation (Fig. 1.24) [17]. These crystals are often encountered in regions of infarction or old hemorrhage. They form yellow-golden radiating crystals that cluster to form star-shaped structures which may be found intracellularly and extracellularly. These crystals may mimic bile pigment.

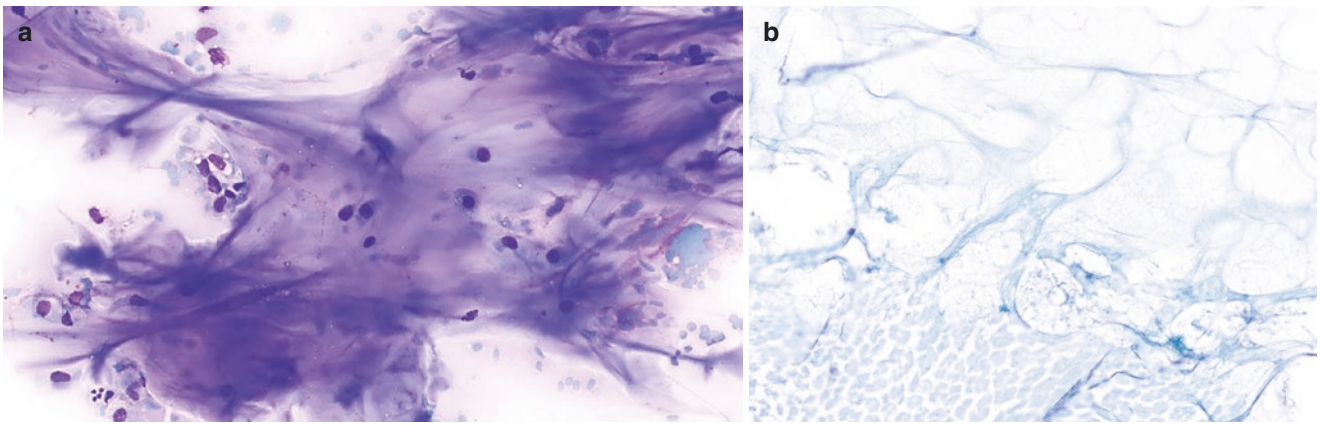

Fig. 1.20 (**a**) Dense mucus with embedded scattered banal epithelial cells and scant macrophages. This mucin has a "smooth" even appearance which helps distinguish it from background myxoid matrix which is more granular. (**b**) Thin, clean, wispy mucus. Mucin derived from the gastrointestinal tract, which often contaminates FNA samples, typically has a "dirty" appearance because it contains debris and bacteria. Air-dried smear preparation, Diff-Quik, 4x magnification (**a**). Alcohol-fixed smear preparation, Papanicolaou stain, 4× magnification (**b**)

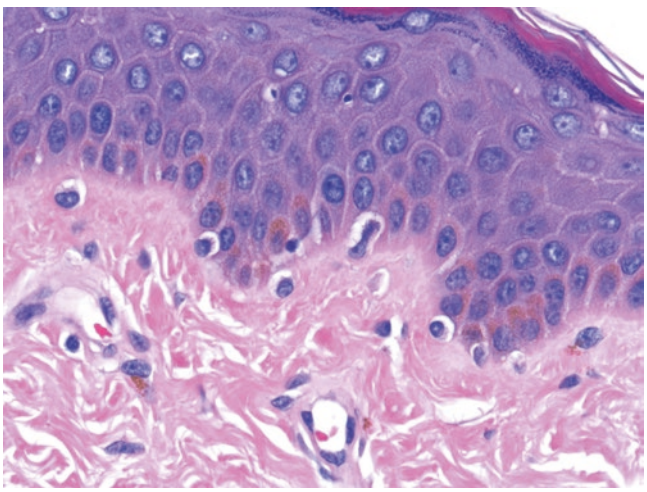

Fig. 1.21 Skin with pigmented melanocytes containing melanin pigment seen along the basal layer of the epidermis. Skin, hematoxylin & eosin, 60× magnification

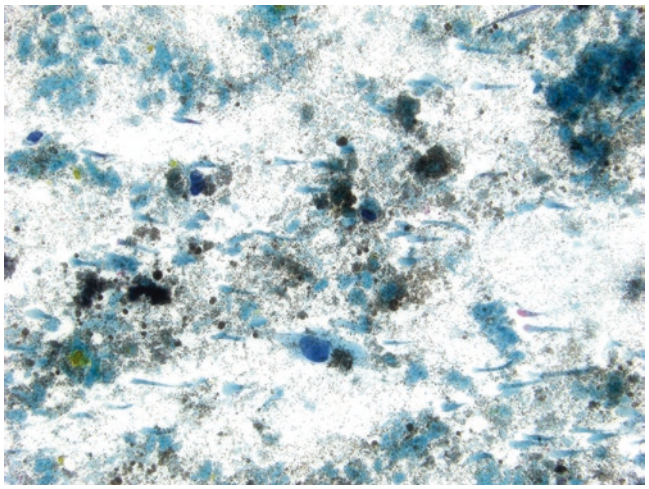

Fig. 1.22 Fine granular extracellular melanin pigment is shown that resembles grains of beach sand. Alcohol-fixed smear preparation, Papanicolaou stain, 40× magnification

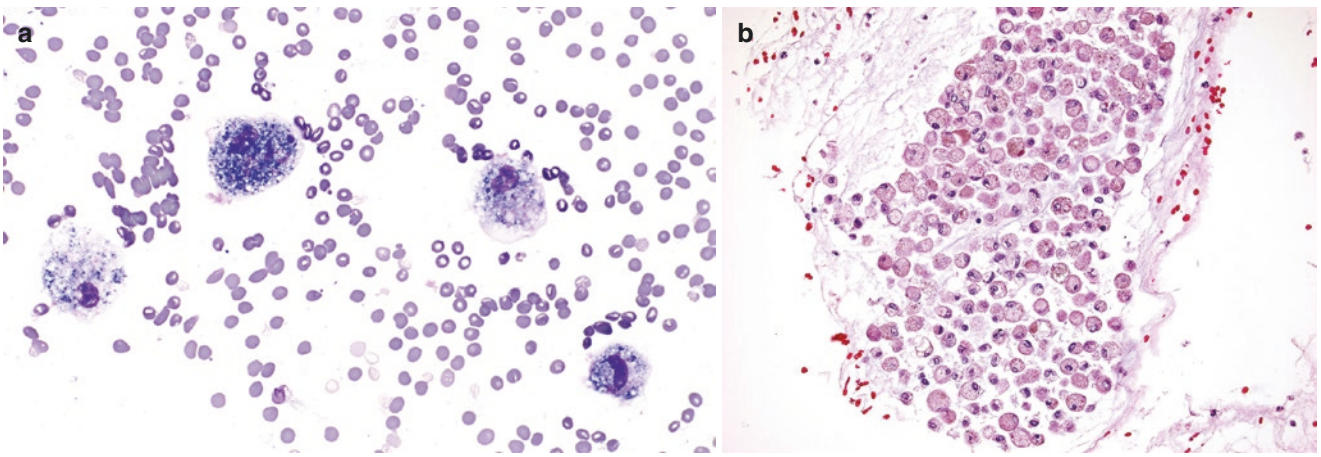

Fig. 1.23 (**a**) Pigment-laden macrophages with coarse intracytoplasmic hemosiderin pigment in a fine needle aspiration of a thyroid cyst with hemorrhage. (**b**) Numerous dust cells containing fine golden-brown pigment are shown in this sputum sample from a patient with a history of smoking. Thyroid, air-dried smear preparation, Diff-Quik, 40x magnification (**a**). Sputum, Cellient cell block, hematoxylin & eosin, 20× magnification (**b**)

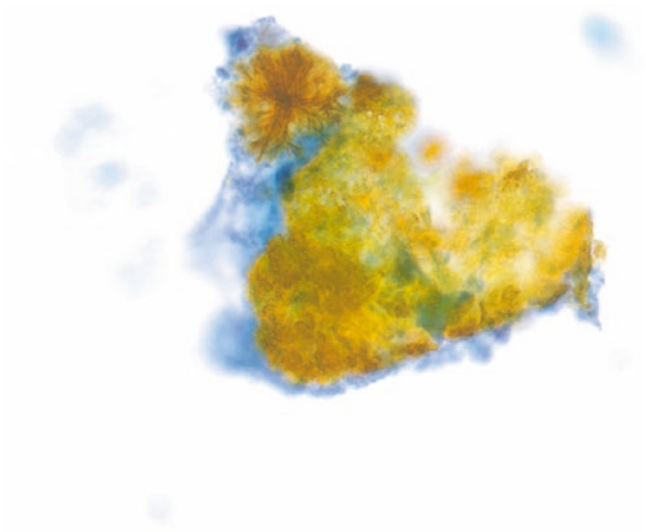

Fig. 1.24 Extracellular yellow hematoidin crystalline material. ThinPrep preparation, Papanicolaou stain, 60× magnification

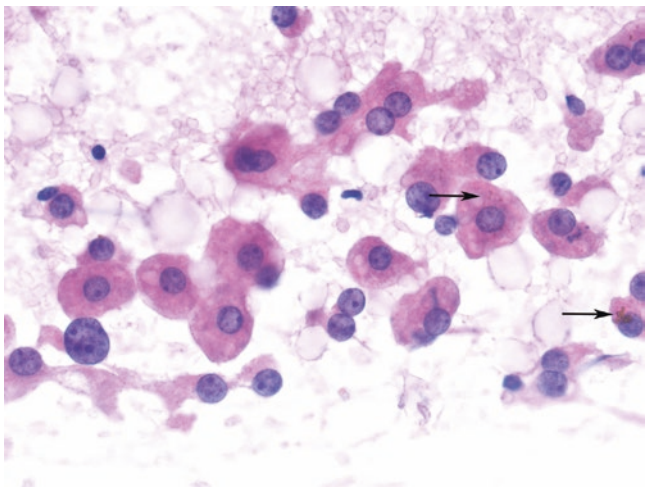

Fig. 1.25 Some of the benign hepatocytes in this aspirate contain scant brown intracytoplasmic lipofuscin pigment (arrow). Alcohol-fixed smear preparation, Papanicolaou stain, 60× magnification

Lipofuscin is a granular "wear-and-tear" oxidized pigment found within intracellular lysosomes that accumulates during normal senescence [18]. Ceroid pigment is similar, but accumulates in pathological conditions such as atrophy, lysosomal disease, and neurodegenerative diseases. Lipofuscin pigment is often yellow-brown in color and may be seen in hepatocytes (Fig. 1.25), cardiac muscle, kidney, seminal vesicles, ejaculatory ducts, adrenal glands, ganglion cells, and the retinal pigment epithelium (RPE) of the eye.

Anthracotic pigment is a black pigment containing carbon particles. Deposition of this pigment is typically seen in the lower respiratory tract, as well as within macrophages of draining hilar and mediastinal lymph nodes (Fig. 1.26). It has no harmful effect on tissue. Anthracotic pigment is usually associated with smoking, air pollution, and, in some cases, prior tuberculosis infection. With certain pneumoconioses (e.g., anthracosis), there may be excess deposition of this pigment in the lungs. Notably, graphite particles that contaminate glass slides when using a pencil to write on slide labels can mimic anthracotic pigment.

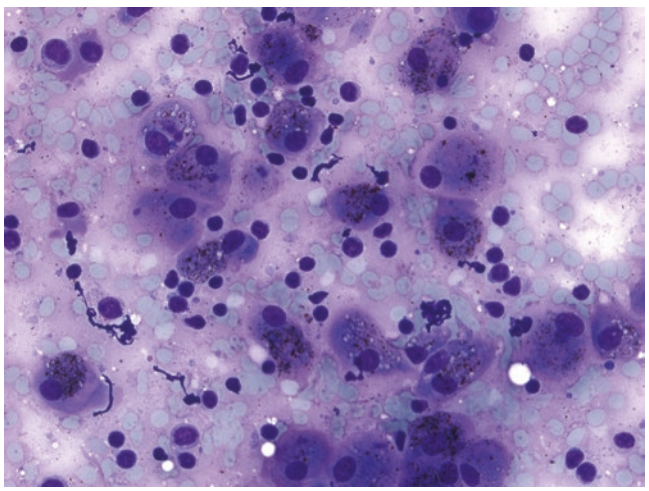

Fig. 1.26 Epithelioid macrophages are shown with black intracytoplasmic anthracotic pigment in a mediastinal lymph node. Lymph node, air-dried smear preparation, Diff-Quik, 40× magnification

Sometimes, one may find various products of degeneration in cytology samples such as cholesterol crystals, calcification, corpora amylacea, amylase crystalloids, Liesegang bodies, and myospherulosis. Many of these structures may mimic microorganisms [19]. Cholesterol crystals are the crystalline form of cholesterol found in gallstones, atherosclerotic plaques, and following tissue breakdown of lipid membranes, usually as a consequence of inflammation or traumatic tissue injury. Cholesterol crystals may also be seen within cyst contents [20]. In cytology samples, they form rhomboid clear structures that often overlap each other (Fig. 1.27a). In histology specimens and cell block material, they form open clefts (Fig. 1.27b). Dystrophic calcification, which refers to calcium deposition in normal tissue usually after long-standing cellular degeneration, is associated with normal calcium and phosphorous levels unlike metastatic calcification or calciphylaxis. Corpora amylacea (CA) are non-calcified, concentric, lamellated structures with a round-oval shape (Fig. 1.28) of variable size (ranging from 30 to 400 μm in diameter). They represent a collection of waste products such as starch-like amyloid and glycoproteins related to aging [21] and can be found in various organs including the brain, spinal cord, prostate gland, and lungs, among others (e.g., bladder, uterus, breast, etc.) [22].

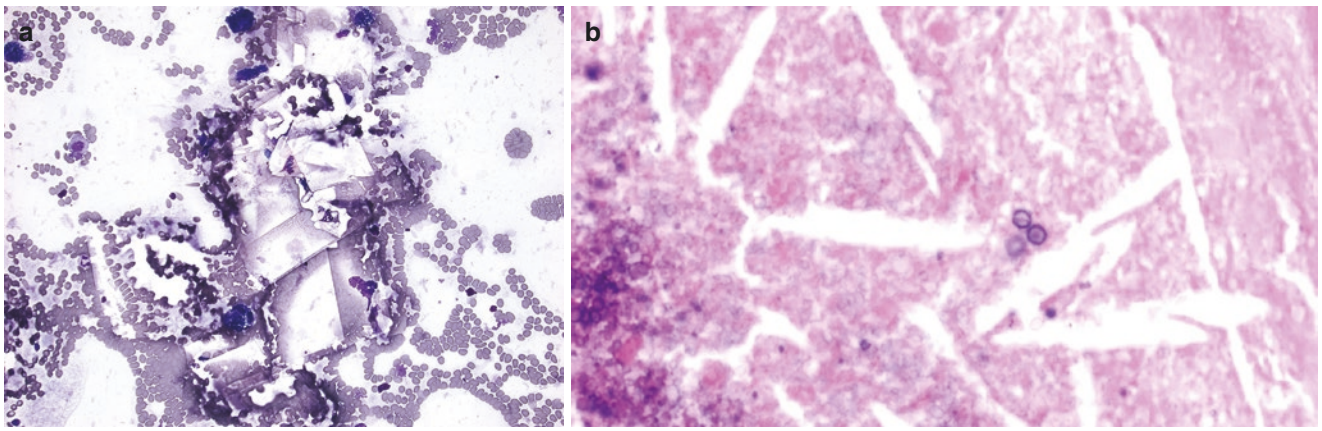

Fig. 1.27 Varied appearance of cholesterol crystals. (**a**) In cytology smear preparations, they can appear as overlapping clear crystals. (**b**) In this histologic section, necrotic acellular material is seen with clear cholesterol clefts with small, round calcifications in the background. These calcifications may mimic the appearance of fungal yeast forms. Air-dried smear preparation, Diff-Quik, 20x magnification (**a**). Histology, hematoxylin & eosin, 20× high magnification (**b**)

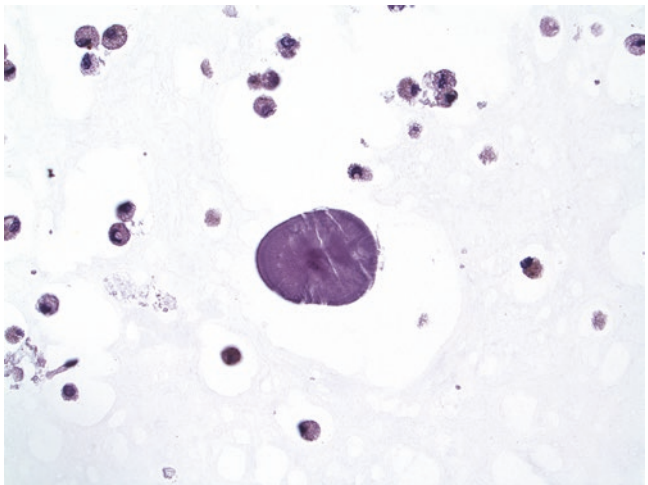

Fig. 1.28 A single round corpus is shown from a lung bronchoalveolar specimen. Note the concentric lamellar pattern. The background of this specimen contains several pigment-laden macrophages. Bronchoalveolar lavage, cell block, hematoxylin & eosin, 40× magnification

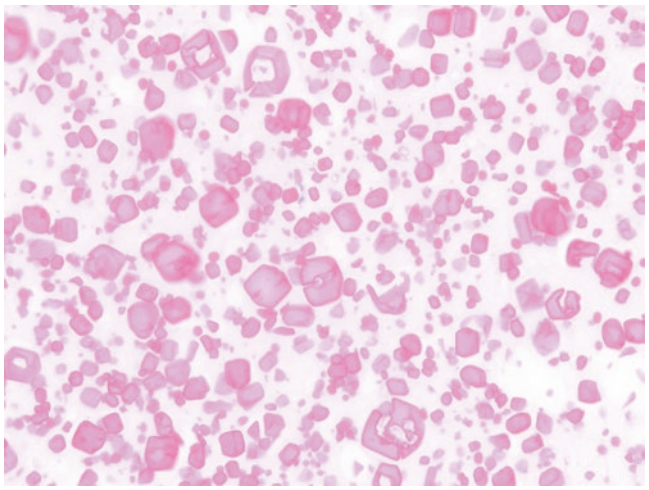

Fig. 1.29 Fragmented amylase crystalloids seen in a parotid fine needle aspiration. Cell block, hematoxylin & eosin, 40× magnification

With the destruction of salivary gland tissue, amylase may leak out from acinar cells and crystallize. These amylase crystalloids are usually a marker of non-neoplastic salivary gland disease. Amylase crystalloids (5–200 μm) are typically fragmented in aspirated material and may accordingly have varied geometric shapes (Fig. 1.29). Liesegang rings (or bodies) are non-polarizable laminated ring-like structures (3–800 μm) that may be associated with hemorrhage and/or found in benign cysts (Fig. 1.30) [23]. They classically have a double-layer outer wall, radial striations, and an amorphous central core.

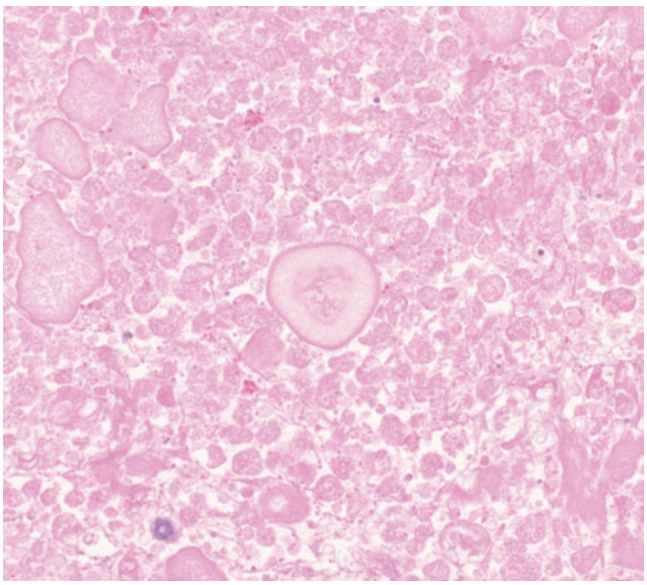

Fig. 1.30 Liesegang rings identified in a hematoma. Soft tissue, hematoxylin & eosin, 40× magnification

References

1. Silverman JF, Frable WJ. The use of the Diff-Quik stain in the immediate interpretation of fine-needle aspiration biopsies. Diagn Cytopathol. 1990;6(5):366–9.
2. Gill GW. Cytopreparation. Principles & practice. New York: Springer; 2013.
3. Chantziantoniou N, Donnelly AD, Mukherjee M, Boon ME, Austin RM. Inception and development of the Papanicolaou stain method. Acta Cytol. 2017;61(4–5):266–80.
4. Yang GC, Alvarez II. Ultrafast Papanicolaou stain. An alternative preparation for fine needle aspiration cytology. Acta Cytol. 1995;39(1):55–60.
5. Allpress SM, Raso DS. The cell. In: Herzberg AJ, Raso DS, Silverman JF, editors. Color atlas of normal cytology. New York: Churchill Livingstone; 1999. p. 1–12.
6. Webster M, Witkin KL, Cohen-Fix O. Sizing up the nucleus: nuclear shape, size and nuclear-envelope assembly. J Cell Sci. 2009;122(10):1477–86.
7. Taxy JB, Chang A. Introduction to the cell. In: Lindberg MR, Lamps LW, editors. Normal histology. 2nd ed. Philadelphia, PA: Elsevier; 2018. p. 4–11.
8. Datar U, Angadi PV, Hallikerimath S, Kale AD. Cytological assessment of Barr bodies using aceto-orcein and Papanicolaou stains in buccal mucosal smears and their sex estimation efficacy in an Indian sample. Acta Cytol. 2013;57(5):516–21.
9. Battistelli M, Falcieri E. Apoptotic bodies: particular extracellular vesicles involved in intercellular communication. Biology (Basel). 2020;9(1):21.
10. Gupta PK, Baloch ZW. Cytohistology. Essentials and basic concepts. Cambridge: Cambridge University Press; 2011.
11. Nguyen M, Mikita G, Hoda RS. "Intercellular bridges" in a case of well differentiated squamous carcinoma. Diagn Cytopathol. 2016;44(2):121–3.
12. Raso DS. Breast. In: Herzberg AJ, Raso DS, Silverman JF, editors. Color atlas of normal cytology. New York: Churchill Livingstone; 1999. p. 387–98.
13. Sidawy MK, Costa M. The significance of paravacuolar granules of the thyroid. A histologic, cytologic and ultrastructural study. Acta Cytol. 1989;33(6):929–33.
14. James LP. Cytopathology of mesenchymal repair. Diagn Cytopathol. 1985;1(2):91–104.
15. Menzel T, Fletcher CD. The emerging role of myofibroblasts in soft tissue neoplasia. Am J Clin Pathol. 1997;107(1):2–5.
16. Sherman JM, Winnie G, Thomassen MJ, Abdul-Karim FW, Boat TF. Time course of hemosiderin production and clearance by human pulmonary macrophages. Chest. 1984;86(3):409–11.
17. Brenner DS, Drachenberg CB, Papdimitriou JC. Structural similarities between hematoidin crystals and asteroid bodies: evidence of lipid composition. Exp Mol Pathol. 2001;70(1):37–42.
18. Katz ML, Robinson WG. What is lipofuscin? Defining characteristics and differentiation from other autofluorescent lysosomal storage bodies. Arch Gerontol Geriatr. 2002;34(3):169–84.
19. Pantanowitz L, Goulart RA, Martínez Girón R. In: Pantanowitz L, Michelow P, Khalbuss WE, editors. Mimics and contaminants. Cytopathology of infectious diseases. New York, NY: Springer; 2011. p. 351–77.
20. Pantanowitz L, Panetti C, Goulart RA, Cooper R. Cholesterol crystals in the thyroid gland. Acta Cytol. 2007;51:249–51.
21. Martínez-Girón R, Pantanowitz L. Corpora amylacea in sputum smears: incidence and clinical significance. Cytopathology. 2021;32(1):108–14.
22. Röcken C. Corpora amylacea in the lung, prostate and uterus. A comparative and immunohistochemical study. Pathol Res Pract. 1996;192(10):998–1006.
23. Raso DS, Greene WB, Finley JL, Silverman JF. Morphology and pathogenesis of Liesegang rings in cyst aspirates: report of two cases with ancillary studies. Diagn Cytopathol. 1998;19:116–9.

Respiratory System

2

Madelyn Lew, Tao Huang, and Xin Jing

The respiratory tract consists of the sinonasal region, larynx, trachea, and the lungs, which contain mainstem bronchi and their progressively smaller divisions of bronchi, bronchioles, and respiratory acini. The airways largely consist of cartilaginous rings supported by fibrous and smooth muscle mesenchymal elements to allow a passageway of air to the lungs. The lungs are paired organs of the respiratory system that function to extract environmental oxygen into the bloodstream via gas exchange. On gross examination, the right lung is divided into three lobes (upper, middle, and lower) while the left lung is divided into two lobes (upper and lower). The left lung also contains a rudimentary appendage, the lingula, which is derived from the left upper lobe and is considered an analogous structure to the right middle lobe. The lobes are further divided into nine and ten bronchopulmonary segments within the left and right lung, respectively. Each segment is partitioned such that fibrous septa derived from the pleura encapsulate each segment, prohibiting free flow of air as well as pathologic processes between bronchopulmonary segments. Lobules are the smallest unit of the lung that can be appreciated grossly and are bound by interlobular septa. A lobule is composed of various numbers of acini, which are the basic units for air exchange. An acinus is composed of respiratory bronchioles, alveolar ducts, alveolar sacs, and alveoli.

Histologically, the bronchus is organized into respiratory epithelium, under which lies a thin layer of smooth muscle, circumferential cartilage, and submucosal seromucous glands (Fig. 2.1a). The respiratory epithelium consists predominantly of pseudostratified tall columnar cells with cilia admixed with goblet cells, basal cells, neuroendocrine cells, and Clara cells. Neuroendocrine cells and Clara cells are inconspicuous on hematoxylin & eosin (H & E) stains (Fig. 2.1b). As the airways subdivide into smaller subunits, some morphologic changes can be identified. The membranous bronchiole lacks cartilaginous rings and shows fewer goblet cells with a proportionally increased number of Clara cells (Fig. 2.1c, d). The alveoli are lined mainly by type I pneumocytes, which are inconspicuous in routine H & E-stained sections but cover 90% of the alveolar surface, and type II pneumocytes (Fig. 2.1e). Although the type II pneumocytes are a small subset of the alveolar lining cells, they are the precursor cells for type I pneumocytes and are the main proliferating cells following alveolar injury (Fig. 2.1f). Within the alveolar spaces, alveolar macrophages are frequently seen and are often pigmented in smokers (Fig. 2.1g). The pigment seen in a smoker's macrophages is red-brown in color and is believed to be a ceroid-like granular autofluorescent pigment in the lysosomes [1]. Incidental findings that can be seen in the lung not too uncommonly include corpora amylacea (Fig. 2.1h), interstitial megakaryocytes (Fig. 2.1i), cytoplasmic Mallory-like hyaline bodies (Fig. 2.1j), carcinoid tumorlets (Fig. 2.1k), and meningothelial-like nodules (Fig. 2.1l). If sampled, these structures may be infrequently encountered in cytology samples.

Evaluation of different types of cytology specimens has played an important role in the diagnosis and staging of lung lesions. Routinely collected cytology specimens include exfoliative samples (sputum, bronchial brushing, bronchial washing, and bronchoalveolar lavage) and fine needle aspiration (FNA) samples obtained via transbronchial (Wang needle), endobronchial ultrasound (EBUS)-guided, endoscopic ultrasound (EUS)-guided transesophageal, or computed tomography (CT)-guided percutaneous approaches. The specimens are often processed using one or multiple preparations, including Diff-Quik- and/or Papanicolaou-stained conventional smears, liquid-based preparations (LBP) such as ThinPrep or SurePath, and cytospins, as well as H & E-stained cell block material. The Papanicolaou Society of Cytopathology previously developed a set of guidelines for pulmonary cytology, including indications and technical recommendations for obtaining the aforementioned lung cytology samples, terminology and classification scheme,

M. Lew (✉) · T. Huang · X. Jing
Department of Pathology, University of Michigan, Ann Arbor, MI, USA
e-mail: lewm@med.umich.edu; taohuang@med.umich.edu; xinjing@med.umich.edu

M. Lew et al. (eds.), *Normal Cytology*, https://doi.org/10.1007/978-3-031-20336-7_2

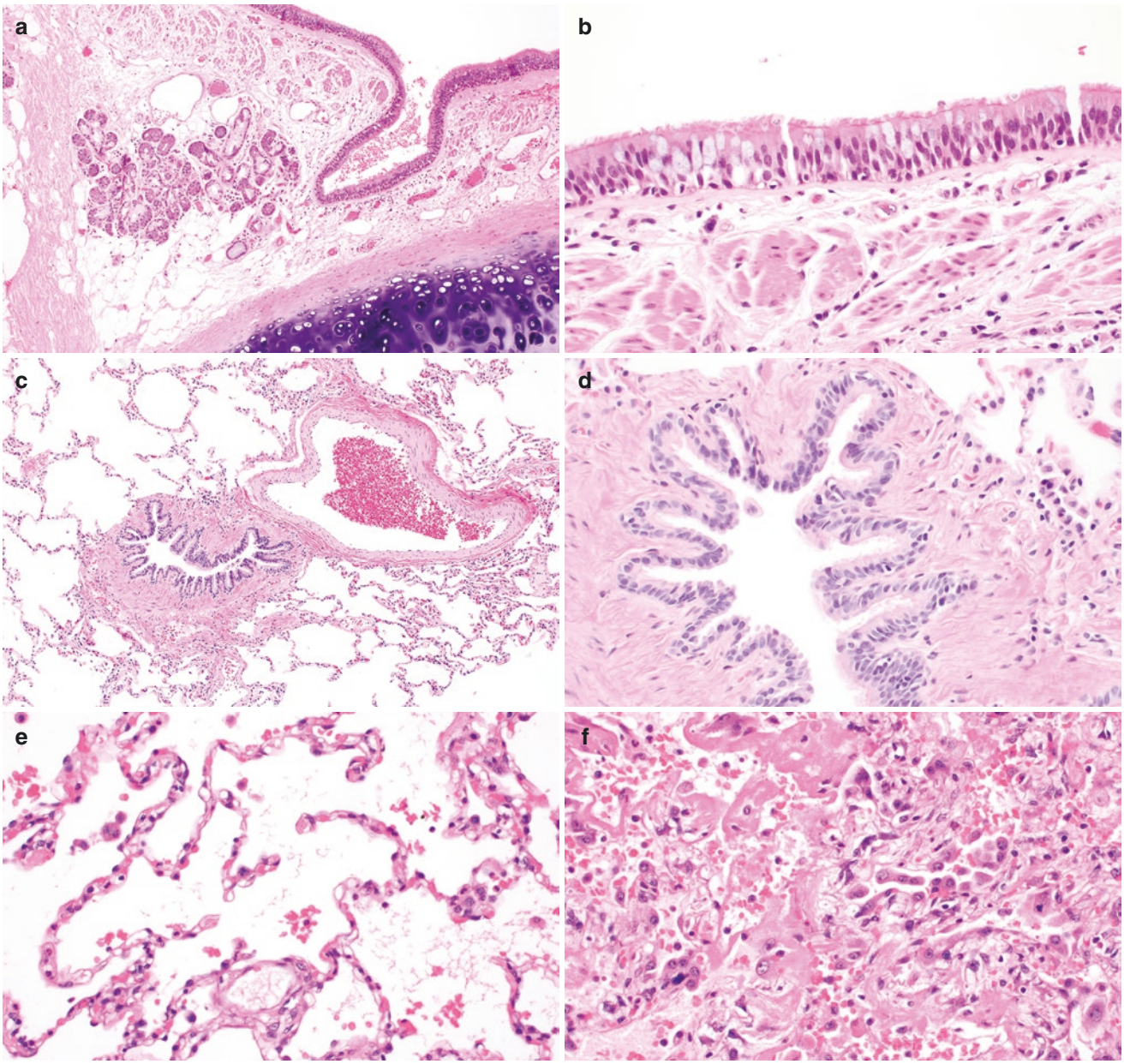

Fig. 2.1 (**a**) A bronchus is shown and composed of respiratory epithelium, an underlying thin layer of smooth muscle, submucosal seromucous glands, and hyaline cartilage. (**b**) The respiratory epithelium lining the bronchus is composed of pseudostratified tall columnar cells including ciliated cells, goblet cells, and basal cells. (**c**) In contrast, the membranous bronchiole does not have a cartilaginous ring and (**d**) is lined by pseudostratified columnar cells with prominent apical cilia, but without obvious goblet cells. (**e**) Type II pneumocytes with a hobnail-like appearance are shown lining the alveoli. (**f**) Type II pneumocytes proliferate to replace damaged cells following acute lung injury (such as acute diffuse alveolar damage) and can show marked cytologic atypia. (**g**) Respiratory bronchiolitis characterized by lightly pigmented alveolar macrophages clustered within the lumina of distal airways and peribronchiolar air spaces is a common finding in smokers. (**h**) Corpora amylacea are shown as amphophilic rounded structures with concentric lamellae within alveolar spaces. (**i**) A megakaryocyte (black arrow) is shown, characterized by a dark staining (on hematoxylin & eosin), irregularly shaped, and elongated nucleus. They should not be misinterpreted as malignant cells or cells with viral cytopathic changes. (**j**) Reactive and proliferating type II pneumocytes in the context of organizing diffuse alveolar damage show cytoplasmic accumulation of brightly eosinophilic amorphous material resembling Mallory's hyaline seen in liver diseases. (**k**) A carcinoid tumorlet focus (<5 mm) of neuroendocrine cells is shown associated with patchy fibrosis. These are often found in close proximity to bronchioles. The cells are cytologically bland with characteristically finely dispersed chromatin, inconspicuous nucleoli, and granular cytoplasm. (**l**) A meningothelial-like nodule is shown composed of a population of cytologically bland oval cells arranged in a nested pattern and distributed randomly within the interstitium. Lung resection, hematoxylin & eosin, 10× (**a**, **c**, **k**), 20× (**l**), and 40× (**b**, **d**–**j**) magnification

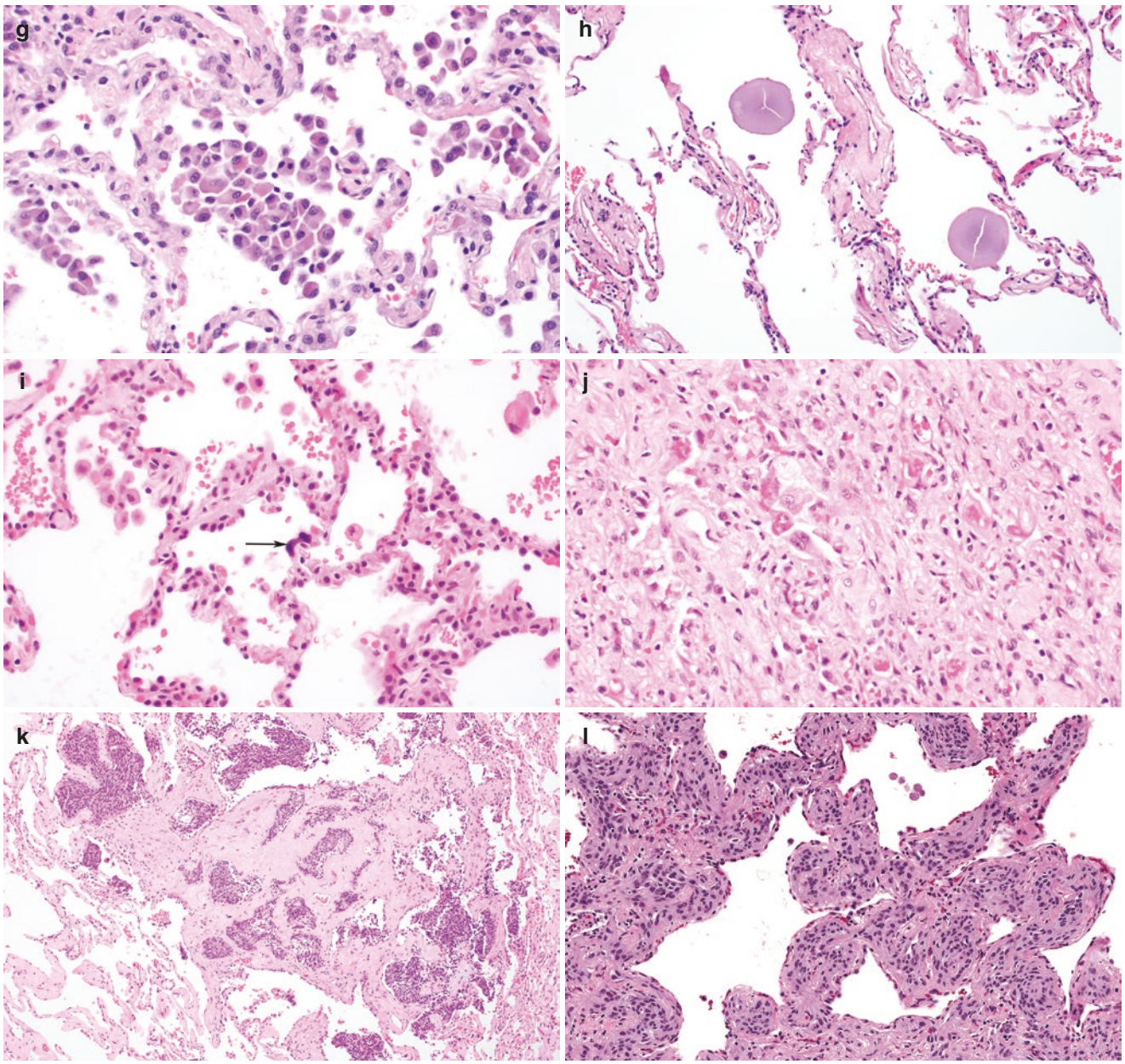

Fig. 2.1 (continued)

recommendations for ancillary testing, as well as recommendations for post-cytologic diagnosis management and follow-up [2–4]. More recently, the WHO System for Reporting Lung Cytopathology has been developed to guide standardized diagnostic categorization while leveraging the use of available ancillary studies.

The various cell types of the respiratory tract can be readily identified on cytologic specimens. Supporting mesenchymal elements (smooth muscle, cartilage, fibrous tissue) and resident pulmonary macrophages can be identified as well. While neuroendocrine or Kulchitsky or K cells may also be present on cytologic specimens, their definitive identification often requires the use of special stains, immunohistochemistry, or electron microscopy. While less common elements may be clearly delineated in histologic examination of biopsies and resection specimens, it is typically uncommon and/or difficult to recognize singly dispersed endocrine cells, type I pneumocytes, myocytes, and fibroblasts in cytologic specimens [5]. The most frequently encountered normal cellular elements in cytology preparations include squamous cells, ciliated columnar cells, goblet cells, basal or reserve cells, type II pneumocytes, and macrophages [6].

Squamous cells line the upper airway from the sinonasal region to the larynx and can be identified as normal components in sputum, bronchial brushing, bronchial washing, and bronchoalveolar lavage specimens. Squamous metaplasia can be seen as a result of reactive changes associated with various etiologies of airway irritation and injury, such as

cigarette smoking, air pollution, infection, or chronic airway disease. Metaplastic squamous cells have dense cytoplasm and bland, round nuclei with smooth nuclear contours, even chromatin distribution, and variably distinct nucleoli [7]. However, some immature metaplastic cells can display cytologic atypia in the form of enlarged, hyperchromatic nuclei. As such, it is important to consider squamous metaplasia as an etiology of atypical squamous cells to avoid a false positive diagnosis of a squamous cell carcinoma.

In cytology preparations, ciliated columnar cells of the trachea and bronchial epithelium are frequently seen in well-spaced monolayer sheets, cohesive clusters with variable nuclear overlapping, or as singly dispersed cells. Like their histologic appearance, they display round or ovoid nuclei with smooth nuclear contours, fine chromatin distribution, and variably distinct nucleoli. When longitudinally oriented, the basal localization of the nucleus is more evident. Most characteristically, the luminal surfaces of bronchial ciliated columnar cells have numerous cilia attached to thick terminal bars (Fig. 2.2a–c). Of note, these cells can display significant morphologic changes in reactive conditions, including nuclear enlargement, multinucleation, coarse chromatin distribution, and large nucleoli.

Caution should be taken to avoid misinterpretation of a well-differentiated neuroendocrine tumor as benign columnar bronchial cells. The spindled- and plasmacytoid-appearing neuroendocrine tumor cells may mimic bronchial columnar cells under low power magnification. However, the tumor cells are often arranged as single cells and lack cilia and terminal bars. The centrally or eccentrically located nuclei of tumor cells have "salt and pepper" chromatin and small but distinct nucleoli (Fig. 2.3a–c).

Tightly clustered benign bronchial cells can also be misinterpreted as well-differentiated adenocarcinoma, particularly in the case of Creola bodies. Creola bodies, first described by Naylor, are well-defined, compact clusters of ciliated columnar cells with peripheral palisading. They are frequently seen in the clinical setting of asthma and are the result of excessive shedding of epithelial cells of the lower respiratory tract [8]. Creola bodies may contain over 100

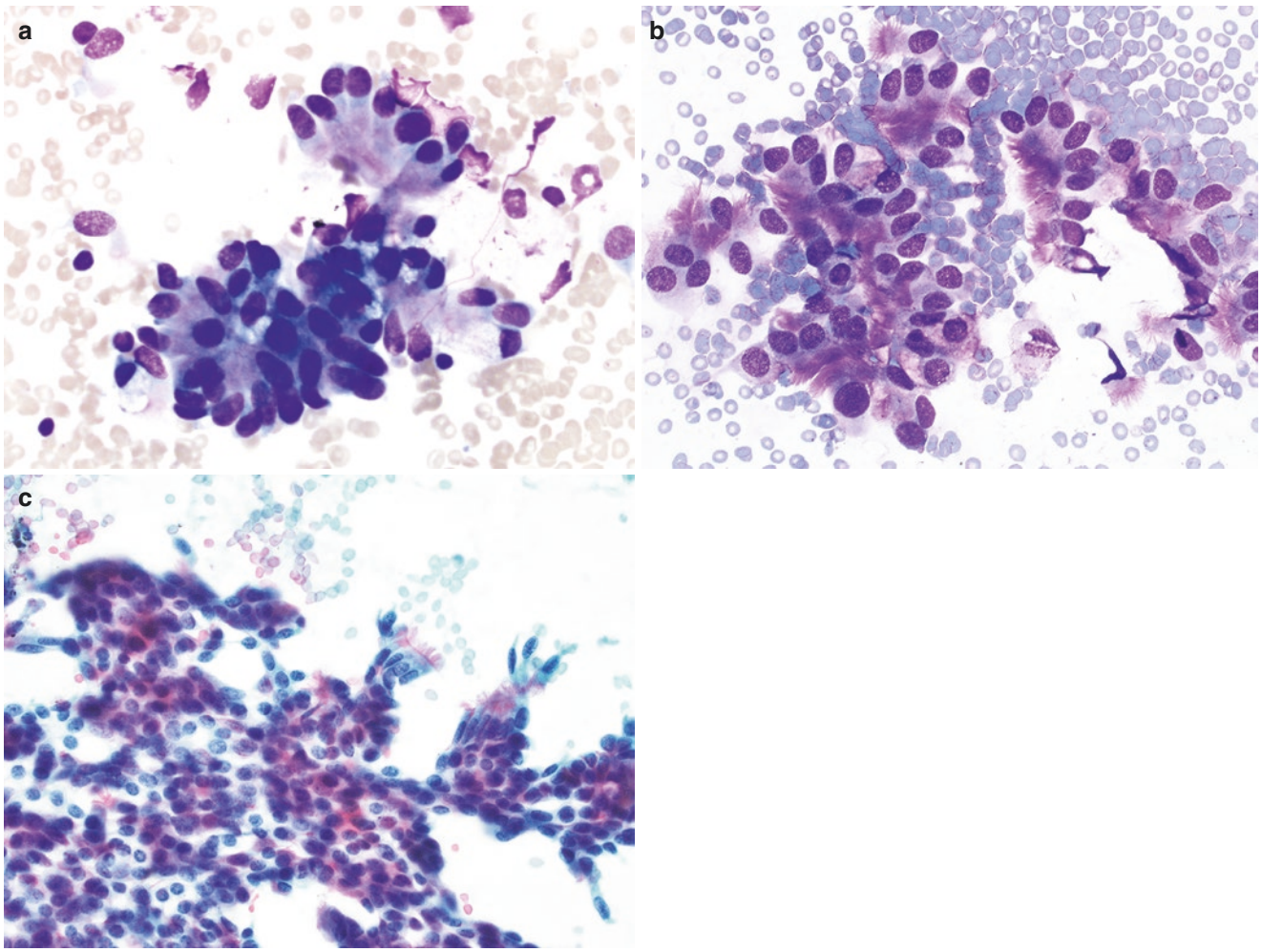

Fig. 2.2 Various bronchial epithelial cells. (**a**) A cohesive cluster of columnar bronchial lining cells with mild nuclear overlapping is shown. The cells have round or oval nuclei, smooth nuclear membranes, fine chromatin distribution, and distinct nucleoli. (**b**, **c**) Cilia attached to thick terminal bars are evident. Lung, air-dried smear preparation, Diff-Quik, 40× magnification (**a**, **b**). Lung, alcohol-fixed smear preparation, Papanicolaou stain, 40× magnification (**c**)

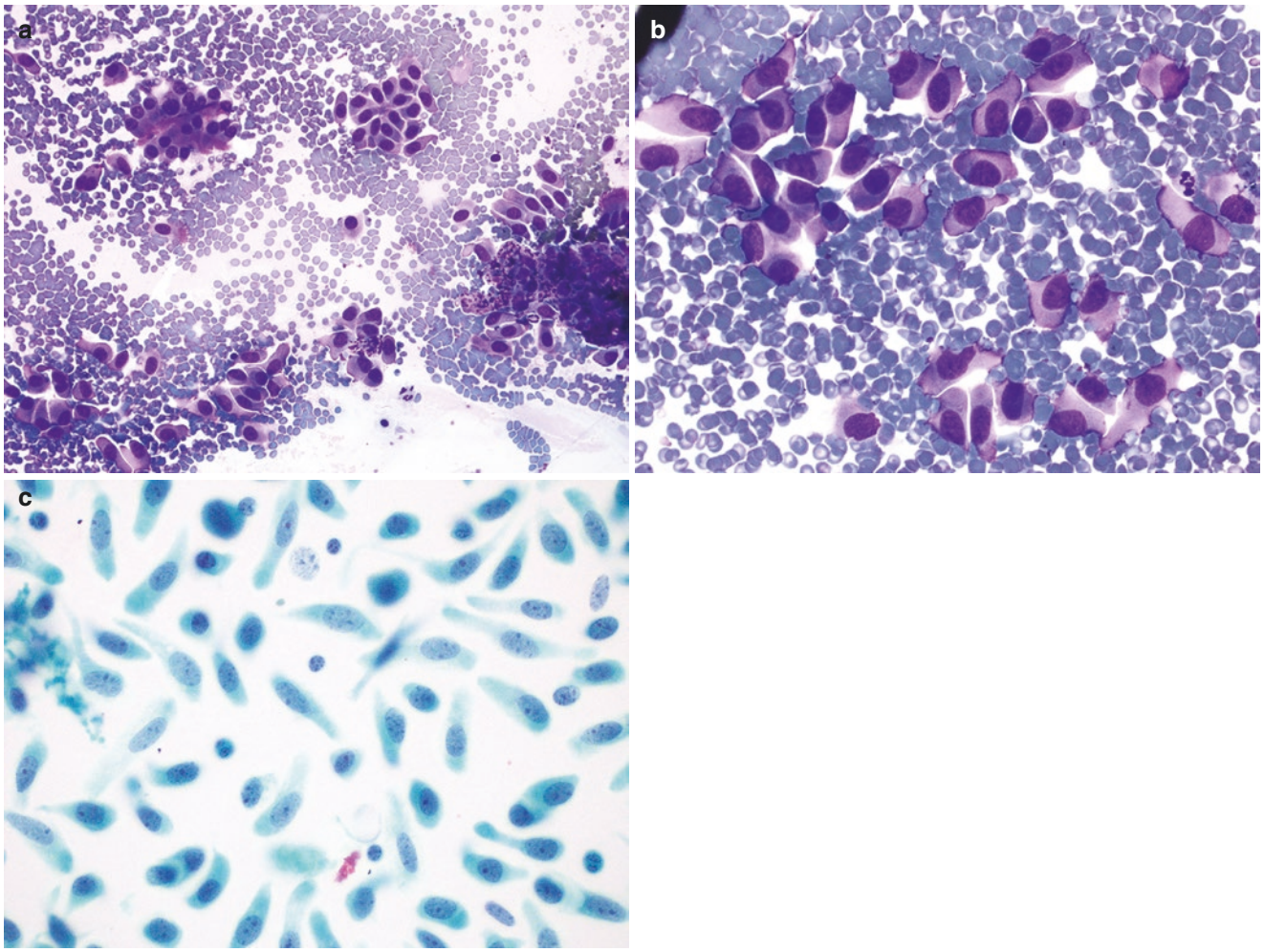

Fig. 2.3 (**a**) Unlike benign bronchial cells (left upper), spindled or plasmacytoid well-differentiated neuroendocrine tumor cells do not have cilia and terminal bars. (**b**, **c**) Neuroendocrine tumor cells are often arranged as single cells or in loosely cohesive clusters. The nuclei are centrally or eccentrically located. "Salt and pepper" chromatin distribution and distinct nucleoli are frequently appreciated. Lung, air-dried smear preparation, Diff-Quik, 20× (**a**) and 40× (**b**) magnification. Lung, alcohol-fixed smear preparation, Papanicolaou stain, 60× magnification (**c**)

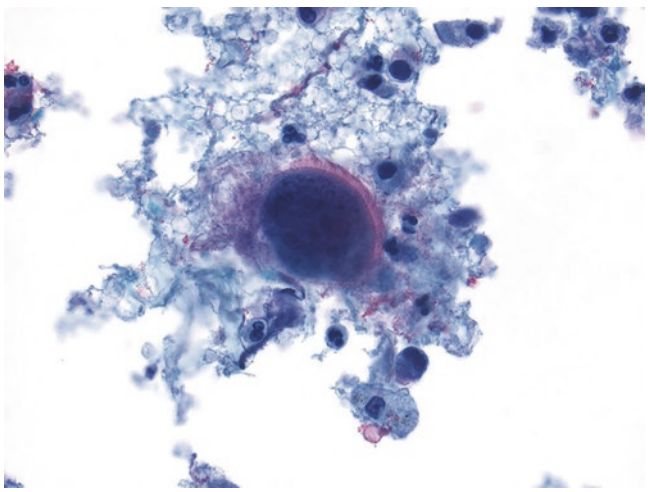

Fig. 2.4 Creola body presenting as a well-defined, compact cluster of uniform, ciliated columnar cells with peripheral palisading. ThinPrep preparation, 60× magnification

columnar cells, are round in shape and may display a papillary architecture. The cytoplasm of the columnar cells can also be vacuolated. However, the presence of cilia (which may be more difficult to identify in tight cell clusters), relatively uniform nuclear size and shape, and peripheral palisading of the papillary groups are helpful features to differentiate Creola bodies from adenocarcinoma (Fig. 2.4).

Another commonly encountered respiratory epithelial component in cytology specimens is the mucin-secreting goblet cell. Goblet cells are interspersed with ciliated columnar cells in a ratio of approximately 1 goblet cell:5–6 columnar cells. Goblet cells contain a single large or multiple smaller cytoplasmic mucin vacuoles, which push nuclei to the periphery. The nuclei have smooth nuclear contours and fine chromatin distribution. Clusters of goblet cells may indicate goblet cell metaplasia and/or hyperplasia associated with reactive processes [7]. Caution should be taken to avoid misinterpretation of goblet cell metaplasia/hyperplasia as a mucin-producing adenocarcinoma (Fig. 2.5a, b). While this

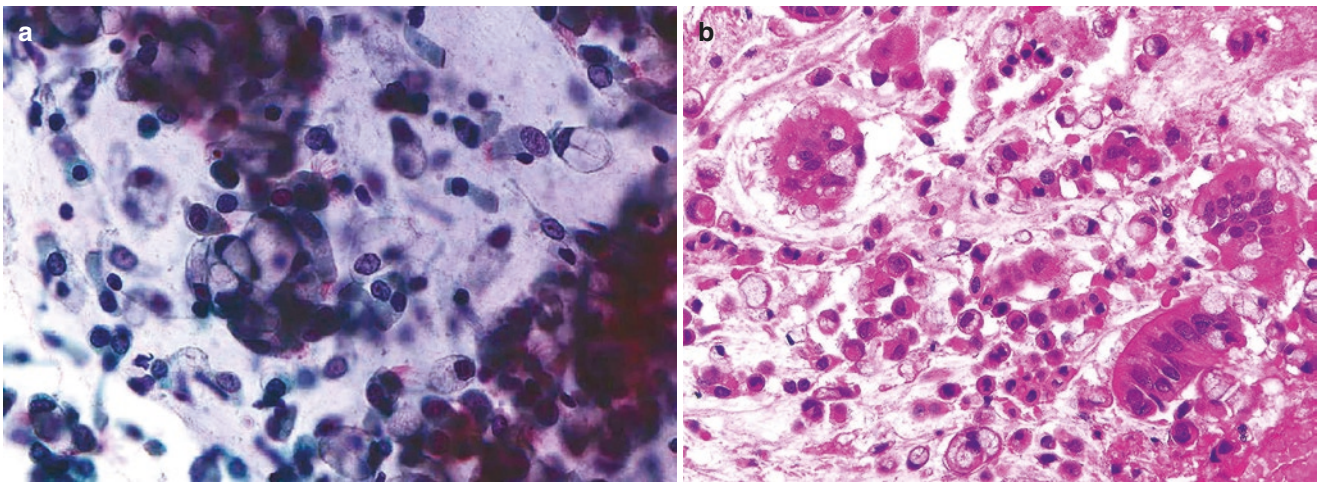

Fig. 2.5 (**a**) Goblet cells with cytoplasmic mucin vacuoles and peripheral nuclei are arranged singly and in clusters. Their nuclei have smooth nuclear membranes and fine chromatin distribution. (**b**) Cell block preparation of a bronchoalveolar lavage shows goblet cells admixed with ciliated bronchial cells. Lung, alcohol-fixed smear preparation, Papanicolaou stain, 40× magnification (**a**). Bronchoalveolar lavage, cell block, hematoxylin & eosin, 40× magnification (**b**)

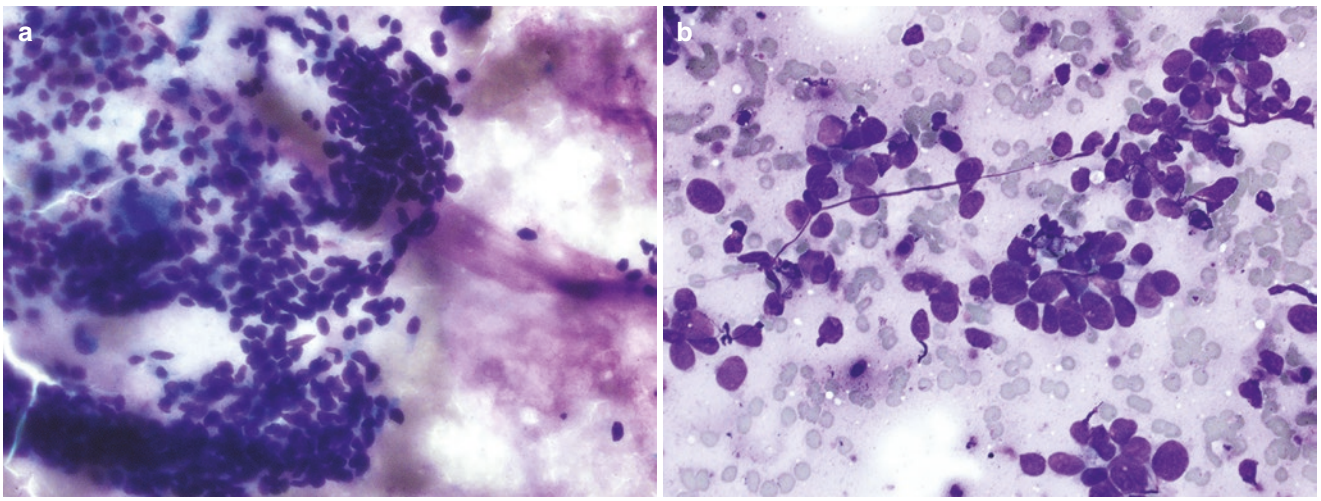

Fig. 2.6 (**a**) Reserve cells are shown as small oval or cuboidal cells with high nuclear:cytoplasmic ratios arranged in clusters that may demonstrate nuclear overlapping and molding. Their nuclei are monotonous. The background contains mucin but there is no associated necrosis. (**b**) Small cell carcinoma cells show cellular disruption, nuclear molding, nuclear enlargement with high nuclear:cytoplasmic ratios, irregular nuclear membranes, and "salt and pepper" chromatin distribution. Note the admixed apoptotic cells in the sample. Lung, air-dried smear preparation, Diff-Quik, 40× magnification (**a**, **b**)

differential may be difficult to distinguish on morphology alone, goblet cell metaplasia will often have a lower quantity of mucin-producing cells in a given sample. Additionally, clinical correlation is key in the identification of long-standing airway disease that could give rise to a reactive process such as goblet cell metaplasia.

Similar to squamous cell metaplasia, reserve or basal cell hyperplasia is also seen as a response to a local insult [7]. In cytology specimens, reserve cells are small columnar or cuboidal cells with high nuclear:cytoplasmic ratios arranged in variably crowded groups which can also contain ciliated columnar cells. They may show mild nuclear molding in which the nuclei compress each other and distort their shapes, potentially raising concern for small cell carcinoma. However, nuclei of reserve cells are monotonous, and the background of reserve cell hyperplasia lacks necrosis and apoptotic debris (Fig. 2.6a). Also in contrast to small cell carcinoma (Fig. 2.6b), mitotic figures are not readily identified.

In cytology specimens, type II pneumocytes are infrequently encountered, but when identified have round nuclei and vacuolated cytoplasm. Their morphology may be hard to distinguish from macrophages when they are singly dispersed. Type II pneumocyte hyperplasia follows injury to the more distal epithelial cells lining the alveolar walls. These are seen as grouped or individual polygonal or rectangular cells, which may show cytoplasmic vacuolization, smooth nuclear membranes, fine chromatin distribution, and distinct nucleoli. No cilia are attached to these cells. The

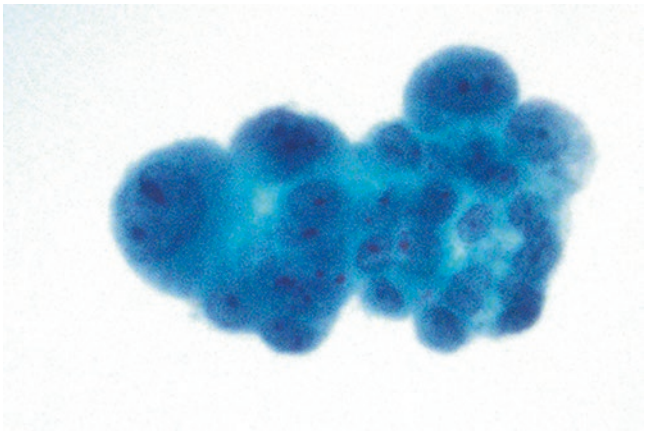

Fig. 2.7 A cluster of type II polygonal pneumocytes with variably sized nuclei, finely vacuolated cytoplasm, smooth nuclear membranes, fine chromatin distribution, and distinct nucleoli. Bronchoalveolar lavage, ThinPrep preparation, 40× magnification

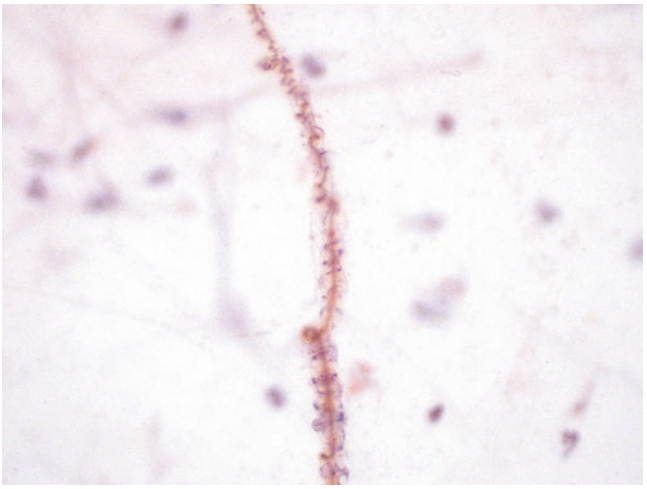

Fig. 2.9 Coiled Curschmann spiral. Lung, alcohol-fixed smear preparation, Papanicolaou stain, 60x magnification

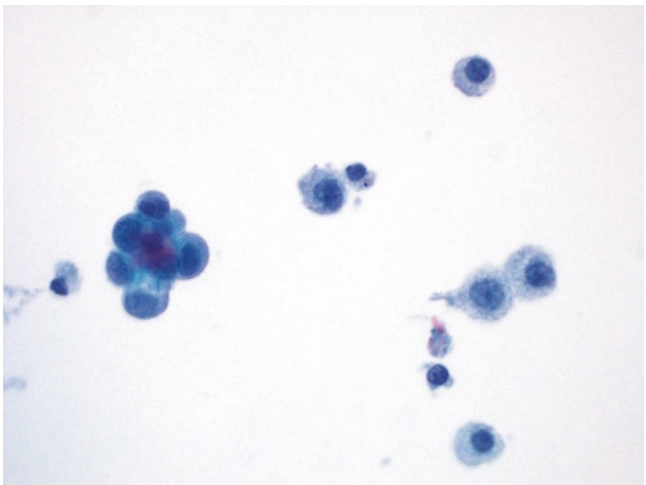

Fig. 2.8 Pulmonary macrophages are arranged as single cells and characterized by abundant pale, vacuolated cytoplasm and small, round nuclei. Bronchoalveolar lavage, ThinPrep preparation, 60× magnification

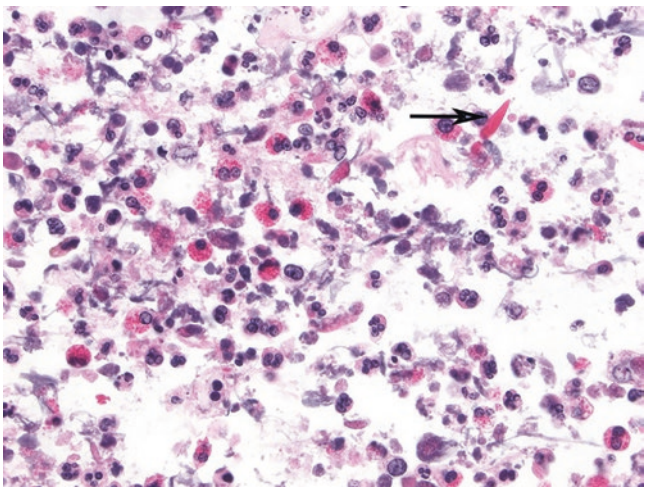

Fig. 2.10 A Charcot-Leyden crystal is present characterized by needle-shaped eosinophilic structure (black arrow). Many eosinophils are seen in the background. Cell block, hematoxylin & eosin, 40× magnification

features of type II pneumocyte hyperplasia may be misinterpreted as adenocarcinoma (Fig. 2.7). As such, in the clinical context of a patient with acute respiratory distress and radiologic findings of diffuse pulmonary infiltrates, one must be cautious to prevent misinterpreting reactive conditions as malignant.

The presence of pulmonary macrophages is required for sputum and bronchoalveolar lavage specimens to be deemed adequate for evaluation. Similar to macrophages seen elsewhere, pulmonary macrophages are characterized by an abundant amount of pale, vacuolated cytoplasm and small round, ovoid, or occasionally indented nuclei (Fig. 2.8). Multinucleation can be seen. Pulmonary macrophages commonly contain cytoplasmic pigment granules which may include finely granular golden brown tobacco pigment, dark and coarse yellow-brown hemosiderin pigment, or black anthracotic pigment from carbon products.

Noncellular components may be encountered in cytology specimens prepared from the respiratory tract, including Curschmann spirals, Charcot-Leyden crystals, asbestos bodies, and corpora amylacea [7, 9]. Curschmann spirals are clumps and casts of mucus from smaller airways, forming coiled structures characterized by densely staining central cores and a lighter staining periphery that can be identified in various chronic respiratory diseases (Fig. 2.9).

Charcot-Leyden crystals are rhomboid or needle-shaped eosinophilic to orangeophilic granule concretions. They may be present in the clinical setting of asthma or any other condition resulting in eosinophilia with degranulation in the respiratory tract (Fig. 2.10).

Asbestos bodies represent asbestos fibers which have been coated by a proteinaceous iron coat derived from alveolar macrophages. Asbestos bodies have a distinguishing thin, transparent fibrous core (Fig. 2.11).

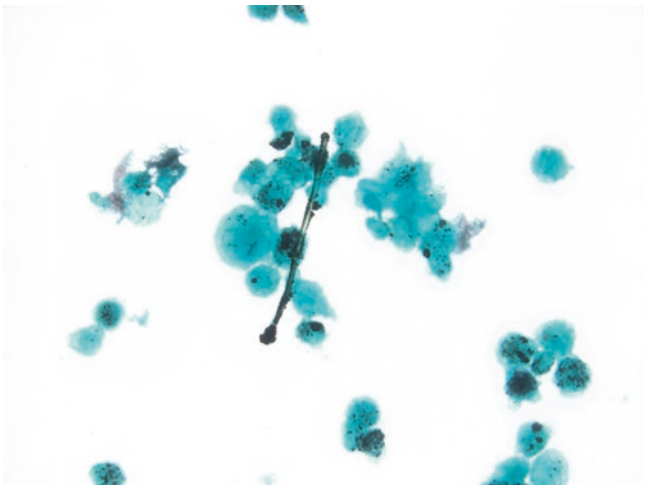

Fig. 2.11 Asbestos body with a thin, transparent fibrous core. Smear preparation, Gomori-methenamine silver (GMS) stain, 40× magnification

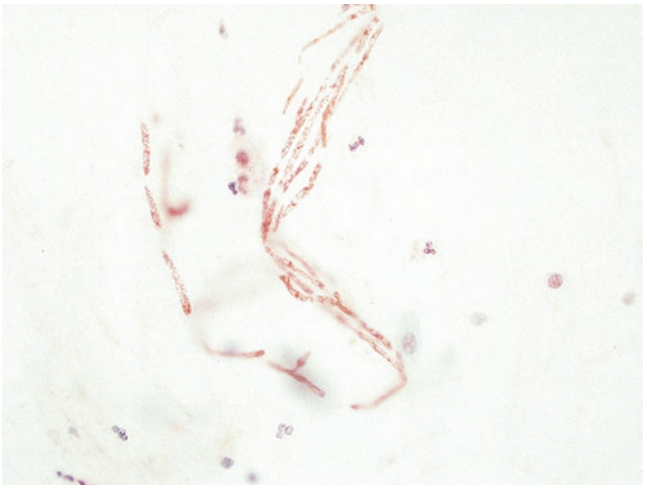

Fig. 2.13 Vegetable matter comprised of degenerated plant cells. Alcohol-fixed smear preparation, Papanicolaou stain, 60× magnification

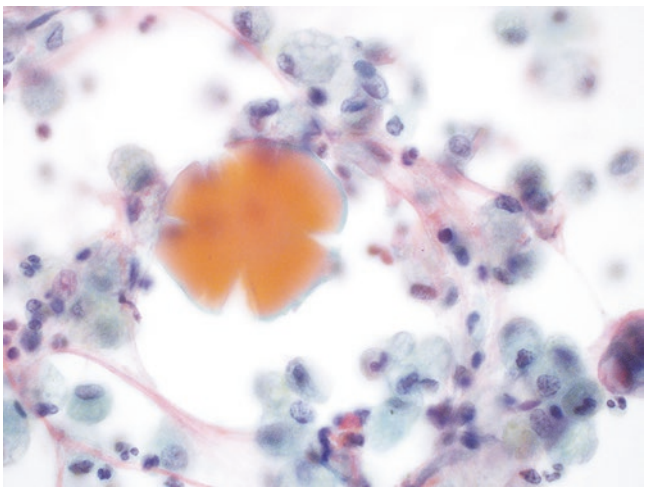

Fig. 2.12 Corpora amylacea, as shown in this image, are noncalcified concentric lamellated structures with a glass-like appearance. Alcohol-fixed smear preparation, Papanicolaou stain, 60× magnification

Corpora amylacea may be seen in bronchoalveolar lavage and sputum cytology specimens as variably sized, noncalcified, round to oval concentrically lamellated structures, sometimes showing a glass-like appearance. The presence of corpora amylacea in sputum smears is related to age, being more frequent in older people, and in nonneoplastic lung diseases such as chronic obstructive pulmonary disease (Fig. 2.12).

In addition, pollen, calcifications, amyloid, and vegetable matter may be rarely seen (Fig. 2.13).

In lung fine needle aspirations, it is important to be cognizant of potential contaminants from other anatomic sites to avoid misinterpretation. In percutaneous approaches to lung lesions, contaminating sheets and clusters of mesothelial cells may be identified and misinterpreted as lesional cells. However, the sheet-like arrangements of mesothelial cells as well as the presence of slit-like spaces between these cells should provide morphologic clues to their mesothelial origin. Similarly, hepatocytes may be seen in specimens collected through a transdiaphragmatic approach or inadvertent sampling when targeting a right lower lobe lung lesion. In addition, transbronchial approaches can result in the sampling of submucosal seromucinous glands and cartilage of the respiratory tract. The morphologic features of seromucinous glands are similar to those of salivary gland acini. While these seromucinous cells often appear bland, it is important to note that, similar to salivary gland acinar cells, they can undergo oncocytic metaplasia that can be misinterpreted as lesional tissue. Stripped individual chondrocytes that get incidentally picked up when placing a needle through bronchial hyaline cartilage may sometimes be mistaken for keratinizing squamous cells.

References

1. Kerényi T, Voss B, Goeckenjan G, Müller KM. Cellular autofluorescent pigment and interstitial fibrosis in smoker's lung. Pathol Res Pract. 1992;188(7):925–30.
2. Michael CW, Hoda RS, Saqi A, Kazakov J, Elsheikh T, Azar N, Ohori NP. Committee I: indications for pulmonary cytology sampling methods. Diagn Cytopathol. 2016;44(12):1010–23.
3. Layfield LJ, Roy-Chowdhuri S, Baloch Z, Ehya H, Geisinger K, Hsiao SJ, Lin O, Lindeman NI, Roh M, Schmitt F, Sidiropoulos N, VanderLaan PA. Utilization of ancillary studies in the cytologic diagnosis of respiratory lesions: the papanicolaou society of cytopathology consensus recommendations for respiratory cytology. Diagn Cytopathol. 2016;44(12):1000–9.
4. Michael CW, Faquin W, Jing X, Kaszuba F, Kazakov J, Moon E, Toloza E, Wu RI, Moreira AL. Committee II: guidelines for cyto-

logic sampling techniques of lung and mediastinal lymph nodes. Diagn Cytopathol. 2018;46(10):815–25.
5. Smith AR, Raso DS. Respiratory system. In: Herzberg AJ, Raso DS, Silverman JF, editors. Color atlas of normal cytology. London: Churchill Livingstone; 1999. p. 101.
6. Sheaff MT, Singh N. The respiratory tract. In: Sheaff MT, Singh N, editors. Cytopathology: an introduction. Berlin: Springer; 2012. p. 49–100.
7. Laucirica R, Ostrowski ML. Cytology of nonneoplastic occupational and environmental diseases of the lung and pleura. Arch Pathol Lab Med. 2007;131(11):1700–8.
8. Naylor B. The shedding of the mucosa of the bronchial tree in asthma. Thorax. 1962;17(1):69–72.
9. Martínez-Girón R, Pantanowitz L. Corpora amylacea in sputum smears: incidence and clinical significance. Cytopathology. 2021;32(1):108–14.

Digestive Tract (Oral Cavity, Esophagus, Stomach, Intestines, and Anus)

3

Judy Pang

Organs of the digestive tract function in the ingestion and digestion of food, absorption of useful products of digestion, and removal of the waste products. The digestive tract includes the oral cavity, esophagus, stomach, intestines, and anus. Direct sampling using a wooden spatula or brush can be performed on the oral cavity and anus. Otherwise, endoscopy is the primary means for obtaining gastrointestinal (GI) tract cytology specimens either via directed brushing or fine needle aspiration (FNA). Recognizing normal GI elements is helpful when dealing with GI contamination in the cytologic sampling of other organs. In countries where resources are limited, cytology is occasionally used to screen for malignancy [1–3].

Oral Cavity

Food is moistened and coated with mucous in the oral cavity, dispersed mechanically by the teeth, and exposed to the digestive enzymes of amylase and ptyalin within saliva. Traces of small molecules such as sugar and salt stimulate the taste buds of the tongue, leading to further secretion of saliva into the oral cavity and stimulation of gastric secretion (cephalic phase of digestion). The act of swallowing is under voluntary control, but the rest of the transfer of food through the pharynx and beyond is a reflex action [4].

Exfoliative cytology is an effective way to evaluate lesions of the oral cavity by using such techniques as brushings and scrapings [5, 6]. Fine needle aspiration biopsy can be utilized for deeper intraoral lesions. Keratinizing squamous mucosa lines the lips, hard palate, gingiva, and dorsal surface of the tongue while the remaining oral cavity, including the buccal mucosa, is lined by nonkeratinizing stratified squamous epithelium.

The predominant cells exfoliated are dependent on the site sampled. Anucleated squamous cells and superficial nucleated squamous cells with small pyknotic nuclei predominate when keratinizing mucosa is sampled, while intermediate squamous cells, which vary in size and shape, but typically have a diameter two to three times that of parabasal cells, predominate in sampling from nonkeratinized squamous mucosa (Fig. 3.1). Shed squamous cells are a normal component of saliva and they may thus be seen in sputum samples. Parabasal cells, with small round nuclei and high nuclear to cytoplasmic ratios, are typically absent and, when present, suggest an ulcer or excessive scraping. Nuclear enlargement can be seen in normal cells as well as in reactive cells. It may be possible to identify the sex chromatin body (Barr body). Respiratory type glandular cells, characterized by simple to pseudostratified columnar ciliated epithelium, can sometimes be sampled from the nasopharynx or salivary gland ducts. Some inflammatory cells and oral flora are usually present [5, 6].

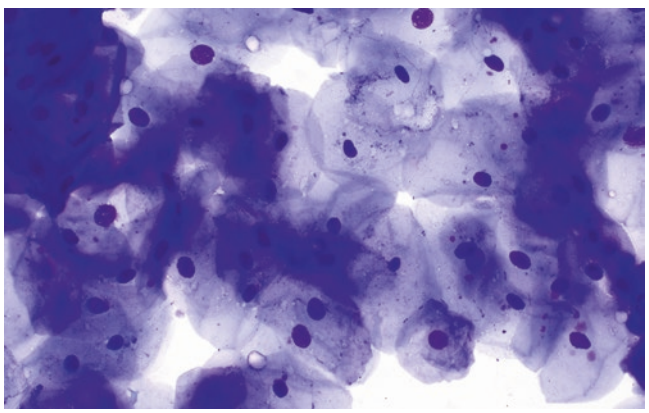

Fig. 3.1 Normal buccal squamous cells in a buccal scraping. Air-dried smear preparation, Diff-Quik, 40× magnification

J. Pang (✉)
Department of Pathology, University of Michigan–Ann Arbor, Ann Arbor, MI, USA
e-mail: jcpang@med.umich.edu

M. Lew et al. (eds.), *Normal Cytology*, https://doi.org/10.1007/978-3-031-20336-7_3

Esophagus

The esophagus is a fibromuscular tube that extends from the neck into the mediastinum. Its primary function is to convey food from the laryngeal pharynx to the cardiac region of the stomach. No enzymatic digestive actions occur. It is divided into the upper, middle, and lower thirds for clinical purposes. Most cytology samples are obtained by direct endoscopic brushings [4–7].

Almost the entire length of the esophagus is lined by nonkeratinizing stratified squamous epithelium (Fig. 3.2a). Brushing samples predominantly consist of intermediate squamous cells with abundant delicate cytoplasm and vesicular nuclei, and scattered superficial squamous cells with pyknotic nuclei that are arranged singly and in sheets (Fig. 3.2b). Keratohyaline granules and squamous pearls can sometimes be seen. The distal 1–2 cm of the esophagus is lined by simple columnar epithelium, with or without mucus production, and is continuous with the stomach. These glandular cells have uniform nuclei, mucinous cytoplasm, and are arranged in flat, honeycomb sheets (Fig. 3.2c) [5–7].

Submucosal mucous glands are rarely sampled by exfoliative cytology, but can be a pick-up contaminant when per-

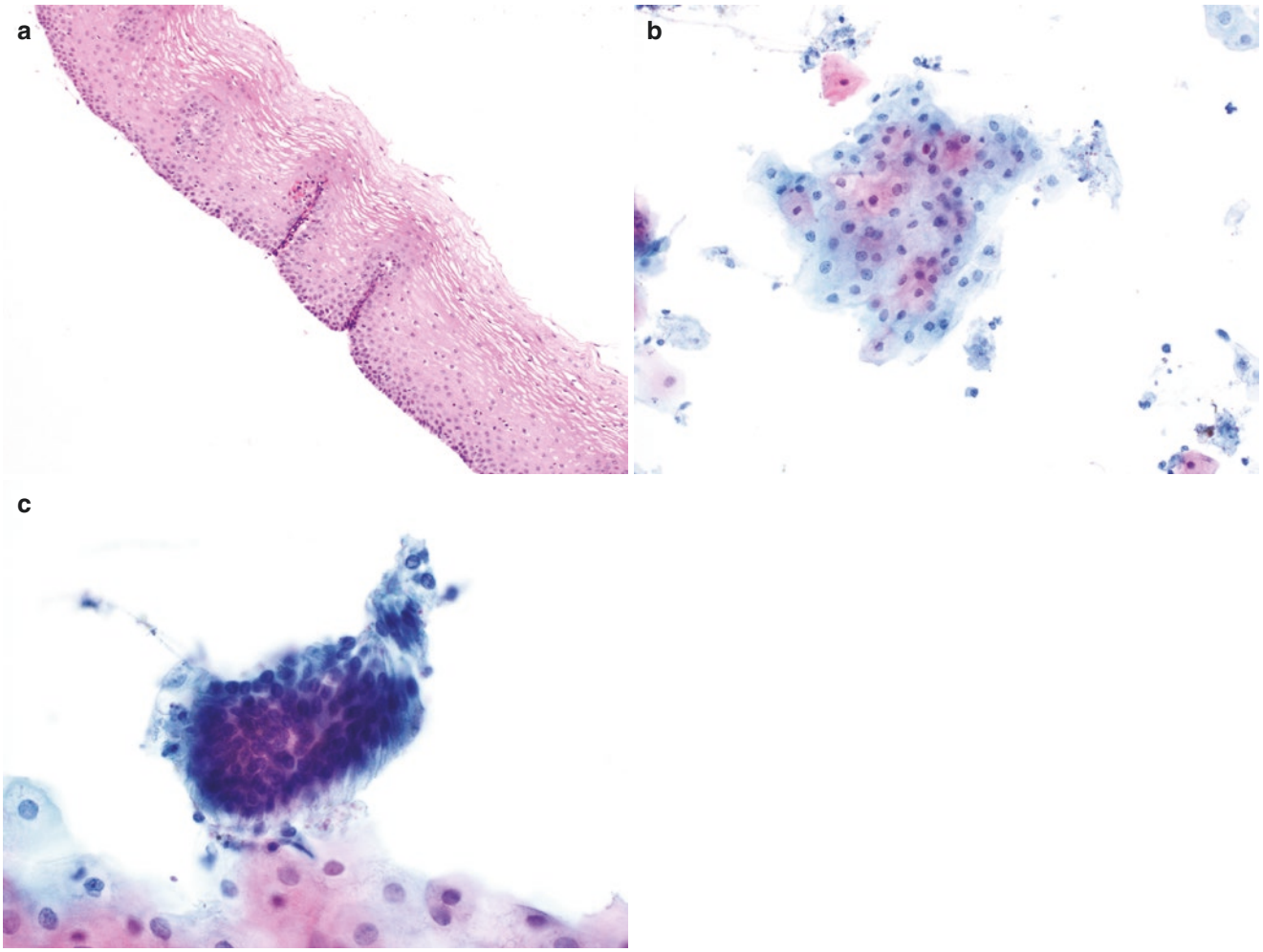

Fig. 3.2 (**a**) Almost the entire length of the esophagus is lined by nonkeratinizing stratified squamous epithelium. (**b**) Intermediate squamous cells with abundant delicate cytoplasm and vesicular nuclei predominate in cytology samples. (**c**) Glandular epithelium with uniform nuclei and mucinous cytoplasm lines the distal 1–2 cm of the esophagus and is continuous with the stomach. Esophagus biopsy, hematoxylin & eosin, 20× magnification (**a**). Esophageal brushing, ThinPrep preparation, 20× (**b**) and 40× (**c**) magnification

forming endoscopic ultrasound-guided procedures. Ciliated columnar cells may be encountered if the nearby respiratory tract was inadvertently traversed. Swallowed respiratory cells including alveolar macrophages can also be present. Bacteria such as Actinomyces, Candida, and inflammatory cells are all common oral contaminants but can also indicate esophageal infection. Food particles (animal and vegetable matter) can sometimes be seen [5–7].

The muscular externa consists of two muscle layers. In the upper third of the esophagus, only skeletal muscle is present, while in the lower third, only smooth muscle fibers are present. Ganglion cells from Auerbach's plexus are found in between the smooth muscle layers of the esophagus. The cervical and thoracic esophagus is surrounded by adventitia. Only the small portion within the abdominal cavity and connecting with the stomach is covered by serosa (peritoneum) [4–7]. Endoscopic ultrasound-guided fine needle aspirations of mediastinal lymph nodes are sometimes performed from within the esophagus, and any of the benign esophageal elements can accordingly be sampled and identified in cytology specimens as pick-up contaminants.

Stomach

Early stages of enzymatic digestion occur in the stomach, which lies between the esophagus and small intestine. It is divided into five regions, from proximal to distal: the cardia, fundus, body, antrum, and pylorus. Histologically, the stomach consists of a glandular mucosa, lamina propria, muscularis mucosa, muscularis propria, and serosa lined by peritoneum. Brushings and washings are rarely utilized for sampling. While evaluation of primary gastric lesions by cytology is unusual, recognizing normal gastric elements is important as they are commonly encountered in the aspirate specimens from submucosal lesions of the stomach or in transgastric sampling of other organs, such as the body and tail of the pancreas [4–7].

The surface epithelium is folded into mucosal glands, which are divided into superficial gastric pits and deeper gastric glands. The wide gastric pits extend from the lumen into the lamina propria. At the base of the gastric pits, the epithelium becomes gastric glands, which are narrower and extend down to the muscularis mucosae. The histology of the gastric mucosa corresponds to a large extent on the aforementioned gross divisions. However, the entire mucosal surface is lined by relatively monotonous tall, columnar cells characterized by small, basally located round to oval nuclei, smooth nuclear membranes, and abundant fine granular or vacuolated cytoplasmic mucin. A mucin pocket above the nucleus can be seen (Fig. 3.3a, b). En face, they form flat cohesive honeycomb-like sheets. Similar cells line the gastric pits which comprise the superficial portion of the mucosa and join the deeper glands. In the fundus and body, these mucus-secreting cells admix with parietal and chief cells (Fig. 3.3c). Since these mucus-secreting cells line the entire surface of the stomach and most of the gastric pits, they are usually the predominant cell type in gastric cytology specimens. Therefore, one cannot specify the portion of stomach mucosa sampled on morphology alone. Given the location of the chief and parietal cells in the deeper layers, they are not readily sampled by exfoliative cytology but may be sampled in fine needle aspirations (Fig. 3.3d, e). Chief cells look similar to acinar cells of the pancreas or salivary gland and contain zymogen granules (proenzymes of the gastric digestive enzymes papain, renin, and lipase). These small cuboidal cells have basophilic cytoplasmic granules and smooth round nuclei with fine chromatin. Parietal cells, in contrast, are large pyramidal or flask-shaped cells which typically have intensely eosinophilic cytoplasm, but can be pale and vacuolated. They have single nuclei with coarse chromatin and prominent nucleoli. Occasional binucleate forms can be seen. Parietal cells secrete intrinsic factor and hydrochloric acid. Endocrine cells are scattered throughout the glands. Endocrine cells present in the pyloric glands produce gastrin, which is released when food enters the stomach and stimulates the release of acid secretions of the main gastric gland. These cells are not readily identified on cytology [4–7].

The lamina propria is not a distinct continuous layer, but instead exists as thin strands of fibrous and smooth muscle elements between the glands. Meissner's neural plexus of the stomach submucosa is fairly prominent. The muscularis externa is distinct in the stomach. There is an additional innermost layer of obliquely oriented smooth muscle in the cardiac region. The middle layer of circularly oriented smooth muscle is thickened at the junction between the pylorus and duodenum forming the pyloric sphincter. A true serosa surrounds all regions of the stomach [4]. Endoscopic ultrasound-guided fine needle aspirations of the pancreas using a transgastric approach can result in the sampling of any of these normal elements in these deeper layers.

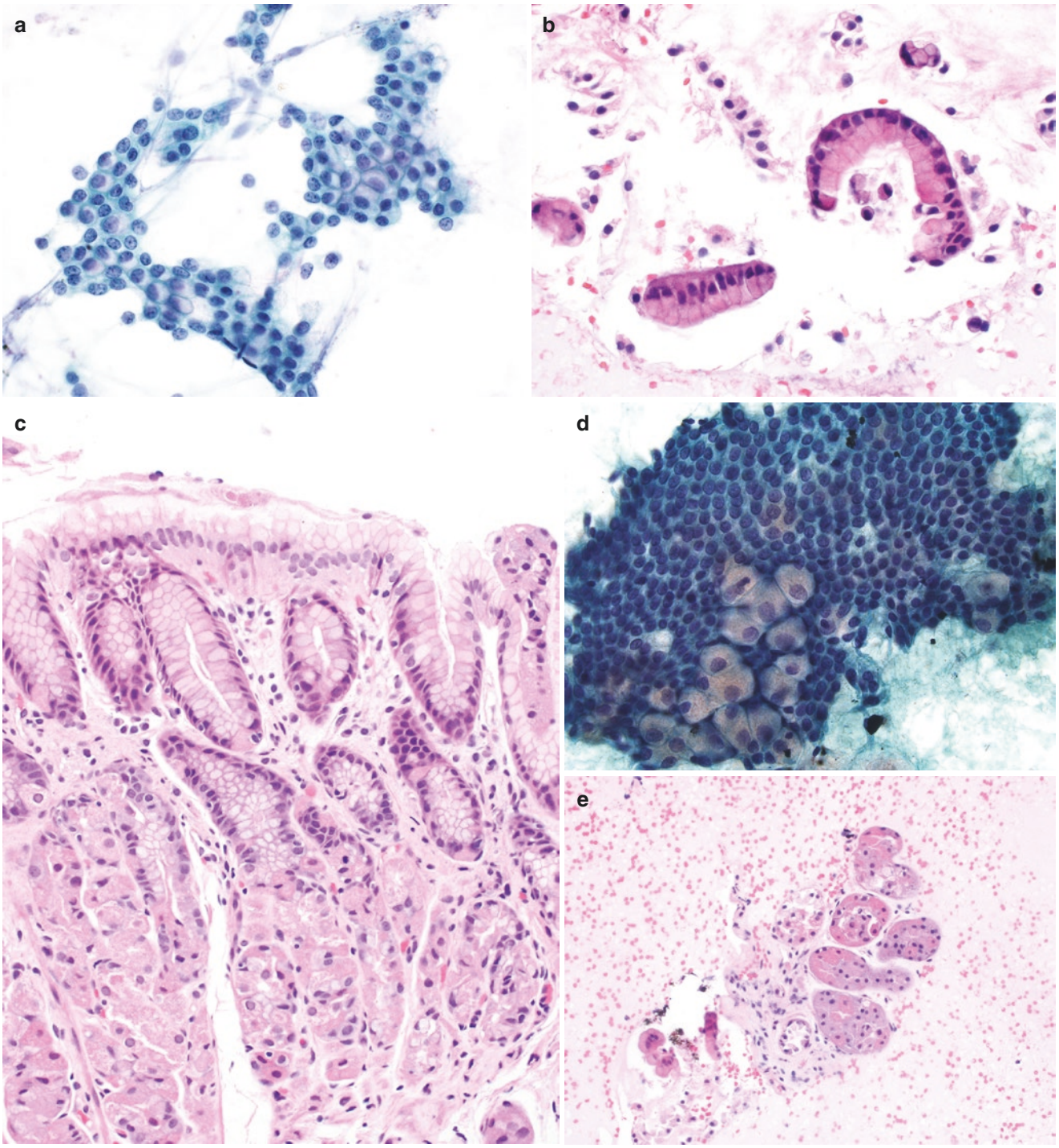

Fig. 3.3 (**a**) On cytologic examination, the mucus-secreting columnar cells form flat cohesive honeycomb sheets en face. (**b**) An apical mucin pocket above the basally located nucleus can be seen in these strips of gastric epithelium. (**c**) The mucosal surface is lined by mucus-secreting columnar cells, as shown in the upper half of this image (gastric pit). Gastric pits and glands are lined by similar cells admixed with parietal and chief cells, shown in the lower half of this image (neck and base). (**d**) Polygonal parietal cells with clear cytoplasm are shown within a flat sheet of mucus-secreting cells in a fine needle aspirate and (**e**) eosinophilic parietal cells and basophilic chief cells in a gastric washing can occasionally be encountered. Stomach, fine needle aspiration, alcohol-fixed smear preparation, Papanicolaou stain, 40× magnification (**a**, **d**), Cell block, hematoxylin & eosin, 40× magnification (**b**). Stomach biopsy, hematoxylin & eosin, 20× magnification (**c**). Gastric washing, Cell block, hematoxylin & eosin, 20× magnification (**e**). (**d** is reprinted with permission from the American Society of Clinical Pathology Press)

Small Intestine

Partially digested food (chyme) passes through the pyloric sphincter and into the small intestine. The components of the small intestine, from proximal to distal, are the duodenum, jejunum, and ileum. The small intestine also contains substances released from the liver and pancreas, as well as the gallbladder, via a combined duct which opens on the duodenal papilla, the ampulla of Vater. Most absorption occurs in the jejunum, but the absorption of vitamin B-12 occurs primarily in the distal ileum. Absorption of water and electrolytes, which begins in the small intestine, is completed in the large intestine [4].

Although the adult small intestine measures approximately 20 ft in length, only the proximal portion of the duodenum which contains the ampulla of Vater is sampled, to any extent, for cytologic examination. Endoscopy allows for access to the duodenum, but does not allow for easy access of the jejunum and ileum. In addition, endoscopic ultrasound-guided fine needle aspirations of the pancreas using a transduodenal approach can result in the sampling of benign elements of all layers of the duodenum [4–7].

Absorption of nutrients occurs in the small intestine, thus requiring specialized mucosa. To optimize absorption, the intestinal wall has a large surface area achieved by folding of the mucosal elements at three levels. The entire mucosa is thrown into deep folds called plicae circulares which run circumferentially beginning in the distal duodenum, reach a maximal size in the jejunum, begin to diminish in the ileum, and are essentially absent in the distal ileum. Superimposed on the plicae are smaller folds of epithelium and lamina propria called crypts (glands) and villi, respectively. Villi are projections into the lumen that cover the intestinal wall giving rise to its velvety texture on gross examination. In between the villi, the epithelium extends down into the mucosa in glands or intestinal crypts (crypts of Lieberkuhn) [4–7].

Throughout the small intestine, the mucosal epithelium is comprised of several cell types. Absorptive cells (enterocytes) are tall columnar cells with a microvillous border found primarily on the villi, but can extend into the crypts. Goblet cells are mucus-secreting cells that serve to coat the surface epithelium, protecting it from digestive juices without hindering absorption of nutrients (Fig. 3.4a). They are present in the villi and glands. On cytology, enterocytes are arranged in honeycomb-like sheets of tall, columnar cells characterized by basally oriented round to ovoid nuclei, small inconspicuous nucleoli, and fine granular or vacuolated cytoplasm. Occasionally, a striated border representing the highly regular microvilli on the absorptive cells can be seen. Interspersed between enterocytes are scattered pale goblet cells characterized by large cytoplasmic mucin vacuoles (Fig. 3.4b). Other cell types which are less likely to be seen in cytology samples are Paneth cells which are serous exocrine cells that secrete lysozyme, an enzyme that digests the cell walls of certain bacteria. Paneth cells are unique to the small intestine and are found at the base of the crypts. Morphologically, they are characterized by a basally oriented nucleus, basophilic cytoplasm, and apical secretory granules. Endocrine cells are also found in the small intestinal crypts and produce polypeptide hormones such as gastric inhibitory polypeptide (GIP), cholecystokinin (CCK), and secretin, which exert their effects on cells in the GI tract and pancreas. Immature cells are found in the base of the crypts.

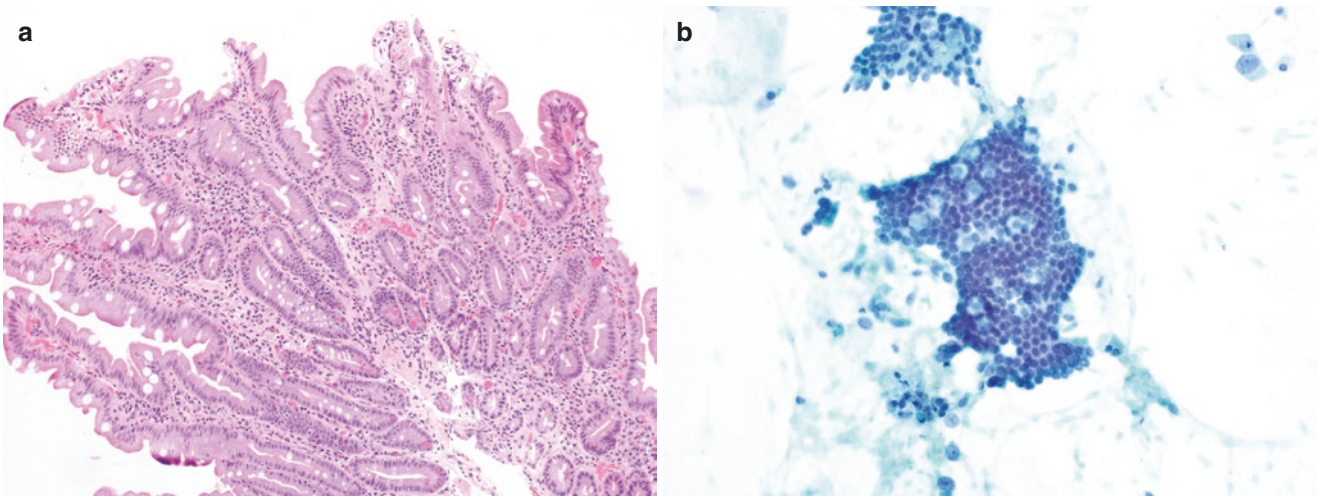

Fig. 3.4 (**a**) Duodenal villi comprised of absorptive enterocytes are shown having tall columnar shape and a microvillous border admixed with vacuolated goblet cells. (**b**) On cytology, enterocytes occur as honeycomb sheets of cells with interspersed pale goblet cells. Duodenum biopsy, hematoxylin & eosin, 10× magnification (**a**). Duodenum fine needle aspiration, alcohol-fixed smear preparation, Papanicolaou stain, 20× magnification (**b**)

These low columnar cells are thought to be precursors of the absorptive cells covering the villi. Intense mitotic activity is seen in these cells.

The cores of villi consist of a lamina propria which is comprised of loose connective tissue with a rich capillary network and large lymphatic vessels. Isolated lymphoid aggregates that form nodules are commonly found throughout the mucosa of the small intestine. Lymphocytes are commonly associated with M cells, microfold cells, which have folds, not microvilli, on their apical surfaces. M cells take macromolecules from the gut lumen and transport antigens to the intercellular space near lymphoid aggregates. These cells are not easily detected but can be more prevalent immediately above lymphoid aggregates in the ileum. Large lymphoid aggregates are common in the ileum and referred to as Peyer's patches. The muscularis mucosae does not protrude into the cores of the villi, but small slips of smooth muscle can be found in the lamina propria of the villi running perpendicular to the muscularis mucosa [4–7].

The submucosa of the duodenum contains the glands of Brunner (Fig. 3.5). They are branched and coiled tubular glands that penetrate the muscularis mucosae and connect with the bases of the crypts of Lieberkuhn. These cells are pale staining but do contain secretory granules. These glands are primarily located in the duodenal submucosa, but can occasionally be found in the distal pylorus and/or proximal jejunum.

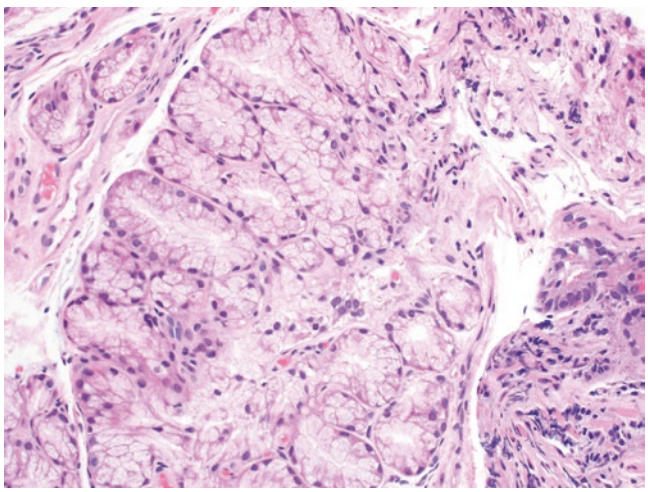

Fig. 3.5 Brunner glands in a duodenum biopsy with pale staining cytoplasm containing secretory granules, hematoxylin & eosin, 20× magnification

The muscularis externa is similar to that seen throughout the GI tract. Except for the portion of duodenum that is retroperitoneal, the small intestine is covered by true serosa which is continuous with the supporting mesentery.

Large Intestine

Food leaves the small intestine through the ileocecal valve and enters the large intestine which consists of the cecum, followed by the ascending, transverse, descending, and sigmoid colon and then finally the rectum and anal canal. No digestive enzymes are produced, but some degradative action continues in the watery chyme from the residual activity of the small intestinal enzymes as well as the putrefactive action of the bacteria that colonizes the large intestine. The large intestine is primarily responsible for the removal of fluid and temporary storage of waste material (feces) [4].

In contrast to the small intestine, the mucosa of the large intestine contains no villi. Instead, the mucosa has a smooth surface marked by deep crypts—straight, nonbranching test tube-like glands (glands of Lieberkuhn) (Fig. 3.6a). The epithelium is columnar, containing similar cell types as the small intestine: absorptive cells with short microvilli, goblet cells, immature cells, and a few endocrine cells. Turnover of the mucosal epithelium is rapid with most mitotic activity occurring in the middle third of the crypts. Cytology specimens from the colon are rare. The cells exfoliate in large, monolayered, cohesive, honeycomb-like sheets en face and palisade when seen from the side. Absorptive cells are tall and columnar with basal nuclei and apical cytoplasm. The nuclei are round and uniform with smooth membranes, fine chromatin, and inconspicuous nucleoli. They have granular cytoplasm with a prominent striated border, which appears as a terminal bar-like apical density. Goblet cells have pale cytoplasm with large mucin vacuoles. The background cells may include scattered neutro-

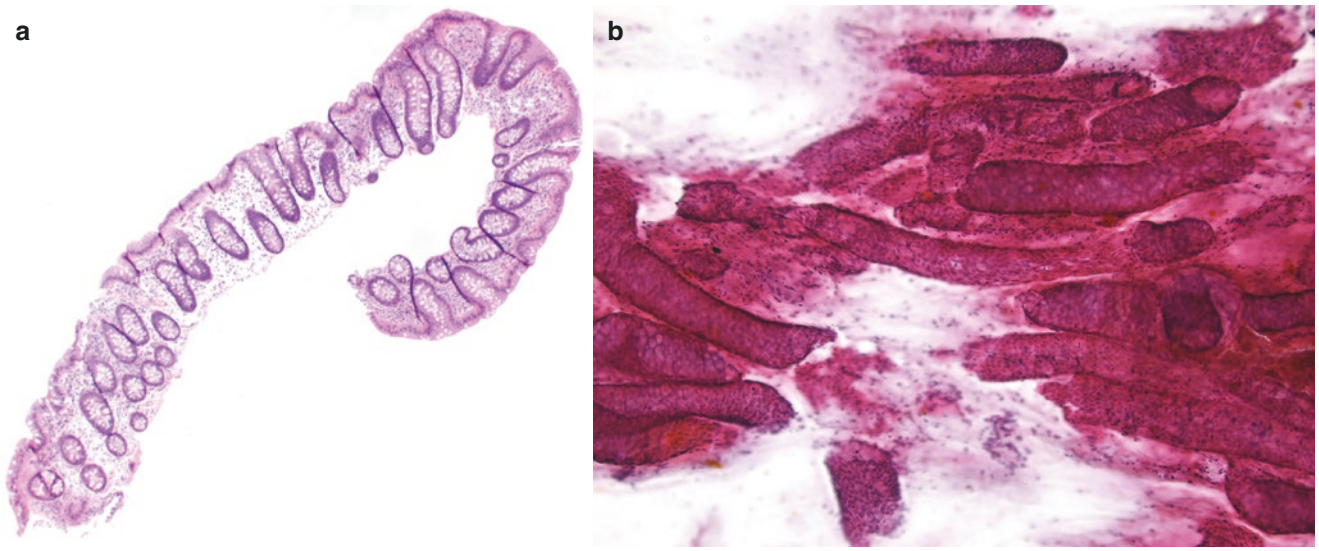

Fig. 3.6 (**a**) Mucosal epithelium with smooth surface marked by non-branching test tube like glands, (**b**) which can sometimes remain intact on fine needle aspirates. Colon biopsy, hematoxylin & eosin, 4× magnification (**a**). Colon fine needle aspiration, alcohol-fixed smear preparation, Papanicolaou stain, 10× magnification (**b**). (**b** is reprinted with permission from the American Society of Clinical Pathology Press)

phils, lymphocytes (which may be numerous), anal squamous cells, mucus, and undigested food and debris. Intact glands may sometimes be seen on fine needle aspirates (Fig. 3.6b) [4–7].

The lamina propria is similar to that of the small intestine with abundant lymphoid tissue presenting as nodules that may be sampled on fine needle aspirations. The muscularis mucosae is present in the cecum, colon, and rectum but disappears in the anal canal where the mucosa and submucosa are less well defined.

The inner circular layer of the muscularis externa is unremarkable, but the fibers of the external longitudinal layer from the cecum to the rectum are gathered into three bundles called the taenia coli. Most of the large intestine is surrounded by serosa. At the level of the rectum, the muscularis externa spreads out. The inner circumferential layer of smooth muscle fibers in the muscularis externa thickens in the anal canal to form the internal anal sphincter. Skeletal muscle from the pelvic floor envelops the anal canal forming the external anal sphincter.

Anus

At the level of the recto-anal junction, the crypts of Lieberkuhn end and an abrupt transition of the columnar glandular mucosa to nonkeratinizing stratified squamous mucosa occur. This mucosa is continuous with the distal epidermis (keratinized stratified squamous epithelium). Exfoliative samples are readily obtained from the anal canal and typically evaluated for squamous dysplasia and malignancy, similar to the cervical cancer screening.

Histologically, at the anorectal junction, colonic type glandular epithelium transitions to a keratinized or nonkeratinized squamous epithelium. This is the transformation zone that may be sampled in an anal pap test. Anucleate squamous cells are typically present and may be numerous on cytologic specimens as the lining of the lower anal canal is keratinized. Parakeratotic cells are also common. The presence of rectal glandular cells or squamous metaplastic cells confirms sampling of the transformation zone. Rectal glandular cells are seen as orderly sheets of uniform columnar cells (Fig. 3.7a, b) [4–7].

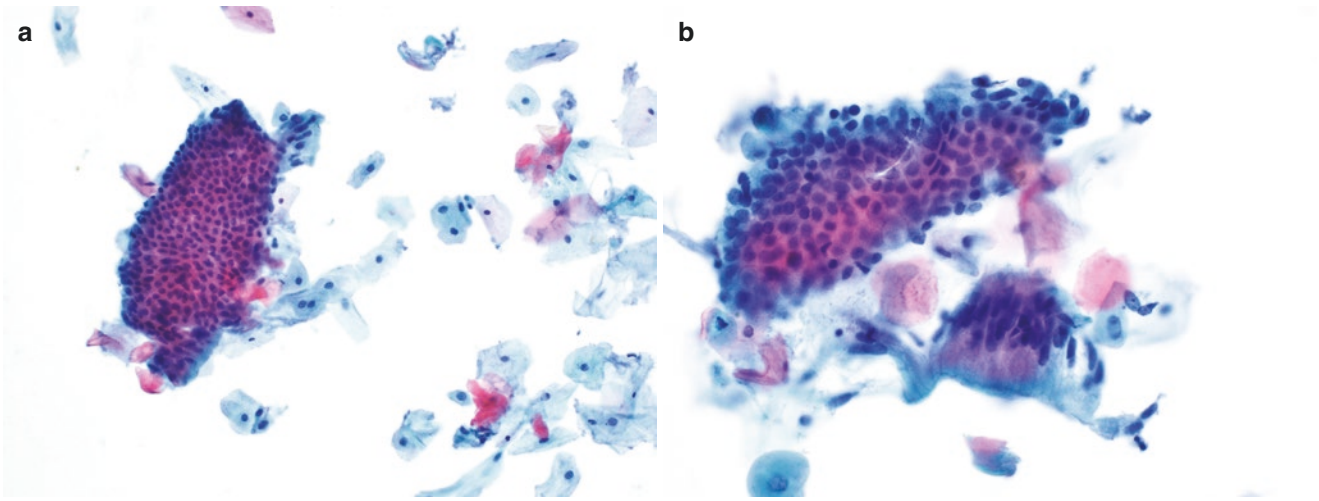

Fig. 3.7 (**a**, **b**) Anal pap test showing orderly sheets of uniform columnar cells and squamous cells. ThinPrep preparation, 20× (**a**) and 40× (**b**) magnification

References

1. Conrad R, Castelino-Prabhu S, Cobb C, Raza A. Role of cytopathology in the diagnosis and management of gastrointestinal tract cancers. J Gastrointest Oncol. 2012;3(3):285–98.
2. Karmarkar P, Wilkinson A, Manohar T, Joshi A, Mahore S. Diagnostic utility of endoscopic brush cytology in the upper gastrointestinal lesions and its correlation with biopsy. IOSR JDMS. 2013;5:32–6.
3. Tyagi R, Kaur J, Kaur G, et al. Cytohistological discordance on gastrointestinal brushings: facts unfolded. Miger Med J. 2016;57(5):299–302.
4. Silverthorn DU. Chapter 21. The digestive system. In: Silverthorn DU, et al., editors. Human physiology: an integrated approach. 7th ed. San Francisco, CA: Pearson; 2016. p. 655–92.
5. DeMay RM. Chapter 3. Fluids. In: DeMay RM, editor. The art & science of cytopathology. Exfoliative cytology. 2nd ed. Chicago, IL: American Society for Clinical Pathology Press; 2012. p. 268–89, 338–341. (Volume 1 of 4).
6. Wang HH, Ayata G. Chapter 7. Gastrointestinal tract. In: Cibas ES, Ducatman BS, editors. Cytology diagnostic principles and clinical correlates. 4th ed. Philadelphia, PA: Saunders, Elsevier; 2014. p. 197–216.
7. Bergman S, Geisinger KR. Chapter 14. Alimentary tract (esophagus, stomach, small intestine, colon, rectum, anus, biliary tract). In: Bibbo M, Wilbur D, editors. Comprehensive cytopathology. 3rd ed. Philadelphia, PA: Saunders, Elsevier; 2008. p. 373–401.

Hepatobiliary System

4

Madelyn Lew

Liver

The liver is a red-brown wedge-shaped organ that consists of a right, left, caudate, and quadrate lobe. It is located in the right upper quadrant of the abdomen, just inferior to the right diaphragm. Apart from a small area where the liver contacts the diaphragm, the liver is covered by a peritoneal surface. In normal adults, the liver often weighs between 600 and 1860 g [1, 2]. It functions in life sustaining processes such as fat, carbohydrate, and protein metabolism, glycogen storage, and the detoxification of various drugs, toxins, and metabolic waste products. Most of the liver volume consists of its cellular functional unit in which the aforementioned processes take place—the hepatocyte. On histologic evaluation, hepatocytes are polyhedral cells characterized by an abundant amount of eosinophilic cytoplasm. Their nuclei are centrally placed, round, and have smooth nuclear contours. Multinucleation, particularly binucleation, is a common morphologic finding among hepatocytes.

Cytoplasmic pigment granules such as lipofuscin or bile can be seen in normal liver histology (Fig. 4.1). Lipofuscin presents as fine light brown granules on hematoxylin & eosin-stained slides while bile presents as coarser yellow-brown to dark brown granules. Additionally, the cytoplasm in a hepatocyte can be clear rather than eosinophilic, depending on the degree of glycogen and/or fat accumulation within the cell. Glycogen accumulation confers a delicately foamy texture to the cytoplasm and can also result in clear, intranuclear vacuoles. Accumulation of lipids within hepatocytes results in small to large clear cytoplasmic vacuoles. The proportion of hepatocytes with these lipid droplets will increase with toxic-metabolic injuries that cause steatosis (Fig. 4.2). However, steatosis can be featured in benign liver lesions, such as focal nodular hyperplasia and hepatic adenomas.

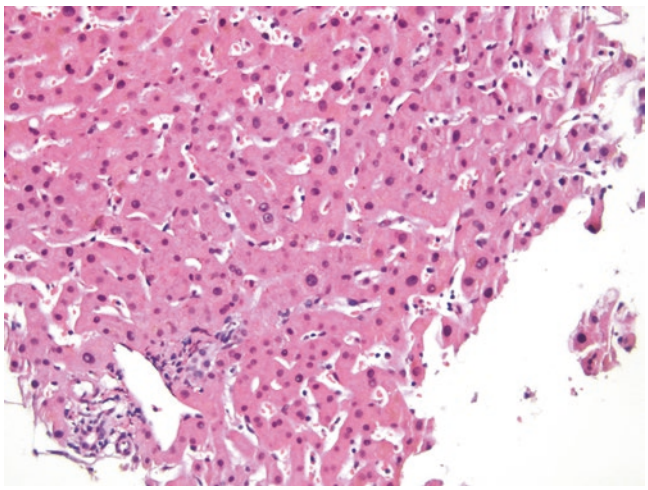

Fig. 4.1 Hepatocytes arranged in cords with mild to moderate anisonucleosis, separated by thin sinusoids. Scattered hepatocytes display cytoplasmic vacuolization and pigment granules. Liver resection, hematoxylin & eosin, 20× magnification

Hepatocytes are arranged as thin plates that are bordered by vascular sinusoids. In adults, these plates are typically one cell in thickness. However, foci of normal and regenerating hepatic parenchyma can also show plates that are two cells thick. The proximity of the hepatocytes with sinusoidal blood allows for absorption and secretion of nutrients and cellular products. The major blood vessels that supply and drain the liver are the hepatic artery and portal vein, respectively, which enter or leave the liver with the common hepatic duct through the porta hepatis, a deep transverse fissure located in the inferomedial portion of the right lobe. The branches of these three structures make up the hallmark histologic feature of the liver—the portal tract (Fig. 4.2).

The role of fine needle aspiration (FNA) in the evaluation of liver lesions has long been a source of debate, especially as imaging modalities have become more adept at diagnosing liver lesions, particularly in cases of hepatocellular carcinoma [3, 4]. In many institutions, core needle biopsies are more frequently utilized to evaluate primary liver lesions due to the

M. Lew (✉)
Department of Pathology, University of Michigan, Ann Arbor, MI, USA
e-mail: lewm@med.umich.edu

M. Lew et al. (eds.), *Normal Cytology*, https://doi.org/10.1007/978-3-031-20336-7_4

consistent acquisition of adequate material and enhanced ability to evaluate architecture of hepatocellular lesions, particularly with respect to hepatic trabeculae. Additionally, on cytologic preparations, there is significant morphologic overlap of hepatic lesions that range from benign to malignant, such as regenerative nodules, dysplastic nodules, focal nodular hyperplasia, hepatocellular adenoma, and hepatocellular carcinoma, limiting the utility of FNA for primary liver lesions. In each of these lesions, cytologic preparations often contain bland appearing polygonal hepatocytes with centrally placed round to oval nuclei, smooth to focally irregular nuclear contours, granular chromatin distribution, and moderate to abundant amounts of granular cytoplasm (Fig. 4.3a, b). The appearance of nucleoli within hepatocytes can be highly variable, ranging from inconspicuous to small and distinct or prominent. In addition to multinucleation and prominent nucleoli, normal hepatocytes can also display significant anisonucleosis (Fig. 4.4). The presence of larger nuclei within hepatocytes indicates polyploidy, which is seen with increasing frequency as a person ages. Although the nuclei in these cells are enlarged, the nuclear to cytoplasmic ratio is often maintained and mitotic figures are rare.

As previously mentioned, intracytoplasmic granules can also be seen in variable conditions in benign liver, including lipofuscin, bile, and, occasionally, hemosiderin. Lipofuscin, associated with normal aging of a cell, is commonly seen as fine to coarse granules that are golden-yellow on Papanicolaou stain and green-brown on Diff-Quik (Fig. 4.5). Meanwhile, bile is associated with cholestatic states and presents as dark green-black granules on both Diff-Quik and Papanicolaou

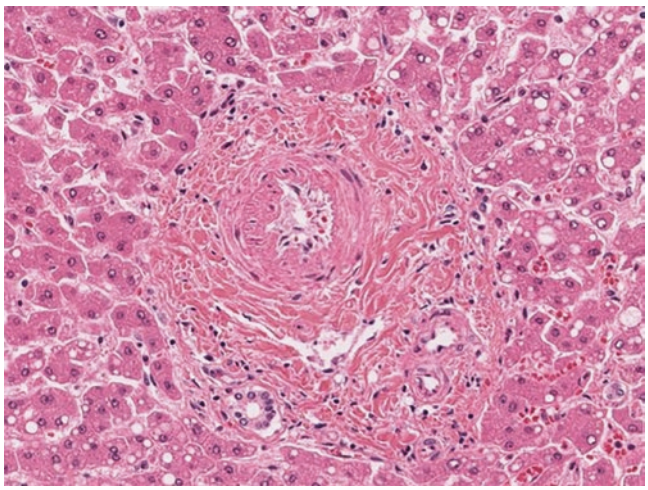

Fig. 4.2 Liver parenchyma highlighting a portal tract (center). Background hepatocytes show steatosis. Liver resection, hematoxylin & eosin, 20× magnification

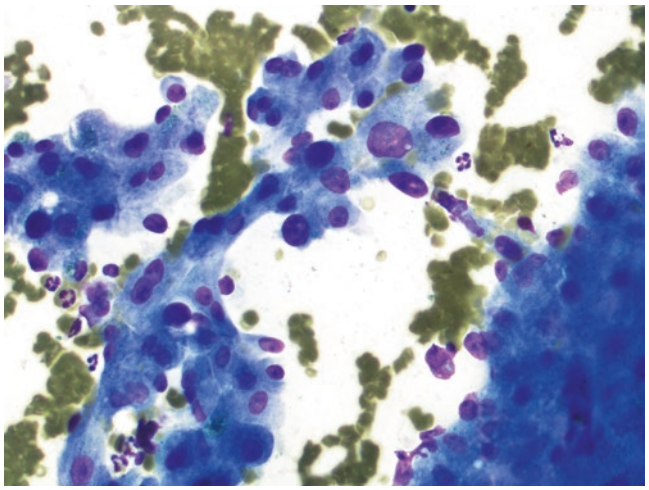

Fig. 4.4 Notable anisonucleosis and prominent nucleoli present in benign hepatocytes. Air-dried smear preparation, Diff-Quik, 40× magnification

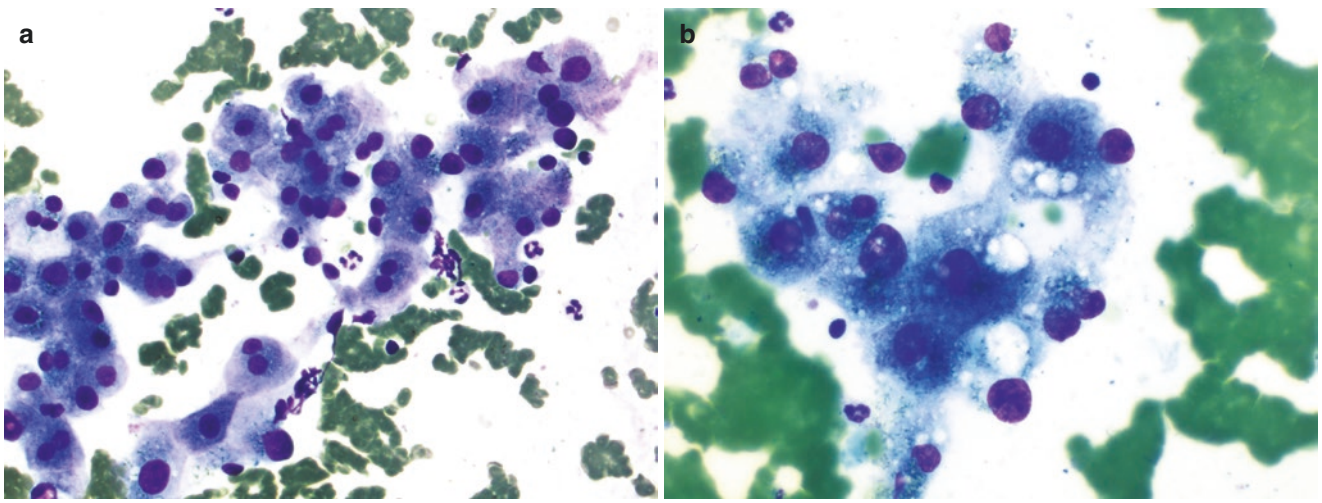

Fig. 4.3 (**a**, **b**) Polygonal hepatocytes on smear preparations with round, smooth nuclear contours and abundant granular cytoplasm with variable vacuolization and intracellular bile (dark, green) pigment. Air-dried smear preparation, Diff-Quik, 20× (**a**) and 40× (**b**) magnification

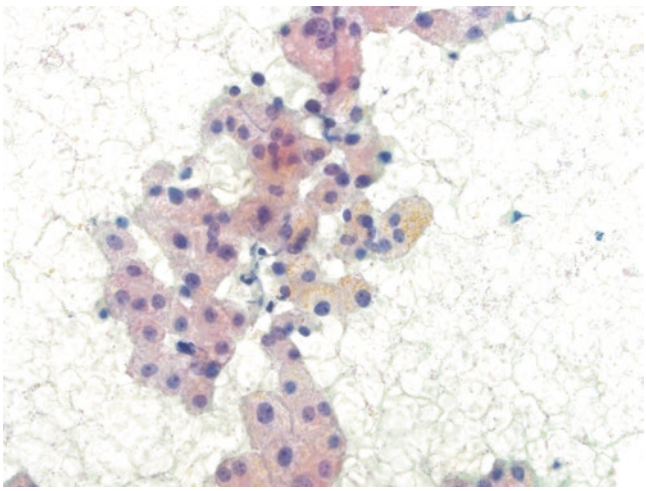

Fig. 4.5 Sheets of hepatocytes with anisonucleosis, binucleation, distinct nucleoli, and yellow-tan cytoplasmic granules, consistent with lipofuscin. Alcohol-fixed smear preparation, Papanicolaou stain, 20× magnification. (Reprinted with permission from [5])

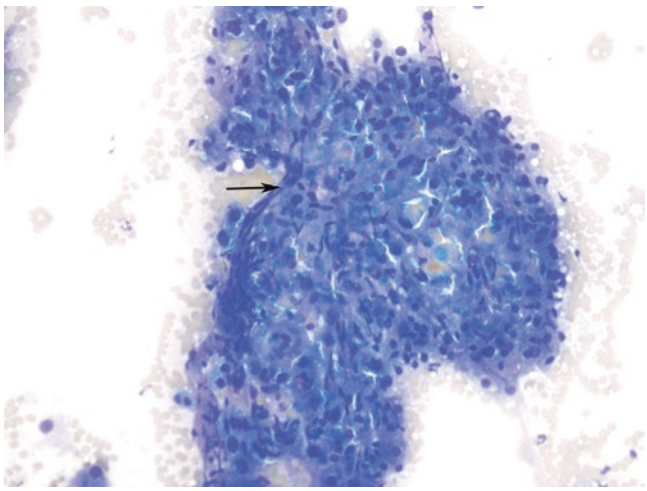

Fig. 4.6 Coursing blood vessel (arrow) through an aggregate of bland hepatocytes. Air-dried smear preparation, Diff-Quik, 20× magnification

stains (Fig. 4.3b). Hemosiderin can be dark brown or blue (more frequently in Diff-Quik staining protocols). Although hemosiderin can be commonly found in the neonatal liver, there is normally only a small amount seen in adult livers. Increased hemosiderin deposition in the liver is associated with chronic bleeding or, if in large quantities, metabolic disorders such as hemochromatosis.

Hepatocytes can be arranged in a variety of architectural patterns on cytologic preparations, including crowded cell clusters, ribbons or trabeculae (up to two hepatocytes in width/thickness), large sheets or aggregates, as well as single cells. Scattered hepatocytes with stripped cytoplasm (naked nuclei) can also be seen in the background of normal liver aspirate specimens, frequently due to poor cellular fixation. In some aspirate preparations, sinusoidal endothelial cells may occasionally be identified coursing through aggregates of hepatocytes (Fig. 4.6).

Given the degree of morphologic overlap of hepatic lesions, accurate assessment of primary liver lesions on morphologic evaluation alone is impractical on cytologic specimens. However, special stains and immunohistochemistry may be applied to cell block material to further delineate the nature of sampled hepatic lesions on cytology. In normal histology, hepatocytes are often arranged in thin plates that are one cell thick in adults (and two cells in thickness in children less than 5 years of age). In cell block material with fragments of liver parenchyma, a reticulin special stain can accentuate the sample's hepatic framework and highlight findings concerning for hepatocellular carcinoma, such as widened cords of hepatocytes or loss of reticulin. However, it is important to note that benign conditions, such as steatohepatitis and steatotic hepatocellular adenomas, can also show loss of reticulin staining, which can affect diagnostic interpretation and reliability of this stain on limited cellular samples [6]. Immunohistochemistry for CD34 may be helpful in showcasing aberrant sinusoidal endothelialization seen in hepatocellular carcinoma. However, of note, other benign hepatic lesions such as focal nodular hyperplasia and hepatic adenomas may also show similar findings [7].

In the evaluation of liver aspirates, there are non-liver-derived elements that can also be seen, depending on the needle approach for sampling. In CT or ultrasound-guided fine needle aspiration, mesothelial cells seen in sheets with variable degrees of nuclear crowding and nuclear contour variation may be seen, which, if not appropriately identified, may raise a concern for a neoplastic process. In aspirates obtained by endoscopic ultrasound as well as in biliary brushings, gastrointestinal contamination may be seen with variable degrees of crowding and nuclear changes depending on concurrent reactive changes in the gastrointestinal tract. In the same vein, mucin, as a component of gastrointestinal contamination, may also be identified in liver aspirates. On the other hand, liver parenchyma can also be identified as a potential contaminant when inadvertently sampled during the targeting of lesions in the right lower lobe of the lung as well as retroperitoneal organs such as the pancreas, right kidney, and right adrenal gland for fine needle aspiration.

Biliary Ducts

Biliary epithelium is the predominant feature in biliary brushing specimens, but is also seen in the background of liver aspirate specimens, where they are differentiated from hepatocytes by their smaller cell size and less abundant cytoplasm. On histologic evaluation, bile ducts are lined by a layer of bland cuboidal epithelial cells. On cytologic evaluation, biliary ductal cells are characterized by basally oriented round nuclei, smooth nuclear contours, even granular chromatin distribution, typically inconspicuous nucleoli, and small to moderately abundant amounts of luminal granular cytoplasm (Fig. 4.7a, b). These ductal epithelial cells appear in "honeycomb" arrangements in which the cells form flat, cohesive sheets with evenly spaced nuclei. In cytologic preparations, the amount of cytoplasm within biliary ductal epithelial cells may appear variable based on cell orientation. As such, cross sections through the short axis of the ductal cells will have less discernible cytoplasm than those seen through the long axis (Fig. 4.8a). While not consistently seen in biliary duct cytology specimens, bile pigment featured as background, yellow to green-yellow granular aggregates, can be seen in biliary stent specimens and brushings (Fig. 4.8b).

While the nuclei of normal biliary ductal cells are frequently bland, there can be a variable amount of nuclear enlargement, slightly coarse chromatin distribution, and distinct nucleoli identified in benign, reactive conditions (Fig. 4.9).

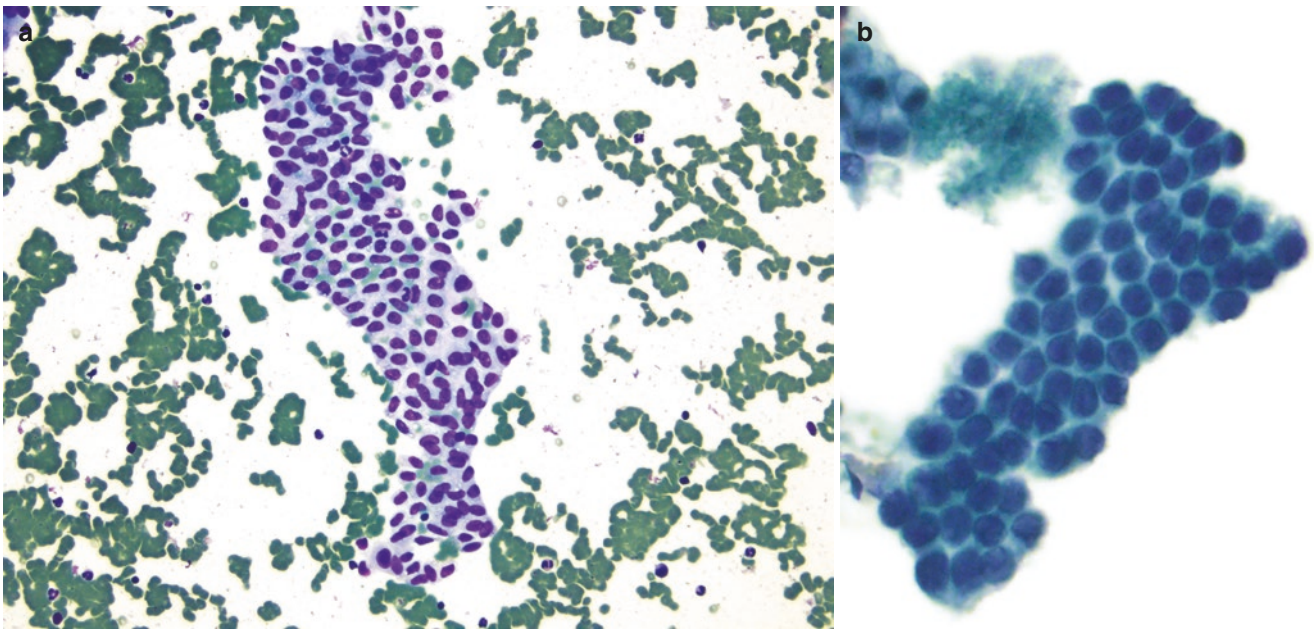

Fig. 4.7 (**a**, **b**) Bile duct epithelial cells arranged in flat sheets. Nuclei are round to ovoid with smooth to slightly irregular nuclear contours. Small to moderately abundant amounts of granular cytoplasm is present. Bile duct brushing, air-dried smear preparation, Diff-Quik, 20× magnification (**a**). Bile duct brushing, ThinPrep preparation, 20× magnification (**b**)

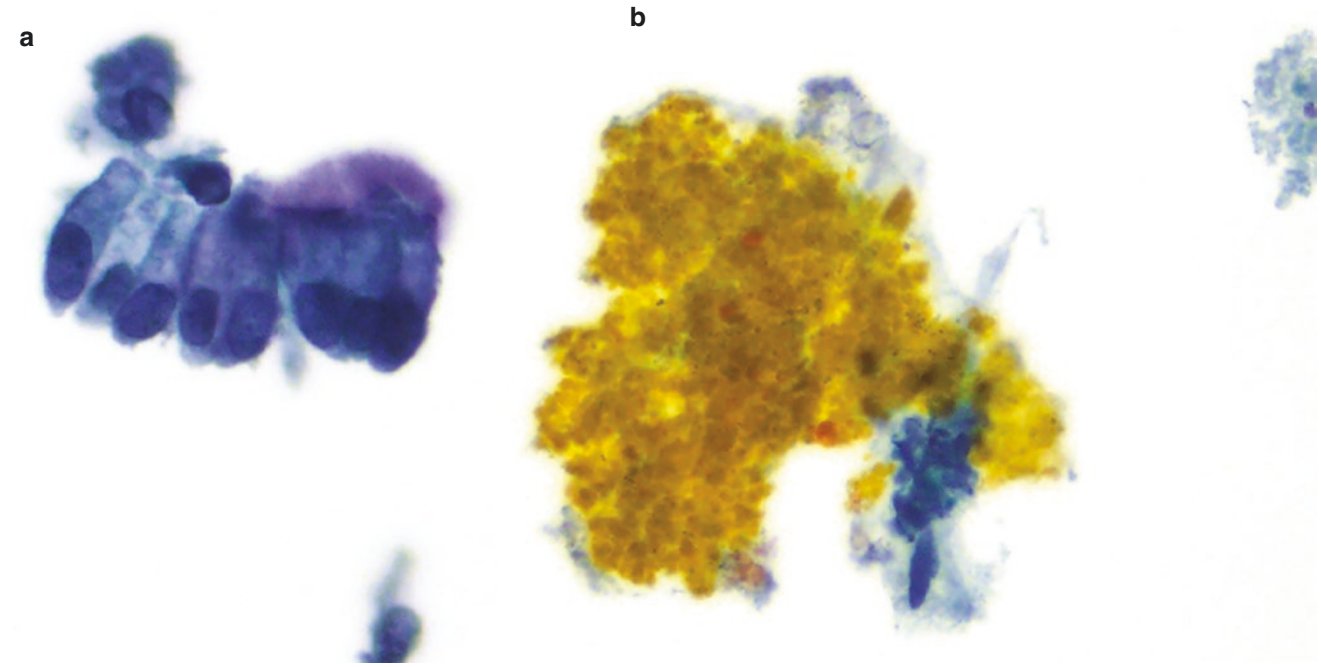

Fig. 4.8 (**a**, **b**) Biliary ductal cells oriented longitudinally show basally oriented nuclei and a more abundant amount of delicately granular cytoplasm in the apical aspect of the cells. Extracellular, amorphous granular yellow aggregates of bile can be seen in the background. Bile duct brushing, ThinPrep preparation, 20× magnification (**a**, **b**)

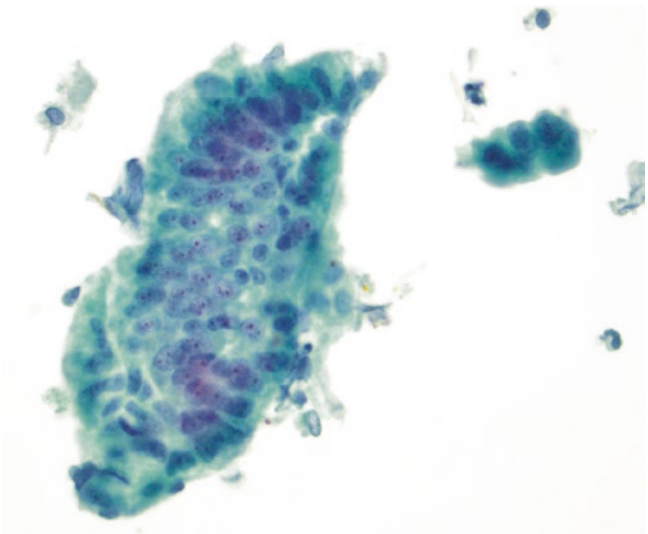

Fig. 4.9 Normal biliary ductal cells show mild nuclear enlargement, slightly coarse chromatin distribution, and distinct nucleoli. However, polarity and even spacing between cells ("honeycomb" arrangement) are maintained. Bile duct brushing, ThinPrep preparation, 40× magnification

Gallbladder

The gallbladder is a pear-shaped organ that is located in the posteroinferior aspect of the right lobe of the liver. The large central body tapers to a thin neck, ultimately connecting to the extrahepatic biliary ducts via the cystic duct. It functions predominantly to concentrate, store, and release bile mediated by neural and humoral mechanisms between and after food intake. The mucosa of the gallbladder is lined by a single layer of columnar epithelial cells typically characterized by basally oriented ovoid nuclei with smooth nuclear contours, even granular chromatin distribution, inconspicuous nucleoli, and moderate to abundant amounts of delicate cytoplasm. The epithelium can be thrown into small folds in the gall bladder's contracted state, and can also be seen in outpouchings delving into the lamina propria or muscularis propria of the gall bladder (Rokitansky-Aschoff sinuses) (Fig. 4.10). At the gallbladder neck, branched mucous glands can be identified in which cuboidal cells with basally oriented nuclei and abundant amounts of clear to basophilic cytoplasm are identified. Rarely, endocrine cells can also be identified in the gallbladder neck, but are frequently absent in normal histologic evaluation [8]. The epithelium overlies lamina propria, smooth muscle, subserosa, and serosa.

Evaluation of the gallbladder by FNA and biopsy is relatively uncommon due to its relatively deep-seated position within the body, making endoscopic access for sampling difficult. This is compounded by the concern of causing biliary peritonitis during sampling. As such, there is limited literature available focusing on the evaluation of gallbladder lesions as well as normal gallbladder cytology. However, some institutions may perform percutaneous ultrasound-guided FNA of gallbladder lesions [9, 10] and have reported

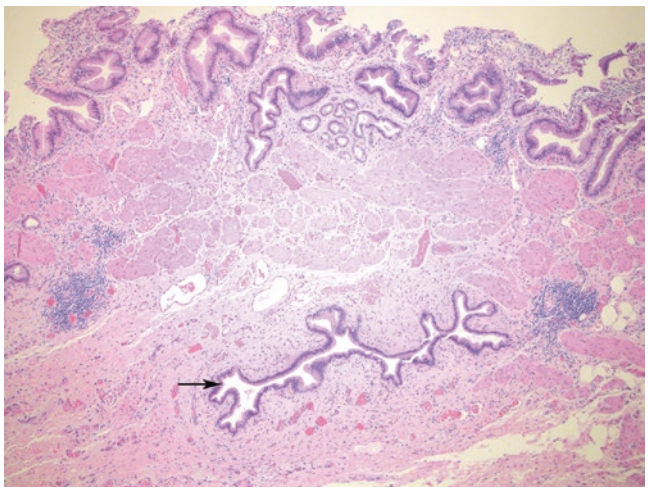

Fig. 4.10 Gallbladder mucosa lined by a single layer of columnar cells with basal nuclei, smooth nuclear contours, inconspicuous nucleoli, and abundant amounts of delicate cytoplasm. Rokitansky-Aschoff sinuses (arrow) can be seen as invaginations of epithelium through the muscularis propria of the gallbladder. Gallbladder resection, hematoxylin & eosin, 5× magnification

their findings which mainly focus on the concordance of FNA and surgical resection specimens of the gallbladder as well as the morphologic features of xanthogranulomatous cholecystitis, abscess, tubercular cholecystitis, and malignant lesions on cytologic preparations. Recent studies have also highlighted the features associated with benign gallbladder epithelium, characterized by uniform epithelial cells with round nuclei, smooth nuclear contours, even granular chromatin distribution, and moderately abundant amounts of granular cytoplasm arranged in flat sheets in the background of bile pigment [11] (Fig. 4.11a, b). Although benign gallbladder epithelial cells are mostly arranged in organized, well-spaced sheets, there can be variable nuclear crowding, mild anisonucleosis, and multinucleation, particularly in inflammatory states, which may make definitive characterization of the nature of the epithelial cells difficult (Fig. 4.12a, b).

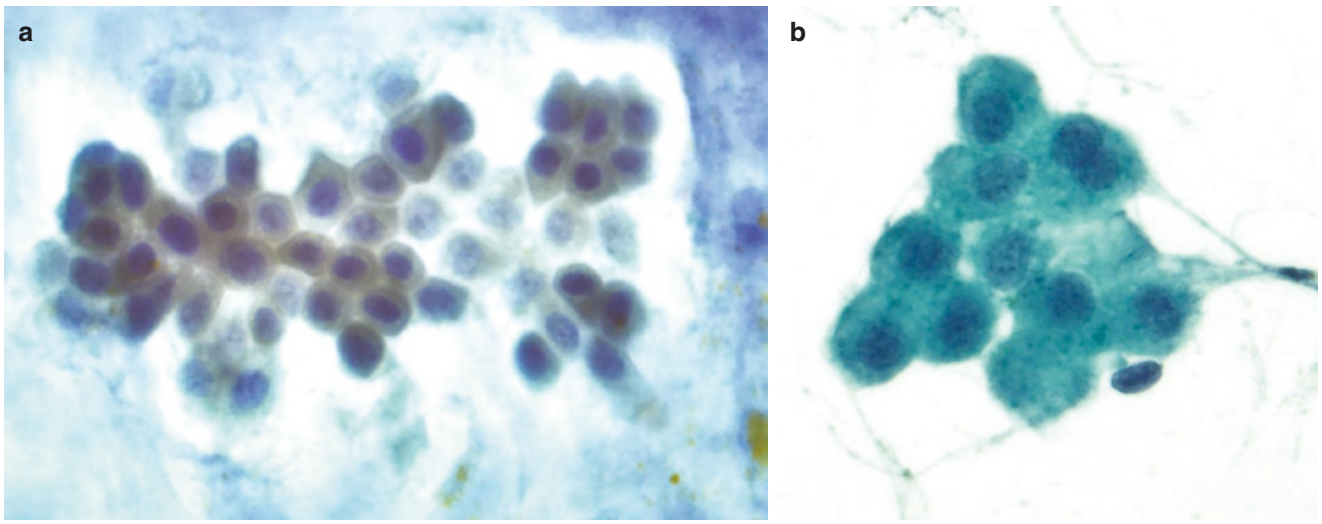

Fig. 4.11 (**a**, **b**) Gallbladder epithelial cells are designated by round nuclei, smooth nuclear contours, even granular chromatin distribution, and moderately abundant amounts of cytoplasm arranged in flat sheets. In some aspirates, extracellular yellow bile pigment may be evident, as in (**a**). Alcohol-fixed smear preparations, Papanicolaou stain, 20× (**a**) and 40× (**b**) magnification

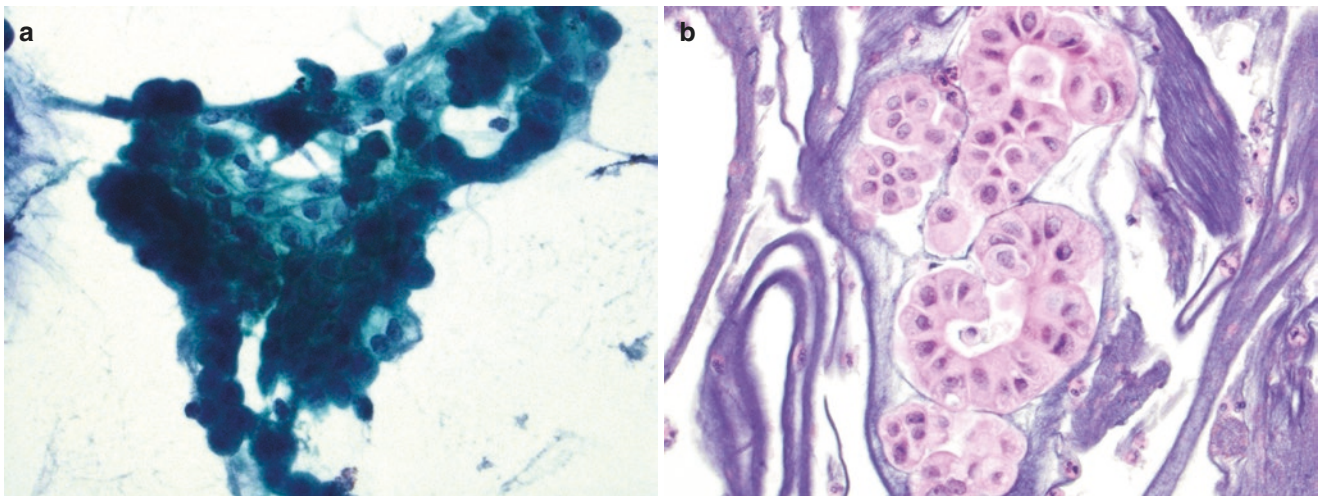

Fig. 4.12 (**a**, **b**) The range of normal to reactive gallbladder epithelial cells can show slightly irregular nuclear contours, coarse chromatin distribution, distinct nucleoli, and variable degrees of nuclear size variation. Alcohol-fixed smear preparation, Papanicolaou stain, 40× magnification (**a**). Cell block, hematoxylin & eosin, 40× magnification (**b**)

References

1. Molina KD, DiMaio VJM. Normal organ weights in men. Am J Forensic Med Pathol. 2012;33(4):368–72.
2. Molina KD, DiMaio VJM. Normal organ weights in women. Am J Forensic Med Pathol. 2015;36(3):182–7.
3. Bruix J, Sherman M. Management of hepatocellular carcinoma. Hepatology. 2005;42(3):1208–36.
4. Wang P, Meng AQ, Chen Z, et al. Diagnostic value and complications of fine needle aspiration for primary liver cancer and its influence on the treatment outcome: a study based on 3011 patients in China. Eur J Surg Oncol. 2008;34(5):541–6.
5. Lew M, Hissong EM, Westerhoff MA, Lamps LW. Optimizing small liver biopsy specimens: a combined cytopathology and surgical pathology perspective. J Am Soc Cytopathol. 2020;9(5):405–21.
6. Singhi AD, Jain D, Kakar S, Wu TT, Yeh MM, Torbsenson M. Reticulin loss in benign fatty liver: an important diagnostic pitfall when considering a diagnosis of hepatocellular carcinoma. Am J Surg Pathol. 2012;36(5):710–5.
7. Wee A. Diagnostic utility of immunohistochemistry in hepatocellular carcinoma, its variants and their mimics. Appl Immunohistochem Mol Morphol. 2016;14(3):266–72.
8. Yamamoto M, Nakajo S, Tahara E. Endocrine cells and lysozyme immunoreactivity in the gallbladder. Arch Pathol Lab Med. 1986;110(3):920–7.
9. Rana C, Krishnani N, Kumari N. Ultrasound-guided fine needle aspiration cytology of gallbladder lesions: a study of 596 cases. Cytopathology. 2016;27(6):398–406.
10. Yadav R, Jain D, Mathur SR, Sharma A, Iyer VK. Gallbladder carcinoma: an attempt of WHO histological classification on fine needle aspiration material. Cytojournal. 2013;10:12.
11. Chandra S, Chandra H, Shukla SK, Sahu S. Fine-needle aspiration cytology of gallbladder with an attempt of cytomorphological classification. Cytojournal. 2019;16:1.

Exocrine Glands (Salivary Gland and Pancreas)

5

Madelyn Lew and Judy Pang

Salivary Glands

The major salivary glands—parotid, submandibular, and sublingual glands—are paired exocrine glands that produce saliva, which is released into the upper aerodigestive tract to moisten mucous membranes, maintain the bacterial flora of the oral cavity, and facilitate digestion of food substances. The major salivary glands can be subclassified not only by their location but also by the quality of the saliva they produce—serous, mucous, or seromucous.

The parotid glands are located in the mandibular rami, anterior and inferior to each ear. As the largest salivary gland, the average size and weight of each parotid is approximately 5.8 cm and 14 g [1], but can weigh up to 28 g. The parotid gland secretions exit through parotid ducts which open on to the mucous membranes of the oral cavity's lateral aspects, typically adjacent to the maxillary second molar. The parotid gland is encapsulated by a fibroadipose capsule and divided into a superficial and deep lobe by the facial nerve. Its functional unit, the acinus, is predominantly composed of serous cells which are characterized by basally oriented and round nuclei, smooth nuclear contours, inconspicuous to small nucleoli, and an abundant amount of densely granular cytoplasm arranged in small nests (Fig. 5.1). The cytoplasm characteristically contains numerous basophilic zymogen granules that contain amylase to begin digestion of starch products. The granules also contribute to initiation of protein digestion with other enzymes like trypsin and chymotrypsin-like proteases, peptidases, and nonspecific bacterial lysozymes [2–4]. Occasional mucous cells that produce the sialomucins of saliva may be present, but are not typically easily identified on histology. Underlying the acinar cells are myoepithelial cells, which aid in emptying acinar cell contents into the central lumen via contraction. The luminal contents of the acinus then empty into an intercalated duct,

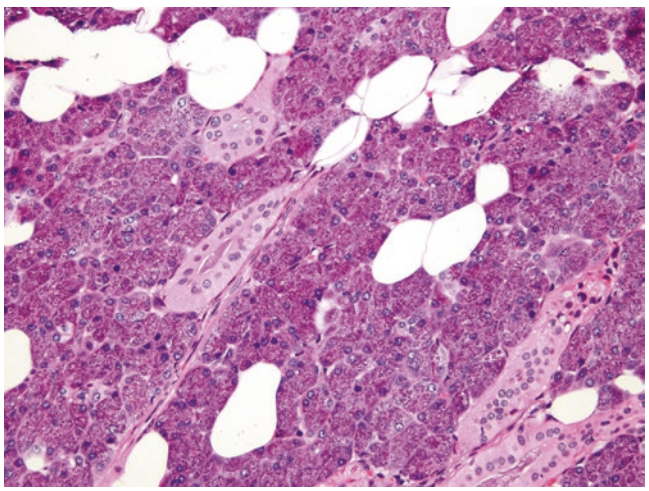

Fig. 5.1 Parotid gland parenchyma composed predominantly of serous acinar units admixed with adipose tissue. Serous acinar cells show basally oriented nuclei with smooth nuclear contours, variably distinct and small nucleoli, and characteristically abundant amounts of basophilic cytoplasmic granules. Striated ducts, lined by pale columnar cells, can be identified traversing through the lobules of acini. Note the scattered admixed adipocytes. Parotid gland resection, hematoxylin & eosin, 20× magnification

which is lined by low cuboidal epithelial cells that lie superficial to the myoepithelial cells. In the parotid, intercalated ducts can be seen traversing through the lobules of acinar cells, eventually becoming striated ducts which are lined by taller, columnar cells and are frequently more evident on histologic sections (Fig. 5.1). As the striated ducts extend into the connective tissue of the parotid septa, they join to form interlobular ducts which are lined by columnar, pseudostratified epithelial cells. Scattered goblet-type cells are intermixed with these columnar cells. These interlobular ducts ultimately join the principal duct through which salivary contents empty into the oropharynx. While the principal duct is largely lined by pseudostratified columnar epithelial cells which may be ciliated, the portion proximal to its oral cavity opening is lined by stratified squamous epithelium. Nests of sebaceous cells characterized by abundant amounts of bub-

M. Lew (✉) · J. Pang
Department of Pathology, University of Michigan, Ann Arbor, MI, USA
e-mail: lewm@med.umich.edu; jcpang@med.umich.edu

M. Lew et al. (eds.), *Normal Cytology*, https://doi.org/10.1007/978-3-031-20336-7_5

bly to vacuolated cytoplasm may be seen within the parotid gland. While these foci may be representative of sebaceous differentiation within the parotid, their function is unclear. Small lymph nodes can also be identified in the superficial aspect of the parotid gland. The medullary portion of these lymph nodes may contain salivary ducts and acini. As a person ages, ductal cells and, less commonly, acinar cells, can undergo oncocytic change characterized by an acquisition of abundant amounts of densely granular, eosinophilic cytoplasm due to an increased cellular proportion of mitochondria. While this occurs more frequently in the parotid gland, it can be observed in other salivary glands as well.

The submandibular glands underlie the floor of the mouth, just above the digastric muscles and typically weigh approximately 15 g each [5]. Each submandibular gland is subdivided into a larger, superficial lobe and a smaller, deeper lobe by the mylohyoid muscle. The secretions from these glands exit through the sublingual caruncles, just lateral to the lingual frenulum. In the submandibular gland, the acini and ductal network are similar to that of the parotid with some key differences. While the functional unit of the submandibular cells is still the acinus, unlike the parotid, there is an easily identified mixture of both serous and mucous cells within the acini (Fig. 5.2a). In histologic sections, the intensely granular serous cells are admixed with mucous cells characterized by abundant clear to lightly eosinophilic cytoplasm and small, round to indented nuclei. While the components of the ductal network (intercalated, striated, interlobular, and principal) in the submandibular gland are the same as those mentioned in the parotid gland, the submandibular gland striated ducts are shorter and may be less easily discernible in histologic sections than those in the parotid gland. In addition to oncocytic metaplastic change, other forms of metaplasia (e.g., mucinous, squamous) can also occur (Fig. 5.2b).

The sublingual glands are the smallest of the three major salivary glands and typically weigh approximately 3 g each [6]. They are located under the tongue, just anterior and superior to the submandibular glands. The secretions of the sublingual glands exit a network of excretory ducts. The largest of the excretory ducts, the sublingual duct of Bartholin, joins with the main submandibular duct to drain into the same exit point in the oral cavity. The general components of acini and ducts seen in the other major salivary glands also apply to the sublingual glands. However, in the sublingual gland, acini are composed predominantly of mucous cells and both the intercalated and striated ducts are significantly shorter and almost indiscernible on histologic evaluation.

Around 800–1000 minor salivary glands are present throughout the oral cavity submucosa, lips, tongue, soft and hard palate, and in the floor of the mouth [7]. In contrast to the aforementioned major salivary glands, the minor salivary glands are small, typically measuring 1–2 mm in greatest dimension, and are unencapsulated. The low number of acini in these small glands are predominantly mucous in nature and serve to moisten the mucous membranes of the oral cavity through saliva released into excretory ducts of their own or common excretory ducts shared with other salivary glands.

Fine needle aspiration (FNA) is a commonly utilized cost-efficient tool in the evaluation of salivary gland lesions, as it has a low complication rate with high diagnostic accuracy in differentiating between non-neoplastic

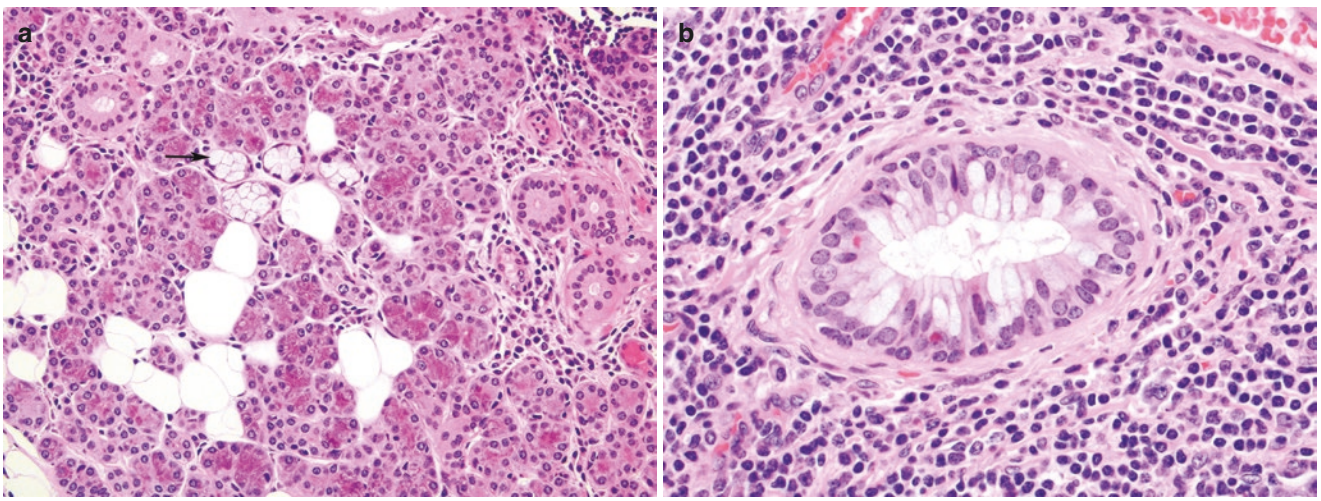

Fig. 5.2 (**a**) Submandibular gland histology showing a mixture of serous and mucous type acini. While the serous acinar cells have characteristically abundant amounts of basophilic cytoplasmic granules, mucous type acinar cells (black arrow) display clear cytoplasm that indents basally oriented nuclei. Adipose tissue and ducts are also seen interspersed in the submandibular gland parenchyma. (**b**) In reactive conditions, metaplastic changes can be seen in ductal cells, such as the featured mucinous metaplasia. Note the presence of periductal chronic inflammation. Submandibular gland resection, hematoxylin & eosin, 20× (**a**) and 40× (**b**) magnification

and neoplastic lesions, as well as between benign and malignant neoplasms [8–10]. While definitive subclassification of salivary gland tumors may be difficult on cytologic assessment alone, the aforementioned utility of salivary gland FNA can help guide appropriate patient management into conservative or surgical approaches, and if surgery is indicated, can also help in surgical planning. Given these treatment implications, it is important to differentiate normal salivary gland elements from neoplastic cells. In this regard, clinical and radiologic correlation is of utmost importance in the interpretation of a salivary gland FNA that yields only normal elements. While these elements may indeed reflect sampling of a prominent normal salivary gland, sialadenosis, or hamartoma, if there is clinical or radiologic evidence of a distinct salivary gland mass or cyst, a FNA specimen containing only normal salivary gland elements should be considered nondiagnostic.

Salivary gland elements such as acini, ducts, lymphoid tissue, and fibroadipose tissue may be observed in cytologic preparations of normal salivary glands. Acinar cells are frequently observed in spherical clusters that confer a "bunch of grapes" appearance, especially when attached to ductal cells (Fig. 5.3a). Serous acinar cells are characterized by an abundant amount of cytoplasm containing granules that range in color from pink to blue-purple on Papanicolaou and Diff-Quik stained preparations, respectively (Fig. 5.3b, c). Their nuclei can be centrally or eccentrically placed with granular chromatin distribution. While nucleoli are often indistinct, acinar cells can sometimes have small nucleoli. Mucous acinar cells have an abundant amount of vacuolated cytoplasm, but in contrast to serous acinar cells, are characterized by cytoplasm with a more clear, delicate quality that lacks cytoplasmic granules (Fig. 5.3d). Mucous acinar cells also have more eccentrically placed nuclei that can be indented by the cell's mucinous cytoplasmic contents.

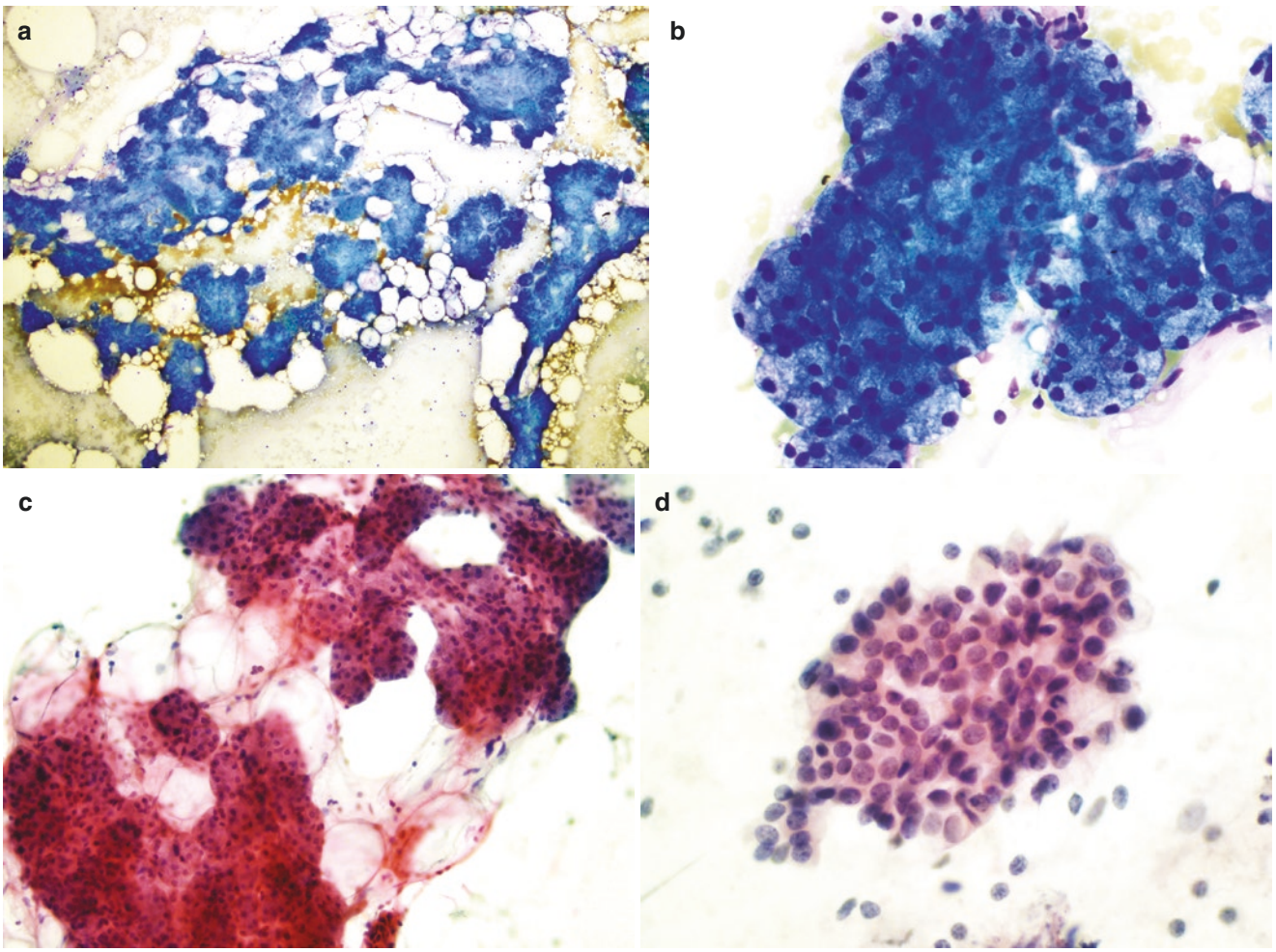

Fig. 5.3 (**a**) Normal salivary gland acini in this parotid gland aspirate are arranged in grape-like clusters admixed with adipose tissue. (**b**, **c**) Serous acinar cells in the parotid are characterized by abundant granular cytoplasm and centrally to basally oriented, round nuclei. (**d**) Mucous acinar cells in this FNA from the submandibular gland are characterized by an abundant amount of clear to delicately vacuolated cytoplasm with basally oriented round nuclei. Parotid gland, air-dried smear preparation, Diff-Quik, 5× (**a**) and 40× (**b**) magnification. Parotid gland, alcohol-fixed smear preparation, Papanicolaou stain, 20× magnification (**c**). Submandibular gland, alcohol-fixed smear preparation, Papanicolaou stain, 60× magnification (**d**)

FNA samples from normal salivary gland are usually limited in cellularity. Given the predominance of acinar cells in normal salivary glands, they are likely to be the most common normal element identified on cytologic evaluation. However, scattered groups of ductal cells can also sometimes be identified. Ductal cells can have a variety of appearances ranging from low cuboidal, to columnar, or ciliated. Regardless, normal ductal cells will display bland nuclear features with round nuclei, smooth nuclear contours, granular chromatin distribution, and indistinct to small nucleoli. The amount of cytoplasm will vary with the portion of the duct sampled, and they may have a high nuclear:cytoplasmic ratio when they resemble basaloid-type cells. Ductal cells are arranged in flat, well-organized sheets with limited nuclear overlap (Fig. 5.4a, b). Myoepithelial cells are usually hard to identify and appear as small dark nuclei superimposed within clusters. Normal ductal cells can undergo various forms of reactive change including mucinous, squamous, and frequently oncocytic metaplasia. Oncocytes are characterized by round to pyramidal cells with an abundant amount of densely granular cytoplasm (Fig. 5.4c, d). While oncocytes arranged singly or in small clusters can be difficult to differentiate from dispersed acinar cells on smear preparations, cell block material can highlight the basophilic granules of acinar cells and the more uniformly dense eosinophilic cytoplasm of oncocytes. Special stains may also be applied to cell block material to further differentiate between cell types as Periodic acid-Schiff with diastase (PASD) and phosphotungstic acid hematoxylin (PTAH) will highlight acinar cells and oncocytes, respectively. Sebaceous cells are infrequently seen, and when present they have multiple small cytoplasmic vacuoles and small bland, round nuclei.

In salivary gland cytology, the aforementioned metaplastic changes in acinar or ductal cells resulting in mucinous, squamous, or oncocytic features can lead to misinterpretation as sampling from neoplastic tissue such

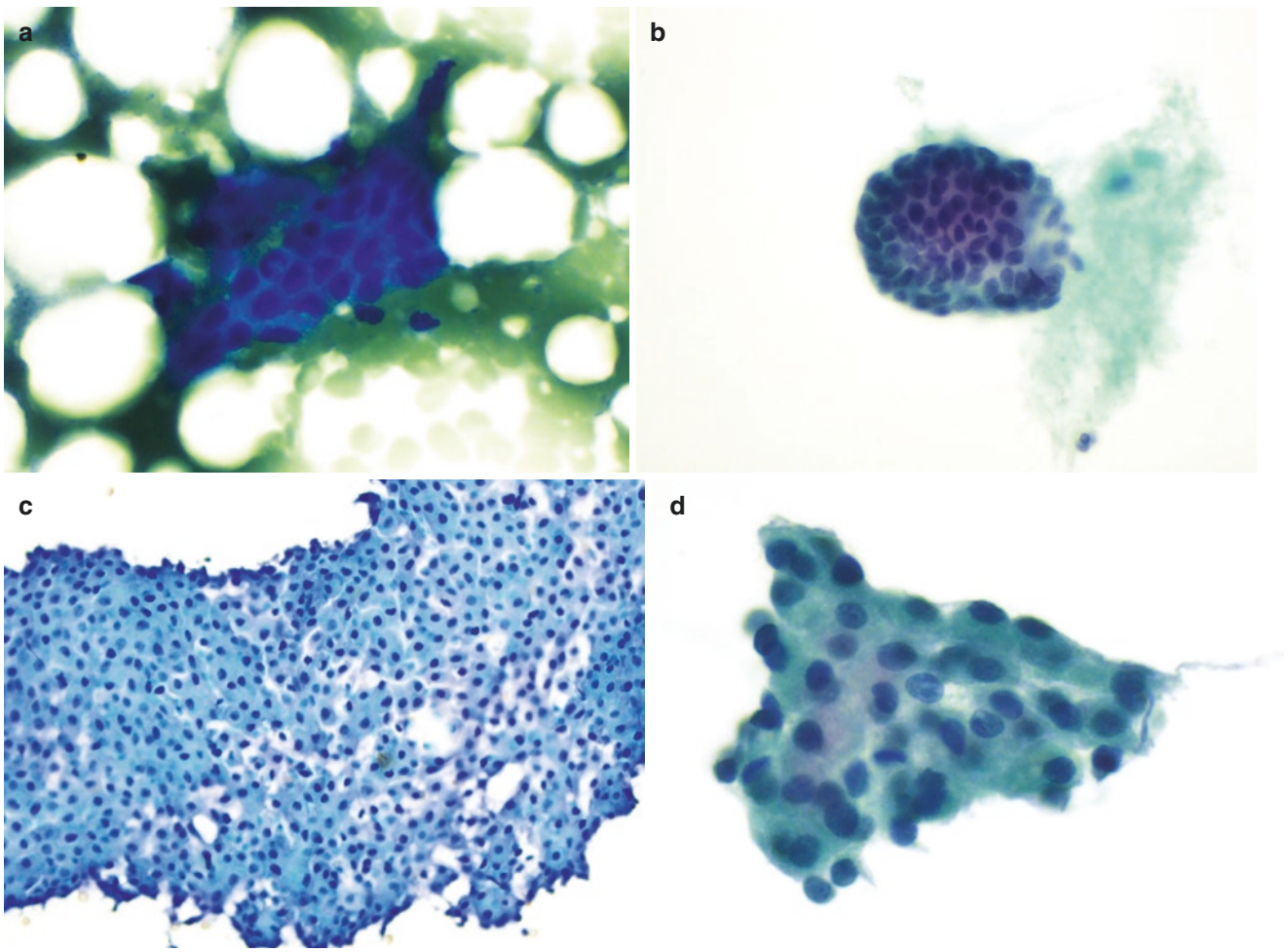

Fig. 5.4 (**a**, **b**) Small sheets of ductal cells are shown that display uniform nuclei with bland nuclear features, even chromatin distribution without visible nucleoli, and scant cytoplasm. (**c**, **d**) Oncocytic metaplasia of ductal cells is shown and is characterized by more densely granular cytoplasm that contains bland, uniform, central, round to ovoid nuclei. Parotid gland, air-dried smear preparation, Diff-Quik, 20× (**c**) and 60× (**a**) magnification. Parotid gland, alcohol-fixed smear preparation, Papanicolaou stain, 60× (**b**, **d**) magnification

as that of a low-grade mucoepidermoid carcinoma. As such, the presence of these cell types in low quantity on cytologic samples, particularly without a mucinous or necrotic background, should be interpreted with caution. While bland acinar cells are typically arranged in tight spherules and "bunch of grapes" configurations, normal architecture can be artifactually disrupted by specimen preparation and/or processing. Aggressive sample preparation could result in a dispersed distribution of acinar cells, mimicking acinic cell carcinoma. In such cases, the presence of other acini with a normal grape-like architectural pattern in other portions of the specimen as well as other normal elements, such as benign ductal cells and adipose tissue, may be helpful in ameliorating concerns. Additionally, acinic cell carcinoma cells often display prominent nucleoli, which may further help discern neoplastic from normal salivary gland acini.

Pancreas

The pancreas is composed of exocrine (acini and ducts) and endocrine (islet cells of Langerhans) tissue arranged in lobules separated by connective tissue septa. The pancreas weighs about 100 g and is 14–20 cm long. There are four anatomic areas: head, neck, body, and tail. The pancreas is enveloped by peritoneum on its anterior surface and connective tissue on its posterior surface. The pancreatic head is the thickest portion of the gland and situated in the C-shaped second portion of the duodenum. The uncinate process extends inferiorly and posteriorly from the head of the pancreas to pass behind the neck and is firmly attached to the third and fourth portions of the duodenum. The neck of the pancreas lies adjacent to the gastric pylorus and is the point at which the gland is surgically transected in a pancreatic head resection (pancreaticoduodenectomy, i.e., Whipple). The antrum of the stomach rests on top of the pancreatic body, which has contact with the left adrenal gland and left kidney. The tail of the pancreas is tapered and flat and is closely related to the hilum of the spleen [11]. FNA is often utilized to obtain tissue during the evaluation of pancreatic lesions including cysts and masses. This is typically performed via endoscopic ultrasound guidance (EUS), but can occasionally be performed percutaneously via computed tomography (CT) or ultrasound guidance. Understanding the anatomy is important as "pick-up" contaminants in fine needle aspirations may occur and are important to recognize and to not misinterpret them as lesional tissue. For example, duodenal epithelium is commonly encountered in EUS-FNA of the pancreatic head and uncinate while gastric epithelium may be seen in sampling the body and tail. In percutaneous interventional guided FNA, hepatocytes and mesothelial cells are potential contaminants.

The exocrine components of the pancreas comprise more than 85% of the pancreatic mass and secrete approximately 1 L of alkaline fluid a day containing digestive enzymes. Acinar cells comprise the vast majority of the exocrine pancreas and produce the proenzymes used to digest food. Through a process called exocytosis, where the membranes of the zymogen granule and cell surface fuse, the proenzymes are released into the acinar lumen where they are transported by the ductal system to the duodenum. In the duodenum, enteropeptidase (enterokinase) converts the inactive proenzyme trypsinogen to active enzyme trypsin, which then catalyzes the cleavage of the other pancreatic proenzymes to their active forms [11–13].

In cytology samples, acinar cells are arranged in small round groups, tubular structures, and anastomosing loops that bud from ductules (Fig. 5.5a). Acinar cells are polygonal with round, basally located nuclei. The perinuclear cytoplasm is basophilic due to the high concentration of rough endoplasmic reticulum while the more abundant granular apical cytoplasm is eosinophilic (Fig. 5.5b). On fine needle aspiration biopsies of normal pancreas, the acinar cells typically predominate and form cohesive three-dimensional grape-like clusters and two-dimensional microacinar structures, sometimes with scattered single cells in the background (Fig. 5.5c, d). Acinar cells have polygonal outlines with indistinct cell borders. The round uniform nuclei are centrally or eccentrically placed and are about the size of a red blood cell. The chromatin is granular and the nucleolus is distinct and can be prominent (Fig. 5.5e). Binucleated forms can occur. Naked nuclei are common when samples are aggressively smeared onto slides. Acinar cells have abundant cytoplasm, which is blue-green on Papanicolaou stain (Fig. 5.5f) and purple on Diff-Quik stain. Coarse cytoplasmic zymogen granules are a characteristic feature; however, clear and vacuolated cytoplasm is relatively common due to degranulation. Acinar cells do not produce mucin. The acinar cells are morphologically similar from different regions of the pancreas. Hypercellular aspirates consisting of predominantly benign acinar cells can potentially lead to a misinterpretation of a neoplasm such as acinar cell carcinoma or pancreatic neuroendocrine tumor. However, some features may be helpful in avoiding this pitfall. Neoplastic acinar cells tend to have higher nuclear:cytoplasmic ratios. Loss of normal acinar architecture will result in large trabeculae and club-shaped aggregates. The predominance of discohesive cells seen in aspirates of neuroendocrine tumors is typically plasmacytoid [14].

Special stains can be used to highlight the zymogen granules which stain with periodic acid Schiff (PAS) stain and are resistant to diastase. The enzymes produced by acinar cells may stain with immunohistochemical labeling with antibodies to trypsin, chymotrypsin, lipase, amylase, and elastase. It is important to note that these stains are also sensitive mark-

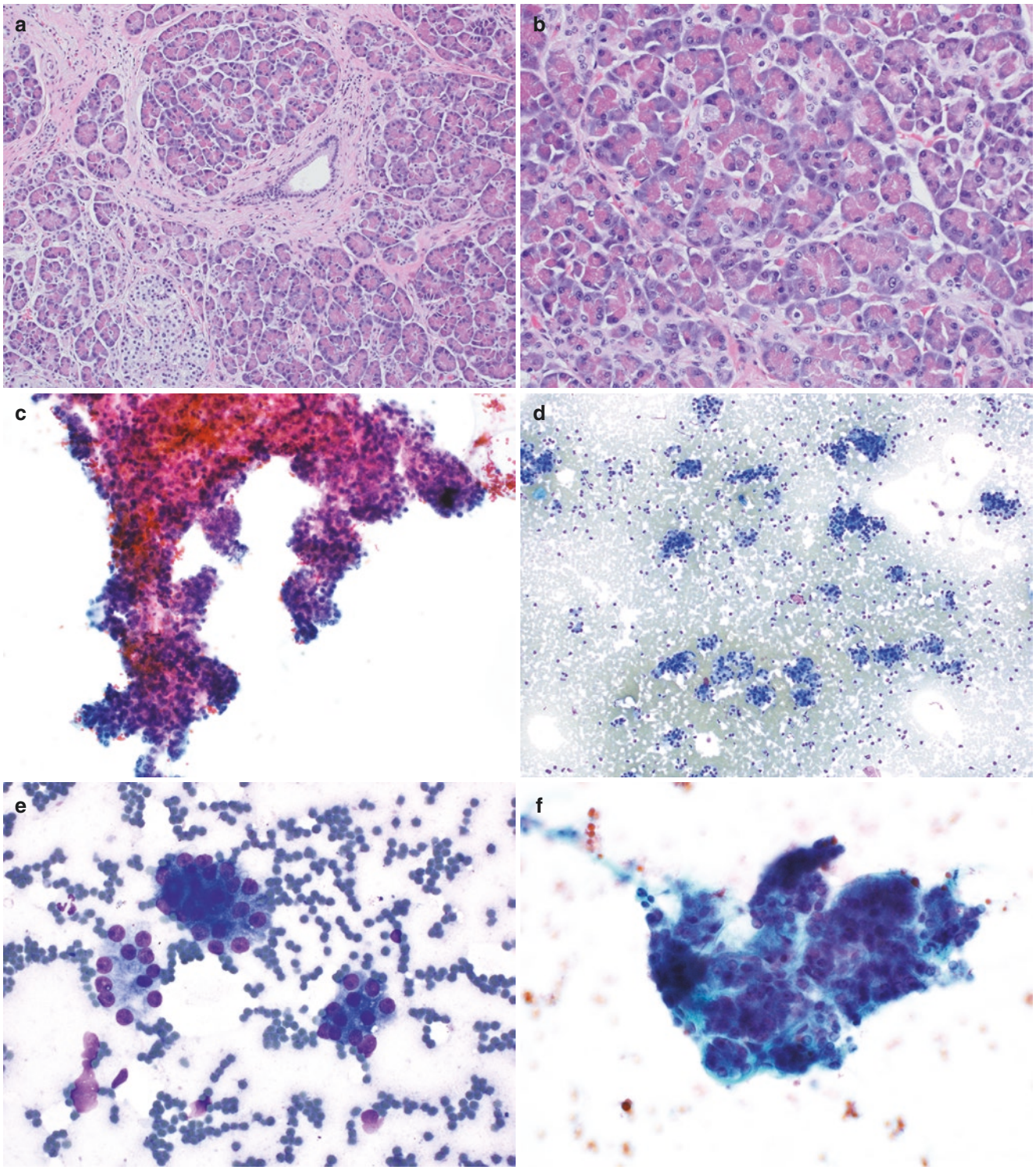

Fig. 5.5 (**a**) Pancreas histology showing acinar cells in rounded groups and tubular structures surrounding small ductules. (**b**) The acinar cells are polygonal with round basally located nuclei, basophilic perinuclear cytoplasm, and abundant granular eosinophilic apical cytoplasm. (**c**) Aspirate of acinar cells showing several cohesive three-dimensional grape-like clusters. (**d**) Two-dimensional microacinar structures with scattered single cells are shown. (**e**) Normal acinar cells can be seen with a distinct nucleolus. (**f**) Acinar cells are shown with abundant cytoplasm which is blue-green on Papanicolaou stain. Pancreas resection, hematoxylin & eosin, 10× (**a**) and 20× (**b**) magnification. Pancreas, alcohol-fixed smear preparation, Papanicolaou stain, 20× (**c**) and 40× (**f**) magnification. Pancreas, air-dried smear preparation, Diff-Quik, 10× (**d**) and 40× (**e**) magnification

ers of acinar differentiation in pancreatic neoplasms. Acinar cells will also stain with antibodies to cytokeratin CAM5.2, CK8, and CK18, but typically do not label with antibodies to cytokeratin AE1/AE3, CK7, and CK20. They also do not label with CA19-9 [11].

The ductal system of the pancreas serves as a conduit for the transport of acinar cell secretions. The ductal epithelial cells secrete water, chloride, and bicarbonate, an alkaline fluid that buffers the acidity of the pancreatic juices, stabilizing the proenzymes. The ductal system starts with the centroacinar cells that connect the acini to intercalated ducts (smallest ducts) which then fuse to form intralobular ducts that drain into interlobular ducts and finally the larger main ducts of Wirsung and Santorini [11]. In fine needle aspirations of normal pancreas, ductal cells are a usually a minor component whereas acinar cells predominate. In both chronic pancreatitis and ductal adenocarcinoma, where normal pancreas may undergo atrophy, ductal cells may outnumber the acinar cells. Benign ductal cells are cohesive and occur in flat two-dimensional honeycomb sheets (Fig. 5.6a, b). The size of ductal cells ranges from cuboidal to columnar and is in direct proportion to the diameter of the duct. Larger ducts may contain ciliated cells. Their nuclei are round and uniform with smooth membranes. Binucleated forms can be seen. Nucleoli are small and inconspicuous. Their cytoplasm is pale and finely vacuolated, best appreciated when the ductal cells are present in strips yielding a "picket-fence" configuration or when the luminal edge in sheets is apparent

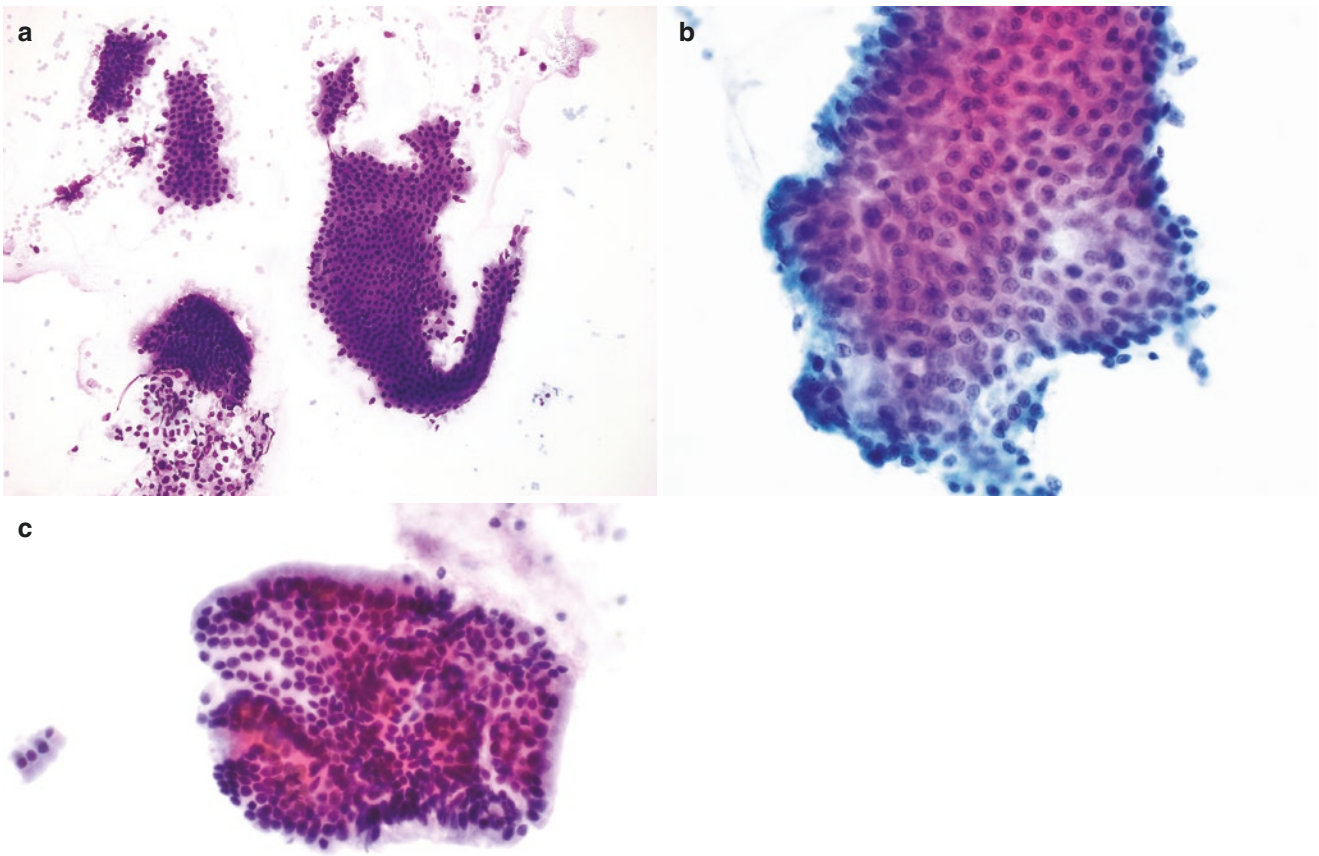

Fig. 5.6 (**a**, **b**) Benign ductal epithelial cells with pale finely vacuolated cytoplasm are arranged in flat honeycomb sheets. The cytoplasm is best appreciated when the ductal cells are present in strips yielding a "picket-fence" configuration or when the luminal edge in sheets is apparent (**c**). Pancreas, air-dried smear preparation, Diff-Quik, 10× magnification (**a**). Pancreas, alcohol-fixed smear preparation, Papanicolaou stain, 40× magnification (**b**). Pancreas, ThinPrep preparation, 40× magnification (**c**)

(Fig. 5.6c). Reactive ductal epithelium can display atypia that may be misinterpreted as adenocarcinoma. Crowding or overlapping of nuclei, nuclear enlargement, and prominent nucleoli are commonly seen in both reactive and malignant ductal cells. However, severe anisonucleosis (i.e., variation in nuclear size greater than 4 times within an epithelial cluster) is typically only seen in malignancy [15]. Metaplastic change includes squamous, oncocytic, intestinal, and acinar metaplasia. Mucin may thus be present in benign ductal cells and a few cells from the large ducts can have substantial mucin (goblet cells), which can be difficult or impossible to differentiate from gastrointestinal contamination or mucinous neoplasms. Abundant mucin, however, is usually pathologic.

Ductal cells label with cytokeratins AE1/AE3, CAM5.2, CK7, and CK19. Normal ductal cells do not label with antibodies to CK20, monoclonal CEA or MUC4. There is no labeling with antibodies to exocrine enzymes or endocrine markers. Of note, scattered endocrine cells (Kulchitsky cells) can be found by immunolabeling within the epithelium of larger ducts [11].

Around 90% of the endocrine cells in the pancreas occur in small, round, compact aggregates called the islets of Langerhans, with the remainder scattered among the acini and larger ducts. Although there are about a million islets of Langerhans in the pancreas, they account for only 1–2% of the total mass of the pancreas and are concentrated in the body and tail of the pancreas (90%). There are four types of islet cells, each producing a single peptide: alpha cells secrete glucagon which is responsible for carbohydrate metabolism (glycogen to glucose), beta cells secrete insulin which is responsible for carbohydrate metabolism (glucose to glycogen), delta cells secrete somatostatin which suppresses gastrointestinal hormones, and PP cells secrete pancreatic polypeptide which regulates the exocrine and endocrine function [11, 12]. The various types of islets cells are morphologically identical and cannot be distinguished without special stains. Although islet cells can be distinguished from acinar cells on morphology alone on histologic examination (Fig. 5.7), islet cells are cytologically similar to acinar cells and are rarely recognized on routine stains in the aspirates of nonendocrine neoplasms [11] without immunohistochemical stains for neuroendocrine markers such as synaptophysin and chromogranin. Nevertheless, compared to acinar cells the islet cells have relatively larger nuclei, tend to appear plasmacytoid, and have denser chromatin. Mild nuclear size variation is an expected finding. While normal islet cells can have enlarged nuclei, these do not exhibit nuclear contour or chromatin irregularities. Increased islet cells (from aggregation or hyperplasia) can potentially be mistaken for a neuroendocrine tumor. However, if sampled, these aspirates are typically hypocellular [16]. It is extremely rare to see mitoses in normal islet cells.

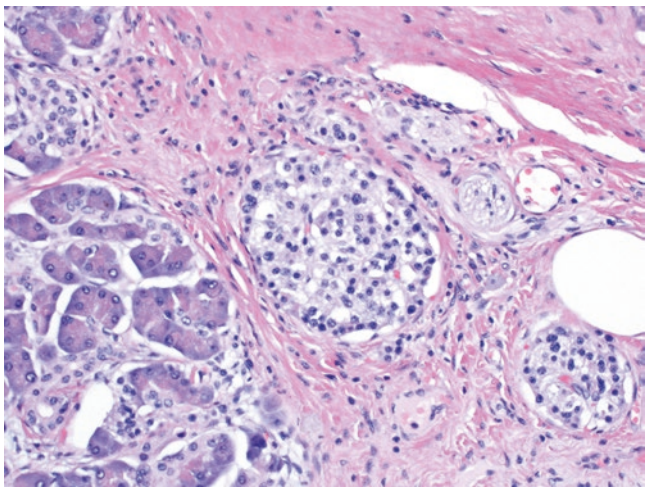

Fig. 5.7 Pancreas histology demonstrating a compact aggregate of islet cells adjacent to acinar cells. Pancreas resection, hematoxylin & eosin, 20× magnification

In addition to the previously discussed mimickers of neoplasms, entities such as intrapancreatic accessory spleen [17], lymphoid tissue and paraganglia as well as intraparenchymal fat may sometimes be encountered. Aspirates of intrapancreatic accessory spleens typically resemble lymphoid tissue with increased vasculature and abundant discohesive single cells with scant cytoplasm (Fig. 5.8a). Pancreatic neoplasms with a similar discohesive pattern include neuroendocrine tumors, acinar cell carcinoma, and solid pseudopapillary neoplasms [16]. The lymphoid nature of the cells can be confirmed by immunostaining with leukocyte common antigen (or CD45) and CD8 which will highlight the endothelial cells of normal vascular channels (Fig. 5.8b).

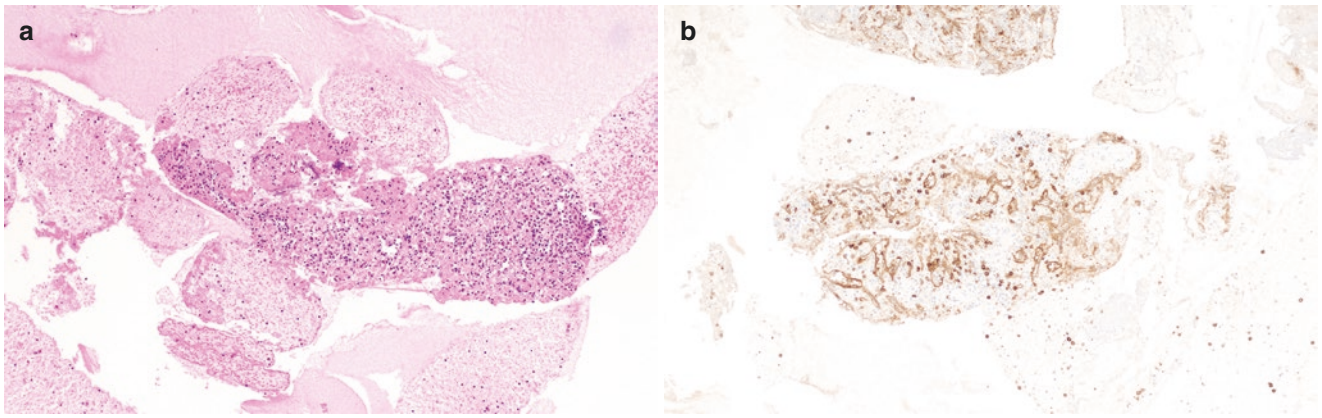

Fig. 5.8 (**a**) Cell block section of intrapancreatic spleen aspirate showing lymphoid cells. (**b**) CD8 immunostain highlights the endothelial cells of the vascular channels. Pancreas aspirate, cell block, hematoxylin & eosin (**a**) and CD8 immunohistochemistry, 10× magnification (**b**)

References

1. Sandrine Jousse-Joulin. Chapter 17: Salivary glands. In: Wakefield RJ, D'Agostino MA, eds. Essential applications of musculoskeletal ultrasound in rheumatology. W.B. Saunders Philadelphia, PA, 2010: 199-206.
2. Xu L, Lal K, Santarpia RP III, Pollock JJ. Salivary proteolysis of histidine-rich polypeptides and the antifungal activity of peptide degradation products. Arch Oral Biol. 1993;38(4):277–83.
3. Caselitz J, Jaup T, Seifert G. Lactoferrin and lysozyme in carcinomas of the parotid gland. A comparative immunocytochemical study with the occurrence in normal and inflamed tissue. Virchows Arch A Pathol Anat Histol. 1981;394(1–2):61–73.
4. Takano K, Malamud D, Bennick A, Oppenheim F, Hand AR. Localization of salivary proteins in granules of human parotid and submandibular acinar cells. Crit Rev Oral Biol Med. 1993;4(3–4):399–405.
5. Langdon JD. Chapter 1: Surgical anatomy, embryology, and physiology of the salivary glands. In: Carlson ER, Ord RA, editors. Textbook and color atlas of salivary gland pathology diagnosis and management. London: Wiley-Blackwell; 2008. p. 3.
6. de Paula F, Teshima THN, Hsieh R, Souza MM, Nico MMS, Lourenco SV. Overview of human salivary glands: highlights of morphology and developing processes. Anat Rec. 2017;300(7):1180–8.
7. Nanci A. Chapter 12: Oral mucosa. In: Nanci A, editor. Ten cate's oral histology: development, structure, and function. 8th ed. Amsterdam: Elsevier; 2013. p. 275.
8. Schmidt RL, Hall BJ, Wilson AR, Layfield LJ. A systematic review and meta-analysis of the diagnostic accuracy of fine-needle aspiration cytology for parotid gland lesions. Am J Clin Pathol. 2011;136(1):45–59.
9. Layfield LJ. Fine-needle aspiration in the diagnosis of head and neck lesions: a review and discussion of problems in differential diagnosis. Diagn Cytopathol. 2007;35(12):798–805.
10. Liu CC, Jethwa AR, Khariwala SS, Johnson J, Sensitivity SJJ. Specificity, and posttest probability of parotid fine-needle aspiration: a systematic review and meta-analysis. Otolaryngol Head Neck Surg. 2016;154(1):9–23.
11. Hruban RH, Pitman MB, Klimstra DS. Chapter 1: The normal pancreas. In: Silverberg SG, editor. AFIP Atlas of tumor pathology, Fourth series, Fascicle tumors of the pancreas. Washington, DC: American Registry of Pathology; 2007. p. 1–15, in collaboration with the Armed Forces Institute of Pathology, Washington, DC.
12. Longnecker DS. Anatomy and histology of the pancreas. Pancreapedia: Exocrine Pancreas Knowledge Base. 2021; https://doi.org/10.3998/panc.2021.01.
13. Chang EB, Leung PS. Pancreatic physiology. In: Leung P, editor. The gastrointestinal system. Dordrecht: Springer; 2014. p. 87–105. https://doi.org/10.1007/978-94-017-8771-0_4.
14. Siegel CS, Slimstra DS. Cytomorphologic and immunophenotypical features of acinar cell neoplasms of the pancreas. Cancer Cytopathol. 2013;121:459–70.
15. Lin F, Staerkel G. Cytologic criteria for well differentiated adenocarcinoma of the pancreas in fine-needle aspiration biopsy specimens. Cancer Cytopathol. 2003;99:44–50.
16. Samedi VG, Bocklage T. Chapter 5: Pancreaticobiliary tract. In: Siddiqui M, editor. Pitfalls in diagnostic cytopathology with key differentiating cytologic features, essentials in cytopathology 27. Springer: Cham; 2016. p. 103–6.
17. Schreiner AM, Mansoor A, Faigel DO, Morgan TK. Intrapancreatic accessory spleen: mimic of pancreatic endocrine tumor diagnosed by endoscopic ultrasound-guided fine-needle aspiration biopsy. Diagn Cytopathol. 2008;36(4):262–5.

Endocrine Glands

6

Tao Huang and Xin Jing

Thyroid Gland

The thyroid is a vascular-rich, butterfly-shaped organ located at the base of the anterior neck that lies on the anterolateral aspect of the cervical trachea, just covering the thyroid cartilage and adjacent tracheal rings. It consists of a left and right lobe, connected by a typically thin isthmus. In adults, the thyroid gland usually weighs 15–25 g, although there can be variation between individuals of different gender, age, weight, and hormonal status as well as exposure to various environmental factors. Each lobe measures approximately 4 cm in length, 2 cm in width, and 2–3 cm in thickness. The isthmus measures approximately 2 cm in length and 2 cm in height, but can have a width that ranges from 2 to 6 cm. It is not uncommon for a normal thyroid lobe to contain an additional thin pyramidal lobe extending superiorly from the isthmus as a remnant of the thyroglossal duct. A small proportion of normal thyroid glands can have nodularity. The thyroid's main function is the production of hormones, the most important of which are thyroxine (T4) and biologically active triiodothyronine (T3) that exert metabolic effects throughout end-organ targets. T4 and approximately 20% of T3 are synthesized by the thyroid. However, the majority of T3 is generated from the conversion of T4 to T3 in extrathyroidal peripheral tissues. These thyroid hormones participate in the regulation of metabolism and growth [1, 2].

On histology, normal thyroid parenchyma is divided into multiple lobules, with each lobule composed of 20–40 various-sized follicles. Follicles have round lumens that are filled with homogeneous eosinophilic colloid, a thick, proteinaceous substance containing thyroglobulin, which serves as a storage point for inactive thyroid hormone precursors and iodine as well as a substrate for the synthesis of thyroid hormones. The follicles are lined by a single layer of flat, cuboidal, or low columnar follicular epithelial cells that display round to ovoid nuclei and fine granular to clumped chromatin. Thyroid follicular cells are responsible for the synthesis of the T4 and T3 hormones and thyroglobulin. The amount of cytoplasm within the follicular cells varies depending on their degree of activity. Flat follicular cells are inactive (Fig. 6.1a), whereas cuboidal cells synthesize thyroglobulin and other proteins to be subsequently stored in luminal colloid. Low columnar cells actively absorb colloid and are therefore often associated with absorption vacuoles (Fig. 6.1b). Calcium oxalate crystals are often present within the colloid material and this finding is thought to be associated with a low functional status of thyroid follicles (Fig. 6.1c) [3]. The shape of these crystals varies and they can be easily detected with polarization. The identification of calcium oxalate crystals within thyroid is helpful during frozen sections in separating thyroid from parathyroid tissue. Follicular cells may show features of Hürthle cell metaplasia manifested by abundant finely granular cytoplasm, a round nucleus, and a variably conspicuous nucleolus (Fig. 6.1d). Sometimes the normal thyroid gland may contain granulomas that originate from ruptured follicles due to palpation. Lymphocytes may be seen in normal thyroid tissue when in close proximity to a lesion or in sampling of an intrathyroidal lymph node [4]. Cytologic samples of the thyroid may also display other elements, such as fragments of skeletal muscle, dystrophic calcification in elderly persons, intrathyroidal parathyroid tissue, ectopic thymic tissue, ectopic cartilage, and adipose tissue as a result of stromal metaplasia.

Additionally, the thyroid contains calcitonin-producing parafollicular or C cells, which are commonly located in the mid- and upper 1/3 of the lateral lobes and comprise less than 0.1% of the total glandular component of the thyroid. In the normal thyroid, C cells are often inconspicuous, and rarely are appreciated under light microscopic examination of hematoxylin & eosin (H & E)-stained sections [5, 6]. C cells show nuclei which are larger than that of the follicular cells, have finely dispersed nuclear chromatin, inconspicuous nucleoli, and variable amounts of pale to eosinophilic granular cytoplasm (Fig. 6.1e). It is noteworthy to mention that the

T. Huang · X. Jing (✉)
Department of Pathology, University of Michigan,
Ann Arbor, MI, USA
e-mail: taohuang@med.umich.edu; xinjing@med.umich.edu

M. Lew et al. (eds.), *Normal Cytology*, https://doi.org/10.1007/978-3-031-20336-7_6

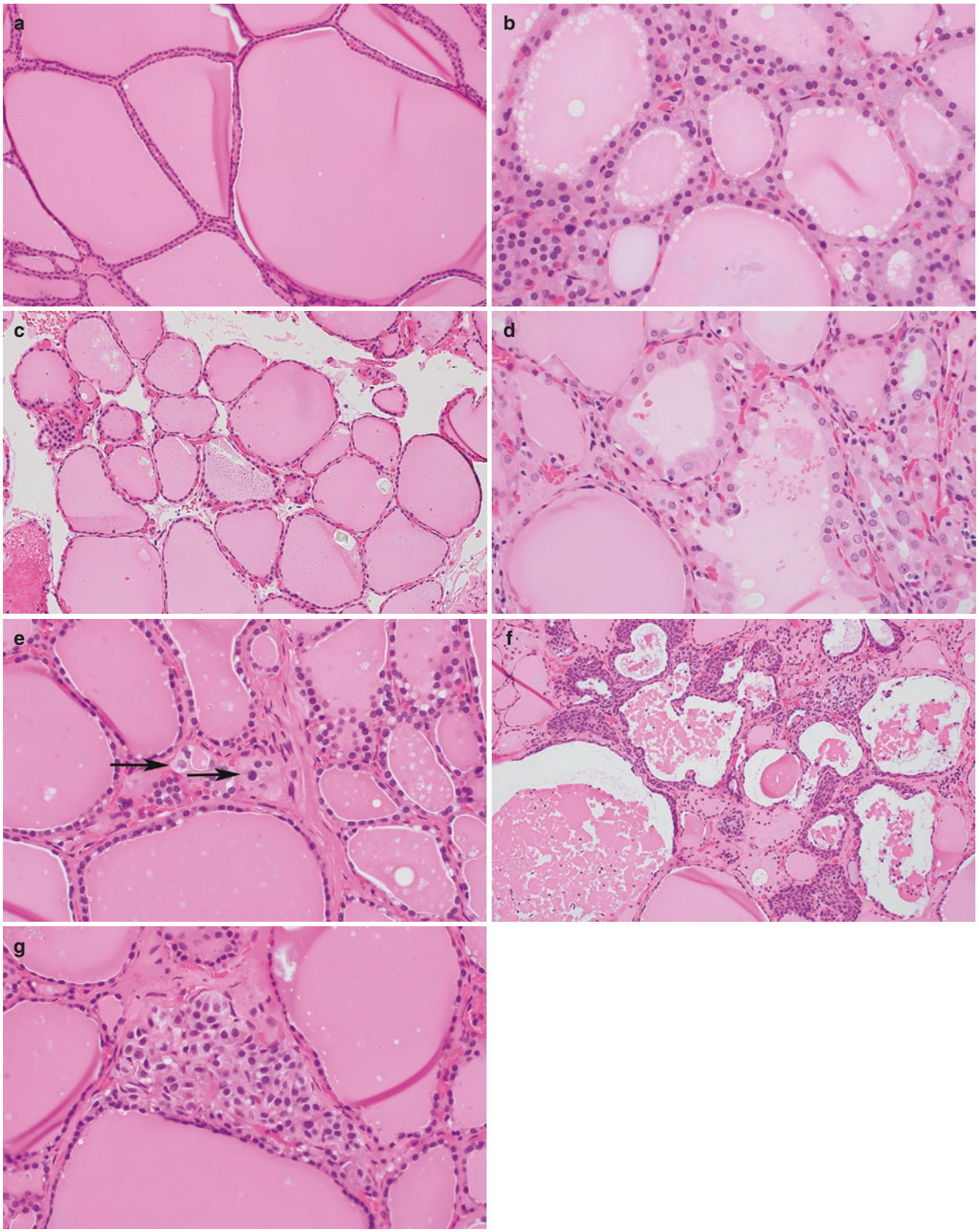

Fig. 6.1 (**a**) Thyroid parenchyma showing variably sized follicles lined by a single layer of flat, inactive, follicular cells (**b**) and/or low columnar cells with absorption vacuoles, filled with (**c**) homogenous eosinophilic colloid with calcium oxalate crystals. (**d**) Metaplastic Hürthle cells with abundant eosinophilic granular cytoplasm can be identified within thyroid parenchyma. (**e**) Parafollicular or C cells can be identified as single cells or as nests of cells (black arrows). (**f**) Small clusters of C cells are readily noted within solid cell nests. (**g**) C cell hyperplasia around a follicle. Thyroid resection, hematoxylin & eosin, 10× (**a**), 20× (**c**), and 40× (**b**, **d**–**g**) magnification

lateral portion of the thyroid lobes may contain solid cell nests, which represent ultimobranchial body remnants derived from the fourth and fifth branchial pouches. Solid cell nests measure from 0.1 to 2 mm and are composed of predominantly basaloid cells and small clusters of C cells (Fig. 6.1f). C cells are more readily identified in abnormal situations, such as C cell hyperplasia in patients with multiple endocrine neoplasia type 2 (Fig. 6.1g). The immunohistochemical stains of calcitonin and neuroendocrine markers including synaptophysin and chromogranin can be used to identify C cells.

Ultrasound is considered the best imaging modality for comprehensive evaluation of the thyroid. Normal thyroid has a homogeneous appearance, and no internal anatomic landmarks are typically defined upon ultrasound exam [7, 8]. Ultrasound-guided fine needle aspiration (FNA) is utilized as an important tool in the clinical assessment and management of thyroid nodules [9]. The anatomy of the thyroid gland on ultrasound imaging and neighboring structures in the neck, such as large vessels, has become increasingly important for cytopathologists to be aware of now that they are performing more ultrasound-guided FNAs of thyroid nodules. Depending on the clinical presentation and laboratory settings, thyroid FNA specimens may be processed as Diff-Quik and/or Papanicolaou-stained conventional smears and/or liquid-based preparations (LBP) [10], which may or may not be accompanied by H & E-stained cell block preparations.

There is considerable overlap in cytologic features between normal thyroid and benign follicular nodules. Occasionally, distinguishing normal from abnormal findings may be problematic. FNA smears of normal thyroid may reveal a mixture of follicular cells and colloid. Background colloid has two main morphologic appearances—thick or thin/watery, both of which display a homogenous texture and appear pale to dark blue or purple with Diff-Quik staining and pink or pale gray with Papanicolaou staining. Colloid may display cracks on Diff-Quik-stained smears as a result of drying and subsequent retraction of colloid from the slide (Fig. 6.2).

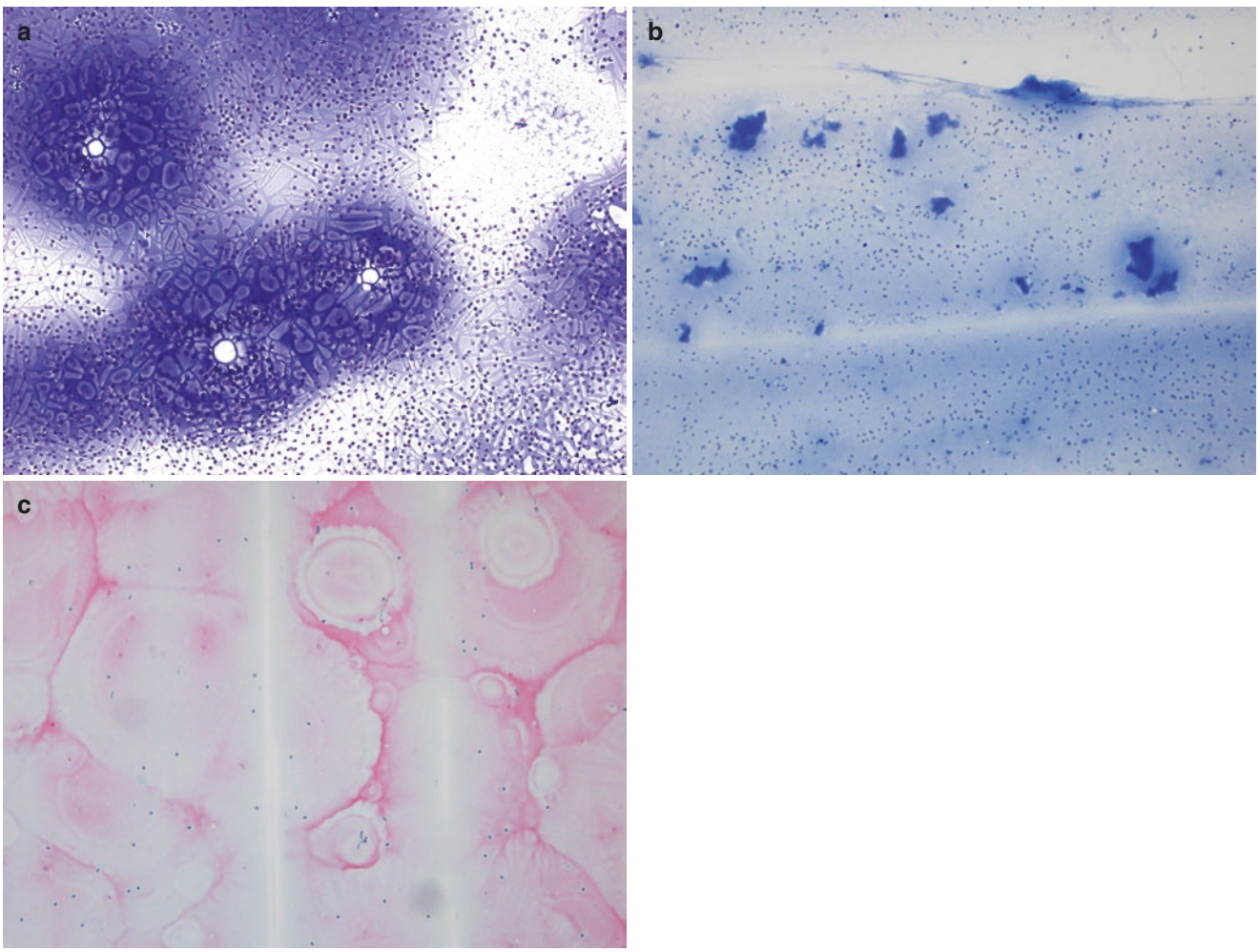

Fig. 6.2 (**a**) Homogenous-appearing thick and thin/watery colloid. Colloid appears blue to purple with Diff-Quik staining and may have cracks as a result of drying and retraction of colloid from the slide. (**b**, **c**) Colloid appears pink or pale gray with Papanicolaou staining. Thyroid, air-dried smear preparation, Diff-Quik, 10× magnification (**a**, **b**). Thyroid, alcohol-fixed smear preparation, Papanicolaou stain, 10× magnification (**c**)

Occasionally smear preparations may show calcium oxalate crystals interspersed with colloid [11, 12]. One should avoid misinterpretation of amyloid and psammomatous calcifications as colloid, which could delay treatment for other disease entities, such as medullary thyroid carcinoma and papillary thyroid carcinoma. Unlike thick and thin colloid material, both of which have homogenous appearance, amyloid material commonly has a coarse, granular texture and is interspersed with elongated and/or spindle-shaped, fibroblast nuclei (Fig. 6.3). Psammoma bodies often show laminated structures.

The majority of follicular cells may be arranged as monolayered honeycomb-like sheets, clusters of loosely arranged macrofollicles with minimal nuclear overlap, and sometimes occasional intact smaller follicles, as well as rare single cells and bare nuclei. In cases where follicular cells are largely stripped of their cytoplasm, the appearance may be similar to that of dispersed lymphocytes. When intact, follicular cells often have a moderate amount of pale, delicate cytoplasm, a centrally located round or oval nucleus, fine chromatin distribution, and inconspicuous or small nucleoli (Figs. 6.4, 6.5, 6.6, and 6.7). Although uncommon, smear preparations of normal (benign) thyroid may also show sheets of Hürthle cells or flame cells. The cytologic features of Hürthle cells are similar to those found in histologic evaluation including abundant, finely granular cytoplasm, large nuclei, and variably prominent nucleoli (Fig. 6.8). However, the quantity of Hürthle cells should be low in sampling of normal thyroid parenchyma. Additionally, in contrast to sampling from Hürthle cell neoplasms, there is a spectrum of Hürthle cell change among follicular cells in the background. Flame cells, which can be seen in Graves' disease, are morphologically distinct in Diff-Quik-stained smear preparations and are characterized by peripheral cytoplasmic vacuoles and an abundant amount of cytoplasm with red to pink frayed edges (Fig. 6.9). Although peripheral vacuoles have been associated with thyroid hyperactivity, as in Graves' disease, some studies have pointed out their nonspecific status and/or demonstrated the lack of correlation between vacuoles and level of thyroid function [3, 5, 6, 13–15]. Rarely, thyroid smear preparations may contain respiratory epithelial cells due to incidental deep sampling of epithelium lining the tracheal wall. Appreciation of the cilia attached to these bronchial epithelial cells is helpful to prevent misinterpretation as a lesional finding (Fig. 6.10). However, ciliated cells may also be identified in sampling of thyroglossal duct cysts. As such, clinical and radiologic correlation of the sampled tissue is of utmost importance in appropriately designating the etiology of these ciliated cells. Usually, the aforementioned calcitonin-producing C cells are not identified in FNA smears of normal thyroid tissue.

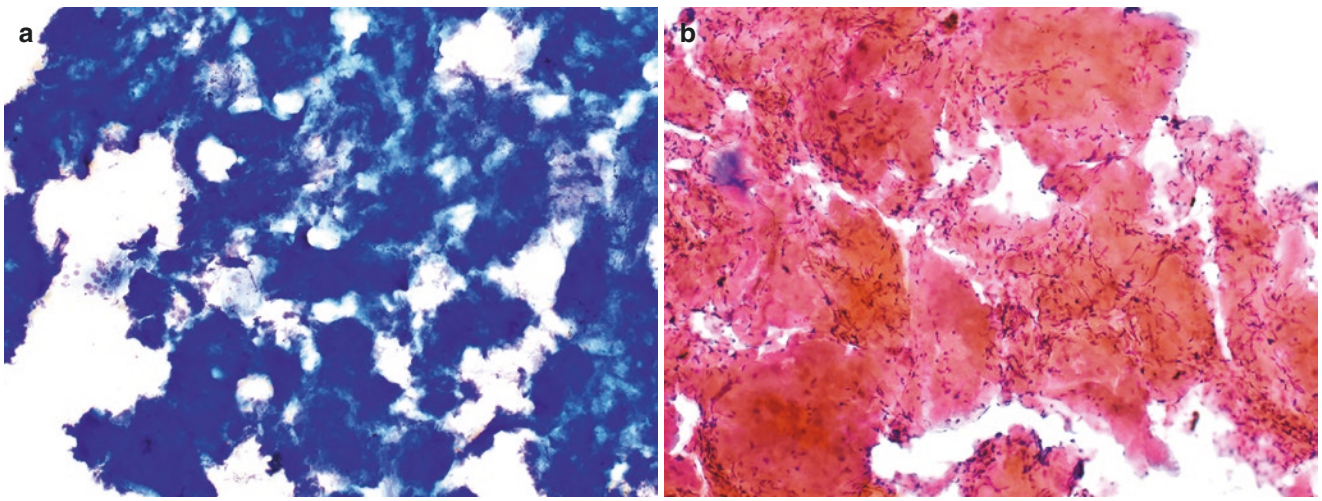

Fig. 6.3 (**a**, **b**) Amyloid material shows a coarse, granular texture that is interspersed with elongated and/or spindle-shaped, fibroblast nuclei. Thyroid, air-dried smear preparation, Diff-Quik, 20× magnification (**a**). Thyroid, alcohol-fixed smear preparation, Papanicolaou stain, 20× magnification (**b**)

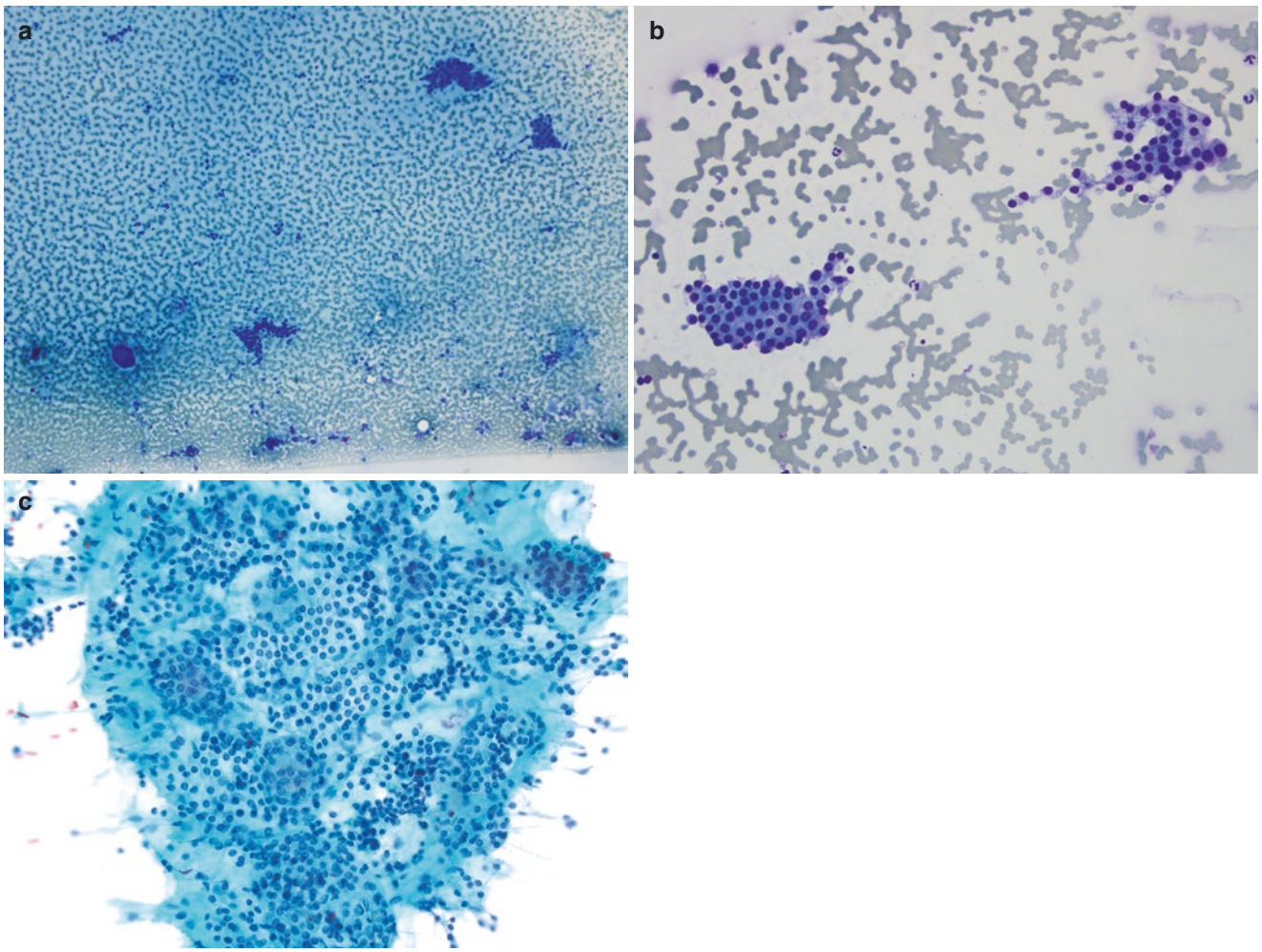

Fig. 6.4 (**a–c**) Background colloid and bland-appearing benign follicular cells which are cohesively arranged in monolayered, honeycomb sheets with even cellular spacing. Note the presence of background watery colloid in these smears. Thyroid, air-dried smear preparation, Diff-Quik, 10× (**a**) and 20× (**b**) magnification. Thyroid, alcohol-fixed preparation, Papanicolaou stain, 20× magnification (**c**)

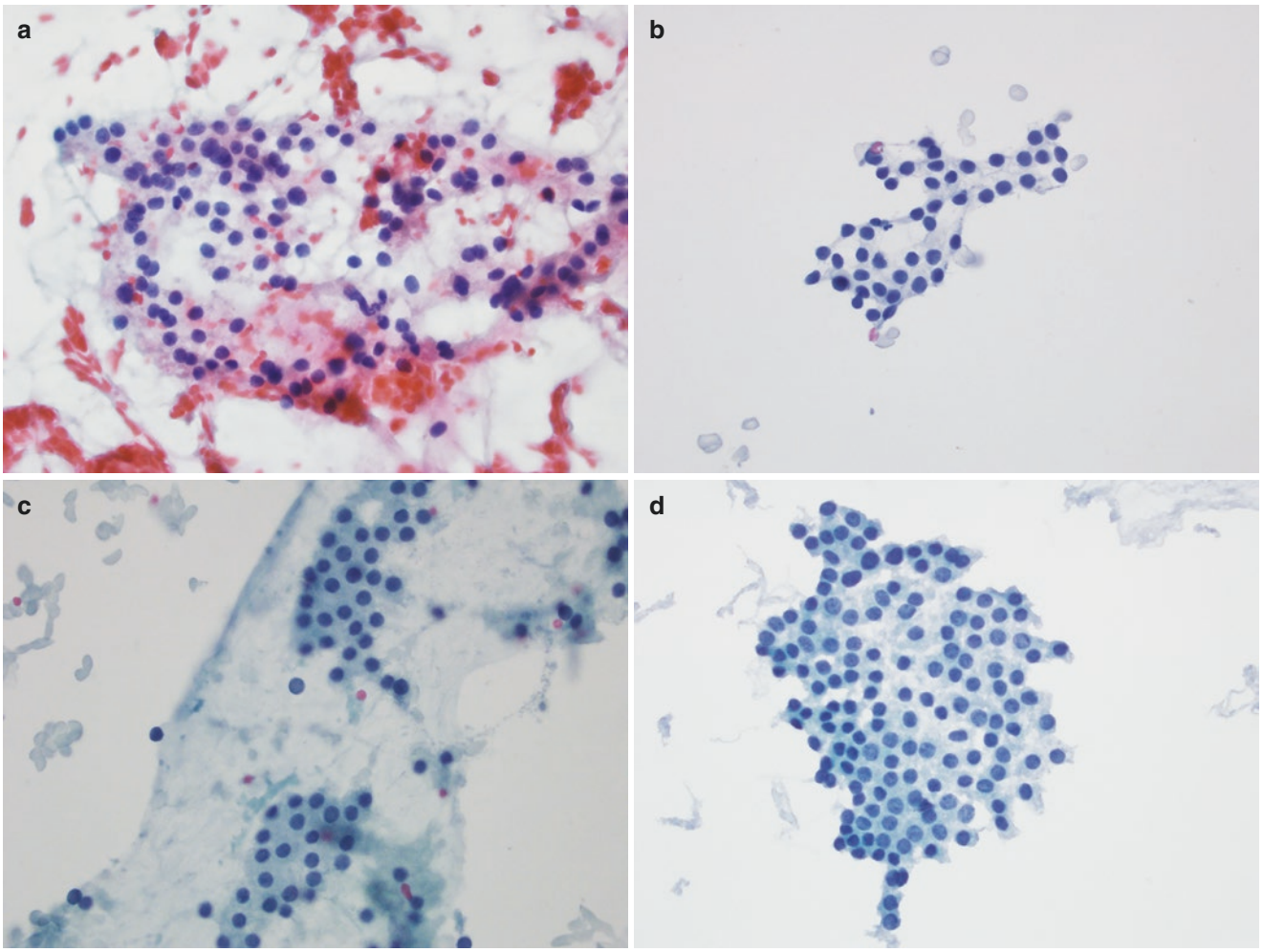

Fig. 6.5 Benign follicular cells arranged as (**a**) a few macrofollicles or (**b**–**d**) monolayered, honeycomb sheets. The follicular cells have a moderate amount of pale cytoplasm, centrally placed round or ovoid nuclei, fine chromatin distribution, and inconspicuous or small nucleoli. Thyroid, alcohol-fixed smear preparation, Papanicolaou stain, 40× magnification (**a**–**c**). Thyroid, ThinPrep preparation, Papanicolaou stain, 40× magnification (**d**)

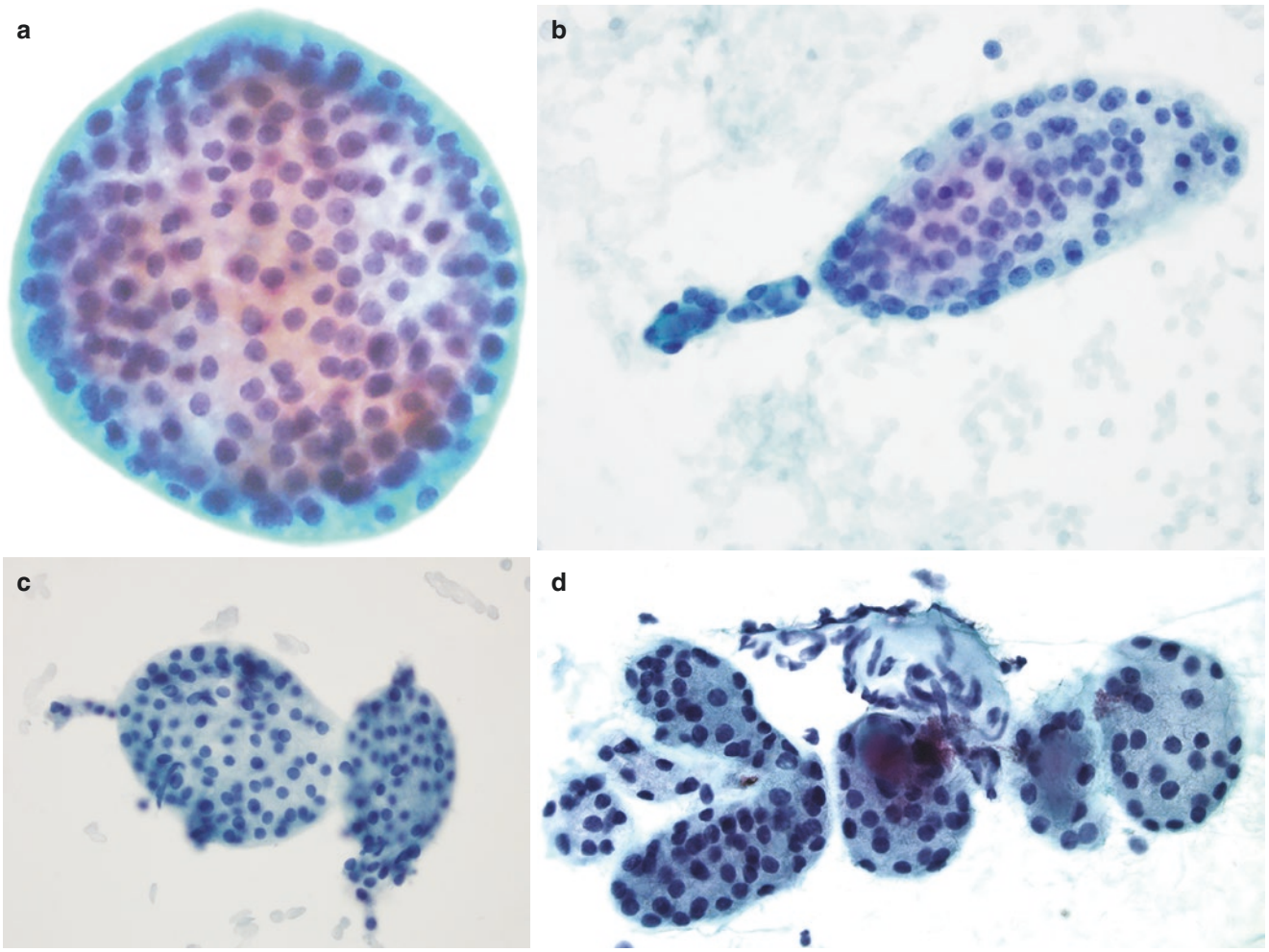

Fig. 6.6 (**a–d**) Benign follicular cells are arranged as intact round follicles which have a smooth outline. The intact follicles may vary in size and contain a few or numerous follicular cells without nuclear overlapping/crowding. Thyroid, alcohol-fixed smear preparation, Papanicolaou stain, 40× magnification (**a–d**)

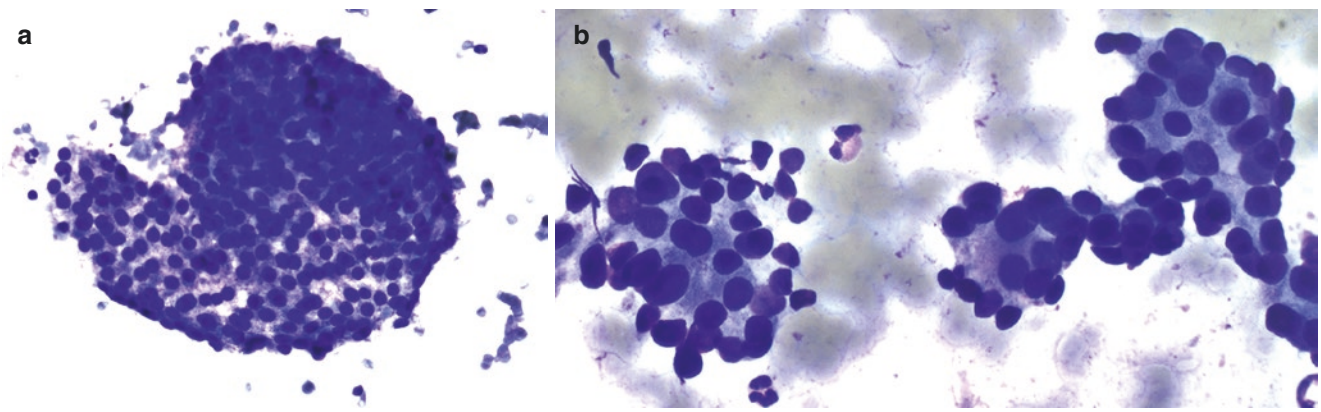

Fig. 6.7 Comparison between (**a**) an intact follicle and (**b**) several smaller microfollicles. Unlike microfollicles, which are defined as crowded cell clusters composed of more than ten follicular cells with significant nuclear overlapping, the intact follicle shows a smooth outline, contains numerous follicular cells in a honeycomb arrangement, and lacks overt nuclear crowding/overlapping. Thyroid, air-dried smear preparation, Diff-Quik, 40× (**a**) and 60× (**b**) magnification

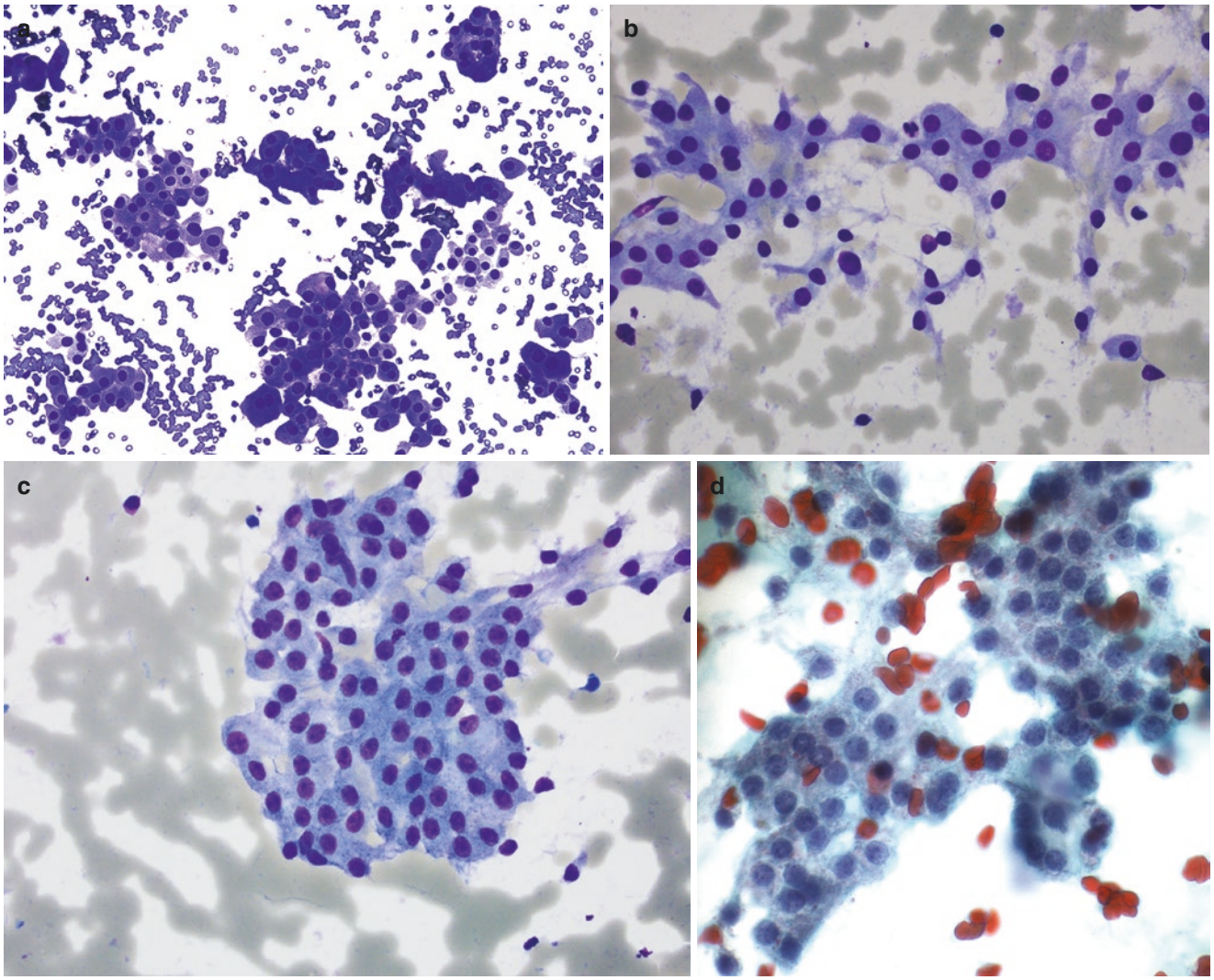

Fig. 6.8 (**a–d**) Singly dispersed and sheets of Hürthle cells with abundant, finely granular cytoplasm, large nuclei, and prominent nucleoli. Thyroid, air-dried smear preparation, Diff-Quik, 20× (**a**) and 40× (**b**, **c**) magnification. Thyroid, alcohol-fixed smear preparation, Papanicolaou stain, 60× magnification (**d**)

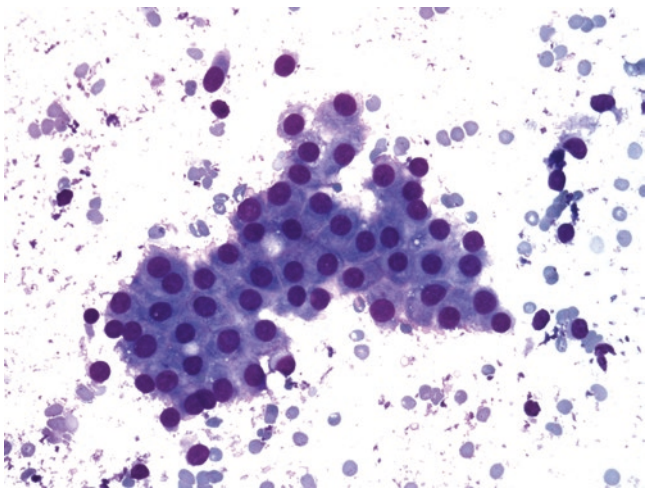

Fig. 6.9 Flame cells have abundant cytoplasm, marginal cytoplasmic vacuoles, and red to pink frayed edges. Thyroid, air-dried smear preparation, Diff-Quik, 40× magnification

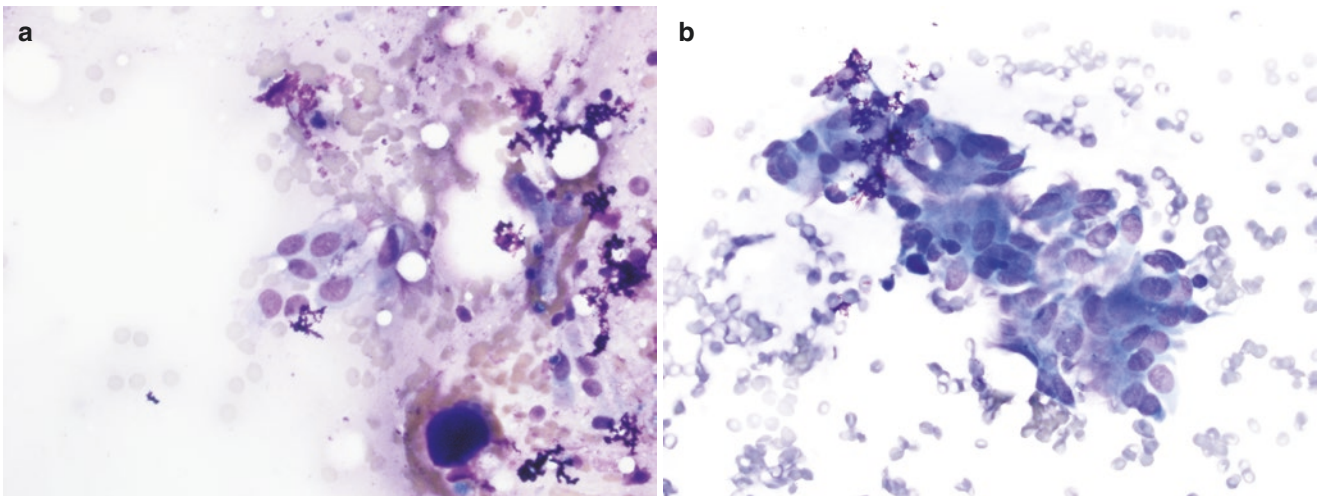

Fig. 6.10 (**a**, **b**) Ciliated respiratory epithelial cells due to contamination from FNA sampling of the trachea. Note the scant dense colloid material in the lower right field of (**a**). Thyroid, air-dried smear preparation, Diff-Quik, 40× magnification (**a, b**)

Parathyroid Glands

Typically, parathyroid glands are present as two paired glands that are located posterior to the upper and lower poles of the thyroid gland. The inferior parathyroid glands may be located anywhere from the level of mandibular angle to pericardium, and the anterior mediastinum is the most common location of finding an ectopic inferior parathyroid gland. Each gland weighs approximately 35–40 mg and measures 0.3–0.8 cm in all three dimensions. Variation in number and location of parathyroids is well described. In this regard, a large autopsy series reported up to 11 glands in normal subjects [1]. Parathyroid glands are responsible for producing parathyroid hormone, which regulates calcium metabolism.

On histology, the parathyroid glands are surrounded by a thin connective tissue capsule and contain a variable amount of adipose tissue within their supporting stroma (Fig. 6.11a, b). This adipose tissue appears after puberty and its amount varies depending on an individual's age and overall functional status of the gland. The average percentage of stromal fat in adult parathyroid glands ranges from 20 to 40% of the entire gland's volume [16, 17]. The parenchyma is rich in vasculature with abundant capillaries surrounding chief cells within lobules (Fig. 6.11c). The chief cells are the predominant cellular element of parathyroid parenchyma, and are characterized by uniform, centrally located, round, and hyperchromatic nuclei, inconspicuous nucleoli, well-defined cell boundaries, and abundant pale-staining to eosinophilic cytoplasm with a variable amount of glycogen and lipid droplets (Fig. 6.11c). Other types of cells identified in the parathyroid include oxyphil and water clear cells, which are postulated to represent morphologic variations of chief cells [18]. Oxyphil cells are characterized by larger nuclei, variably conspicuous nucleoli, and abundant eosinophilic granular cytoplasm (Fig. 6.11d). Water clear cells are rarely seen in normal parathyroid glands and are characterized by well-demarcated cell boundaries and abundant optically clear cytoplasm as a result of glycogen accumulation (Fig. 6.11e). Occasionally, chief cells form small acinar or glandular structures containing eosinophilic colloid-like material within the lumen, mimicking the appearance of thyroid follicles (Fig. 6.11f). When these follicles form and become abundant, the distinction between parathyroid and thyroid tissue can be challenging especially on frozen sections. As mentioned previously, identification of calcium oxalate crystals within colloid is a helpful morphologic clue to confirm thyroid origin.

Due to their location, small size, and thyroid-like pattern of parenchyma, parathyroid glands are not typically detectable on any imaging modality. Preoperative FNA has been used for locating suspected parathyroid tissue. It has been claimed that cytomorphologic features along with ancillary studies (i.e., immunostaining, chemical analysis of FNA rinses, or molecular testing) may aid in confirming parathyroid origin of sampled cells. However, definitive differentiation between normal parathyroid, parathyroid hyperplasia, and a parathyroid adenoma cannot be made by evaluation of cytomorphologic features alone and requires histologic evaluation [19–21].

FNA samples from normal parathyroid glands contain variable amounts of relatively monotonous small round or ovoid chief cells which can be arranged as single cells, cords, loose two-dimensional sheets, papillary structures, three-dimensional clusters, and occasionally microfollicles (Fig. 6.12a, c). Isolated cells and naked nuclei are commonly present. The majority of the cells have moderately abundant amounts of granular and delicate cytoplasm, round nuclei, granular chromatin distribution, and inconspicuous nucleoli.

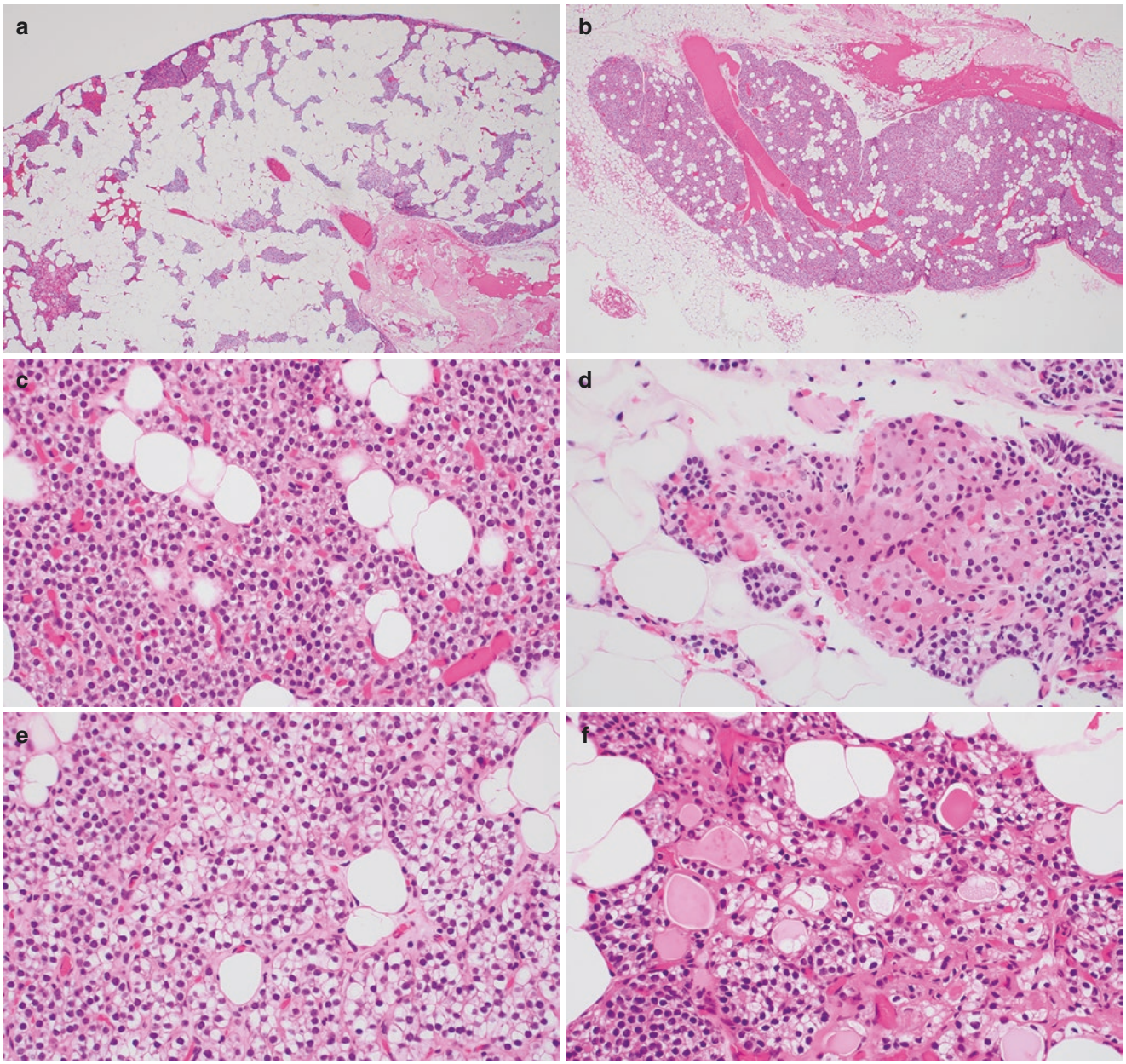

Fig. 6.11 (**a**, **b**) Normal parathyroid glands show a variable amount of stromal fat (**c**) with an extensive delicate capillary network intimately associated with chief cells, (**d**) oxyphil cells, and (**e**) water clear cells. (**f**) Chief cells can occasionally be arranged in acinar or glandular formations with colloid-like material within the lumen mimicking the appearance of thyroid follicles. Parathyroid resection, hematoxylin & eosin, 5× (**a–b**) and 40× (**c–f**) magnification

In addition, a prominent vascular network, mild nuclear pleomorphism, hyperchromatic nuclei, distinct nucleoli, a granular background due to disrupted fragile cytoplasm, and/or colloid-like material may occasionally be present [19–22]. There is considerable overlap in the cytomorphological features of parathyroid and thyroid aspirate samples. However, the presence of stippled chromatin patterns, a vascular network with attached epithelioid cells, and numerous singly dispersed cells and naked nuclei favor a parathyroid origin [19, 20]. Given the significant overlap in cytomorphology, ancillary studies are typically performed to differentiate between these two tissue origins, including chemical analysis of aspirate material (i.e., PTH) and immunohistochemistry on cell block material. PTH will be positive in parathyroid cells (Fig. 6.12h) while thyroid follicular cells are highlighted by PAX-8, TTF-1, and thyroglobulin. Odronic et al. compared the cytomorphological features of parathyroid aspirates between ThinPrep preparations and conventional

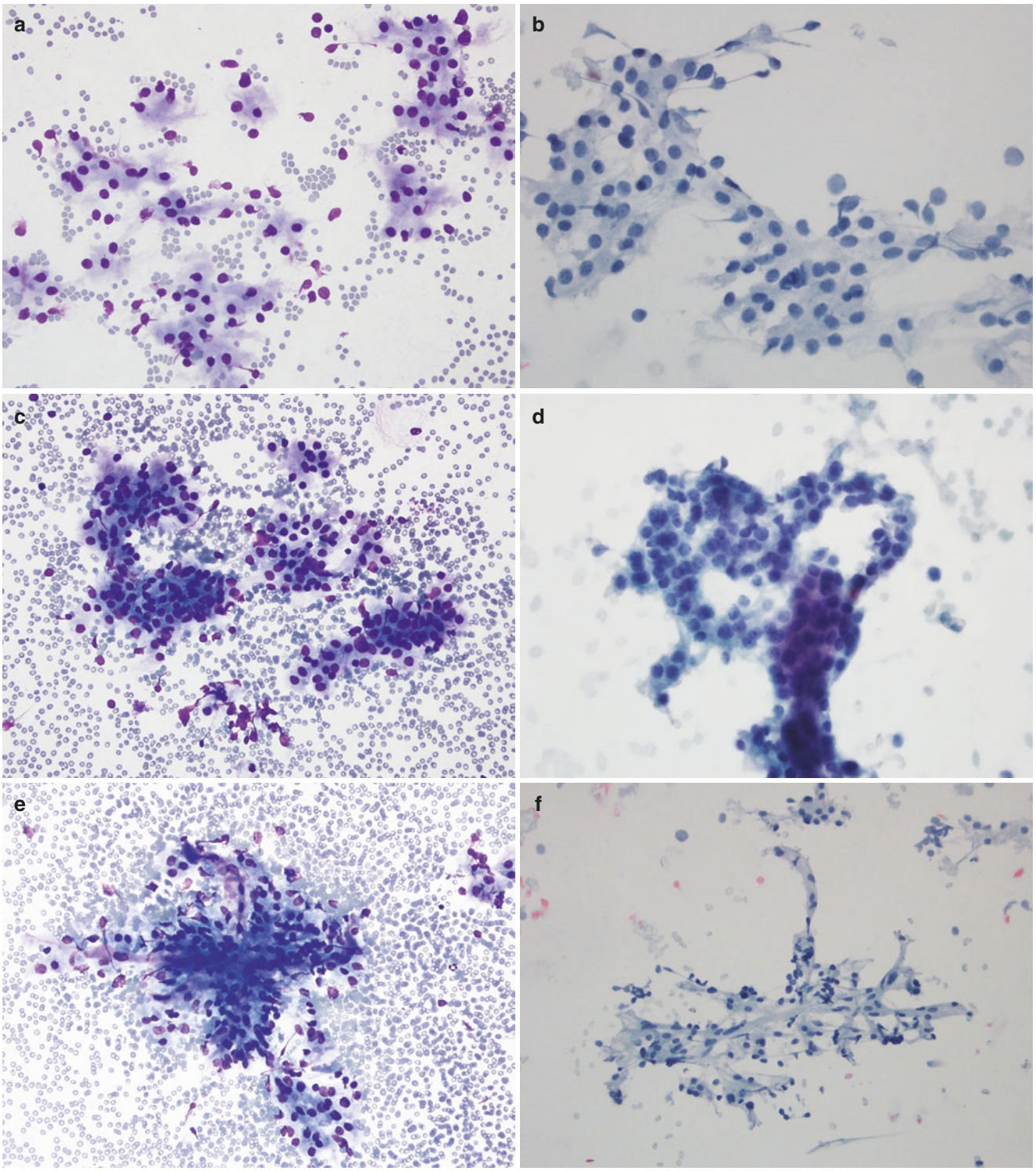

Fig. 6.12 (**a**, **b**) Normal parathyroid cells are arranged as single cells, loose two-dimensional sheets, three-dimensional clusters, and microfollicles. Cells with more abundant granular cytoplasm and prominent nuclei represent oxyphil cells while cells containing relatively smaller amounts of cytoplasm are (**c**, **d**) chief cells. (**e**, **f**) A prominent vascular network and (**g**) colloid-like material may present. (**h**) Positive immunostaining for parathyroid hormone (PTH) can facilitate confirmation of parathyroid cell origin on cell block material. Air-dried smear preparation, Diff-Quik, 20× magnification (**a**, **c**, **e**). Alcohol-fixed smear preparation, Papanicolaou stain, 20× (**f**, **g**) and 40× (**b**, **d**) magnification. Cell block, PTH immunohistochemistry, 10× magnification (**h**)

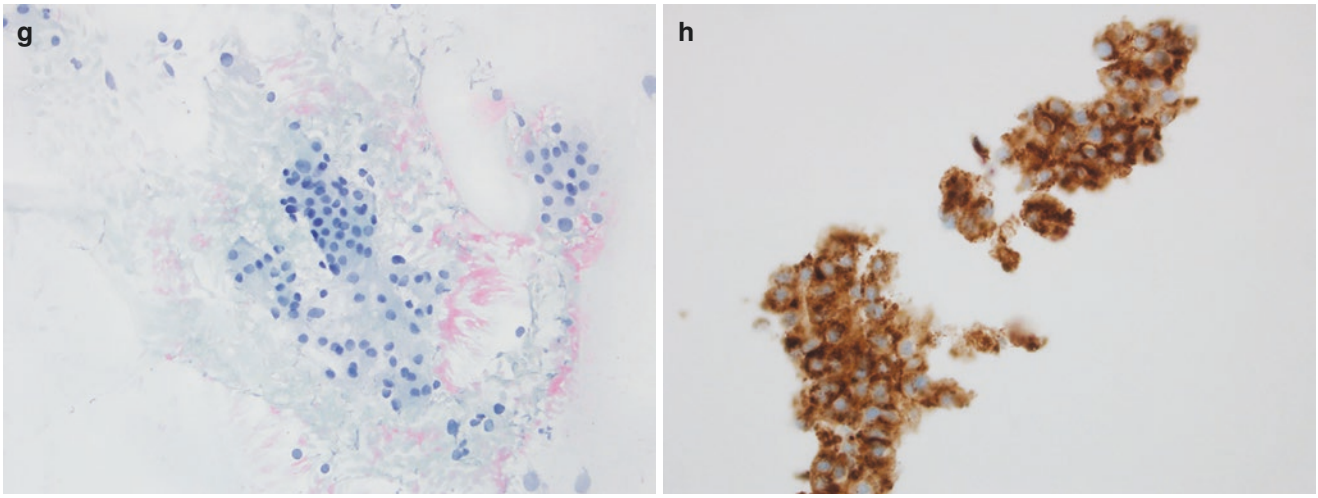

Fig. 6.12 (continued)

smears. Accordingly, ThinPrep preparation did not show papillary architecture and naked nuclei but demonstrated more microfollicles [23, 24].

Adrenal Glands

The right and left adrenal glands are each located superior and medial to the ipsilateral kidney in the retroperitoneum. These glands are composed of a cortex and medulla (Fig. 6.13a). The adrenal cortex is divided into three layers including the outer layer or zona glomerulosa, the middle layer or zona fasciculata, and the inner layer or zona reticularis (Fig. 6.13b). The adrenal cortex secretes several steroid hormones including aldosterone, glucocorticoids, and sex hormones produced by the cortical cells of the zona glomerulosa, zona fasciculata, and zona reticularis, respectively. The zona glomerulosa forms a thin layer and is located directly beneath the fibrous capsule that encompasses the adrenal gland. The cells within zona glomerulosa are arranged in tightly packed small nests with variably scant eosinophilic to amphophilic cytoplasm. In contrast, the adjacent zona fasciculata cells display voluminous finely vacuolated cytoplasm (Fig. 6.13c). The zona fasciculata accounts for the majority of the adrenal cortex and is composed of large cells with vacuolated lipid–rich cytoplasm arranged in two cell-thick cords (Fig. 6.13b, c). The cells of the zona reticularis are large cells with abundant, deeply eosinophilic cytoplasm (Fig. 6.13d). The zona reticularis cells may show prominent golden brown lipofuscin pigment within the cytoplasm (Fig. 6.13e). The central adrenal medulla is mainly composed of large polygonal chromaffin cells with large vesicular nuclei, small nucleoli, and abundant basophilic granular cytoplasm. They are arranged in small nests associated with a delicate capillary network (Fig. 6.13f). Sustentacular cells are located at the periphery of the nests, which are difficult to identify on routine H & E stain, but can be readily highlighted by an S100 immunohistochemical stain.

FNA has been a useful tool in evaluating adrenal lesions including those identified incidentally. In comparison to a percutaneous image-guided approach, endoscopic ultrasound (EUS)-guided FNA is preferred, particularly for the left adrenal gland due to markedly improved specimen adequacy, a less invasive approach, and rare post-procedure complications [25–29]. Normal elements of other viscera may be accidentally sampled in each approach as the needle may traverse other organs to collect adrenal gland samples. Aspirates of the right adrenal gland collected through the percutaneous approach may contain hepatocytes. Similarly, EUS-guided FNAs may contain glandular epithelial cells from the luminal gastrointestinal tract.

The published literature associated with FNA of adrenal glands mainly describes elements of the adrenal cortex. It has been emphasized that cells of the normal adrenal cortex cannot be distinguished from those of adrenal cortical hyperplasia and adenoma merely based on cytomorphological features, as all these three conditions exhibit overlapping cytomorphological findings. Clinical and radiological correlation thus plays an important role for accurate interpretation. FNA smears may show a lipid-rich, bubbly background characterized by small, punched-out, round vacuoles, and single and/or loose clusters of cells. The cells have ill-defined, fragile, vacuolated or foamy cytoplasm, centrally or eccentrically located round nuclei, evenly distributed chromatin, and inconspicuous or distinct nucleoli (Fig. 6.14a–d). Variation in nuclear size may be observed, and should not always be regarded as pleomorphism of neoplasia. In addition, abundant stripped nuclei in the background of large,

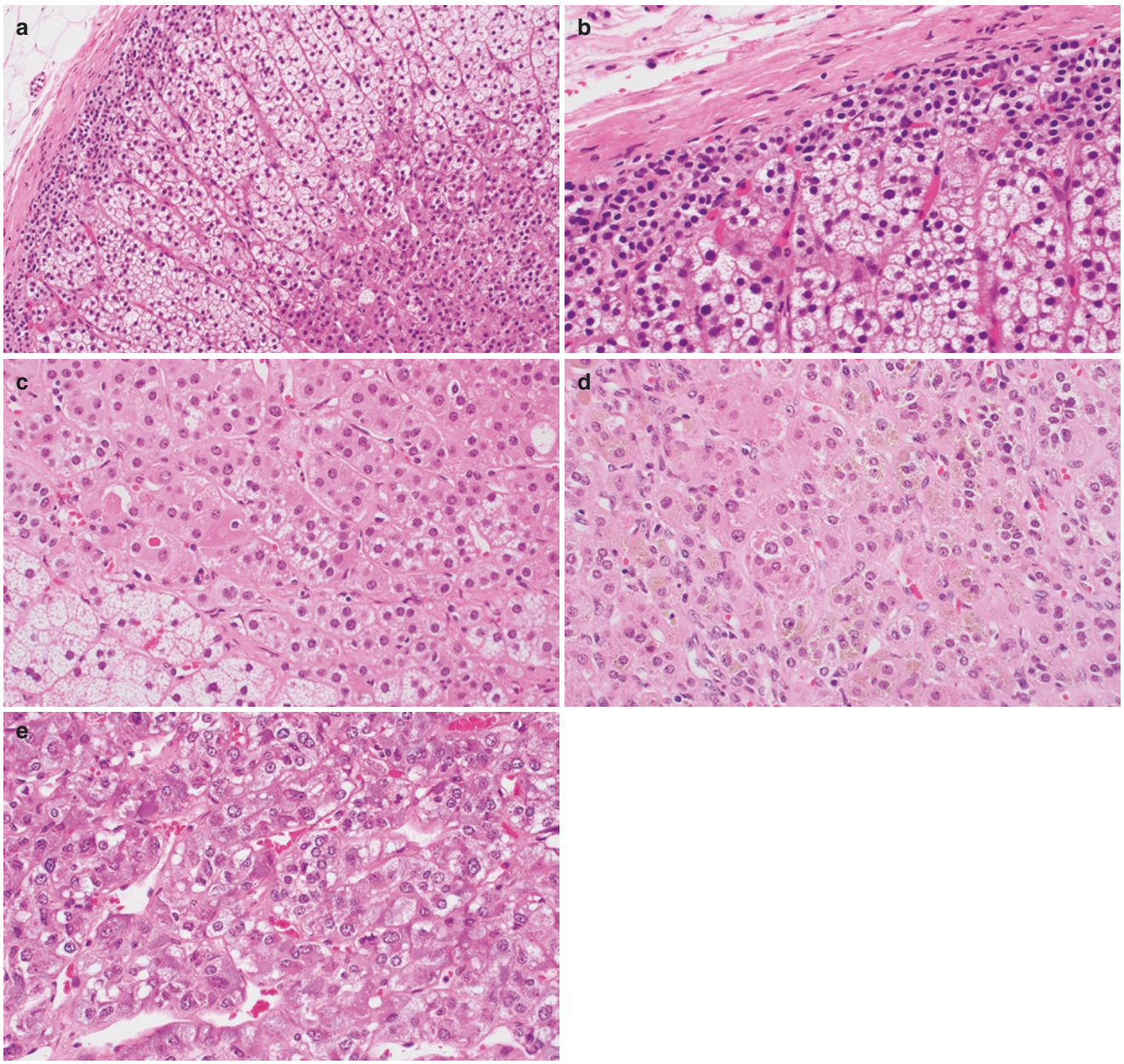

Fig. 6.13 (**a**) The adrenal cortex is composed of three distinct layers including the outermost zona glomerulosa, middle zona fasciculata, and innermost zona reticularis. (**b**) The zona glomerulosa cells are located directly underneath the capsule with scant eosinophilic to amphophilic cytoplasm in contrast to the voluminous finely vacuolated and lipid-rich cytoplasm of the zona fasciculata cells. (**c**) The zona reticularis cells are large with abundant, deeply eosinophilic cytoplasm and (**d**) occasionally display intracytoplasmic golden-brown lipofuscin pigment. (**e**) The adrenal medulla is composed of mainly large polygonal chromaffin cells arranged in small nests. Adrenal gland resection, hematoxylin & eosin, 20× (**a**) and 40× (**b**–**e**) magnification

cohesive tissue fragments composed of adrenal cortical cells (Fig. 6.14e, f) in syncytial and nested arrangements admixed with sinusoidal endothelial cells (Fig. 6.14g, h) are frequently observed. The combination of a lipid-rich, bubbly background along with bare nuclei (Fig. 6.14i–k) and large tissue fragments (Fig. 6.14l) thus favors sampling of benign adrenal gland over metastatic disease (e.g., renal cell carcinoma or hepatocellular carcinoma) [28–30]. A panel of immunohistochemistry with inhibin, PAX-8, Hep-par 1, and arginase performed on cell block material with adequate cellularity may also be helpful in delineating the etiology of cell types. Inhibin will highlight adrenal cortical cells while PAX-8 frequently highlights renal cell carcinoma and Hep-par 1 and arginase highlight hepatocytic cells.

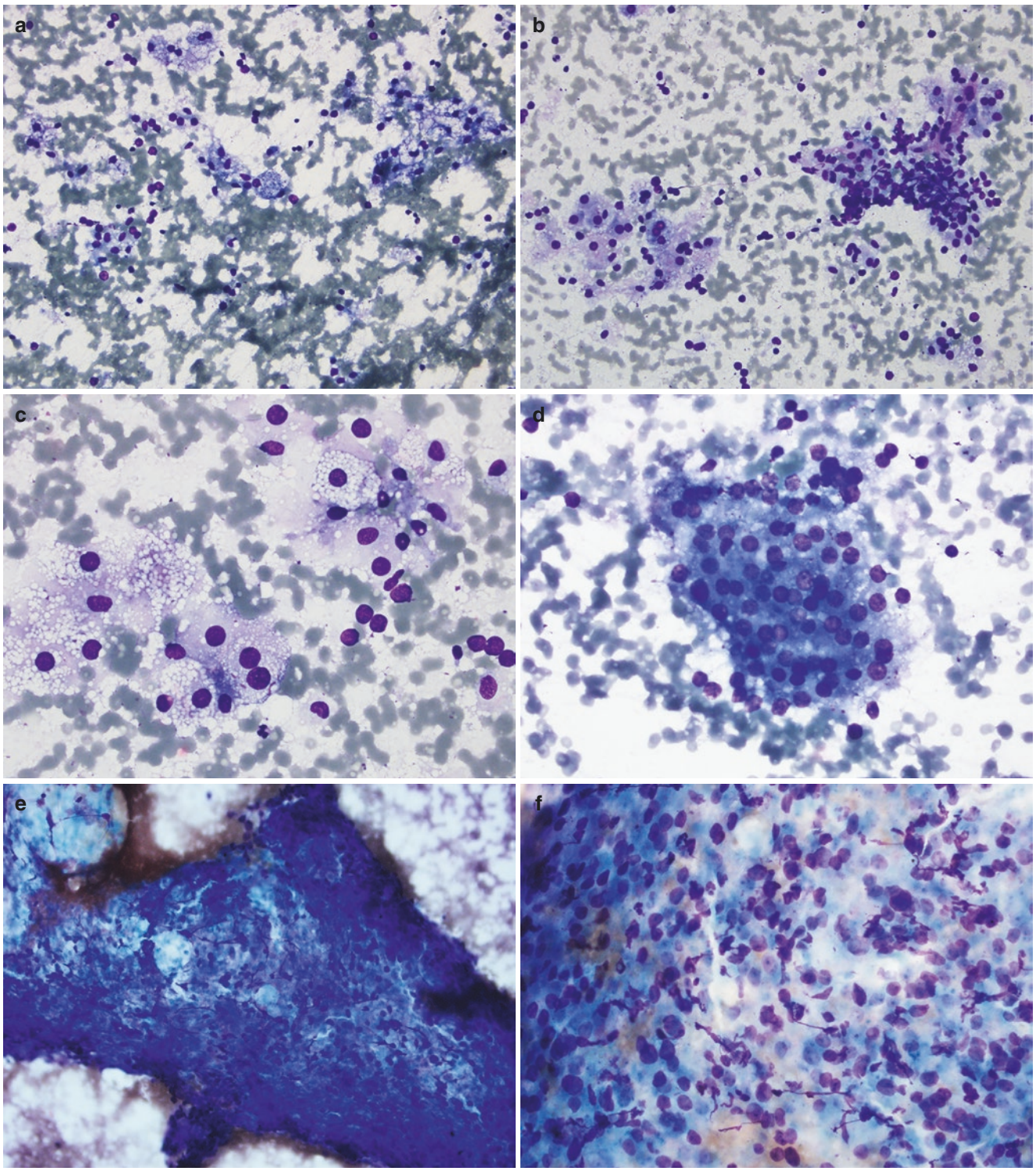

Fig. 6.14 (**a**–**d**) Adrenal cortical cells with ill-defined, vacuolated or foamy cytoplasm, centrally or eccentrically located round nuclei, evenly distributed chromatin, and inconspicuous or distinct nucleoli arranged singly and in loose clusters. (**e**, **f**) Adrenal cortical cells can also be identified in large, cohesive tissue fragments admixed with sinusoidal endothelial cells. (**g**, **h**) Abundant stripped or naked nuclei can also be seen in the background of cortical cells arranged as (**i**–**k**) clusters or (**l**) sheets. Adrenal gland, air-dried smear preparation, Diff-Quik, 20× (**a**, **b**, **e**) and 40× (**c**, **d**, **f**) magnification. Adrenal gland, alcohol-fixed smear preparation, Papanicolaou stain, 20× (**g**, **h**), 40× (**i**, **l**), and 60× (**j**, **k**) magnification

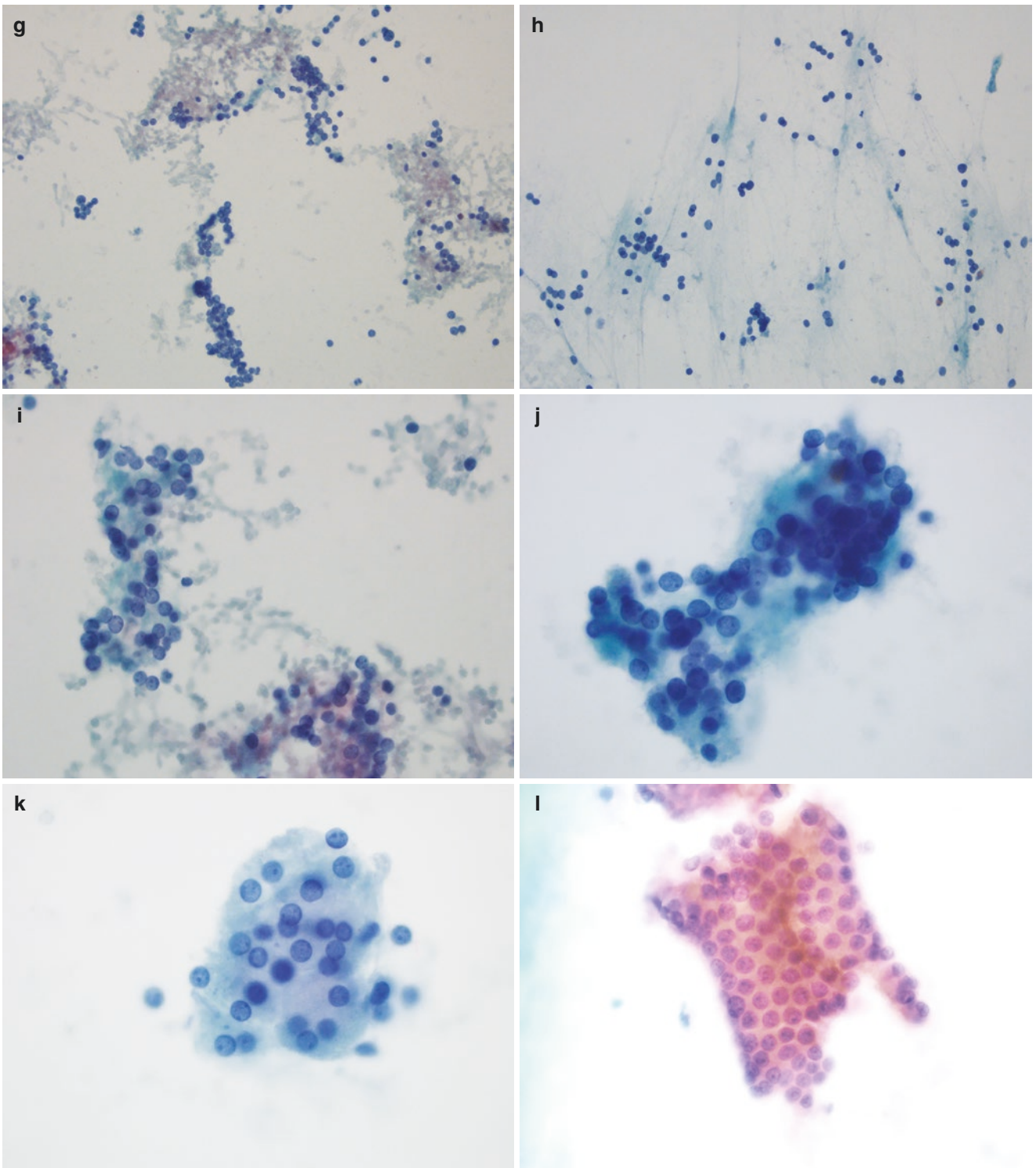

Fig. 6.14 (continued)

References

1. Mohebati A, Shaha AR. Anatomy of thyroid and parathyroid glands and neurovascular relations. Clin Anat. 2012;25(1):19–31.
2. Allen E, Fingeret A. Anatomy, head and neck, thyroid. Treasure Island, FL: StatPearls; 2020.
3. Katoh R, et al. Nature and significance of calcium oxalate crystals in normal human thyroid gland. A clinicopathological and immunohistochemical study. Virchows Arch A Pathol Anat Histopathol. 1993;422(4):301–6.
4. Shawky MS, Meyer-Rochow W. Aberrant intrathyroid tissue: a report of intrathyroid lymph node metastasis and a review of literature. Indian J Surg. 2017;79(2):148–52.
5. Herzberg AJ, Raso DS, Silverman JF. Thyroid. In: Herzberg AJ, Raso DS, Silverman JF, editors. Color atlas of normal cytology. Philadelphia: Churchill Livingstone; 1999. p. 197–8.
6. Galera-Davidson H, González-Cámpora R. Thyroid. In: Bibbo M, Wilbur D, editors. Comprehensive cytopathology. Philadelphia: Saunders Elsevier; 2008. p. 636.
7. Germano A, et al. Normal ultrasound anatomy and common anatomical variants of the thyroid gland plus adjacent structures—a pictorial review. Clin Imaging. 2019;58:114–28.
8. Richman DM, Frates MC. Ultrasound of the normal thyroid with technical pearls and pitfalls. Radiol Clin North Am. 2020;58(6):1033–9.
9. Haugen BR, et al. 2015 American Thyroid Association Management Guidelines for adult patients with thyroid nodules and differentiated thyroid cancer: the American Thyroid Association Guidelines Task Force on thyroid nodules and differentiated thyroid cancer. Thyroid. 2016;26(1):1–133.
10. Nagarajan N, et al. Conventional smears versus liquid-based preparations for thyroid fine-needle aspirates: a systematic review and meta-analysis. J Am Soc Cytopathol. 2015;4(5):253–60.
11. Cibas ES, Ali SZ. The 2017 Bethesda system for reporting thyroid cytopathology. Thyroid. 2017;27(11):1341–6.
12. Pusztaszeri M. Birefringent crystals in thyroid fine-needle aspiration cytology. Diagn Cytopathol. 2016;44(10):814–5.
13. Layfield LJ, Wax T, Jones C. Cytologic distinction of goiterous nodules from morphologically normal thyroid: analyses of cytomorphologic features. Cancer. 2003;99(4):217–22.
14. Das DK. Marginal vacuoles (fire-flare appearance) in fine needle aspiration smears of thyroid lesions: does it represent diffusing out of thyroid hormones at the base of follicular cells? Diagn Cytopathol. 2006;34(4):277–83.
15. Gupta A, et al. Cytomorphologic significance of marginal vacuoles in diffuse thyroid enlargements. J Cytol. 2013;30(2):125–9.
16. Dufour DR, Wilkerson SY. The normal parathyroid revisited: percentage of stromal fat. Hum Pathol. 1982;13(8):717–21.
17. Obara T, Fujimoto Y, Aiba M. Stromal fat content of the parathyroid gland. Endocrinol Jpn. 1990;37(6):901–5.
18. Roth SI, Capen CC. Ultrastructural and functional correlations of the parathyroid gland. Int Rev Exp Pathol. 1974;13:161–221.
19. Dimashkieh H, Krishnamurthy S. Ultrasound guided fine needle aspiration biopsy of parathyroid gland and lesions. Cytojournal. 2006;3:6.
20. Owens CL, et al. Parathyroid hormone assay in fine-needle aspirate is useful in differentiating inadvertently sampled parathyroid tissue from thyroid lesions. Diagn Cytopathol. 2008;36(4):227–31.
21. Domingo RP, et al. Identification of parathyroid tissue in thyroid fine-needle aspiration: a combined approach using cytology, immunohistochemical, and molecular methods. Diagn Cytopathol. 2017;45(6):526–32.
22. Absher KJ, et al. Parathyroid cytology: avoiding diagnostic pitfalls. Head Neck. 2002;24(2):157–64.
23. Odronic SI, Reynolds JP, Chute DJ. Cytologic features of parathyroid fine-needle aspiration on ThinPrep preparations. Cancer Cytopathol. 2014;122(9):678–84.
24. Park GS, et al. Liquid-based cytology in the fine needle aspiration of parathyroid lesions: a comparison study with the conventional smear, ThinPrep, and SurePath. Int J Clin Exp Pathol. 2015;8(10):12160–8.
25. Chang KJ, Erickson RA, Nguyen P. Endoscopic ultrasound (EUS) and EUS-guided fine-needle aspiration of the left adrenal gland. Gastrointest Endosc. 1996;44(5):568–72.
26. Fassina AS, Borsato S, Fedeli U. Fine needle aspiration cytology (FNAC) of adrenal masses. Cytopathology. 2000;11(5):302–11.
27. Lumachi F, et al. CT-scan, MRI and image-guided FNA cytology of incidental adrenal masses. Eur J Surg Oncol. 2003;29(8):689–92.
28. Jhala NC, et al. Endoscopic ultrasound-guided fine-needle aspiration biopsy of the adrenal glands: analysis of 24 patients. Cancer. 2004;102(5):308–14.
29. Stelow EB, et al. Sampling of the adrenal glands by endoscopic ultrasound-guided fine-needle aspiration. Diagn Cytopathol. 2005;33(1):26–30.
30. Wu HH, et al. Fine needle aspiration cytology of benign adrenal cortical nodules. A comparison of cytologic findings with those of primary and metastatic adrenal malignancies. Acta Cytol. 1998;42(6):1352–8.

7 Lymphoid and Hematopoietic Systems (Lymph Nodes, Thymus, Spleen, Bone Marrow)

Efrain A. Gutierrez-Lanz, Winston Y. Lee, and Liron Pantanowitz

Lymph Nodes

Lymph nodes are secondary lymphoid organs that serve as sites for mounting an adaptive immune response and are distributed along the lymphatic system throughout the body. A lymph node contains the following structures: cortex, paracortex, medulla, and a network of lymphoid sinuses (Fig. 7.1a) [1, 2].

The cortex contains scattered follicles (Fig. 7.1b) that are predominantly populated by mature B cells. In quiescence, the lymphoid follicles appear as nodular aggregates of small mature lymphocytes with condensed chromatin and are termed primary follicles [1]. During an immune response, the follicles develop germinal center reactions with the help of T-follicular helper cells and become secondary follicles, where the B cells undergo the iterative process of affinity maturation [2–4]. During this process, the B cells alter the affinity of their immunoglobulins to the targeted antigens through controlled somatic mutations. Through interactions with the targeted antigens presented by meshworks of specialized stromal cells called follicular dendritic cells (FDCs), these B cells then downregulate their proliferative activity to undergo selection. The B cells with increased affinity to an antigen will continue to proliferate while those with low affinity are negatively selected and undergo apoptosis. The apoptotic debris is subsequently engulfed by tingible body macrophages (TBMs). This process manifests as distinct anatomic compartments within the germinal center with a zone of proliferation, often referred to as the "dark zone" due to increased density of darkly stained nuclei and a zone of apoptosis, often referred to as the "light zone" due to decreased nuclear density. The proliferative B cells in the dark zone, termed centroblasts, are enlarged, have open chromatin, and multiple distinct nucleoli. In contrast, the B cells in the light zone, termed centrocytes, appear smaller in size with irregular to cleaved nuclear contours, and have condensed chromatin and inconspicuous nucleoli. The germinal center reaction iterates and ultimately affinity-matured memory B cells and plasma cells merge. Some of the stimulated naive B cells do not undergo affinity maturation and differentiate into short-lived IgM-secreting plasma cells at the medullary cords [2, 3]. In contrast, the affinity-matured plasma cells reside in the bone marrow and are long-lived to provide long-term humoral immunity [5]. Surrounding the germinal centers is an inner ring of small naive B cells, called the mantle zone, and an outer ring of memory B cells, called the marginal zone.

The paracortex, the zone of lymphocytes between cortex and medulla, is mainly populated by T cells admixed with a number of other cells types, including dendritic cells, histiocytes, immunoblasts, and plasma cells [1–4]. High endothelial venules, specialized vessels lined by tall columnar endothelial cells in the paracortex, serve as the conduit for recruiting T cells from the circulation into the lymph node as the first step of T cell activation. The dendritic cells then activate T cells through antigen presentation and co-stimulation. In the paracortex are scattered immunoblasts, which are larger lymphoid cells that represent activated T or B cells that exited from the germinal centers.

The medulla is composed of medullary cords and sinuses and serves as the entry point of the artery, veins, and afferent lymphatics at the hilum [1–4]. Medullary cords are thin protrusions of tissue enriched with lymphocytes, plasma cells, and histiocytes. The medullary sinuses are the terminal portions of a lymph drainage network in the lymph node. The lymph, carrying antigens and cells, initially enters the lymph node through the afferent lymphatics and flows through the subcapsular sinus, cortex, and paracortex, eventually draining into the medullary sinus and exiting through the efferent lymphatics.

Fine needle aspirations (FNAs) are commonly performed as the initial study to evaluate lymphadenopathy [6–9]. The

E. A. Gutierrez-Lanz · W. Y. Lee
Department of Pathology, University of Michigan, Ann Arbor, MI, USA
e-mail: efgu@med.umich.edu; winstonl@med.umich.edu

L. Pantanowitz (✉)
Department of Pathology, Michigan Medicine, Ann Arbor, MI, USA
e-mail: lironp@med.umich.edu

M. Lew et al. (eds.), *Normal Cytology*, https://doi.org/10.1007/978-3-031-20336-7_7

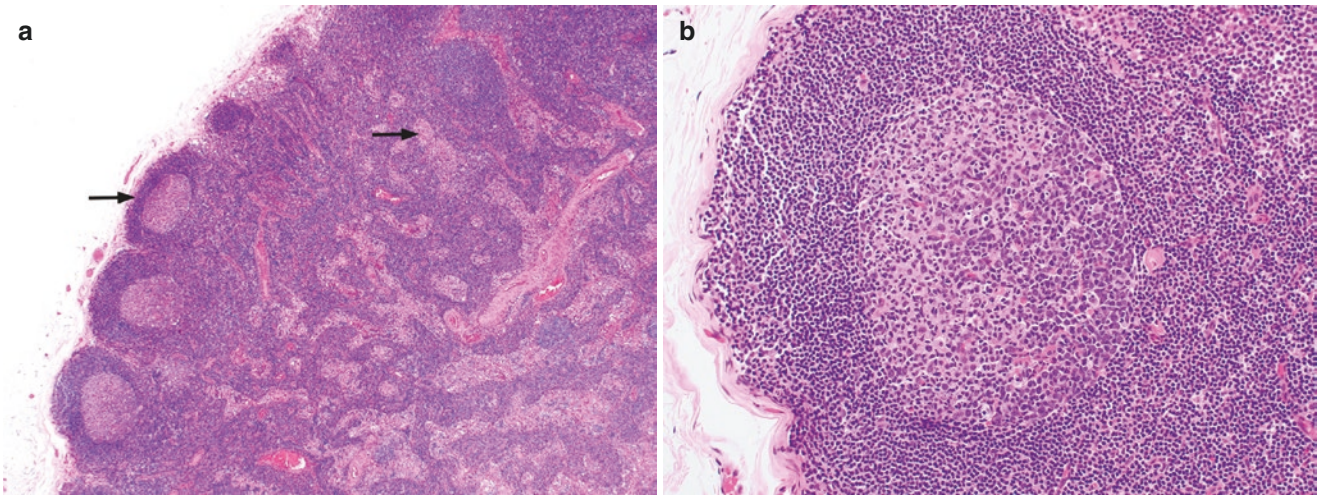

Fig. 7.1 (**a**) A normal lymph node is shown with intact architecture and well-delineated cortex, which contains follicles (left arrow), paracortex, and medulla, which contains sinuses (right arrow). (**b**) The cortex contains a secondary follicle with a polarized germinal center that includes a dark (right) and light (left) zone. Lymph node excision, hematoxylin & eosin, 5× (**a**) and 20× (**b**) magnification

differential diagnosis includes reactive lymphadenopathy, lymphoma, and metastatic cancer. FNAs can be performed readily on superficial palpable lymph nodes and safely on deep-seated lymph nodes with image guidance. Rapid on-site evaluation allows for optimal triaging of the specimen for ancillary testing, including immunohistochemistry performed on cell block preparation, flow cytometry analysis, microbial culture studies, and genetic studies.

Most sampled lymph nodes are enlarged and unlikely to be quiescent lymph nodes. Reactive lymphadenopathy is the most common nonneoplastic cause of lymphadenopathy. Subclassification of reactive lymphadenopathy is based upon nodal architectural patterns: follicular, interfollicular/mixed, predominant sinus, and diffuse patterns [10]. Each pattern can elicit a set of associated differential diagnoses. While the FNA smear samples, in principle, will reflect the cellular constituents of the lymph node, the lack of preserved tissue architecture often precludes reliable recognition of these reactive patterns [11]. Nevertheless, knowing the common cytologic features of a lymph node with nonneoplastic processes is essential in appropriately differentiating benign samples from lymphoproliferative disorders. Of note, given the lack of tissue architecture in FNA samples, low-grade lymphomas or partially involved lymph nodes by lymphoma cannot be entirely excluded on cytomorphology alone. As such, if there is a clinical suspicion of a lymphoproliferative disorder, triaging the sample for flow cytometric evaluation is essential.

FNA of a benign lymph node consists of a heterogenous (polymorphous) population of frequent small lymphocytes admixed with fewer larger lymphocytes, sinus histiocytes, and plasma cells (Fig. 7.2a). An erythrocyte or nucleus of a histocyte can be used as a reference when determining the size of a lymphocyte. A small size lymphocyte is smaller than the size of a histiocytic nucleus, an intermediate-size lymphocyte is equivalent in size, and a large size lymphocyte is bigger. On high power, distinct cell types can be recognized (Fig. 7.2b). The nonactivated T or B cells are the small lymphocytes with smooth to slightly irregular nuclear contours, dark and coarse chromatin textures, indistinct nucleoli, and scant cytoplasm. Based on cytomorphology alone, it is not possible to reliably discern T from B cells. While these small lymphocytes contain minimal cytoplasm, they can be easily disrupted during processing of smear preparations, resulting in linear streaks of DNA content in the direction the slide was smeared. This finding is often absent in liquid-based preparations. Lymphoglandular bodies, which are small, pale blue, disrupted isolated globoid fragments of cytoplasm, may be conspicuous in the background of a lymphoid population on smears (Fig. 7.3). They can mimic apoptotic debris, platelets, stain artifact, organisms, or contaminating material. Cells aspirated from germinal centers, including centroblasts, centrocytes, TBMs, and FDCs, are often present in variable numbers and are often indicative of a reactive process. However, TBMs can also be seen in certain high-

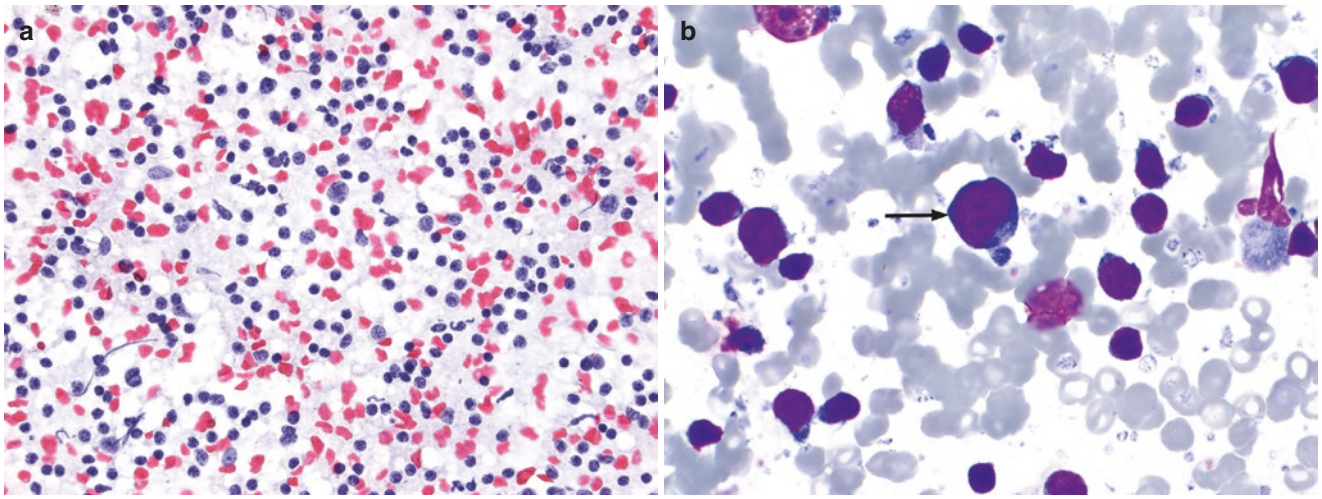

Fig. 7.2 (**a**) Direct smear of a reactive lymph node showing a polymorphous population of lymphoid cells. (**b**) At higher power, this heterogeneous population of lymphocytes includes a centroblast (arrow) and centrocytes (smaller surrounding lymphocytes). Lymph node, air-dried smear preparation, Diff-Quik, 40× (**a**) and 100× (**b**) magnification

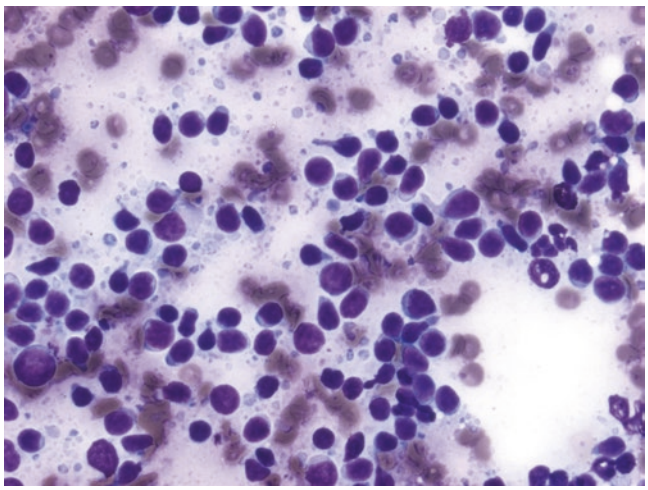

Fig. 7.3 Reactive lymph node comprised of polymorphous mature lymphocytes and many scattered small background lymphoglandular bodies. Lymph node, air-dried smear preparation, Diff-Quik, 60× magnification

grade lymphomas (e.g., Burkitt lymphoma) that undergo extensive apoptosis. Centroblasts are large cells, usually 2–3 times the size of a small lymphocyte, with round nuclear contours, vesicular chromatin, multiple distinct nucleoli, and a moderate amount of cytoplasm. Vesicular refers to a pale or open face appearance due to abundant nucleoplasm with minimal chromatin. Centrocytes are intermediate-sized cells, usually 1.5–2 times the size of a small lymphocyte, with cleaved or indented nuclear contours, condensed chromatin, inconspicuous nucleoli, and a small amount of cytoplasm. TBMs (Fig. 7.4a, b) vary in size and have oval nuclear contours, pale chromatin, occasional distinct nucleoli, a moderate to large amount of cytoplasm, and angular cellular borders, rendering an epithelioid appearance to the cells. These cells often contain intracytoplasmic phagocytic cellular debris. Sinus-type histiocytes also have abundant pale cytoplasm that is granular or vacuolated, and contain central oval or reniform-shaped nuclei with vesicular chromatin, and distinct nucleoli. Occasional plasma cells and immunoblasts can be present. Immunoblasts are large lymphocytes with dark basophilic cytoplasm, a large vesicular nucleus, and prominent single central nucleolus. Plasma cells are round to oval in shape and have abundant deep blue cytoplasm with a characteristic pale perinuclear hof that corresponds to their Golgi apparatus (Fig. 7.5). Their nucleus is typically round, eccentrically placed, has coarse chromatin in a clock-face pattern, and inconspicuous nucleoli. Mott cells are plasma cells that contain globular cytoplasmic PAS-positive inclusions of immunoglobulin called Russell bodies. Similar inclusions (Dutcher bodies) found within the nucleus are only seen in neoplastic plasma cells. Also found in aspirates with secondary follicles are scattered cohesive fragments of germinal centers (Fig. 7.6a–c), composed of centroblasts, centrocytes, small lymphocytes, FDCs, and

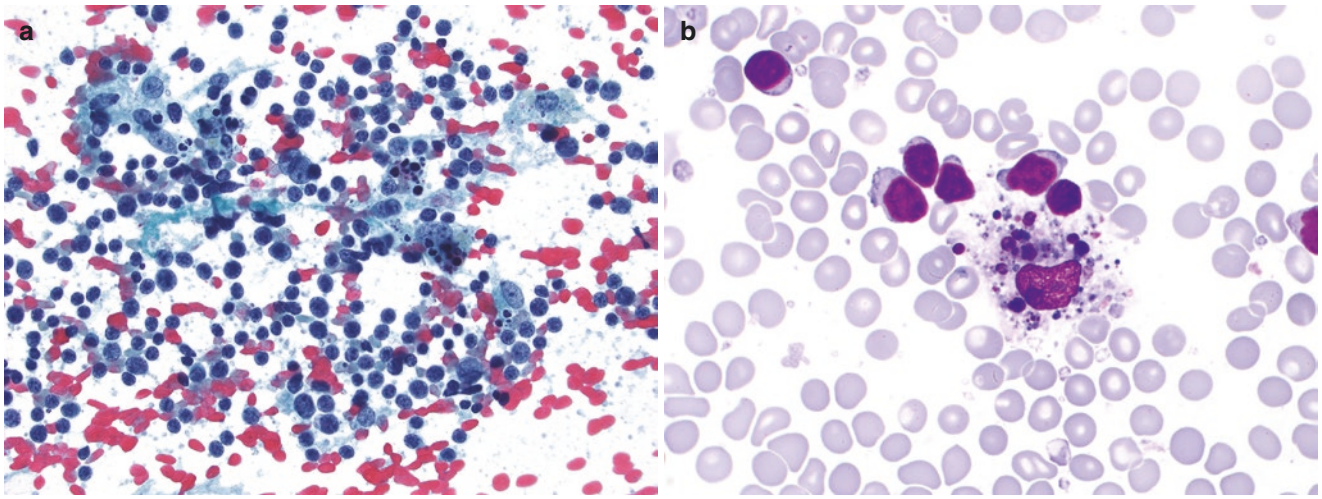

Fig. 7.4 (**a**) Reactive lymph node with several tingible body macrophages admixed with mature lymphocytes and dendritic cells. (**b**) A single tingible body macrophage with phagocytosed cellular debris. The reniform vesicular nucleus of this macrophage is of similar size to that of the nearby small lymphocytes. Lymph node, alcohol-fixed smear preparation, Papanicolaou stain, 40× magnification (**a**). Lymph node, air-dried smear preparation, Diff-Quik, 100× magnification (**b**)

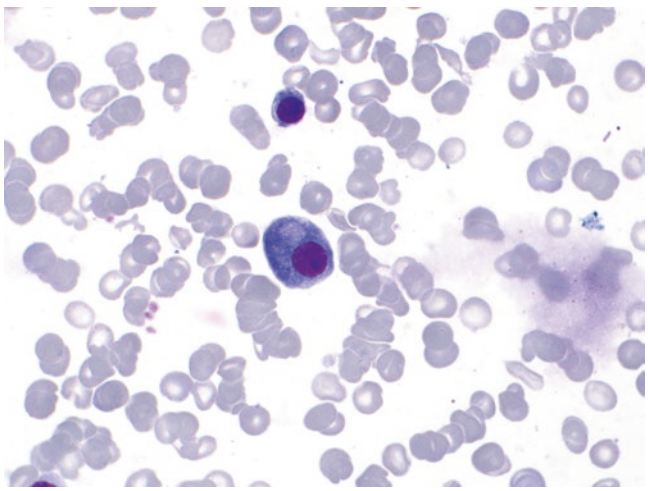

Fig. 7.5 The plasma cell in the lower field of this image has abundant basophilic cytoplasm, a pale perinuclear cytoplasmic hof, and an eccentric nucleus. The nucleus of the smaller plasma cell in the upper field of the image shows heterochromatin present in a clock-face arrangement. Air-dried smear preparation, Diff-Quik, 100× magnification

TBMs, also known as lymphohistiocytic aggregates (LHAs) [12, 13]. These follicular center structures tend to be more abundant in reactive follicular hyperplasia [14, 15] and can form flat sheets or three-dimensional cell clusters on cytologic preparations. FDCs have pale oval nuclei, delicate chromatin, small central nucleoli, and long slender cytoplasmic processes which are usually not easily seen in routine cytology preparations (Fig. 7.7a–c). They may be multinucleated, and accordingly may be mistaken for Reed-Sternberg cells as their nuclei are characteristically pressed together (kissing nuclei).

Lymph node aspirates may contain scattered fibroblasts from the nodal capsule or trabeculae, and endothelial cells from intranodal vessels. Rarely, lymph nodes may also contain adipocytes, ectopic nevus nest cells, as well as bland epithelioid cells from epithelial or mesothelial inclusions. Pigment may sometimes be identified within normal lymph nodes, such as the black anthracotic carbon pigment located within macrophages of thoracic hilar lymph nodes.

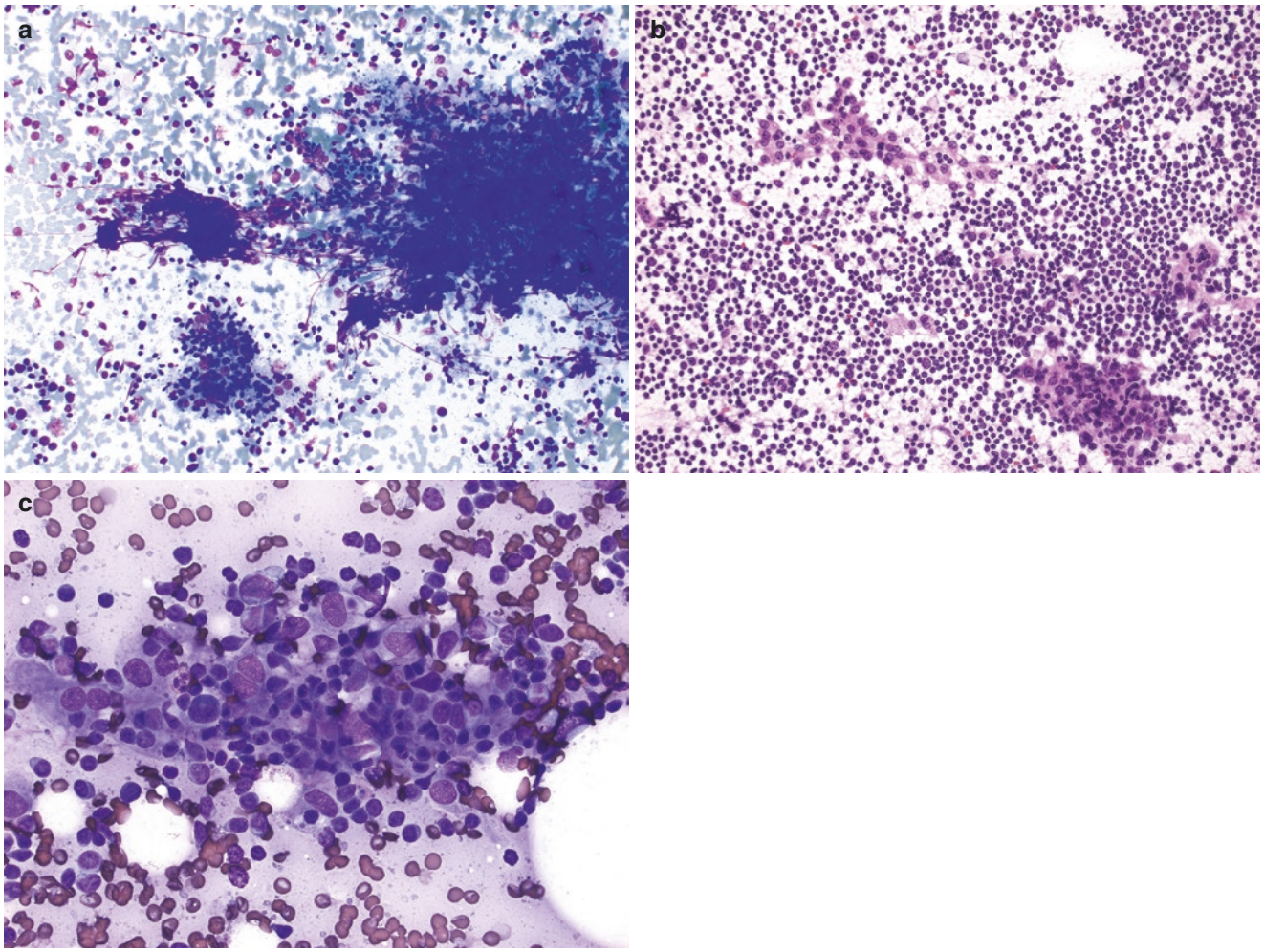

Fig. 7.6 (**a**) Lymphohistiocytic aggregates are shown representing a partially disrupted germinal center. (**b**) Cohesive dendritic cell clusters from lymphohistiocytic aggregates admixed with dispersed lymphocytes. (**c**) High power view of this lymphohistiocytic aggregate shows dendritic cells with abundant pale cytoplasm admixed with smaller mature lymphocytes. Lymph node, air-dried smear preparation, Diff-Quik, 20× (**a**) and 40× (**c**) magnification. Lymph node, air-dried smear preparation, hematoxylin & eosin, 20× magnification (**b**)

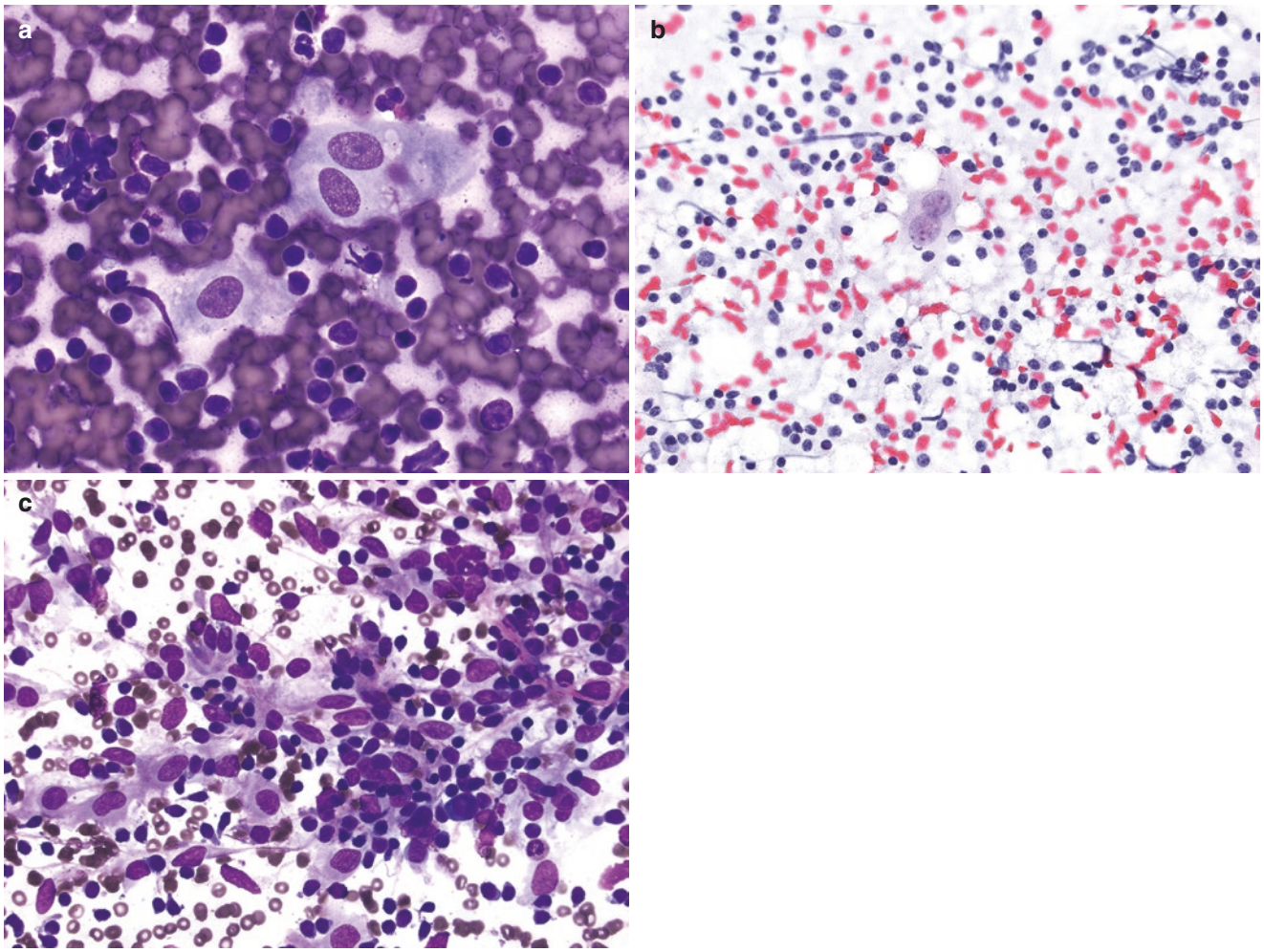

Fig. 7.7 (**a**) Follicular dendritic cells with abundant pale cytoplasm and central oval nuclei that contain delicate chromatin and small nucleoli. (**b**) A follicular dendritic cell in the center of this image with kissing nuclei. (**c**) Follicular dendritic cells with more spindle-shaped cytomorphology and long slender cytoplasmic processes. Lymph node, air-dried smear preparation, Diff-Quik, 60× magnification (**a**, **c**). Lymph node, alcohol-fixed smear preparation, Papanicolaou stain, 40× magnification (**b**)

Spleen

The spleen is a major secondary lymphoid organ located in the left upper quadrant of the abdominal cavity. Its functions include mounting an adaptive immune response against antigens captured from peripheral blood, acting as a phagocytic filter to eliminate blood-borne bacterial or parasitic organisms, as well as remove degenerated or nondeformable red blood cells. The spleen also serves as a major storage site for mature hematopoietic elements, including lymphocytes and platelets [2, 16].

The histologic features of the spleen reflect its functions. In adults, the spleen normally weighs between 115 and 139 g and is encased in a fibrous capsule with an overlying mesothelial lining [17, 18]. The spleen parenchyma can be divided into distinct histological compartments with different functions: the white pulp (Fig. 7.8a) and red pulp (Fig. 7.8b). The white pulp comprises approximately a quarter of the spleen by volume and is composed of lymphoid tissue. T cells within the white pulp are predominantly present around arterioles, forming periarteriolar lymphoid sheets (PALS), where T cell activation through antigen presentation can occur. Contiguous to the PALS, but away from the arterioles are follicles, where most of the B cells in the spleen reside. Like the lymph node, the follicles in the spleen can progress from quiescent primary follicles to active secondary follicles with germinal centers, a mantle zone and marginal zone during an adaptive immune response. The arterial system feeding the spleen eventually transitions into flexible splenic cords (of Billroth), marking the beginning of the red pulp, which comprises the remaining three quarters of the spleen by volume. As blood drains from the splenic cords (sinuses) into the venous sinusoid system, the blood cells need to pass through slit-like structures formed by a discontinuous CD8-positive endothelial lining (also known as littoral cells) [19]. Nondeformable or degen-

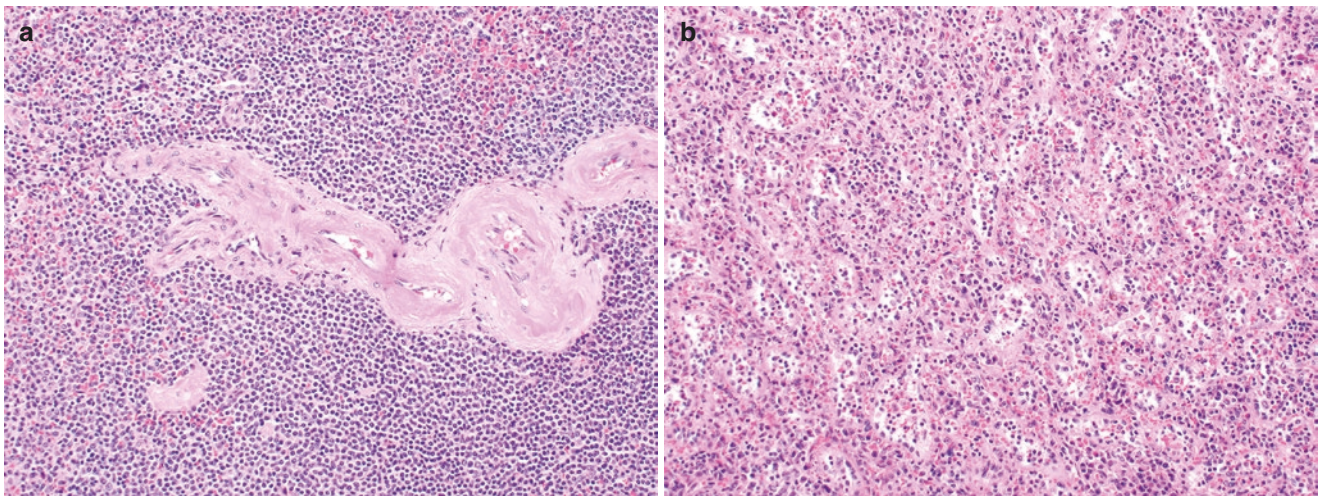

Fig. 7.8 (**a**) Spleen white pulp with a periarteriolar lymphoid sheet (PALS) and (**b**) red pulp with splenic cords containing erythrocytes. Splenectomy, hematoxylin & eosin, 20× magnification (**a**, **b**)

erated red blood cells, which fail to pass through these slits, are phagocytized by macrophages. These macrophages can also sense the presence of bacteria or parasitic organisms and hence mount an innate immune response that results in phagocytosis of these organisms or infected blood cells. The cords may also contain immature blood cells due to extramedullary hematopoiesis (EMH). EMH can be physiologic (e.g., during fetal development) or pathologic (e.g., compensatory expansion of bone marrow with severe anemia).

FNA of the spleen is not commonly performed in all regions of the world. The main indication for a splenic biopsy is to evaluate isolated splenic lesions. The diagnostic considerations include infections, inflammatory processes, sarcoidosis, vascular malformation, cystic lesions, vascular neoplasms, metastatic cancer, and lymphoma. Splenomegaly without discrete lesions is another common abnormality. The differential diagnosis in this setting includes sequestration of blood elements, infection, inflammatory processes, extramedullary hematopoiesis, and lymphoma. Many of these conditions can be diagnosed without a tissue biopsy. Rare complications from splenic FNA can occur and include splenic rupture and hemorrhage. However, a substantial number of retrospective studies have demonstrated that splenic FNA with image guidance can be done safely and effectively [20–24].

An accessory spleen presents as nodular splenic tissue found outside the spleen proper and is present in approximately 10–30% of people [25, 26]. Approximately 75% of accessory spleens are found near the hilum of the spleen. Another 20% are found in the tail of the pancreas, also known as intrapancreatic accessory spleen (IPAS). They can also rarely be found in the mesentery and other organs such as the stomach and intestine. Although these accessory spleens are small, they are histologically identical to the spleen. Importantly, these ectopically located accessory spleens can mimic mass lesions on imaging studies [27, 28]. In particular, it can be difficult to preoperatively distinguish an IPAS from a neuroendocrine tumor of the pancreas [29]. Therefore, it is important to be able to identify normal splenic cellular constituents in order to recognize an unexpected encounter of an accessory spleen in aspirate specimens. Identification of splenic littoral cells by morphologic evaluation along with the use of a CD8 immunostain on histologic or cell block material would aid in differentiating IPAS from a lymph node or nonspecific chronic inflammatory cells. Splenosis, presenting as small splenic nodules along the peritoneum resulting from splenic rupture, is another possibility of encountering splenic tissue outside the spleen proper.

The aspirate smears of a normal spleen show variable amounts of lymphoid cells with aggregates of platelets in a bloody background, representing disaggregated constituents of white and red pulps (Fig. 7.9). Occasionally, fragments of crushed white pulp with entrapped lymphocytes may be present. A predominance of small mature lymphocytes is expected. If secondary follicles are sampled, scattered centrocytes and centroblasts along with TBMs may be present. The cytology of these lymphoid cells is identical to those seen within a reactive lymph node as described above. Sometimes lymphocytes may be seen aggregating around blood vessels in a "starburst" pattern. A closer look at the bloody background reveals the presence of red pulp elements, including scattered macrophages, lymphocytes, erythrocytes, and sinusoid endothelial cells. Some of the macrophages may be laden with hemosiderin derived from phagocytosis of red blood cells. When aspirated, sinusoid endothelial cells appear spindled in shape with an oval nucleus and "double-tailed" pointy polar cytoplasmic ends, which, as noted previously, can be highlighted on cell block sections with a CD8 immunostain

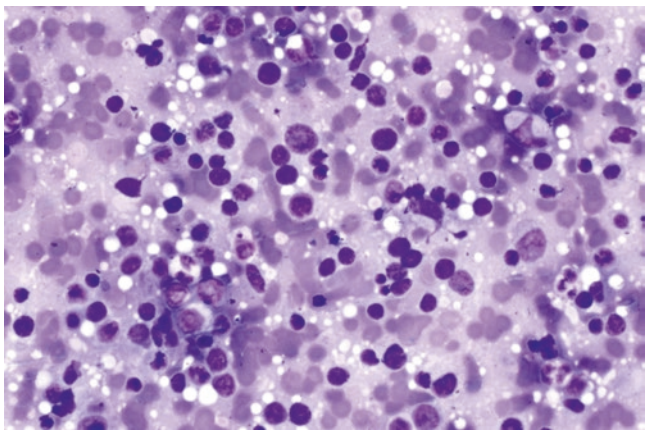

Fig. 7.9 Normal spleen showing polymorphous lymphoid cells in a bloody background. Spleen, air-dried touch preparation, Diff-Quik, 40× magnification

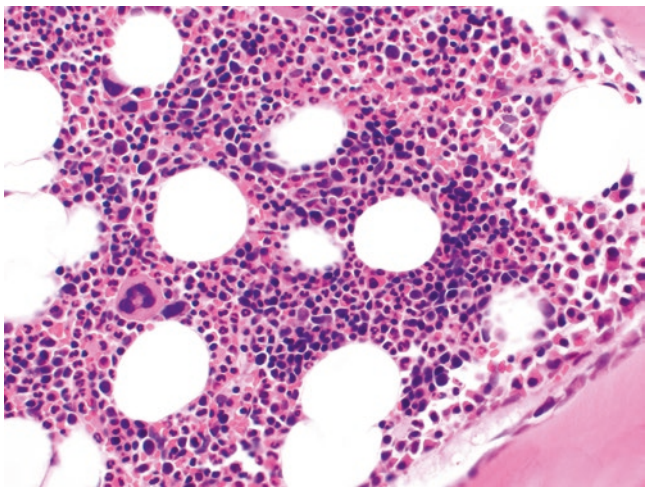

Fig. 7.10 Bone marrow with maturing myeloid elements (enriched near the bony trabecula), maturing erythroid elements (nontrabecular loose aggregates of small cells with densely stained round nuclei), and large megakaryocytes. Bone marrow core biopsy, hematoxylin & eosin, 40× magnification

Bone Marrow

Bone marrow is present in the medullary cavities in bones. The medullary cavity contains loose thin bony protrusions, also known as bony trabeculae, rendering a spongy appearance to the marrow. Grossly, marrow can be divided into yellow marrow with high fat content, serving as an energy storage, and red marrow with high blood forming activity, serving as the primary site of hematopoiesis. The marrow cellularity of hematopoietic elements is highest at birth and steadily decreases with age. In adults, the red marrow is enriched in the vertebrae, ribs, and pelvic bones [30, 31].

The process of hematopoiesis, which produces on average approximately 300 billion cells daily [32], begins with hematopoietic stem cells (HSCs). Under physiologic conditions, most of the HSCs are quiescent and reside in the endosteal niches located within a few cell lengths from the osteoblasts overlaying bony trabeculae [33–35]. When activated, HSCs migrate to the vascular niche near the marrow sinuses to undergo rapid proliferation and differentiation into cells of myeloid and lymphoid lineages. The cells of myeloid lineage include erythrocytes, megakaryocytes, granulocytes, monocytes, dendritic cells, and mast cells, whereas the cells of lymphoid lineage include T cells, NK cells, and B cells. The hierarchical trajectory of lineage differentiation branches in a tree-like pattern [35–38]. Consistent with this model of lineage differentiation, HSCs are rare, estimated to be approximately 1:10,000 cells in the marrow [39]; too few to be detected by conventional morphologic studies. The myeloid blasts, erythroid blasts, and lymphoid blasts are the earliest morphologically recognizable progenitors. The bustling activity of hematopoiesis is reflected by the histologic section of a bone marrow core biopsy, where one can observe megakaryopoiesis and progressive myeloid and erythroid maturation (Fig. 7.10). The immature myeloid cells tend to be enriched near the bony trabeculae and the sinus, while the mature myeloid cells are stored in the intervening central areas. On the other hand, the maturing erythroid elements are present as loose aggerates. Lastly, the marrow also harbors plasma cells derived from germinal center reactions [5].

Standard cytology specimens are not used to routinely assess bone marrow pathology. Instead, diagnostic evaluation of bone marrow is routinely performed by hematopathologists using a standard set of procedures, including marrow core biopsy and marrow aspirate, which is made into smears and clot sections [40]. However, bone marrow elements can be inadvertently sampled in a FNA (Fig. 7.11) of a bone lesion or a soft tissue lesion with extramedullary hematopoiesis. Occasionally, a cerebrospinal fluid (CSF) sample may also contain contaminating bone marrow cells from a misguided lumbar puncture. The differential diagnosis of a bone lesion is broad and can include reactive and neoplastic processes. Therefore, knowing the morphologic features of marrow elements will aid in diagnosis.

A marrow aspirate smear shows disaggregated marrow elements and residual nondispersed fragments of marrow. The maturing granulocytic elements and maturing erythroid elements should be the predominant cell types at a ratio of 1.2–3 (the so-called myeloid-to-erythroid ratio) with scattered megakaryocytes in the background. In addition to maturing hematopoietic elements, these bone marrow parti-

cles tend to be enriched for mast cells and other supporting cells, such as endothelial cells and mesenchymal fibrocytes. Individual cells within the spectrum of maturing myeloid and erythroid series, and megakaryocytes as well as plasma cells are best recognized on air-dried, Romanowsky-stained smears due to more pronounced cytoplasmic and nuclear details.

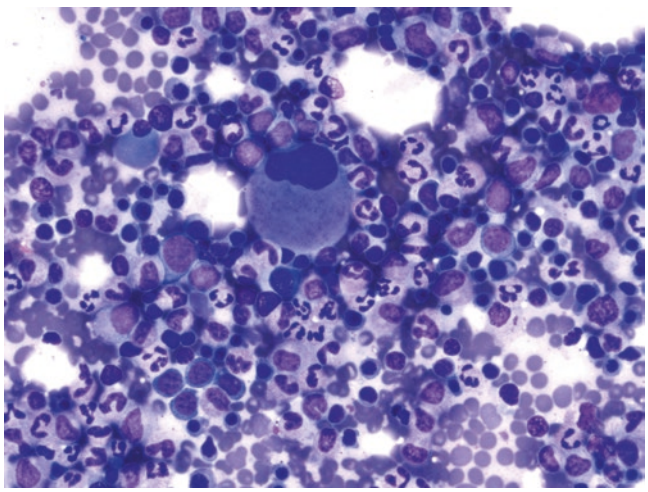

Fig. 7.11 Bone marrow showing a central megakaryocyte surrounded by maturing myeloid and erythroid cells. Bone marrow, air-dried touch preparation, Diff-Quik, 40× magnification

The maturing myeloid series is a continuum, but by convention is divided in the order of maturation into myeloblasts, progranulocytes, myelocytes, metamyelocytes, band cells, and segmented granulocytes (Fig. 7.12). Normally, the myeloblasts comprise less than 3–5% of marrow cellularity and are characterized as intermediate-sized cells with a high nuclear:cytoplasmic ratio, smooth nuclear contours, dispersed fine chromatin, variably prominent nucleoli, and a small amount of cytoplasm that may be sparsely granular. In becoming promyelocytes, their cytoplasm increases with a gain of primary/azurophilic granules, and their nuclei appear to be eccentrically displaced with retained fine chromatin texture and increasingly prominent nucleoli. The primary granules contain defensive enzymes such as myeloperoxidase, defensins, lysozymes, and others. The appearance of secondary cytoplasmic granules which contain lactoferrin, leukocyte alkaline phosphatase and other constituents, marks the transition to myelocytes. The secondary granules are lilac and pink in color and are smaller than the primary granules. At this point, the chromatin condenses and nucleoli become indistinct. As maturation toward metamyelocytes, band cells, and neutrophils continues, the chromatin continues to condense and segmentation of nuclei occurs. Other granulo-

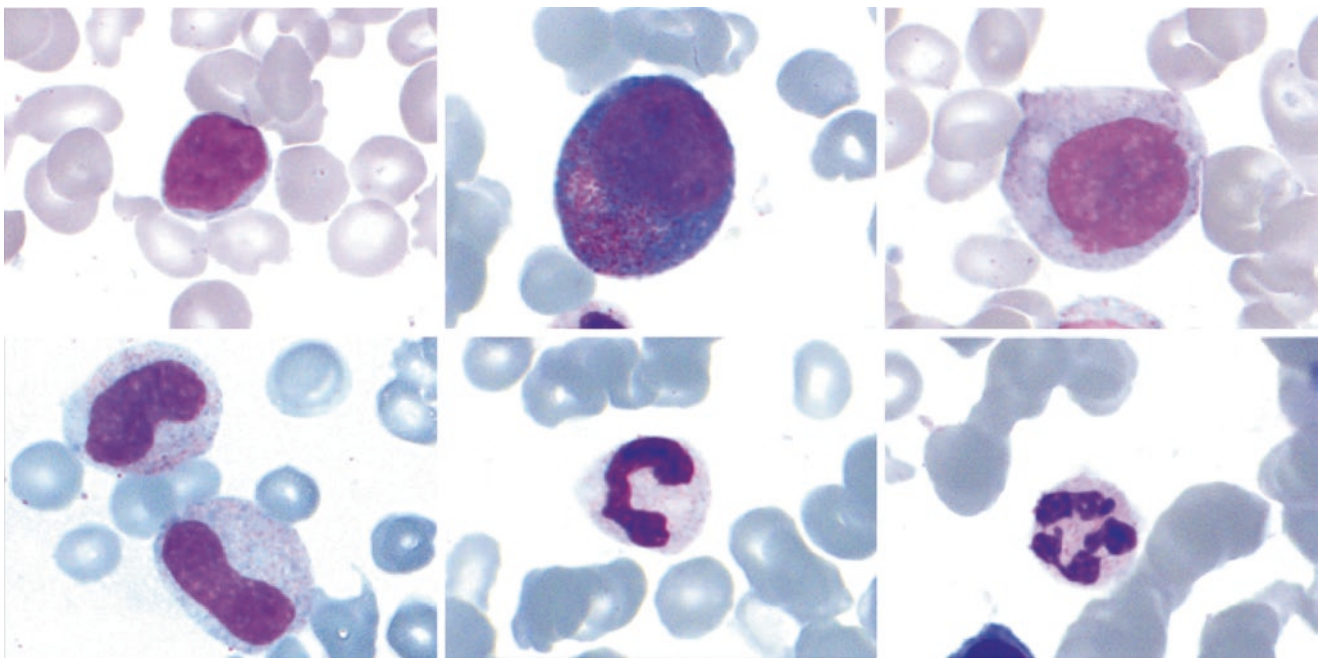

Fig. 7.12 Maturing myeloid series including: myeloblast, promyelocytes, myelocytes, metamyelocyte, band neutrophil, and segmented neutrophil (from top left to bottom right). Bone, air-dried smear preparation, Diff-Quik, 100× magnification

cytes, basophils, and eosinophils also follow a similar trajectory, but are normally fewer in number in the marrow.

The maturing erythroid series can be divided into the following stages of maturation: erythroblasts/pronormoblasts, basophilic normoblasts, polychromatophilic normoblasts, orthochromic normoblasts, reticulocytes, and red blood cells (Fig. 7.13). The erythroblasts are intermediate in size with round nuclear contours, fine chromatin texture, and a rim of deeply basophilic cytoplasm. With maturation, the chromatin condenses and the cell slightly decreases in size to become a basophilic normoblast. The production of hemoglobin synthesis marks the transition to a polychromatophilic normoblast. In becoming orthochromic normoblasts, the cell size decreases further, and the nuclei also condense further rendering a pyknotic appearance. The cells then become reticulocytes upon extrusion of their nuclei with retention of ribosomal RNAs. The extruded nuclei are ingested by macrophages. With the regression of ribosomal RNA, the erythrocyte is considered fully mature.

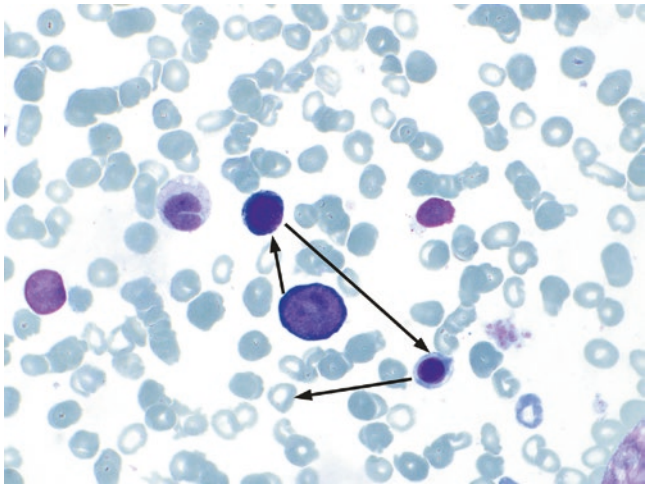

Fig. 7.13 Maturing erythroid series (arrows) including: pronormoblast, basophilic normoblast, polychromatophilic normoblast, orthochromic normoblast (not shown), and mature red blood cell. Bone, air-dried smear preparation, Diff-Quik, 100× magnification

Normal bone marrow also contains scattered megakaryocytes. They are responsible for the production of platelets. These are large cells (50–100 μm in diameter) and usually 10× larger than typical erythrocytes. They contain a single nucleus that is lobulated, has dense even or "smudged" chromatin, and no visible nucleoli. At first glance these cells may appear to contain many nuclei, but when changing planes of focus, it will be evident that these are connected lobes of a single large nucleus (Fig. 7.14a). Megakaryocytes may be mistaken for malignant cells, such as metastatic carcinoma involving the bone marrow or when present in a pleural fluid specimen (Fig. 7.14b). Other cell types that can be seen in marrow aspirates include plasma cells and monocytes, while osteoblasts and osteoclasts are infrequently present.

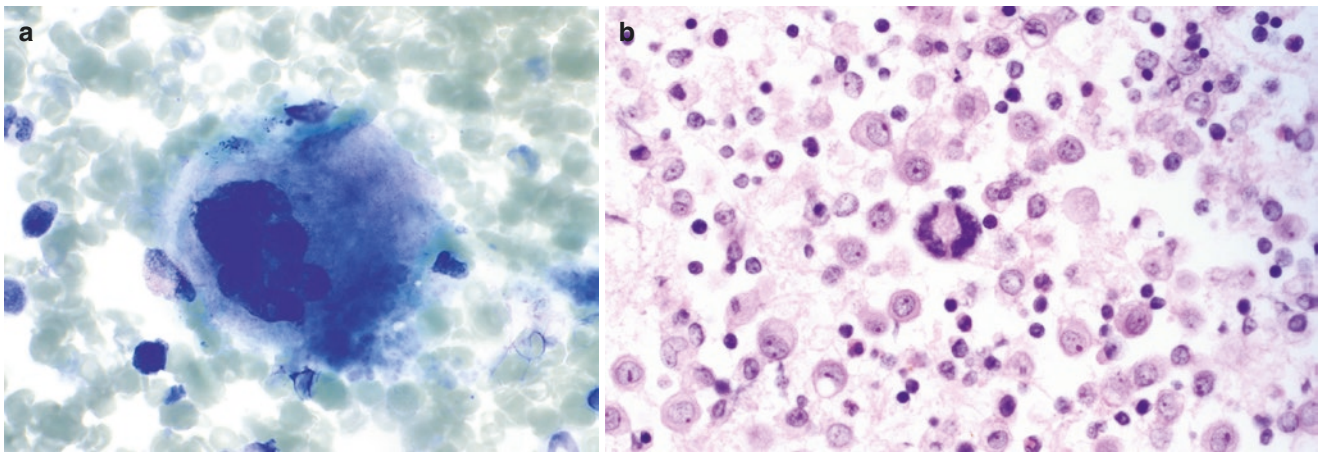

Fig. 7.14 (**a**) Megakaryocyte characterized as a large cell with abundant cytoplasm and single lobated nucleus. (**b**) A megakaryocyte is shown in the center of this pleural fluid sample surrounded by macrophages and lymphocytes. Bone, air-dried smear preparation, Diff-Quik, 100× magnification (**a**). Pleural fluid, cell block, hematoxylin & eosin, 60× magnification (**b**)

Blood and Inflammatory Cells

Blood that circulates throughout the body is comprised of red blood cells (RBCs), white blood cells (leukocytes), platelets, and plasma. Plasma is a yellow liquid that makes up about half of the blood content. It contains many proteins (e.g., clotting factors), glucose, hormones, and other dissolved chemicals. Most cytology samples, especially FNA specimens, contain contaminating blood. In fact, certain samples may only contain blood and are often considered unsatisfactory for cytologic evaluation (i.e., nondiagnostic). While cytology slide preparations are unlike formal peripheral blood smears, it is nevertheless important for cytologists to recognize normal blood elements in order to identify abnormalities (e.g., acute inflammation, chronic lymphocytic lymphoma).

Erythrocytes (RBCs), which contain hemoglobin that carries oxygen, are accountable for nearly half of the blood volume. Their life cycle is 120 days. The normal size of a RBC is 7–8 μm, which can serve as a rough guide to measure the size of other nearby cells in cytology specimens. RBCs are anucleate, uniformly round to oval, and when stained with Romanowsky stains, such as Diff-Quik, have eosinophilic cytoplasm with central pallor. RBCs may be easily disrupted with vigorous smear preparations or due to hemolytic agents included in certain liquid-based fixatives.

White blood cells (WBCs) only account for around 1% of blood and are normally manufactured from the bone marrow. They include granulocytes and monocytes. Their precursor cells (e.g., myelocytes, band cells) are normally not readily identified in peripheral blood, unless there is an abnormality (e.g., left shift or leukemoid reaction). Neutrophils are the most common WBC, but are short lived. Together with basophils and eosinophils, they belong to the polymorphonuclear (PMNs) cell family. Circulating segmented (mature) neutrophils measure 10–15 μm, are round to oval, and have a nuclear:cytoplasmic ratio of around 1:3. Their segmented nuclei are multi-lobed (2–5 connected lobes) with clumpy chromatin and no nucleoli (Fig. 7.15a, b). Their abundant pale pink cytoplasm can contain a variable amount of granules, which increase with infection (toxic granulation).

Eosinophils are the same size and shape as neutrophils. Their abundant cytoplasm contains many uniform orange-red refractile granules (Fig. 7.16a, b), which can sometimes even obscure their nuclei. With Papanicolaou-stained preparations, these granules are not well stained and are not evident. Hence, in such cytology preparations (e.g., ThinPrep) eosinophils may be mistaken as neutrophils. Most eosinophils have two equal-sized nuclear lobes connected by a thin filament. Sometimes, they can have 3–5 nuclear lobes. Prolonged eosinophilic inflammation in tissue can be associated with bipyramidal Charcot-Leyden crystals. Basophils are mostly

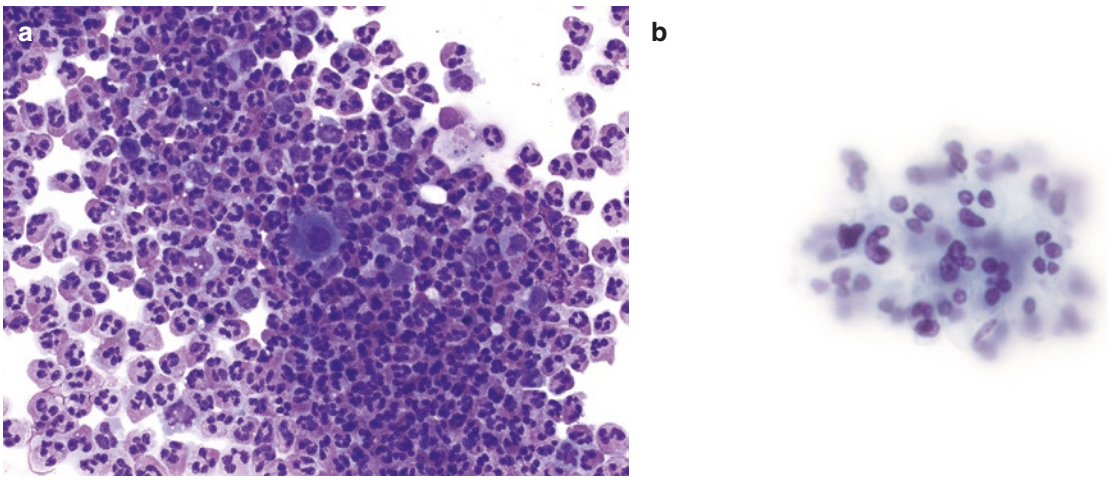

Fig. 7.15 (**a**) Abundant segmented neutrophils are shown in a pleural fluid specimen. This specimen also contains a larger central mesothelial cell and scattered admixed mononuclear lymphocytes of equivalent size. (**b**) Multilobed neutrophils are shown with indistinct cytoplasmic borders, which often occurs with liquid-based preparations. Pleural fluid, cytospin preparation, Diff-Quik, 40× magnification (**a**). Pleural fluid, ThinPrep preparation, 60× magnification (**b**)

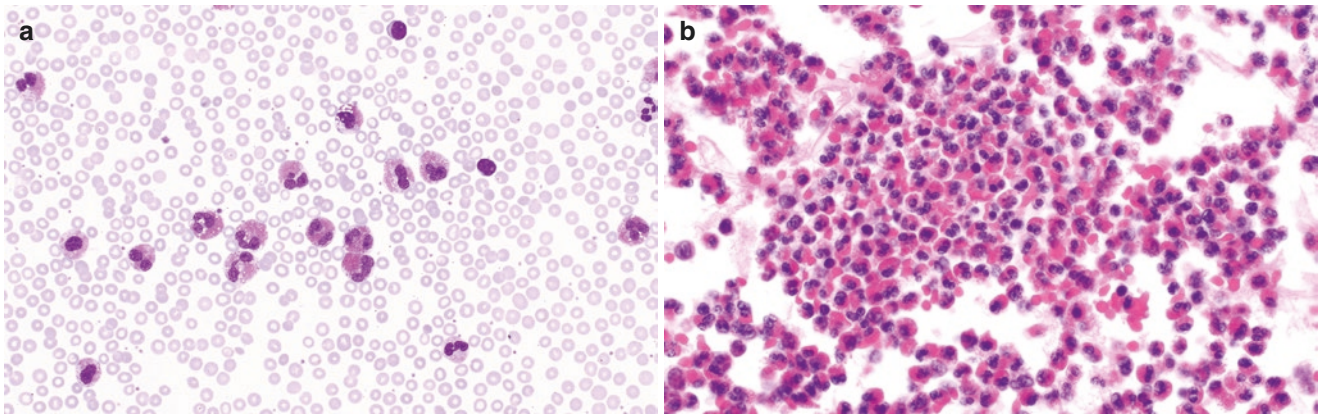

Fig. 7.16 (**a**, **b**) Numerous eosinophils characterized by orange-red cytoplasmic granules and bilobed nuclei (resembling headphones). Blood, air-dried smear preparation, Wright-Giemsa stain, 40× magnification (**a**). Cell block, hematoxylin & eosin, 60× magnification (**b**)

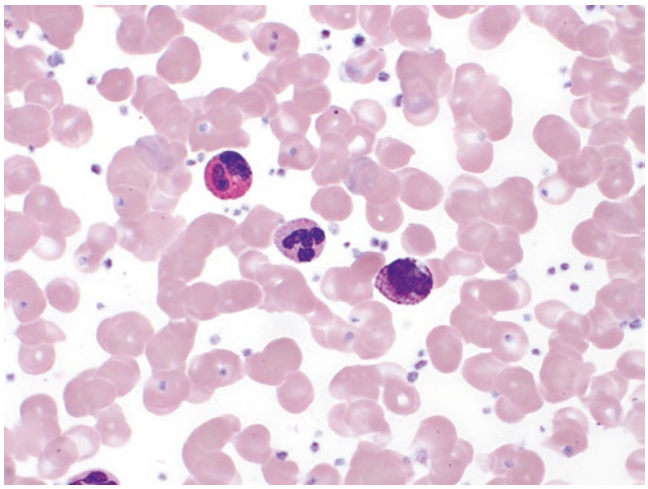

Fig. 7.17 Peripheral blood smear showing a basophil (right), a neutrophil (center), and an eosinophil (left). Blood, air-dried smear preparation, Wright-Giemsa stain, 100×

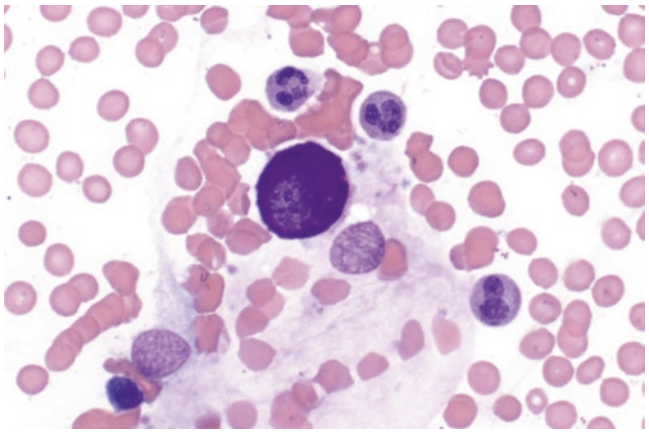

Fig. 7.18 Bone marrow aspirate showing a mast cell densely packed with cytoplasmic granules that are partially obscuring the nucleus. Bone marrow, air-dried smear preparation, Diff-Quik, 60× magnification

confined to blood (Fig. 7.17). They are similar to eosinophils, but can be differentiated because of their large, dense cytoplasmic basophilic granules. Mast cells (also known as tissue basophils) measure 15–30 μm and may vary in shape (round to spindled). Their round nuclei are often hard to visualize because their cytoplasm is densely packed with blue-black to purple metachromatic granules (Fig. 7.18). These granules contain histamine and play an important role in wound healing, immunity, and allergy. In normal connective tissue, they can usually be found near small blood vessels. Mast cells are only seen in peripheral blood in neoplastic conditions.

Monocytes are the largest of the normal blood cells (12–20 μm). They are derived from either bone marrow or splenic reserves and only circulate for up to 24 h. While they can be round, cytoplasmic extensions may confer an irregular cell shape. Their nuclear:cytoplasmic ratio is 2–4:1. They have a round or indented (reniform) nucleus, with some chromatin clumping and typically no nucleolus. Their cytoplasm when reactive may contain vacuoles. Monocytes that get recruited from the blood into tissue during inflammation or injury give rise to CD68-positive macrophages (histiocytes). Macrophages are larger than monocytes and can measure up to 80 μm. Their nuclear:cytoplasmic ratio is around 3:1 and

they have a round central nucleus with vesicular or clumped chromatin. Their nucleoli are usually small, but may become prominent when reactive. Macrophages may contain variable intracytoplasmic vacuoles, granules, and/or phagocytosed matter (e.g., hemosiderin, carbon, debris, other cells, microorganisms, foreign material) (Fig. 7.19a–c). Macrophages may coalesce to form multinucleated giant cells (MNGs) (Fig. 7.20a, b). Macrophages may also migrate into body fluids or form part of cyst fluid contents (Fig. 7.21a, b). In body cavity effusions, macrophages are smaller than mesothelial cells. Within tissues, one can also find dendritic cells including Langerhans cells in the skin, microglial cells in the brain, Kupffer cells in the liver, and osteoclasts in bone.

Lymphocytes circulate in the blood when traveling between lymphoid organs. Their average life span is 4–5 years. Mature lymphocytes appear morphologically similar, irrespective of whether they belong to the T lymphocyte, B lymphocyte, or Natural Killer (NK) subset. Flow cytometry is necessary to subtype these lymphocytes, as well as assess for their clonality. T cells, which mature in the thymus, are the main lymphoid cells (70–80%) seen in peripheral blood and functionally include T-helper (CD4+), T-regulatory, and T-suppressor/cytotoxic cells (CD8+). Normally there are fewer B cells (20–30%) in peripheral blood. NK cells comprise <10% of circulating lymphocytes. Mature lymphocytes measure

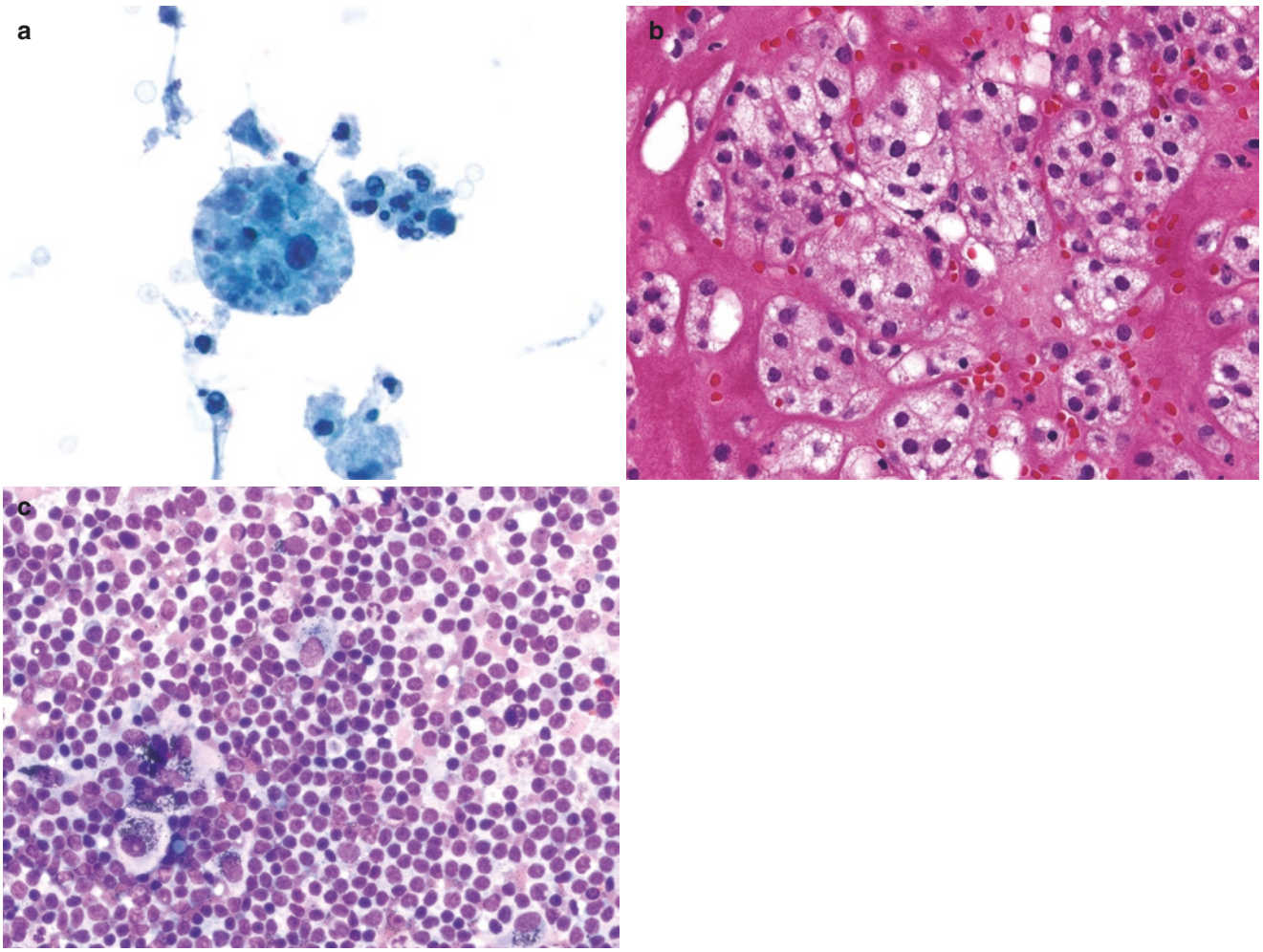

Fig. 7.19 (**a**) Macrophage with abundant cytoplasm containing phagocytosed material. (**b**) Numerous macrophages with vacuolated cytoplasm and uniform, round central nuclei in a pleural effusion. (**c**) Sinus histiocytes with black granular cytoplasmic pigment from a thoracic hilar lymph node in a background of polymorphous mature lymphocytes. ThinPrep preparation, 60× magnification (**a**). Pleural effusion, cell block, hematoxylin & eosin, 40× magnification (**b**). Lymph node, air-dried touch preparation, Diff-Quik, 40× magnification (**c**)

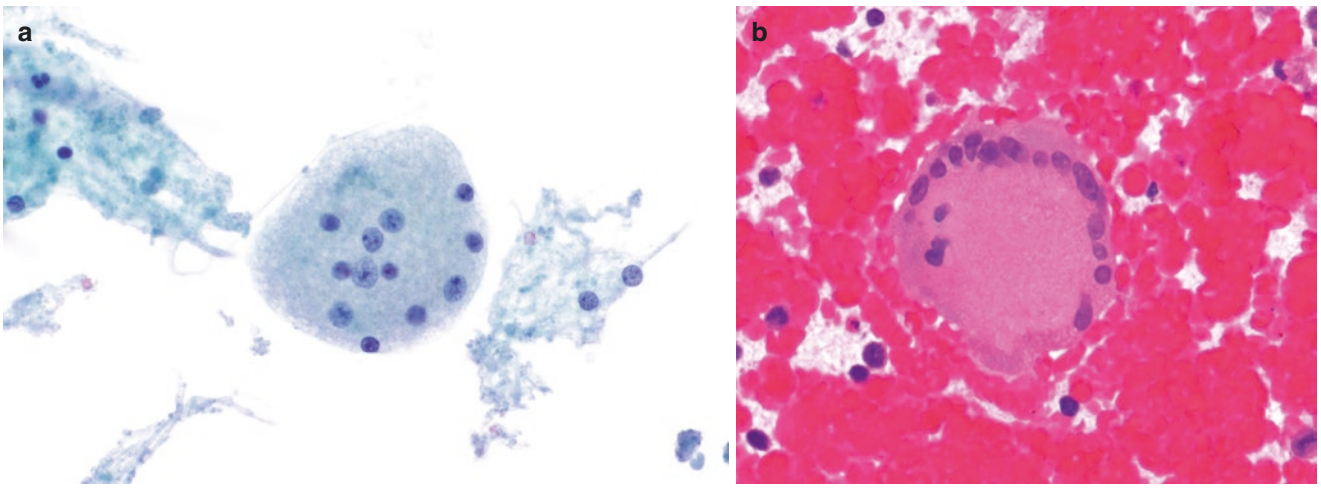

Fig. 7.20 (**a**) Multinucleated macrophage (foreign body-type giant cell) with relatively equal-sized nuclei scattered randomly throughout the cytoplasm. (**b**) Multinucleated macrophage with an arcuate arrangement of multiple nuclei along the periphery of the cell. ThinPrep preparation, 60× magnification (**a**). Cell block, hematoxylin & eosin, 40× magnification (**b**)

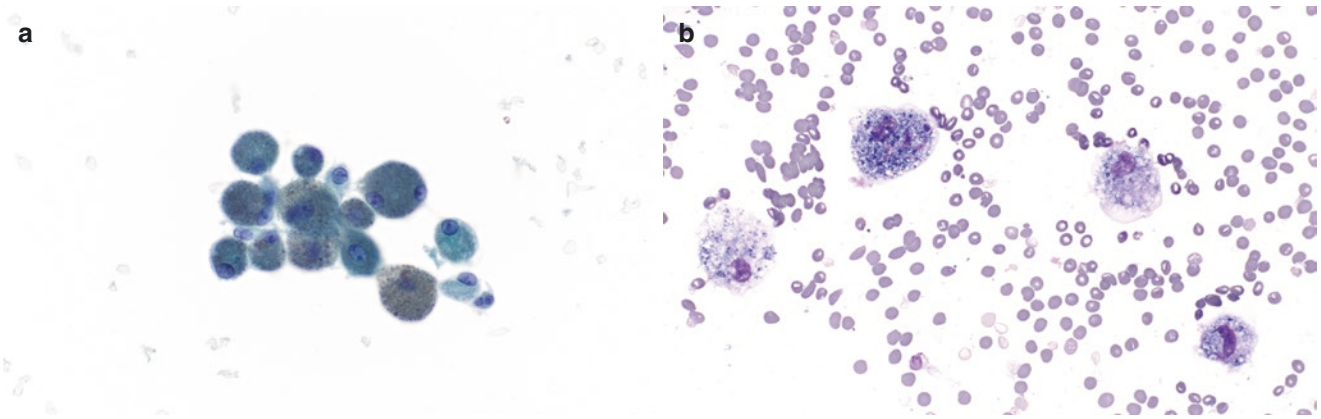

Fig. 7.21 (**a**, **b**) Macrophages within cyst fluid contents often contain abundant pigment-laden cytoplasm. The nuclei are uniform, small, round to oval, and in reactive conditions may contain a central distinct nucleolus and occasionally can be binucleate. Alcohol-fixed smear preparation, Papanicolaou stain, 40× magnification (**a**). Air-dried smear preparation, Diff-Quik, 40× magnification (**b**)

7–15 μm, are round to oval, have a relatively high nuclear:cytoplasmic ratio of 2–5:1 due to their scant agranular cytoplasm, and contain a round to oval nucleus with dense chromatin and indistinct nucleolus. Their cell edges may become frayed due to harsh smear preparation, and their nuclear material may similarly artifactually streak. Reactive lymphocytes can exhibit varying cytomorphology including taking on a plasmacytoid appearance (so-called plymphs) and/or undergo nuclear changes such as indentation (Fig. 7.22) and formation of distinct

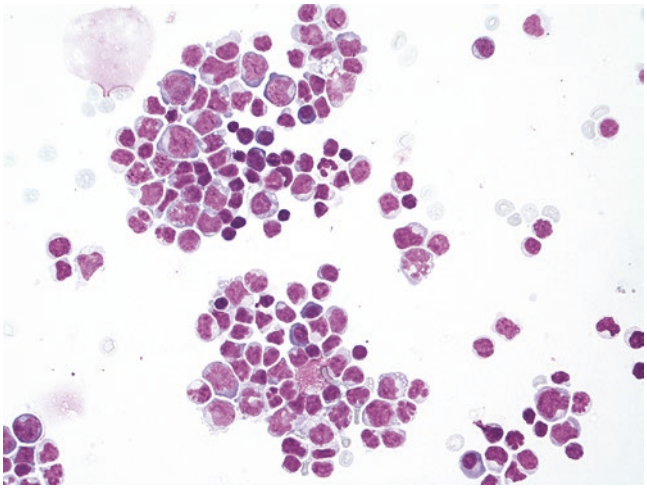

Fig. 7.22 CSF sample in a patient with lupus cerebritis showing polymorphous lymphocytes with variable cell sizes and nuclear features. Note the scattered smaller plasma cells with dark blue cytoplasm. Normal CSF should be paucicellular. CSF, cytospin preparation, Diff-Quik, 40× magnification

nucleoli. Plasma cells are rarely seen in peripheral blood and are more common constituents of various tissues (e.g., lymph node, bone marrow, spleen, soft tissue). Their cytomorphology is described above in the lymph node section (Fig. 7.5).

Platelets (thrombocytes) are the smallest blood cells (1–5 μm) and they help control bleeding. They are typically round with pale scant cytoplasm. They may be evenly distributed among RBCs or can sometimes aggregate/clump together (Fig. 7.23a, b). In FNA samples that are not immediately smeared, blood can begin to clot. In such clotted preparations, one may find clumped platelets around string-like fibrin material along with entrapped cells. Platelets can be mistaken for lymphoglandular bodies, extracellular microorganisms, or stain precipitate.

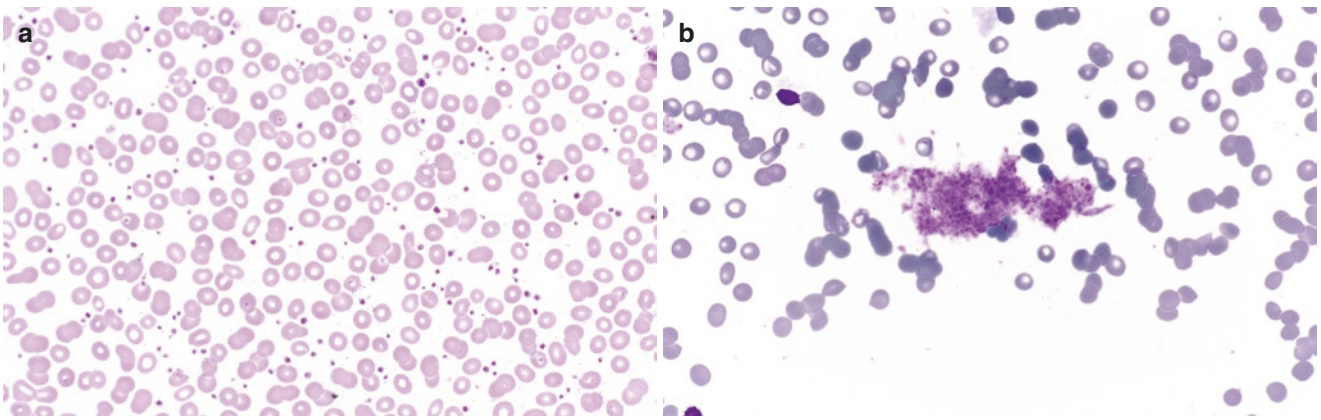

Fig. 7.23 (**a**) This peripheral blood smear is characterized by numerous anucleate erythrocytes and scattered among them are small, isolated, darkly stained platelets (thrombocytosis). Note the central pallor within the eosinophilic cytoplasm of some RBCs. (**b**) Clumped platelets. Blood, air-dried smear preparation, Wright-Giemsa stain, 60× magnification (**a**). Blood, air-dried smear preparation, Diff-Quik, 60× magnification (**b**)

Thymus

The thymus (thymic gland) is a primary lymphoid organ located in the anterior mediastinum that serves as the site of T cell selection and maturation. The production of T cells in the thymus is most active from birth to puberty [41]. In adulthood, the production of T cells steadily decreases with age, as the thymus involutes with fatty replacement. The changes in activity are reflected by changes in weight [42]. The thymus weighs 14 g on average at birth, increases to 25 g during adolescence, and steadily decreases with age. For reference, a 50-year-old person would have a thymus with an average weight of 15 g, over 50% of which is comprised of adipose tissue.

Grossly, a well-developed thymus (as seen in the first two decades of life) is composed of two connected lobes of lobulated tissue with an outline that resembles a thyme leaf. The organ is encased in a thin capsule, which extends into the parenchyma forming interlobular septa. The histological organization of the thymus is intimately linked to the process of T cell selection and maturation [41, 43, 44]. The parenchyma of the thymus contains two histologically discernable compartments: the cortex and the medulla (Fig. 7.24a). The cortex contains more lymphocytes whereas the medulla contains more thymic epithelial cells. The epithelial cells have moderate cytoplasm with thin processes, large oval nuclei, and 1–2 nucleoli.

Histologically, the cortex contains numerous densely packed small lymphocytes that greatly outnumber thymic epithelial cells. The T cells continue their path of maturation in the medulla, where they interact with specialized thymic epithelial cells capable of antigen expression from diverse tissue types. This interaction allows further editing of autoreactive T cells. Furthermore, emerging evidence suggests that these specialized epithelial cells also play an important role in the production of regulatory T cells, which are the major

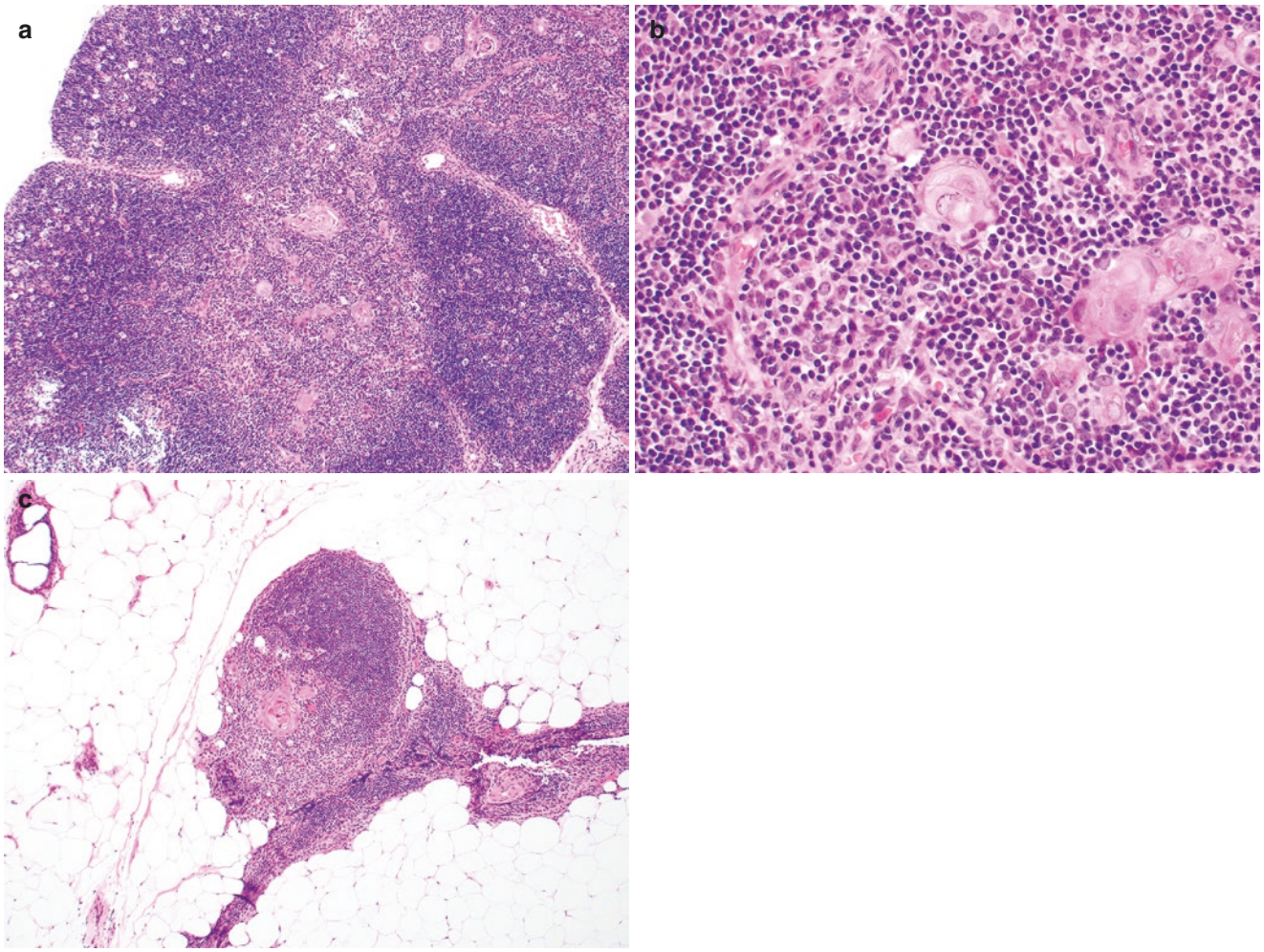

Fig. 7.24 Pediatric thymus (**a**) with well-delineated outer cortex that contains maturing thymocytes and central medulla that contains (**b**) Hassall's corpuscles. Adult thymus (**c**) with atrophic change and fatty replacement. Thymus resection, hematoxylin & eosin, 10× (**a**, **c**) and 40× (**b**) magnification

repressor cells that limit an adaptive immune response to prevent an overreactive or autoimmune response [44]. Histologically, the medulla contains two hallmark structures with a background of T cells at a lower density than those seen in the cortex. First, there are Hassall's corpuscles (Fig. 7.24b), which are distinctive structures composed of keratinizing squamous epithelial cells arranged in a whorled configuration. Hassall's corpuscles play a role in the differentiation of regulatory T cells, which function as suppressors to prevent autoimmunity [45]. They may undergo dystrophic calcification and glandular metaplasia featuring goblet, ciliated, or columnar cells. The second hallmark structure in the medulla is the perivascular space (PVS), which refers to a connective tissue structure containing blood vessels delineated by a tightly formed rim of thymic epithelial cells [46]. On histologic sections, the PVS appears as blood vessels that float in a void with a rim of epithelial cells. Often, scattered mature T cells, B cells, plasma cells, and monocytes can be present in the void. For patients under 2 years of age, mature eosinophils can be prominently present in the PVS. Despite its localization in the thymic medulla, the compartment within the PVS does not exhibit thymopoietic activity. The function of the PVS is not well-established. Some studies have suggested the possibility of an entry and exit site for lymphoid cells that may be involved in localized immune response [47, 48]. With age, the PVS increases in proportion while thymic involution occurs [46]. Therefore, in adults the thymus takes on an appearance of regressed thymic lobules with a relative prominence of medullary tissue in a background of abundant mature adipose tissue (Fig. 7.24c).

While some reports suggest that FNA has some utility in the evaluation of a thymic mass, tissue core biopsy or resection is often chosen as an alternative to allow preservation of tissue architecture, thereby providing more accurate diagnostic information. Additionally, collection of more robust tissue samples through biopsy and resection facilitates adequate sampling for ancillary tests [49–51]. The differential diagnosis of a thymic mass is broad and includes nonneoplastic and neoplastic processes. Thymic parenchymal hyperplasia, by definition, is a histologically normal thymus with increased cell number and weight. Thymic lymphoid hyperplasia refers to increased mature lymphoid cells, primarily in the medulla. Both forms of hyperplasia can be associated with autoimmune diseases, as evidenced by normalization of hyperplasia upon successful treatment of Graves' disease [52]. Thymic cysts, if unilocular, are likely developed during embryological development. Multilocular thymic cysts, on the other hand, are likely acquired and may be associated with inflammation [53].

Recognizing the cytologic features of thymic tissue, including ectopic tissue, on an aspirate smear can avoid misdiagnosis. Unexpected sampling of normal thymic tissue may mislead one to interpret the cellular constituents, such as maturing lymphocytes as acute lymphoblastic lymphoma, or thymic epithelial cells as carcinoma. Ectopic thymic tissue can be present along the track of thymic descent to the anterior mediastinum from the third and fourth pharyngeal pouches during embryological development [54]. Common sites of ectopic thymic tissue include the parathyroid glands, thyroid gland, paratracheal region, submandibular region, and, less commonly, other anatomic locations within the mediastinum, such as the posterior mediastinum [55].

Sampling of well-developed pediatric thymic tissue by FNA often demonstrates a predominance of heterogeneous small lymphocytes admixed with discohesive epithelioid to spindle-shaped oncocytic thymic epithelial cells (Fig. 7.25). The epithelial cells can form clusters. Lymphocytes may form a cuff around these groups and also infiltrate between the epithelial cells. Thymocytes can be of varied shape (usually round to polygonal) and contain a round to oval nucleus with finely granular cytoplasm and small nucleolus. Hassall's corpuscles and TBMs are infrequently present [56]. Hassall's corpuscles when aspirated will yield keratinized squamous cells. Admixed adipocytes, granulocytes, histiocytes, dendritic cells, and plasma cells are also infrequently present. In patients less than 2 years old, a prominence of mature eosinophils can sometimes be observed [46]. The predominant lymphocytes are composed of T cells at different stages of maturation. Scattered lymphoid cells with blastoid features are expected, but also

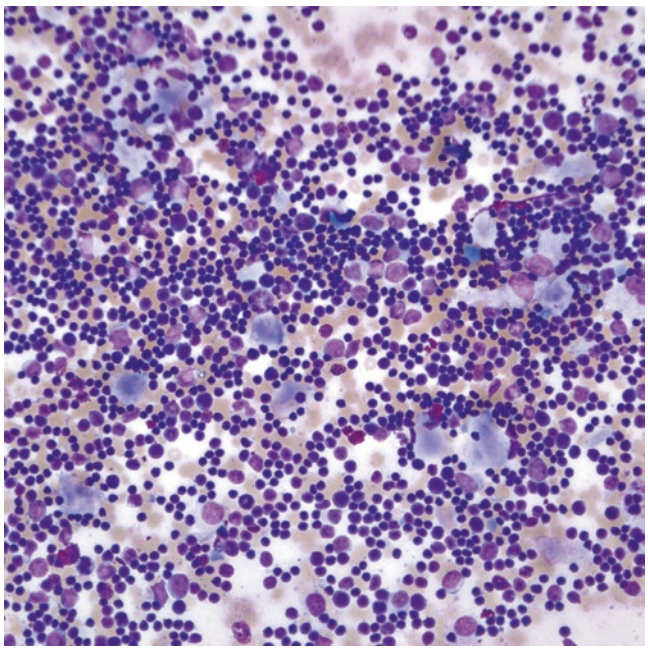

Fig. 7.25 Pediatric thymus showing a polymorphous lymphoid population. Thymus, air-dried smear preparation, Diff-Quik, 40× magnification

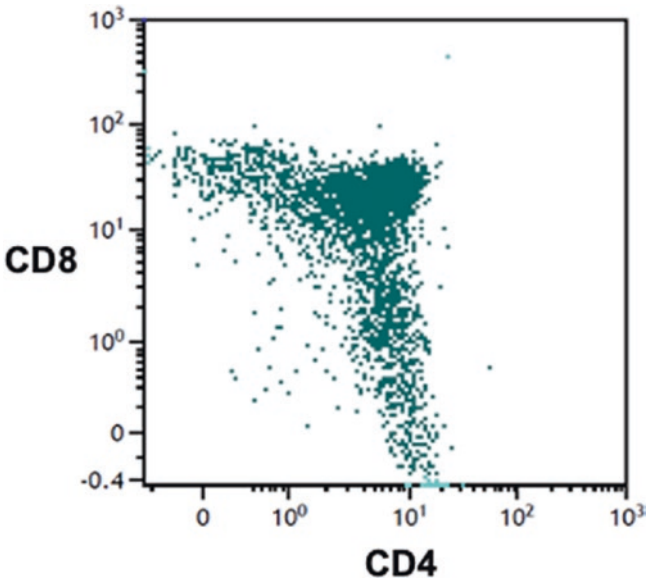

Fig. 7.26 Flow cytometry analysis of a normal thymus demonstrating maturing thymocytes (gated on CD3 positive cells) with single CD4 or CD8 positive as well as CD4/CD8 double positive populations

raise the differential diagnosis of lymphoblastic lymphoma. Further evaluation by flow cytometry analysis can confirm the diagnosis of normal thymic tissue. Specifically, the maturing T cells will appear heterogenous and include populations of CD4+ T cells, CD8+ T cells, and T cells doubly positive for CD4 and CD8, which also partially co-express immature markers, such as TdT and CD1a (Fig. 7.26). In contrast, a T lymphoblastic lymphoma will lack heterogeneity and often exhibit immunophenotypic aberrancy. These cytologic features are not unique to benign thymic tissue but can also be seen in ectopic thymic tissue and lymphocyte-rich thymoma [57].

References

1. Campo E, Jaffe ES, Harris NL. Normal lymphoid organs and tissues. In: Jaffe ES, Arber DA, Campo E, Harris NL, Quintanilla-Martinez L, editors. Hematopathology. 2nd ed. Philadelphia, PA: Elsevier; 2011. p. 97–117.
2. Murphy K, Weaver C. The humoral immune response. In: Murphy K, Weaver C, editors. Janeway's immunobiology. 9th ed. New York, NY: Garland Science/Taylor and Francis; 2017. p. 406–13.
3. De Silva NS, Klein U. Dynamics of B cells in germinal centres. Nat Rev Immunol. 2015;15(3):137–48.
4. Victora GD, Nussenzweig MC. Germinal centers. Annu Rev Immunol. 2012;30:429–57.
5. Radbruch A, Muehlinghaus G, Luger EO, Inamine A, Smith KGC, Dörner T, et al. Competence and competition: the challenge of becoming a long-lived plasma cell. Nat Rev Immunol. 2006;6(10):741–50.
6. Nasuti JF, Gupta PK, Baloch ZW. Diagnostic value and cost-effectiveness of on-site evaluation of fine-needle aspiration specimens: review of 5,688 cases. Diagn Cytopathol. 2002;27(1):1–4.
7. Stewart CJR, Duncan JA, Farquharson M, Richmond J. Fine needle aspiration cytology diagnosis of malignant lymphoma and reactive lymphoid hyperplasia. J Clin Pathol. 1998;51(3):197–203.
8. Hsu C, Leung BSY, Lau S-K, Sham JST, Choy D, Engzell U. Efficacy of fine-needle aspiration and sampling of lymph nodes in 1,484 Chinese patients. Diagn Cytopathol. 1990;6(3):154–9.
9. Frederiksen JK, Sharma M, Casulo C, Burack WR. Systematic review of the effectiveness of fine-needle aspiration and/or core needle biopsy for subclassifying lymphoma. Arch Pathol Lab Med. 2015;139(2):245–51.
10. Hsi ED, Schnitzer B. Chapter 9. Reactive lymphadenopathies. In: Jaffe ES, Arber DA, Campo E, Harris NL, Quintanilla-Martinez L, editors. Hematopathology. 2nd ed. Philadelphia, PA: Elsevier; 2017. p. 153–78.
11. Monaco SE, Khalbuss WE, Pantanowitz L. Benign non-infectious causes of lymphadenopathy: a review of cytomorphology and differential diagnosis. Diagn Cytopathol. 2012;40(10):925–38.
12. DeMay RM. Lymph nodes. In: DeMay RM, editor. Practical principles of cytopathology. Chicago, IL: American Society for Clinical Pathology; 2007. p. 227–79, revised edition.
13. Wieczorek TJ, Wakely PE. Lymph nodes. In: Cibas E, Ducatman B, editors. Cytology diagnostic principles and clinical correlates. 5th ed. Philadelphia, PA: Elsevier; 2020. p. 379–424.
14. O'Dowd GJ, Frable WJ, Behm FG. Fine needle aspiration cytology of benign lymph node hyperplasias. Diagnostic significance of lymphohistiocytic aggregates. Acta Cytol. 1985;29(4):554–8.
15. Suh YK, Shabaik A, Meurer WT, Shin SS. Lymphoid cell aggregates: a useful clue in the fine-needle aspiration diagnosis of follicular lymphomas. Diagn Cytopathol. 1997;17(6):467–71.
16. van Krieken JHJM, Orazi A. Spleen. In: Mills SE, editor. Histology for pathologists. 5th ed. Philadelphia, PA: Wolters Kluwer Health; 2020. p. 799–852.
17. Molina DK, DiMaio VJM. Normal organ weights in men: part II-the brain, lungs, liver, spleen, and kidneys. Am J Forensic Med Pathol. 2012;33(4):368–72.
18. Molina DK, DiMaio VJM. Normal organ weights in women: Part II-The brain, lungs, liver, spleen, and kidneys. Am J Forensic Med Pathol. 2015;36(3):182–7.
19. Steiniger BS. Human spleen microanatomy: why mice do not suffice. Immunology. 2015;145(3):334–46.
20. Barone S, Baer MR, Sait SNJ, Lawrence D, Block AW, Wetzler M. Ultrasound-guided fine needle biopsy of the spleen: high clinical efficacy and low risk in a multicenter Italian study. Am J Hematol. 2001;67(2):93–9.
21. Caraway NP, Fanning CV. Use of fine-needle aspiration biopsy in the evaluation of splenic lesions in a cancer center. Diagn Cytopathol. 1997;16(4):312–6.
22. Gómez-Rubio M, López-Cano A, Rendón P, Muñoz-Benvenuty A, Macías M, Garre C, et al. Safety and diagnostic accuracy of percutaneous ultrasound-guided biopsy of the spleen: a multicenter study. J Clin Ultrasound. 2009;37(8):445–50.
23. Kang M, Kalra N, Gulati M, Lal A, Kochhar R, Rajwanshi A. Image guided percutaneous splenic interventions. Eur J Radiol. 2007;64(1):140–6.
24. Zeppa P, Vetrani A, Luciano L, Fulciniti F, Troncone G, Rotoli B, et al. Fine needle aspiration biopsy of the spleen: a useful procedure in the diagnosis of splenomegaly. Acta Cytol. 1994;38(3):299–309.
25. Varga I, Babala J, Kachlik D. Anatomic variations of the spleen: current state of terminology, classification, and embryological background. Surg Radiol Anat. 2018;40(1):21–9.
26. Vikse J, Sanna B, Henry BM, Taterra D, Sanna S, Pękala PA, et al. The prevalence and morphometry of an accessory spleen: a meta-analysis and systematic review of 22,487 patients. Int J Surg. 2017;45:18–28.
27. Bhutiani N, Egger ME, Doughtie CA, Burkardt ES, Scoggins CR, Martin RCG, et al. Intrapancreatic accessory spleen (IPAS):

a single-institution experience and review of the literature. Am J Surg. 2017;213(4):816–20.
28. Tatsas AD, Owens CL, Siddiqui MT, Hruban RH, Ali SZ. Fine-needle aspiration of intrapancreatic accessory spleen: cytomorphologic features and differential diagnosis. Cancer Cytopathol. 2012;120(4):261–8.
29. Kim G, Morris J, Anand N, Depalma F, Greenwald B, Kim R, et al. Recognizing intrapancreatic accessory spleen via EUS: interobserver variability. Endosc Ultrasound. 2019;8(6):392–7.
30. Hayman JA, Callahan JW, Herschtal A, Everitt S, Binns DS, Hicks RJ, et al. Distribution of proliferating bone marrow in adult cancer patients determined using FLT-PET imaging. Int J Radiat Oncol Biol Phys. 2011;79(3):847–52.
31. Campbell BA, Callahan J, Bressel M, Simoens N, Everitt S, Hofman MS, et al. Distribution atlas of proliferating bone marrow in non-small cell lung cancer patients measured by FLT-PET/CT imaging, with potential applicability in radiation therapy planning. Int J Radiat Oncol Biol Phys. 2015;92(5):1035–43.
32. Sender R, Milo R. The distribution of cellular turnover in the human body. Nat Med. 2021;27(1):45–8.
33. Calvi LM, Link DC. The hematopoietic stem cell niche in homeostasis and disease. Blood. 2015;126(22):2443–51.
34. Doulatov S, Notta F, Laurenti E, Dick JE. Hematopoiesis: a human perspective. Cell Stem Cell. 2012;10(2):120–36.
35. Hoggatt J, Kfoury Y, Scadden DT. Hematopoietic stem cell niche in health and disease. Annu Rev Pathol Mech Dis. 2016;11:555–81.
36. Adams GB, Scadden DT. The hematopoietic stem cell in its place. Nat Immunol. 2006;7(4):333–7.
37. Boulais PE, Frenette PS. Making sense of hematopoietic stem cell niches. Blood. 2015;125(17):2621–9.
38. Höfer T, Rodewald HR. Differentiation-based model of hematopoietic stem cell functions and lineage pathways. Blood. 2018;132(11):1106–13.
39. Ng AP, Alexander WS. Haematopoietic stem cells: past, present and future. Cell Death Discov. 2017;3:2–5.
40. Swerdlow SH, Campo E, Harris NL, Jaffe ES, Pileri SA, Stein H, Thiele J. WHO classification of tumours of haematopoietic and lymphoid tissues. Lyon: International Agency for Research on Cancer; 2017. Revised 4th edition.
41. Hale LP. Histologic and molecular assessment of human thymus. Ann Diagn Pathol. 2004;8(1):50–60.
42. Kendall MD, Johnson HR, Singh J. The weight of the human thymus gland at necropsy. J Anat. 1980;131(Pt 3):483–97.
43. Germain RN. t-cell development and the CD4-CD8 lineage decision. Nat Rev Immunol. 2002;2(5):309–22.
44. Takahama Y. Journey through the thymus: stromal guides for T-cell development and selection. Nat Rev Immunol. 2006;6(2):127–35.
45. Laan M, Salumets A, Klein A, Reintamm K, Bichele R, Peterson H, et al. Post-aire medullary thymic epithelial cells and Hassall's corpuscles as inducers of tonic pro-inflammatory microenvironment. Front Immunol. 2021;12:1–9.
46. Flores KG, Li J, Sempowski GD, Haynes BF, Hale LP. Analysis of the human thymic perivascular space during aging. J Clin Invest. 1999;104(8):1031–9.
47. Nuñez S, Moore C, Gao B, Rogers K, Hidalgo Y, Del Nido PJ, et al. The human thymus perivascular space is a functional niche for viral-specific plasma cells. Sci Immunol. 2016;1(6):139–48.
48. Mori K, Itoi M, Tsukamoto N, Kubo H, Amagai T. The perivascular space as a path of hematopoietic progenitor cells and mature T cells between the blood circulation and the thymic parenchyma. Int Immunol. 2007;19(6):745–53.
49. Goel D, Prayaga AK, Sundaram C, Raghunadharao D, Rajappa SJ, Rammurti S, et al. Utility of fine needle aspiration cytology in mediastinal lesions: a clinicopathologic study of 161 cases from a single institution. Acta Cytol. 2008;52(4):404–11.
50. Adler OB, Rosenberger A, Peleg H. Fine-needle aspiration biopsy of mediastinal masses: evaluation of 136 experiences. AJR Am J Roentgenol. 1983;140(5):893–6.
51. Marchevsky A, Marx A, Ströbel P, Suster S, Venuta F, Marino M, et al. Policies and reporting guidelines for small biopsy specimens of mediastinal masses. J Thorac Oncol. 2011;6(7 Suppl 3):S1724.
52. Popoveniuc G, Sharma M, Devdhar M, Wexler JA, Carroll NM, Wartofsky L, et al. Graves' disease and thymic hyperplasia: the relationship of thymic volume to thyroid function. Thyroid. 2010;20(9):1015–8.
53. Illei PB, Shyu S. Fine needle aspiration of thymic epithelial neoplasms and non-neoplastic lesions. Semin Diagn Pathol. 2020;37(4):166–73.
54. Wee T, Lee AF, Nadel H, Bray H. The paediatric thymus: recognising normal and ectopic thymic tissue. Clin Radiol. 2021;76(7):477–87.
55. Klimek-piotrowska W, Mizia E, Kuzdzał J, Lazar A, Lis M, Pankowski J. Ectopic thymic tissue in the mediastinum: limitations for the operative treatment of Myasthenia gravis. Eur J Cardiothorac Surg. 2012;42(1):61–5.
56. Monaco SE, Escobar F, Simons JP. Hassall's corpuscles in the fine-needle aspiration cytology of pediatric ectopic thymic tissue. Diagn Cytopathol. 2017;45(8):735–7.
57. Escobar FA, Pantanowitz L, Picarsic JL, Craig FE, Simons JP, Viswanathan PA, et al. Cytomorphology and sonographic features of ectopic thymic tissue diagnosed in paediatric FNA biopsies. Cytopathology. 2018;29(3):241–6.

Urinary Tract

8

Madelyn Lew

Kidney

The kidneys are bean-shaped organs located in the left and right retroperitoneal space of the upper abdominal cavity. They typically measure up to 12 cm in length, 7.5 in width, and 3 cm in thickness, with variation in weight dependent on body surface area, age, gender, and ethnicity [1]. Due to the presence of the liver, the right kidney is often positioned slightly more inferomedial and is slightly smaller than its left counterpart. Each kidney has a medial concave hilum in which the renal artery enters the kidney to supply blood and the renal vein exits to distribute deoxygenated blood to the inferior vena cava. The ureter carrying urine from the renal calyces also exits from the hilum. The kidney is surrounded by a fibrous renal capsule, which is surrounded by perirenal fat.

The kidney is responsible for the excretion of various metabolic products into urine. The nephron is its structural and functional unit and is composed of a glomerulus and its associated Bowman's capsule, proximal tubule, loop of Henle with descending and ascending limbs, and distal tubule. The nephron's function is to process blood through filtration, reabsorption, secretion, and excretion of specified substances to produce a concentrated filtrate that will become urine. The production of urine is critical in homeostasis as it plays a role in regulating acid-base balance, electrolyte levels, body fluid volume, and blood pressure. The different components of the nephron are housed in two regions of the kidney—the outer renal cortex and inner medulla. The renal cortex houses glomeruli as well as proximal and distal tubules and a rich capillary network (Fig. 8.1a). The glomerulus refers to a rounded structure made up of a capillary tuft supported by connective tissue of the mesangium. The capillaries are lined by endothelial cells and are covered by the pedicles of podocytes, which are epithelial cells of Bowman's capsule. Systemic blood enters through the glomerular structure via an afferent arteriole for filtration in the glomerulus. As blood is processed through the glomerulus filtration barrier, large substances such as proteins are retained while a filtrate of water and other soluble substances are collected in Bowman's capsule that encloses the glomerulus. This filtrate then enters the proximal tubule for reabsorption of substances such as glucose, amino acids, urea, uric acid, and electrolytes into peritubular capillaries. On histology, proximal tubules are characterized by cuboidal to columnar epithelial cells with moderately abundant amounts of eosinophilic granular cytoplasm and basally oriented nuclei. A Periodic acid-Schiff (PAS) stain can highlight the terminal brush border of these cells. The filtrate becomes further refined through reabsorption as well as secretion as it descends through the inner medulla in the terminal portion of the proximal tubules and descending thin limb of Henle's loop. The descending limb is histologically characterized by a tubular structure lined by flattened, attenuated epithelial cells. The loop of Henle then makes a hairpin turn to return the filtrate back towards the cortex in the distal tubules. The distal tubules are lined by low cuboidal epithelial cells that contain less abundant and eosinophilic cytoplasm than those of the proximal tubule (Fig. 8.1b). Additionally, the distal tubular cells lack the PAS-positive brush border seen in the proximal tubular cells. After passing through the distal tubules, the filtrate undergoes the final processing step of excretion into the collecting ducts, which are characterized by low cuboidal to columnar epithelial cells with light eosinophilic to clear cytoplasm and distinct lateral cell borders. After this point, the filtrate enters the ureter and is renamed urine.

The role of fine needle aspiration (FNA) in the initial evaluation of renal masses has been the subject of several studies. Many of these studies highlight the higher average sensitivity and diagnostic accuracy of core needle biopsies compared to FNAs, as they typically provide more tissue that allows for evaluation of architecture patterns within renal neoplasms [2, 3]. Therefore, core needle biopsy is the pre-

M. Lew (✉)
Department of Pathology, University of Michigan, Ann Arbor, MI, USA
e-mail: lewm@med.umich.edu

M. Lew et al. (eds.), *Normal Cytology*, https://doi.org/10.1007/978-3-031-20336-7_8

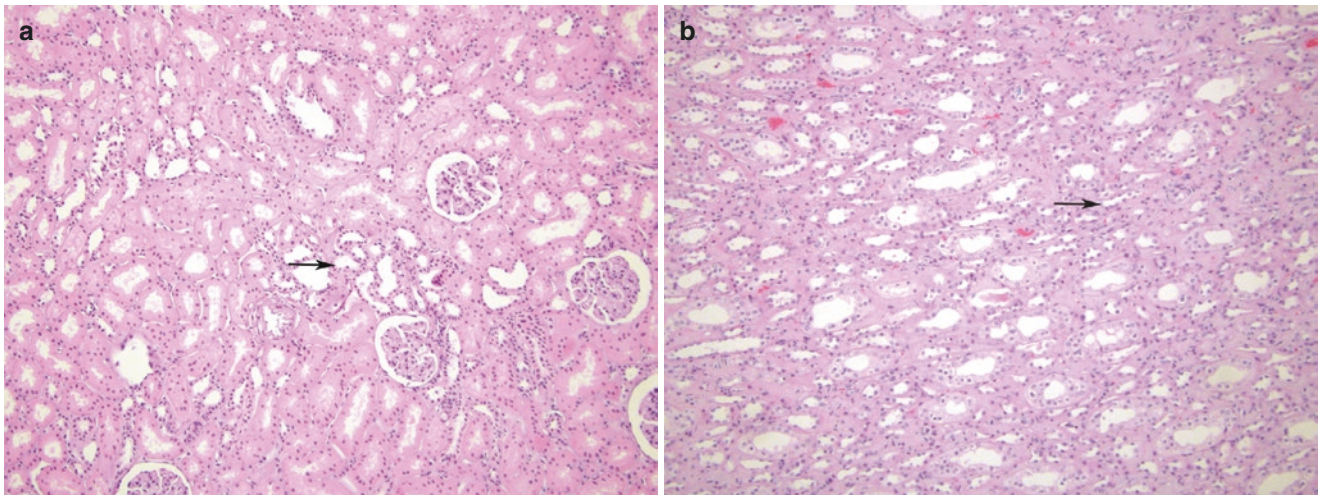

Fig. 8.1 (**a**) In the renal cortex, a mixture of glomeruli, proximal tubules, and distal tubules can be seen. Glomeruli are designated by rounded structures composed of a capillary tuft with supporting soft tissue surrounded by Bowman's capsule. Adjacent to glomeruli, proximal tubules with cuboidal epithelial cells characterized by abundant amounts of eosinophilic cytoplasm are seen. Comparatively, distal tubules (black arrow) are lined by low cuboidal epithelial cells with a small amount of cytoplasm. (**b**) The renal medulla contains the distal portions of the proximal tubules, loops of Henle, and collecting ducts. The descending thin limbs of Henle's loop (black arrow) are lined by attenuated epithelial cells. Kidney resection, hematoxylin & eosin, 10× magnification (**a**, **b**)

ferred specimen collection method for initial evaluation of renal masses by the American Urologic Association [4]. However, FNA is less invasive, allows for more extensive sampling of regions within a renal mass, and also provides an opportunity for rapid on-site assessment to optimize sampling and specimen triaging, including preparation of appropriate cell block material for immunohistochemical and/or molecular studies [5]. Studies have shown that the combination of FNA and core needle biopsy has a higher sensitivity and diagnostic accuracy than either modality on its own [3, 6–9]. Therefore, as an increased number of small renal masses are detected by imaging, renal aspirates may become more common, highlighting the importance of recognizing normal elements to avoid their misinterpretation as lesional cells. In these scenarios, the identification of only normal renal elements in a FNA or touch preparation of core biopsies should be considered nondiagnostic, as it indicates that the targeted lesion of interest was not adequately sampled.

On aspirate material, glomeruli are featured as large cohesive and densely cellular globular or rounded structures. On high power evaluation, there is increased cellularity in the central portion due to the intermix of endothelial cells and mesangial cells. This cellularity may account for variable staining. The nuclei are bland in appearance with round to ovoid shapes, smooth to slightly irregular nuclear contours, and have a granular chromatin distribution (Fig. 8.2a). In some glomeruli, the segmentation of the glomerular structure as well as its coursing capillaries can be highlighted (Fig. 8.2b), potentially raising the concern for papillary architecture seen in a variety of renal neoplasms such as papillary renal cell carcinoma and clear cell papillary renal cell tumor. However, in contrast to these neoplasms, the periphery of normal glomerular structures can feature thin capillary loops and there should be no pleomorphism. On cytologic preparations, proximal tubular cells have round nuclei, smooth nuclear contours, even chromatin distribution, and distinct nucleoli. Characteristically, they have a moderate amount of granular cytoplasm (Fig. 8.3). While these proximal tubules are often found in small clusters with indistinct cell boundaries, when singly dispersed and if they constitute the predominant cell type present, they can be difficult to distinguish from cells derived from oncocytic neoplasms such as oncocytoma or chromophobe renal cell carcinoma. However, when clustered in groups they may be easier to recognize, as oncocytic neoplastic cells tend to have more sharply defined cell boundaries and scattered multinucleation. Chromophobe renal cell carcinomas also display a higher degree of nuclear atypia with nuclear enlargement, nuclear contour irregularities, and coarse chromatin distribution. Distal tubular cells have similar bland nuclear features to their proximal tubular counterparts but are typically differentiated by more well-defined cell borders and a lower quantity of clear to granular cytoplasm, as well as inconspicuous nucleoli (Fig. 8.3). When aspirated, distal tubules are often arranged in small clusters or as singly dispersed cells. Although these cells look bland, in isolation, they can be difficult to differentiate from low-grade renal cell carcinomas.

While neoplastic lesions tend to be more cellular on aspirate material, in paucicellular samples, it can be difficult to definitively distinguish between benign renal elements and poor sampling of a renal neoplasm on morphology alone. In these cases, immunohistochemistry

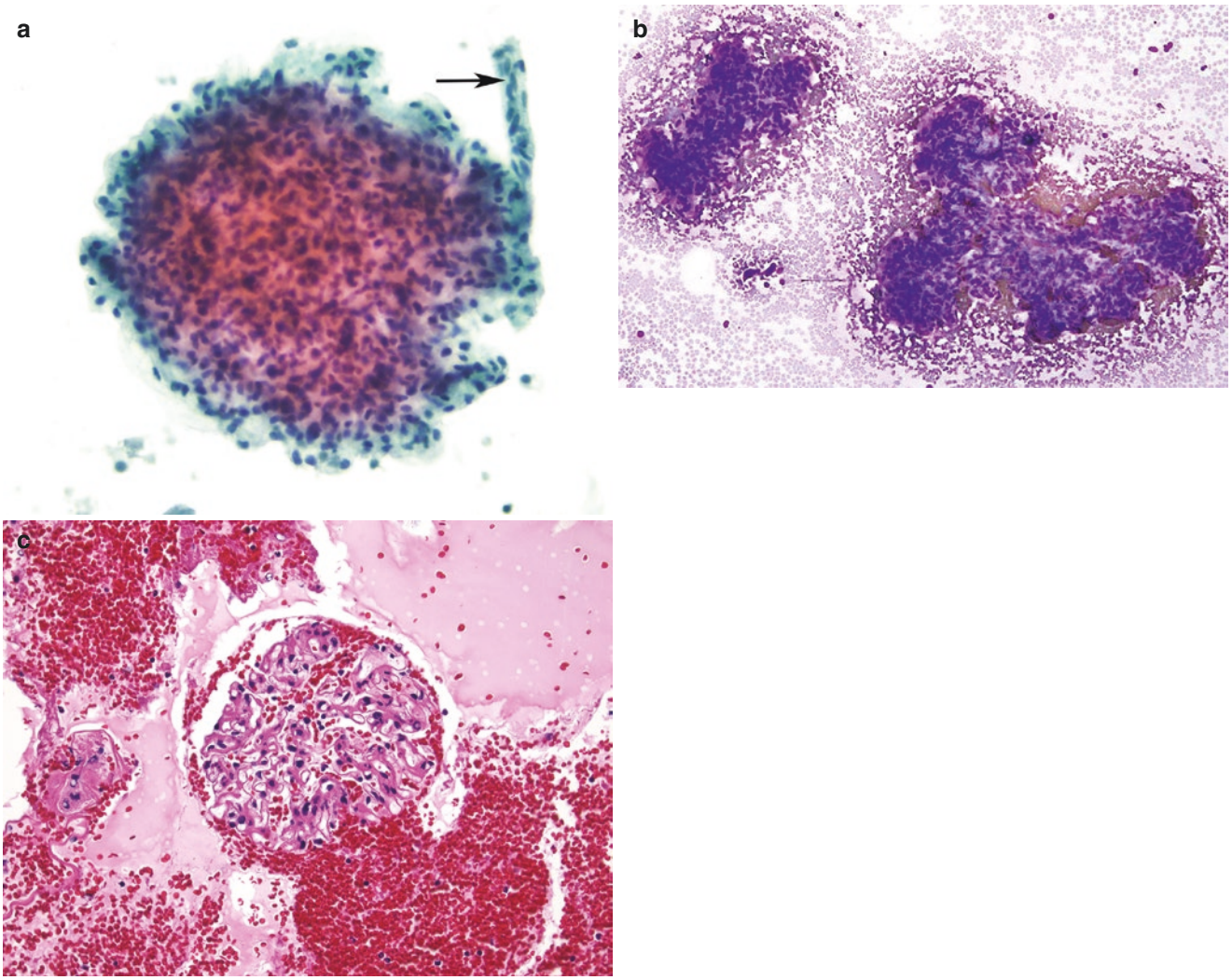

Fig. 8.2 (**a**) A glomerulus seen as a cellular rounded/globular structure with central cellular density, comprised of a mixture of mesangial and endothelial cells that lack atypia. Note that the cells are denser in the center compared to the periphery. Arterioles (black arrow) can be occasionally seen at the poles of a glomerulus. (**b**) Glomeruli seen as a cohesive lobulated structure (left) and more segmented architecture (right) with coursing blood vessels. (**c**) Glomeruli are seen as isolated lobulated structures with well-defined capillary loops on cell block material. Kidney, alcohol-fixed smear preparation, Papanicolaou stain, 20x magnification (**a**). Kidney, air-dried smear preparation, Diff-Quik, 10x magnification (**b**). Kidney, cell block, hematoxylin & eosin, 40× magnification (**c**)

may be useful in further delineating the etiology of procured cells. PAX8 nuclear staining can be utilized to confirm the renal etiology of the cells in question, although it does not differentiate between neoplastic and non-neoplastic lesions [10]. Carbonic anhydrase-IX (CA-IX) is a hypoxia-induced protein and is frequently overexpressed in clear cell renal cell carcinoma and clear cell papillary renal cell tumor. Although CA-IX has been reported to have variable positivity in papillary renal cell carcinomas, it is typically negative in chromophobe renal cell carcinomas, oncocytomas, and normal renal tubules. However, focal weak staining in rare renal tubular cells has been reported in a small number of cases [11, 12]. Of note, CA-IX is not entirely specific for renal cell carcinomas. As a hypoxia marker, it can be expressed within and near necrotic regions as well as in other malignancies from other organ sites such as cholangiocarcinomas [11]. As previously mentioned, normal renal elements can raise concern for a papillary renal cell carcinoma. In this context, AMACR positivity is a feature of papillary lesions of the kidney including papillary adenomas and papillary renal cell carcinomas. Although AMACR expression can be seen in other renal cell carcinomas as well as normal renal tubules, normal glomeruli are negative [13]. Additionally, immunohistochemistry for CK7 can be utilized as a significant subset of papillary renal cell carcinomas will be positive for this marker while normal glomeruli and tubular cells will be negative.

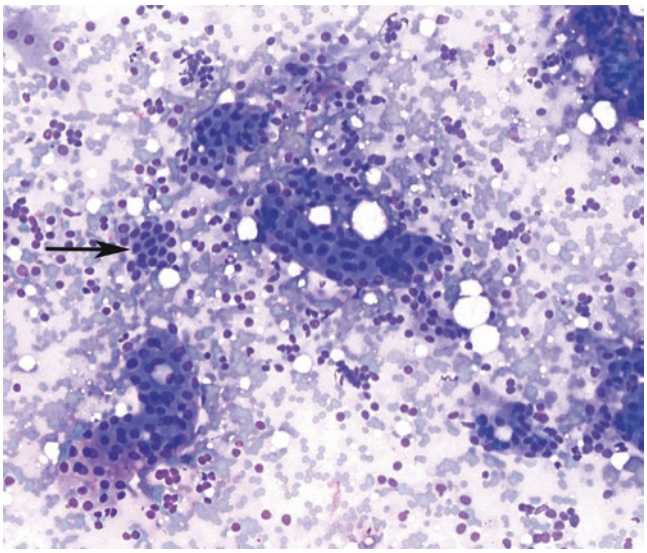

Fig. 8.3 Proximal tubular cells are shown arranged in cohesive cell groups that are characterized by round nuclei, smooth nuclear contours, and moderately abundant amounts of granular cytoplasm which confer indistinct cellular boundaries. While adjacent distal tubular cells (black arrow) have similarly bland nuclear features, they have notably less cytoplasm. Kidney, air-dried touch preparation of core needle biopsy, Diff-Quik, 10× magnification

However, normal epithelial cells from the collecting ducts will be positive. Although immunohistochemistry can be helpful in differentiating some renal neoplasms from normal elements, there are likely to be cases in which these stains are not beneficial. Both chromophobe renal cell carcinoma and oncocytoma are thought to originate from the intercalated cells of renal collecting tubules. These oncocytic neoplasms are positive for CD117, which is helpful in differentiating them from eosinophilic variants of clear cell renal cell carcinoma. However, studies have shown that proximal renal tubules are also CD117 positive [14], making a clear delineation between oncocytic lesions and proximal tubular cells difficult on limited cell block material.

Inadvertent sampling of the adjacent organs may also be misinterpreted as evidence of a renal neoplasm. Samples targeting the superior aspect of the right kidney may yield cells from the liver, which given their distinct nucleoli, moderate to abundant amounts of granular cytoplasm, and propensity for binucleation can be mistaken for a renal oncocytic neoplasm. On the left side, inadvertent sampling of the spleen results in aspirate samples with a significant population of small, mature appearing lymphocytes, which may raise concern for involvement of the kidney by a lymphoproliferative disorder.

Renal Pelvis and Ureters

The major calyces of the kidney join together to form the renal pelvis which is lined by urothelium. The renal pelvis serves to funnel urine to the ureter. The ureters are thin tubular structures approximately 30 cm in length that empty urine filtrated in the kidney downward into the bladder through the ureteral orifices. Similar to the bladder and renal pelvis, the ureter is lined by urothelium under which lie the lamina propria and muscularis propria (Fig. 8.4a). The urothelium is composed of three main cell types—basal cells, intermediate urothelial cells, and superficial (umbrella) cells (Fig. 8.4b). Basal cells are round to cuboidal cells that lie on the basement membrane and are characterized by having small amounts of cytoplasm with round nuclei, smooth nuclear contours, and even chromatin distribution. On top of the basal cells is a variable number of layers of intermediate cells. The intermediate urothelial cells often have moderately abundant amounts of eosinophilic to clear cytoplasm and ovoid nuclei with smooth to grooved nuclei, and finely stippled chromatin. Nucleoli in these intermediate cells are variably seen and their cytoplasm may appear vacuolated. The top layer of urothelium that faces the lumen is composed of superficial cells, otherwise called umbrella cells. These cells frequently have larger nuclei than those seen in the underlying intermediate and basal cells. However, the overall cell size of umbrella cells is also considerably larger, which typically confers a low nuclear to cytoplasmic ratio. Additionally, multinucleation, slightly coarse chromatin distribution, and distinct nucleoli are frequently identified in superficial cells.

Cytologic samples from the ureters and renal pelvis are most commonly obtained in the setting of ureteral strictures as well as ureteral and/or renal pelvic masses identified on imaging. Additionally, patients with reported voided urine abnormalities in the absence of concurrent urinary bladder lesions may undergo ureteroscopy and have subsequent ureteral washings and brushings to look for a possible upper urinary tract urothelial neoplasm. Obtaining sufficient biopsy material for upper urinary tract abnormalities may be hindered by the technical difficulty associated with accessing upper urinary tract sites compared to the lower urinary tract [15]. As such, upper urinary tract washings and brushing cytology specimens are useful in the evaluation of potential abnormalities given the wider area of urothelium sampled in these specimens compared to biopsy specimens.

Upper tract washing and brushing cytology samples contain the same spectrum of urothelial cells as seen in the lower

urinary tract. However, there may be more basal cells due to abrasion of the urothelium during these collections. The cells may be arranged singly and in clusters. Interpretation of normal upper urinary tract cytology samples can be difficult to interpret due to their high cellularity and abundance of cell clusters. Additionally, featured urothelial cells from the upper urothelial tract often display larger nuclei, variably distinct nucleoli, and have slightly coarser chromatin distribution (Fig. 8.5a) compared to those identified in voided urine and bladder washing samples. These features, in conjunction with variable nuclear crowding and pleomorphism within cell clusters (Fig. 8.5b), can mistakenly be attributed to a neoplastic urothelial process [16]. As such, comparison with a contralateral upper urinary tract sample may be helpful in the evaluation of urothelial atypia in the ureter or renal pelvis. Similar to the diagnostic pitfalls seen in the evaluation of lower tract urine specimens, the presence of stones, history of chemotherapy or radiation, as well as other inflammatory conditions can give rise to reactive changes that can be mistaken for malignancy.

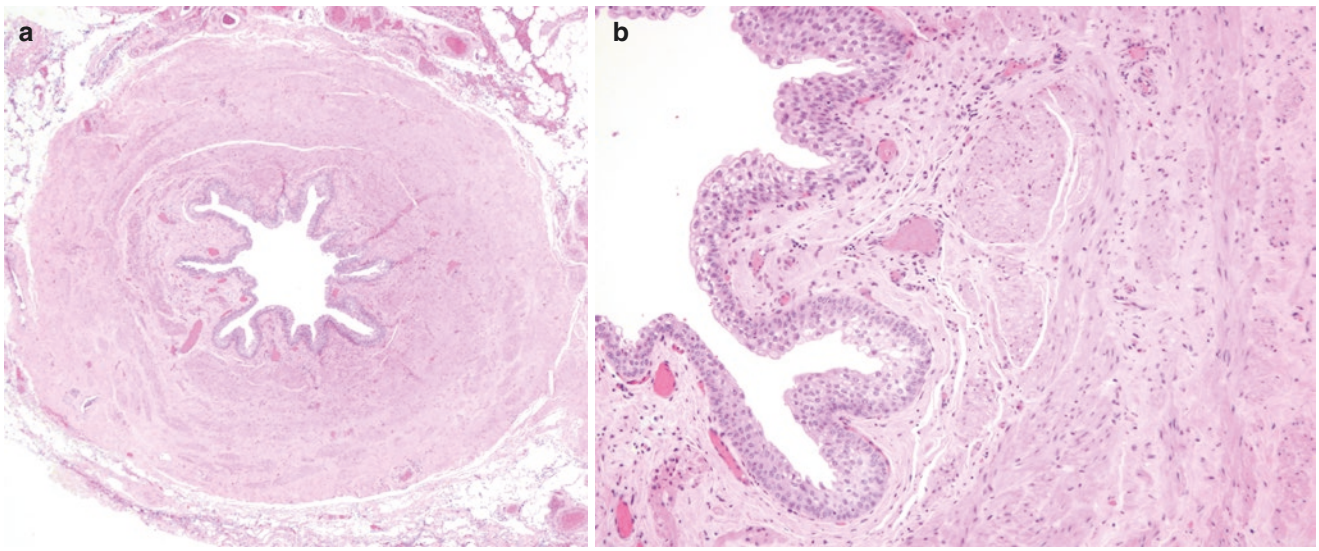

Fig. 8.4 (**a**) Cross section of a benign ureter with undulating urothelium showing underlying loose connective tissue of the lamina propria and smooth muscle bundles of the muscularis propria. (**b**) Multilayered urothelium showing basal cells, intermediate urothelial cells, and superficial (umbrella) cells. Ureter resection, hematoxylin & eosin, 2× (**a**) and 10× (**b**) magnification

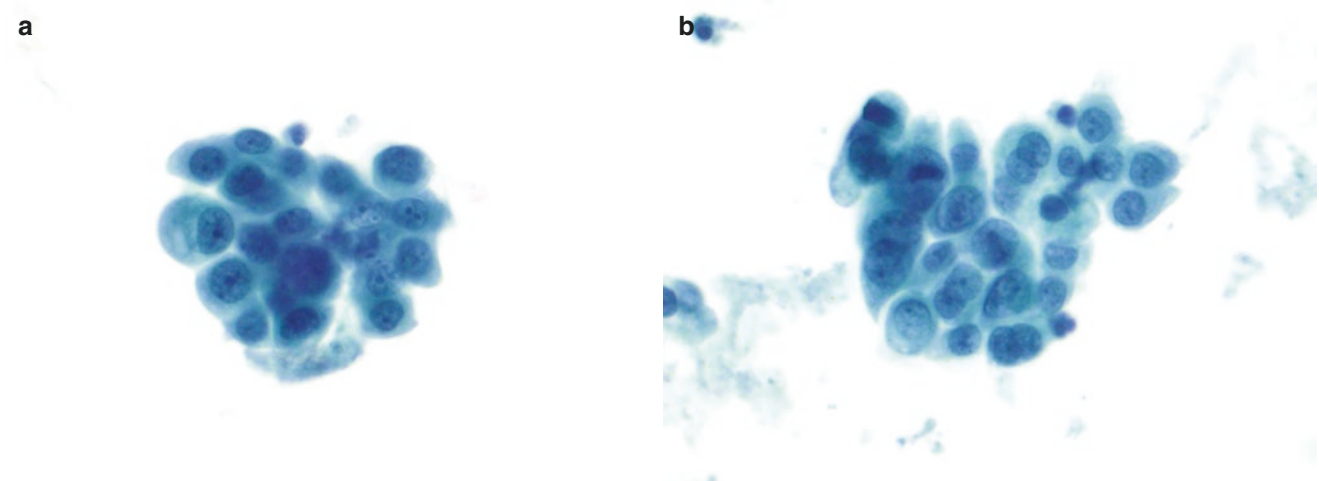

Fig. 8.5 (**a**) Ureteral wash with intermediate urothelial cells displaying larger nuclei than those of lower urinary tract urothelial cells. Note the slightly coarse chromatin distribution and distinct nucleoli, and (**b**) variable pleomorphism in these urothelial cells. Ureteral washing, ThinPrep preparation, 5× (**a**) and 40× (**b**) magnification

Urinary Bladder

The urinary bladder is a muscular sac-like organ within the pelvis that typically is set superior and posterior to the pubic bone. Pubovesicle and puboprostatic ligaments hold the urinary bladder in its place in females and males, respectively [17, 18]. Urine that is filtered from the kidneys and passed through the ureters enters the urinary bladder through ureteral orifices. The thick bundles of the muscularis propria or detrusor muscle of the bladder relaxes and expands to allow storage of urine, conferring a more rounded appearance to the bladder. Upon contraction, the bladder empties urine through the urethra, which confers a pear-shaped appearance to the bladder.

On histologic evaluation, the bladder has four main components—the urothelium lining, lamina propria, muscularis propria, and outer adventitia. The urothelium has a variable cell thickness depending on the degree of urinary bladder distention and regional location within this organ. A distended bladder has a thin urothelium as opposed to a contracted one. The urothelium is composed of the same three main cell types as previously described in the ureters—basal cells, intermediate urothelial cells, and superficial (umbrella) cells (Fig. 8.6).

In normal variants of urinary bladder histology, the urothelium can undulate and invaginate into the underlying lamina propria as von Brunn's nests. In some cases, these can take on a cystic appearance (cystitis cystica) or undergo glandular metaplasia (cystitis glandularis), where the cells take on a cuboidal to columnar shape and can be mucin-secreting (Fig. 8.7). In some cases of cystitis glandularis, the cells recapitulate the appearance of intestinal-type goblet cells. While the presence of glandular epithelium in the bladder can raise the concern for an adenocarcinoma, the cells of cystitis glandular often display bland nuclear features, which is helpful in mitigating concern. All of these histologic variants can be seen in a spectrum of normal or reactive bladders. Squamous metaplasia is also frequently identified in the urinary bladder. While this is more often associated with chronic irritation from varying etiologies including infection, stones, and frequent catheterization, it can also be readily apparent in the posterior aspect or trigone in the female bladder. Mucus, derived from the vagina or glands in the lower urinary tract, can contaminate normal urine.

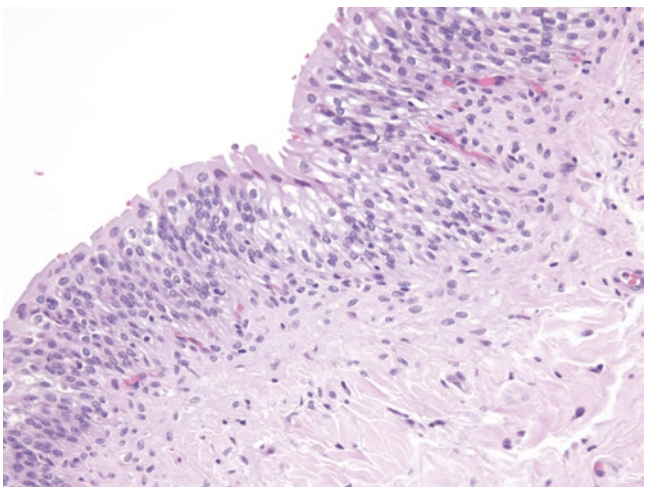

Fig. 8.6 Multilayered urothelium showing basal cells, many intermediate urothelial cells, and superficial (umbrella) cells. This urothelium is composed predominantly of intermediate urothelial cells with eosinophilic to clear cytoplasm, round to grooved nuclei, and variably distinct nucleoli. The superficial cells have an abundant amount of eosinophilic cytoplasm. Urinary bladder resection, hematoxylin & eosin, 20× magnification

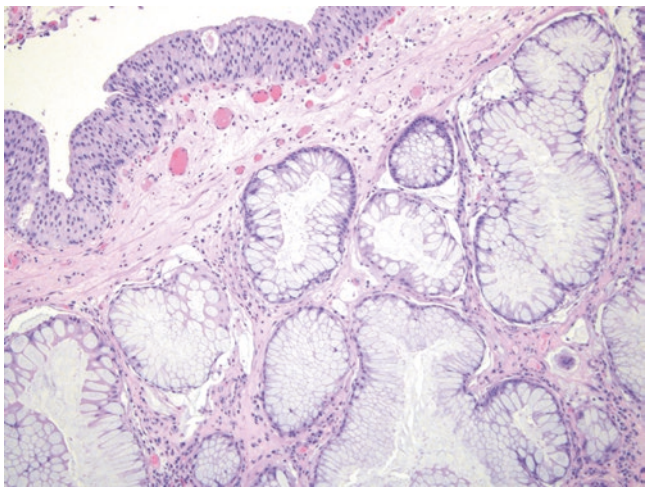

Fig. 8.7 Invaginations of urothelium may undergo glandular metaplasia in cystitis glandularis. Bladder biopsy, hematoxylin & eosin, 20× magnification

The lamina propria underlies the urothelial mucosa and is composed of connective tissue, lymphovascular vessels, nerves, and elastic fibers. Thin bands of smooth muscle fibers of the muscularis mucosae can be identified in the lamina propria. These smooth muscle bands are typically discontinuous, but can occasionally become hyperplastic and continuous, which on biopsy or transurethral resection specimens can make it difficult to differentiate muscularis mucosae from the thicker bundles of muscularis propria. The muscularis propria has three layers— an inner longitudinal layer, a central circular layer, and an outer longitudinal layer. However, in many parts of the bladder these layers are intimately intertwined without definitive orientation. Unlike other organs, such as the colon, surrounding fat tissue is intimately associated between the thick smooth muscle bundles of the muscularis propria and, occasionally, the lamina propria [19].

Fine needle aspirations (FNA) of the urinary bladder are generally not performed in humans, although they have

been reported to be useful in veterinary pathology [20]. Instead, urothelium is most commonly evaluated as a part of urine samples. Urine cytology is a convenient method that allows clinicians to screen and triage patients with urinary symptoms such as hematuria or exposure to known bladder-toxic agents such as aniline dyes, aromatic amines, or cyclophosphamide. Urine cytology samples can be processed in a variety of ways including smears, liquid-based specimens (ThinPrep® and SurePath®), and cytospin preparations.

In normal urine cytology specimens, the various cells of the urothelium can be identified. Urothelial cells arranged as clusters are uncommon in normal voided urine specimens. Samples may contain basal, intermediate, and superficial (umbrella) cells. The basal cells are infrequently detected in voided samples. The basal and intermediate cells are usually round, but can sometimes be more elongated or columnar. Similar to their histologic appearance, basal cells are characterized by high nuclear to cytoplasmic ratios, smooth nuclear contours, even dark chromatin distribution, indistinct nucleoli, and scant amounts of dense cytoplasm (Fig. 8.8a). In some cases, the high nuclear to cytoplasmic ratios and occasionally hyperchromatic nuclei may be misinterpreted as malignant. However, the size of the basal cell nucleus is smaller or similar to those of adjacent intermediate urothelial cells. Intermediate urothelial cells are the most common urothelial cell type in voided urine samples and are characterized by smooth nuclear contours, granular chromatin distribution, and more moderately abundant amounts of cytoplasm (Fig. 8.8b). In reactive conditions,

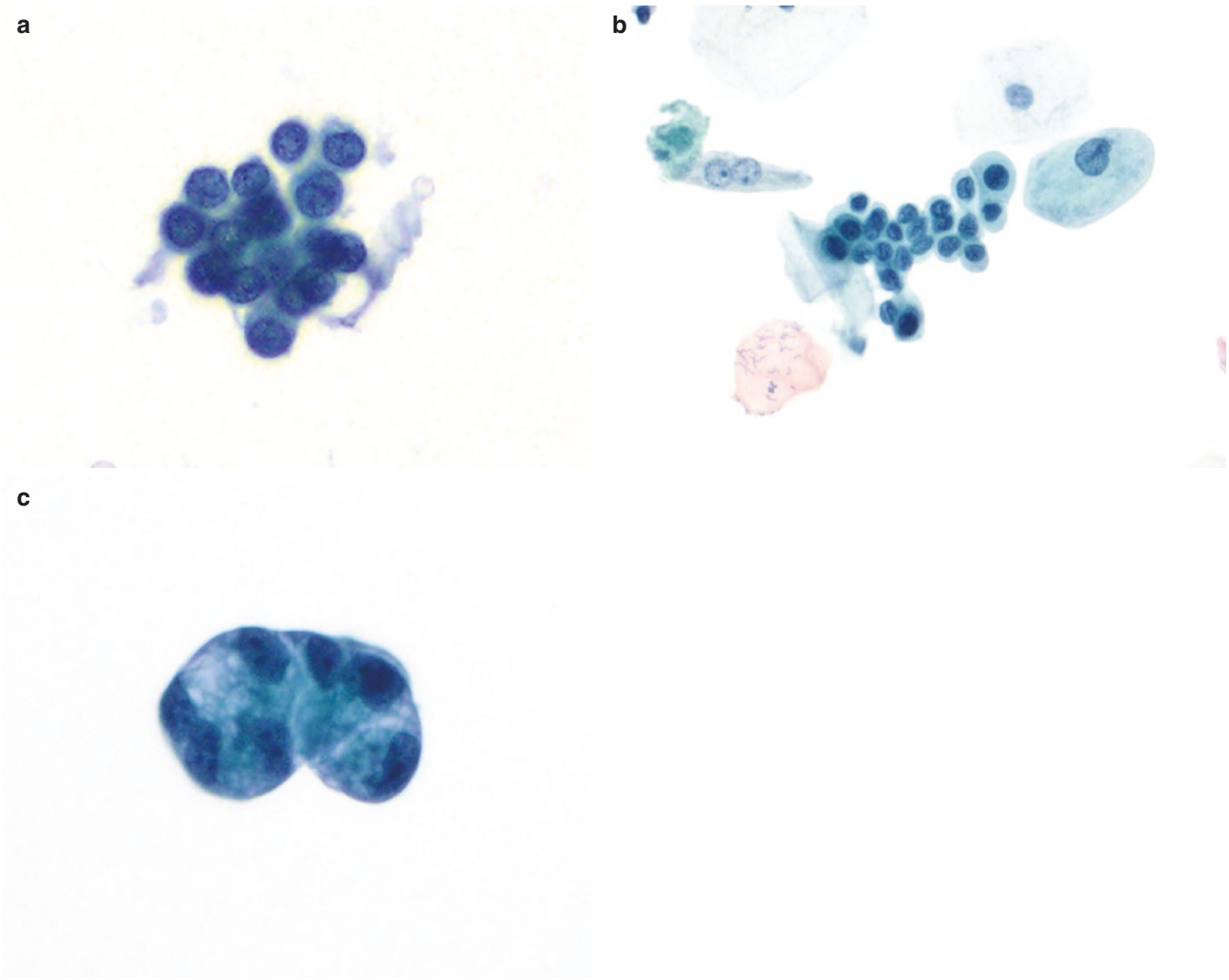

Fig. 8.8 (**a**) In normal urine cytology, basal cells show high nuclear to cytoplasmic ratios, smooth nuclear contours, even granular chromatic distribution, indistinct nucleoli, and scant cytoplasm. (**b**, **c**) Intermediate urothelial cells typically have similarly bland nuclear features. These cells also are characterized by moderate amounts of granular cytoplasm which can occasionally be finely to coarsely vacuolated. Urine, ThinPrep preparation, 20× (**a**) and 40× (**b**, **c**) magnification

there may be notable nucleoli and the cytoplasmic quality can appear more vacuolated, which may be misinterpreted as a feature of adenocarcinoma when extensive (Fig. 8.8c). However, the degree of nuclear atypia in adenocarcinoma should be higher than that seen in reactive urothelial cells. Rarely, true glandular-type epithelial cells can be identified in urine specimens. The differential diagnosis for glandular cells in urine is quite broad and includes cystitis glandularis (Fig. 8.9a, b), colovesical fistulas, contamination from the vaginal or gastrointestinal tract, müllerianosis, villous adenoma of the bladder, adenocarcinoma and urothelial carcinoma with gland-like differentiation [21]. In both benign and malignant urothelial cells undergoing degenerative changes, red to green-blue intracytoplasmic inclusions called Melamed-Wolinska bodies can be seen (Fig. 8.10). The pathogenesis and significance of these cytoplasmic inclusions is unclear [22], but is important to differentiate them from inclusions seen in viral infections or lead toxicity. Their presence outside of the urothelial tract may also give rise to diagnostic consideration of a metastatic urothelial carcinoma [23]. Superficial or umbrella cells are much larger cells and often display enlarged nuclei with smooth to slightly irregular nuclear contours, variably distinct nucleoli, and abundant amounts of delicate cytoplasm. Their nuclear to cytoplasmic ratio is low. Binucleation or multinucleation and reactive changes can frequently be identified in umbrella cells (Fig. 8.11).

Urine cytology specimens are most frequently collected as voided or mid-stream ("clean catch") specimens. Often in these specimens, there are also many squamous cells derived from the external urogenital region or distal urethra. Typically, there should be very few red blood cells. In post-adolescent males, sperm can be identified in normal urine cytology (Fig. 8.12). Sperm can also occasionally be detected in women after vaginal intercourse. In urine samples from patients who had previously undergone total cystectomy, ileal conduits or neobladders are constructed by connecting a portion of small intestine to the urinary tract. Urine specimens from such urinary diversions are frequently notable for yielding cellular specimens with extensive intestinal epithelial degeneration, mucus and variable amounts of inflammatory cells and bacteria (Fig. 8.13). The degenerated epithelial

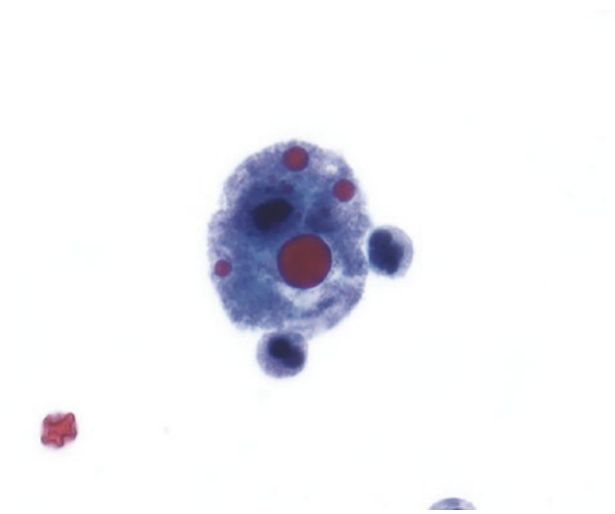

Fig. 8.10 Intracytoplasmic round, often red Melamed-Wolinska bodies can be identified in degenerating urothelial cells. Urine, ThinPrep preparation, 40× magnification

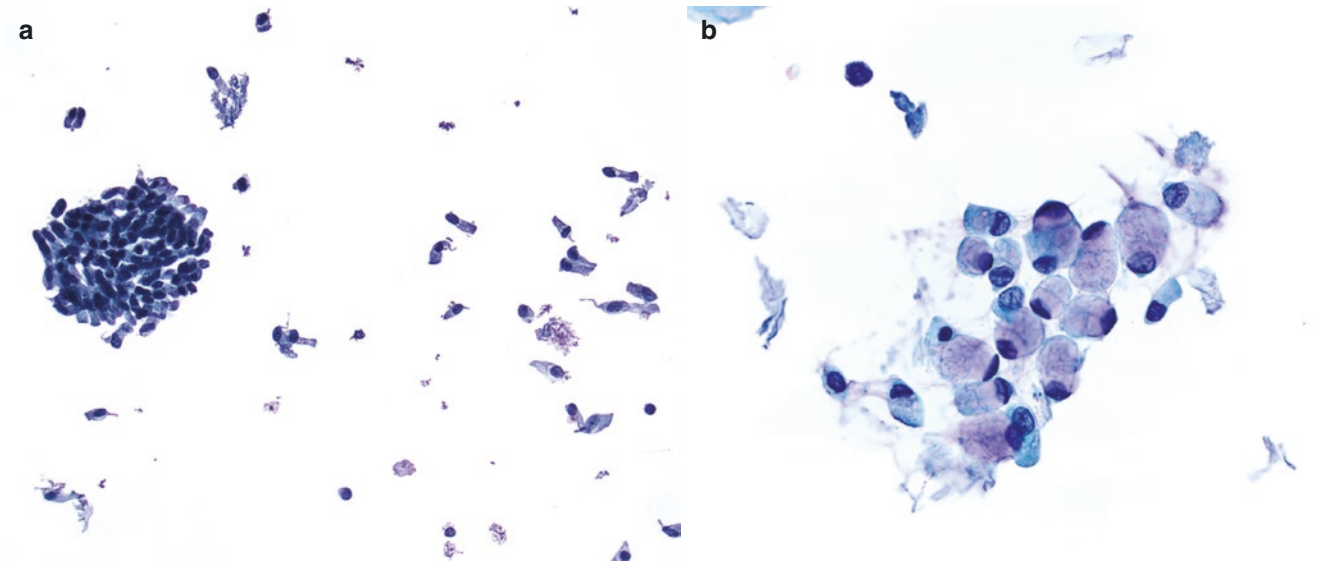

Fig. 8.9 Glandular cells from cystitis glandularis can occasionally be identified in urine cytology specimens. They can be (**a**) columnar or (**b**) round mucin-secreting cells that recapitulate the appearance of goblet cells in the colorectal tract. Their nuclei are bland with round to ovoid nuclei and exhibit even chromatin distribution. These glandular cells also display low nuclear to cytoplasmic ratios. Urine, ThinPrep preparation, 10× (**a**) and 40× (**b**) magnification

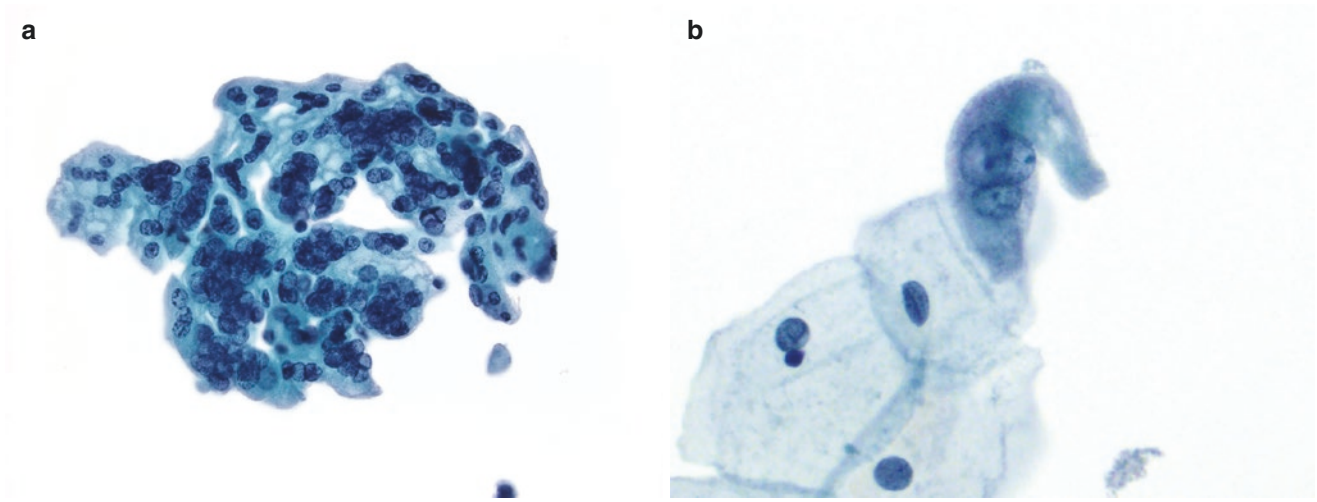

Fig. 8.11 (**a**, **b**) Umbrella cells can be of variable size and show extensive multinucleation with granular to coarse chromatin distribution. Urine, ThinPrep preparation, 40× (**a**, **b**) magnification

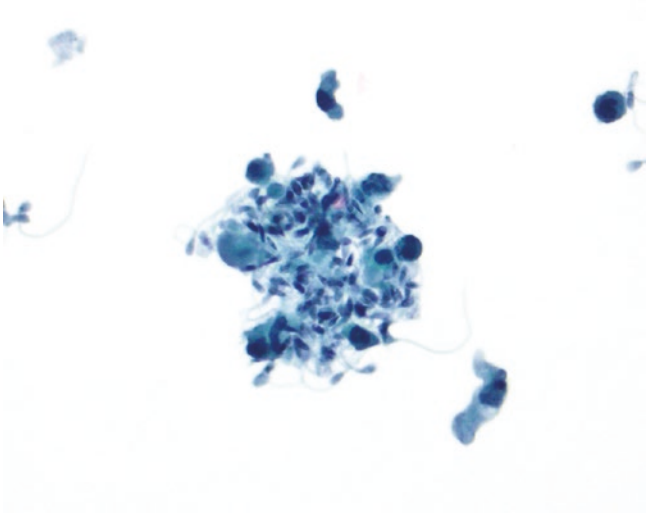

Fig. 8.12 Spermatozoa can be identified in urine cytologic samples. Voided urine, ThinPrep preparation, 40× magnification

cells resemble macrophages. Lubricant material and vegetable-like cell structures can occasionally be seen as a contaminant in urinary diversion specimens [24]. Urine cytology specimens can also be collected through instrumentation such as catheterization or irrigation during cystoscopy (bladder washings). In bladder washings, urothelial cells can normally form clusters with variable nuclear crowding and overlap in which the cell boundaries between these cells can become indistinct (Fig. 8.14). The appearance of these clusters may initially cause concern, as they can contain various types of urothelial cells which may be mistakenly interpreted as nuclear pleomorphism seen in urothelial carcinoma. However, the cells at the edges of these benign clusters typically display an outer cytoplasmic collar of superficial cells and true fibrovascular cores in these pseudopapillary clusters are absent. Clusters of urothelial cells can also be identified in voided urine samples, although these are more often associated with conditions resulting in the disruption of urothelium, such as the presence of urinary tract calculi, prior instrumentation, trauma, or inflammatory states. While low-grade urothelial neoplasms can also result in clusters of urothelial cells, it is not feasible to differentiate low-grade neoplastic urothelial clusters from other causes without cystoscopic evidence of tumor or urothelial cell clusters with notable fibrovascular cores. In any urine cytology specimens, crystals (e.g., calcium oxalate, calcium phosphate, triple phosphate, uric acid), casts (e.g., red blood cell, granular, waxy), or other structures (e.g., corpora amylacea) may also be identified. The specification of crystal types is typically reported as part of urinalysis on wet preparations rather than cytologic specimens.

Other elements seen in normal urine cytology may be striking and raise concern for a neoplastic process. Patients with a history of urothelial carcinoma treated with intravesicular Bacillus Calmette-Guérin (BCG) can have granulomas present in urine cytology specimens (Fig. 8.15). In contrast to urothelial cell clusters, histiocyte nuclei are round, ovoid, bean-shaped, and/or spindled and will show more contour variability. Additionally, the chromatin distribution is often finely granular and there are typically distinct nucleoli. Changes from radiation and chemotherapy can also give rise to reactive atypia that may be misinterpreted as malignant in nature [25]. These reactive changes include nuclear enlargement and hyperchromasia, cytoplasmic and nuclear vacuolization, as well as cytoplasmic polychromasia. However, in contrast to urothelial carcinoma, there is a concurrent increase in cell size or cytomegaly, thereby maintaining the cell's low nuclear to cytoplasmic ratio.

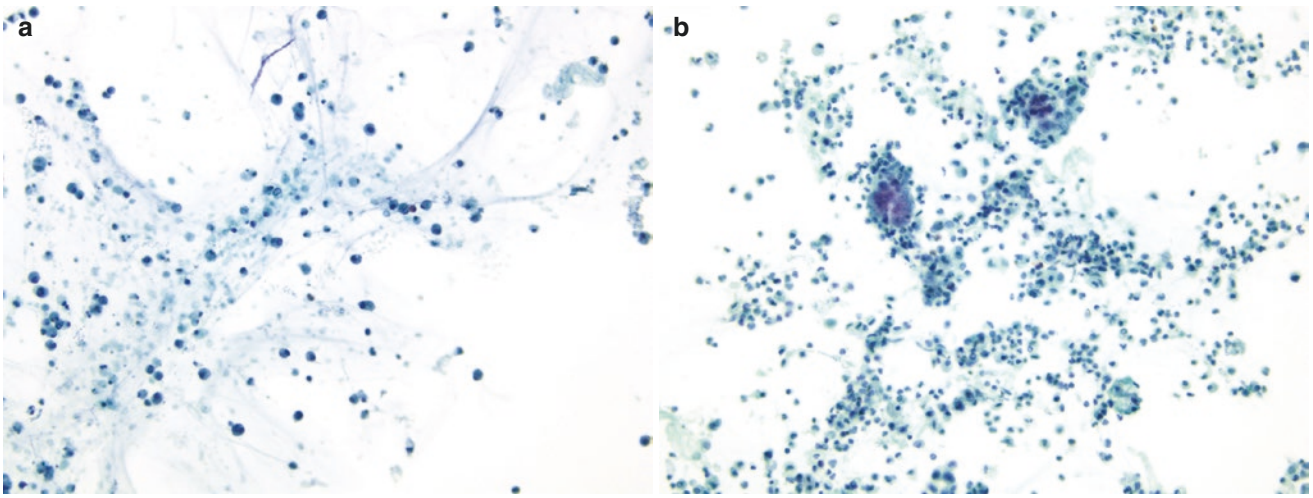

Fig. 8.13 (**a**, **b**) Ileal conduit urine cytology sample highlighting degenerated epithelial cells, macrophages, scattered inflammatory cells within a background of granular debris. Urine, ThinPrep preparation, 10× (**a**) and 20× (**b**) magnification

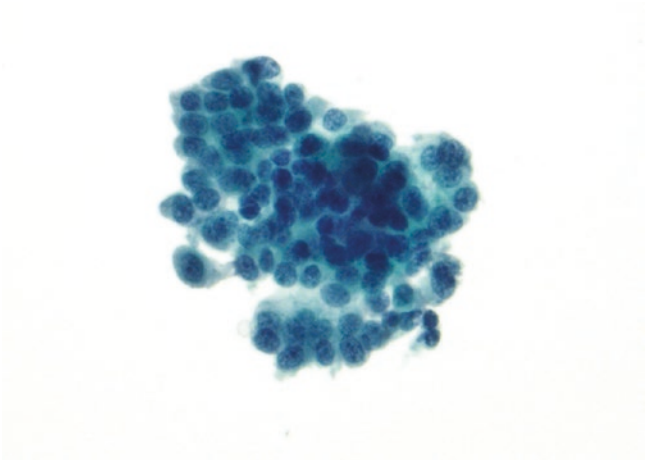

Fig. 8.14 Instrumentation change showing a cohesive cluster of basal and intermediate urothelial cells with bland nuclear features. Within the cluster, cell boundaries are indistinct and there is nuclear crowding. Bladder washing, ThinPrep preparation, 40× magnification

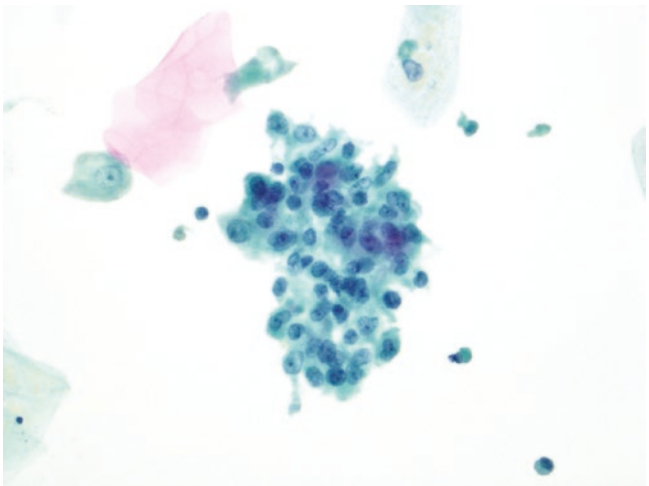

Fig. 8.15 Cluster of epithelioid macrophages characterized by ovoid to bean-shaped nuclei, finely granular chromatin distribution, and abundant amounts of delicate cytoplasm with indistinct cell boundaries in a patient with a history of BCG treatment for urothelial carcinoma. Urine, ThinPrep preparation, 40× magnification

Additionally, the nuclear hyperchromasia induced by these treatment-related changes is degenerative in nature, which confers a dark and smudgy appearance in nuclei rather than the coarse chromatin distribution associated with high-grade urothelial carcinoma. Persistent trauma and irritation of urothelium by urinary tract stones can result in the appearance of atypical urothelial cell clusters displaying enlarged nuclei, coarse chromatin distribution, and irregular nuclear contours, which mimics the appearance of urothelial carcinoma [26]. As such, clinical correlation with radiology and cystoscopy reports is of utmost importance to avoid this diagnostic pitfall. Rarely, epithelial cells from the seminal vesicle, which are notable for enlarged, hyperchromatic, and irregular nuclei, can be mistaken for malignant cells. However, the presence of coarse yellow-brown cytoplasmic granules of lipofuscin is helpful in mitigating concern. Renal tubular epithelial cells may be observed in small sheets or casts. They can be polygonal and have moderate amounts of cytoplasm, round nuclei, and granular hyperchromatic chromatin with degeneration.

Urethra

In both men and women, the urethra is a tubular structure that serves as a conduit for urine (and sperm in men) to leave the body to the external environment. In men, the urethra is composed of three main sections—the prostatic urethra, the membranous urethra, and penile urethra. The prostatic urethra, as occurs in the bladder and ureter, has a urothelial lining. The short membranous urethra traverses through the pelvic floor and deep perineal pouch and is lined by pseudostratified columnar epithelium. Underlying bulbourethral (Cowper's) glands eject mucoprotein-rich secretions into the membranous urethra. The penile urethra, which traverses through the corpus spongiosum of the penis, is proximally lined by a similar pseudostratified columnar epithelium, but transitions to a stratified squamous epithelium more distally until its endpoint at the external urethral orifice. The epithelial lining of the urethra in all sections is surrounded by a smooth muscle wall.

The urethra in women is shorter than in men as it extends from the bladder neck inferiorly through the pelvic floor until its endpoint at the urethral orifice, just anterior to the vaginal opening. The proximal portion of the female urethra, as seen in the bladder and ureters, has a urothelial lining and the distal portion is lined by stratified squamous epithelium. Close to the urethral orifice, periurethral Skene's glands secrete lubricating fluid through ducts into the vulvar vestibule with openings to both sides of the urethral orifice.

Urethral elements may be seen in the collection of voided urine samples. More directed urethral washings may be performed, particularly in the surveillance of patients who have previously undergone cystectomy for urothelial carcinoma. Similar to the aforementioned urine samples, urethral washings will contain scattered bland appearing urothelial and, rarely, squamous cells.

References

1. Kasiske BL, Umen AJ. The influence of age, sex, race, and body habitus on kidney weight in humans. Arch Pathol Lab Med. 1986;110(1):55–60.
2. Volpe A, Finelli A, Gill IS, Jewett MAS, Martignoni G, Polascik TJ, Remzi M, Uzzo RG. Rationale for percutaneous biopsy and histologic characterization of renal tumours. Eur Urol. 2012;62(3):491–504.
3. Yang CS, Choi E, Idrees MT, Chen X, Wu HH. Percutaneous biopsy of the renal mass: FNA or core needle biopsy? Cancer Cytopathol. 2017;125(6):407–15.
4. Campbell S, Uzzo RG, Allaf ME, Bass EB, Cadeddu JA, Chang A, Clark PE, Davis BJ, Derweesh IH, Giambarresi L, Gervais DA, Hu SL, Lane BR, Leibovich BC, Pierorazio. Renal mass and localized renal cancer: AUA guideline. J Urol. 2017;198(3):520–9.
5. Eikren O, Walter TC, Flatberg A, Beisvag V, Strauss P, Farstad M, Beisland C, Koch E, Mueller TF, Marti HP. Fine needle aspirates of kidneys: a promising tool for RNA sequencing in native and transplanted kidneys. BMC Neprhol. 2018;19(1):221.
6. Cate F, Kapp ME, Arnold SA. Core needle biopsy and fine needle aspiration alone or in combination: diagnostic accuracy and impact on management of renal masses. J Urol. 2017;197(6):1396–402.
7. Tsivian M, Rampersaud EN Jr, del Pilar Laguna Pes M, et al. Small renal mass biopsy—how, what and when: report from an international consensus panel. BJU Int. 2014;113(6):854–63.
8. Bawari K, Jummerlin IP, ten Kate FH, Algaba F, Trias I, Wijkstra H, De la Rosette JJ, Laguna P. What is the added value of combined core biopsy and fine needle aspiration in the diagnostic process of renal tumours? World J Urol. 2013;31(4):823–7.
9. Parks GE, Perkins LA, Zagoria RJ, Garvin AJ, Sirintrapun SJ, Geisinger KR. Benefits of combined approach to sampling of renal neoplasms as demonstrated in a series of 351 cases. Am J Surg Pathol. 2011;35(6):827–35.
10. Tong GX, Yu WM, Beaubier NT, Weeden EM, Hamele-Bena D, Mansukhani MM, O'Toole KM. Expression of PAX8 in normal and neoplastic renal tissues: an immunohistochemical study. Modern Pathol. 2009;22(9):1218–27.
11. Luong-Player A, Liu H, Wang HL, Lin F. Immunohistochemical reevaluation of carbonic anhydrase IX (CA IX) expression in tumors and normal tissues. Am J Clin Pathol. 2014;141(2):219–25.
12. Donato DP, Johnson MT, Yang XJ, Zynger DL. Expression of carbonic anhydrase IX in genitourinary and adrenal tumours. Histopathology. 2011;59(6):1229–39.
13. Szponar A, Beothe T, Kovacs G. How useful is alpha-methylacyl-CoA racemase (AMACR) immunohistochemistry in the differential diagnosis of kidney cancers? Histopathology. 2009;56(20):263–5.
14. Miliaras D, Karasavvidou F, Papanikolaou A, Sioutopoulou D. KIT expression in fetal, normal adult, and neoplastic tissues. J Clin Pathol. 2004;57(5):463–6.
15. Bagley DH, Huffman JL, Lyon ES. Flexible ureteropyeloscopy: diagnostic and treatment in the upper urinary tract. J Urol. 1987;138(2):280–85.
16. Potts SA, Thomas PA, Cohen MB, Raab SS. Diagnostic accuracy and key cytologic features of high-grade transitional cell carcinoma in the upper urinary tract. Mod Pathol. 1997;10(7):657–62.
17. Moore KL. The pelvis and perineum. In: Clinically oriented anatomy. 2nd ed. Baltimore: Williams & Wilkins; 1985.
18. Tanagho E. Anatomy of the lower urinary tracts. Campbell's urology. 6th ed. Philadelphia: WB Saunders; 1992.
19. Philip AT, Amin MB, Tamboli P, Lee TJ, Hill CE, Ro JY. Intravesical adipose tissue: a quantitative study of its presence and location with implications for therapy and prognosis. Am J Surg Pathol. 2000;24(9):1286–90.
20. Liffman R, Courtman N. Fine needle aspiration of abdominal organs: a review of current recommendations for achieving a diagnostic sample. J Small Anim Pract. 2017;58(11):599–609.
21. Pantanowitz L, Otis CN. Cystitis glandularis. Diagn Cytopathol. 2008;36(3):181–2.
22. Rashidi B, Tongson-Ignacio JE. Melamed-Wolinska bodies in urine cytology an interesting aggregate in a degenerated urothelial cell. Diagn Cytopathol. 2011;39(2):117.
23. Renshaw AA, Madge R, Granter SR. Intracytoplasmic eosinophilic inclusions (Melamed-Wolinska bodies). Association with metastatic transitional cell carcinoma in pleural fluid. Acta Cytol. 1997;41(4):995–8.
24. Quiroga-Garza G, Nassar D, Khalbuss WE, Monaco SE, Pantanowitz. Vegetable cell contaminants in urinary bladder diversion cytology specimens. Acta Cytol. 2012;56(3):271–6.
25. Bastacky S, Ibrahim S, Wilczynski SP, Murphy WM. The accuracy of urinary cytology in daily practice. Cancer Cytopathol. 1999;87(3):118–28.
26. Kannan V, Gupta D. Calculus artifact. A challenge in urinary cytology. Acta Cytol. 1999;43(5):794–800.

Female Reproductive System

9

Richard L. Cantley, Brian Smola, Kalyani Naik, and Liron Pantanowitz

Ectocervix and Vagina

The Papanicolaou (Pap) test is directed primarily at obtaining exfoliated cells from the ectocervix and endocervical canal, including the squamocolumnar junction. Squamous cells from the ectocervix and adjacent vaginal canal account for the majority of cellular elements in most Pap test samples. Benign squamous cells are typically large, polygonal cells with abundant cytoplasm and centrally located nuclei (Fig. 9.1). On Papanicolaou (Pap)-stained liquid-based cytology (LBC) preparations, squamous cells may be present as single cells or in clusters. The cytoplasm of squamous cells ranges from green-blue to pink-orange [1, 2].

The appearance of squamous cells varies depending on which layer of the ectocervical lining they are sampled from and the degree of maturation [1]. The three cell types typically seen on a Pap test, in ascending order of maturation, are parabasal, intermediate (midzone), and superficial squamous cells. The maturation index (MI), although no longer used to assess the hormonal status of women, refers to the proportion (%) of parabasal:intermediate:superficial cells. Most reproductive-aged women have a predominance of superficial and intermediate cells on Pap test sampling, with superficial cells predominating during the first half (follicular phase, estrogen dominant) of the menstrual cycle and intermediate cells predominating during the second half (luteal phase, progesterone dominant) (Fig. 9.2a). Postmenopausal women and those with squamous cell atrophy have a predominance of parabasal and intermediate cells (Fig. 9.2b).

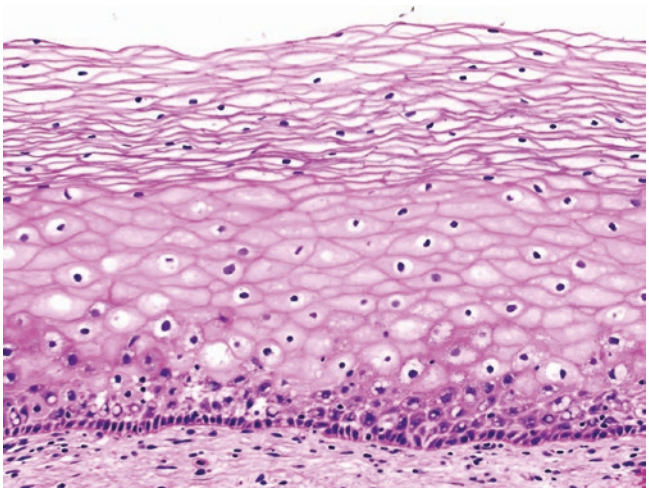

Fig. 9.1 Normal squamous epithelium of the ectocervix. The outer surface superficial squamous cells have abundant glycogenated cytoplasm and small pyknotic nuclei, while the middle intermediate cells have larger, more pale nuclei and less intracytoplasmic glycogen. A uniform, single layer of basal-type squamous cells is present at the base. Cervical biopsy, hematoxylin & eosin, 40× magnification

Superficial cells are the largest type of squamous cell (50 uM in diameter), located at the mucosal surface of the squamous epithelium. Their nuclei are very small (5 uM) and pyknotic. The cytoplasm is usually delicate and tends to be pink-orange due to intracytoplasmic keratin accumulation. Intermediate cells, just deep to the superficial cells in the squamous lining, are slightly smaller (45 uM in diameter) with slightly larger nuclei (7–8 uM). The chromatin of intermediate cells is more pale than superficial cells. Like superficial cells, intermediate cells tend to be polygonal in shape but have less cytoplasm, which more commonly appears green on Pap stain. Parabasal cells are the smallest (20–30 uM in diameter) and most deeply located of the commonly encountered squamous cells seen on a Pap test. They are typically round in shape and have small centrally located nuclei that are slightly larger than intermediate cell nuclei. Their cytoplasm is dense, often appearing similar to meta-

R. L. Cantley (✉) · B. Smola · K. Naik
Department of Pathology, University of Michigan, Ann Arbor, MI, USA
e-mail: rcantley@med.umich.edu; bsmola@med.umich.edu; knaik@med.umich.edu

L. Pantanowitz
Department of Pathology, Michigan Medicine, Ann Arbor, MI, USA
e-mail: lironp@med.umich.edu

M. Lew et al. (eds.), *Normal Cytology*, https://doi.org/10.1007/978-3-031-20336-7_9

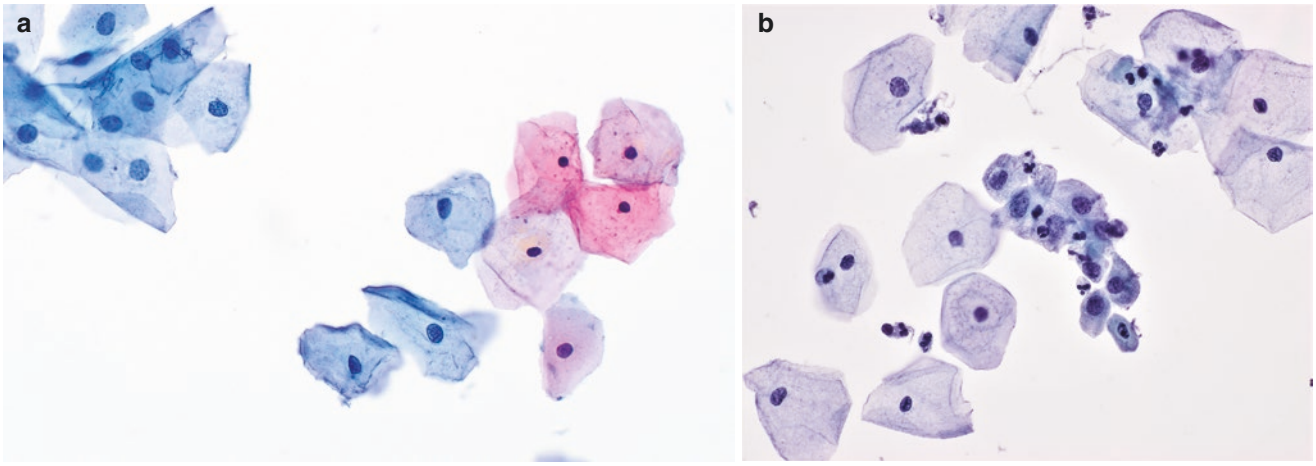

Fig. 9.2 (**a**) Superficial and intermediate cells predominate in this Pap test from a woman of reproductive age. The intermediate cells have slightly larger, paler nuclei (left) than the pyknotic nuclei of the superficial cells (right). (**b**) Parabasal cells, shown in the center of this image, are less than half the diameter of adjacent intermediate cells, and also have slightly larger nuclei and denser cytoplasm. Cervical Pap, ThinPrep preparation, Papanicolaou stain, 40× magnification (**a**, **b**)

plastic squamous cells. Basal (reserve) cells are uncommonly encountered in the Pap test. They are approximately 10 uM in diameter, with very scant but dense cytoplasm, and contain central nuclei similar to those seen in parabasal cells. Reserve cells are more likely to be encountered with reserve cell hyperplasia related to microglandular hyperplasia.

Squamous metaplastic cells are immature epithelial cells present at the squamocolumnar junction (transformation zone). They are typically present in cohesive sheets with interlocking cells that have distinctive cell borders [1, 3]. Approximately the size of parabasal cells and containing similarly dense cytoplasm, squamous metaplastic cells are difficult to distinguish from parabasal cells in practice when present singly or in small groups (Fig. 9.3). Like other benign squamous cell types, the nuclei of these metaplastic cells are smooth bordered with evenly distributed chromatin. Immature squamous metaplasia is marked by groups of small, nonkeratinizing metaplastic squamous cells with relatively scant cytoplasm which can impart a hyperchromatic appearance that resembles a high-grade squamous intraepithelial lesion (HSIL) at low to mid scanning magnification. However, nuclear overlap is minimal and the nuclei are not enlarged or irregular.

Squamous cells may show a variety of benign, physiological changes that are important to recognize, as these morphologic changes can overlap with those seen in cervical dysplasia. Navicular cells are intermediate cells seen normally during increased endogenous or exogenous progesterone exposure, such as during the luteal phase of the menstrual cycle, pregnancy, and with progesterone-based birth control [4]. They are so named because of their "boat-shaped" appearance, with a thick outer rim of dark cytoplasm and an inner portion of yellowish-brown cytoplasm

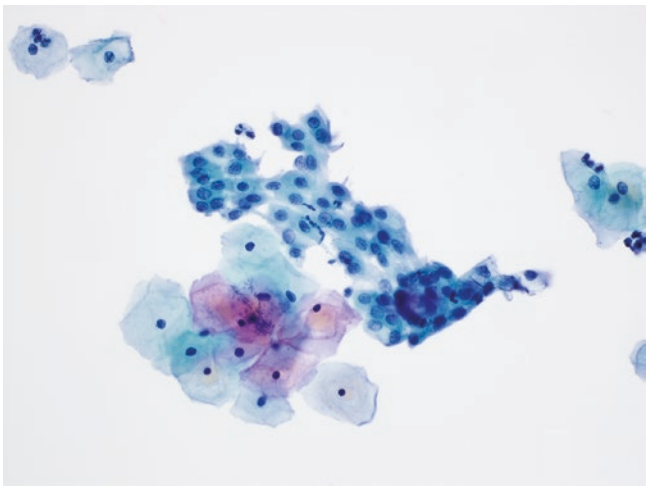

Fig. 9.3 Squamous metaplastic cells are shown present in a cohesive streaming sheet. Nuclei are approximately the size of intermediate cell nuclei, with euchromatin and smooth nuclear borders. Cervical Pap, ThinPrep preparation, 40× magnification

that is rich in glycogen. As a result, navicular cells can take on a pseudo-koilocyte appearance. However, the nuclei remain typical of benign intermediate cells, and the yellowish appearance of the central cytoplasm is distinct from the achromic clearing seen in koilocytes. The background in navicular cell-rich Pap tests will typically show naked intermediate cell nuclei, due to cytolysis, and increased lactobacilli (Fig. 9.4a, b). The naked nuclei may resemble inflammatory cells and sometimes can mimic *Trichomonas vaginalis* parasitic organisms. Occasionally, keratinizing squamous cells can contain Herxheimer spirals, which are twisted or coiled keratin fibrils (tonofilaments) seen within

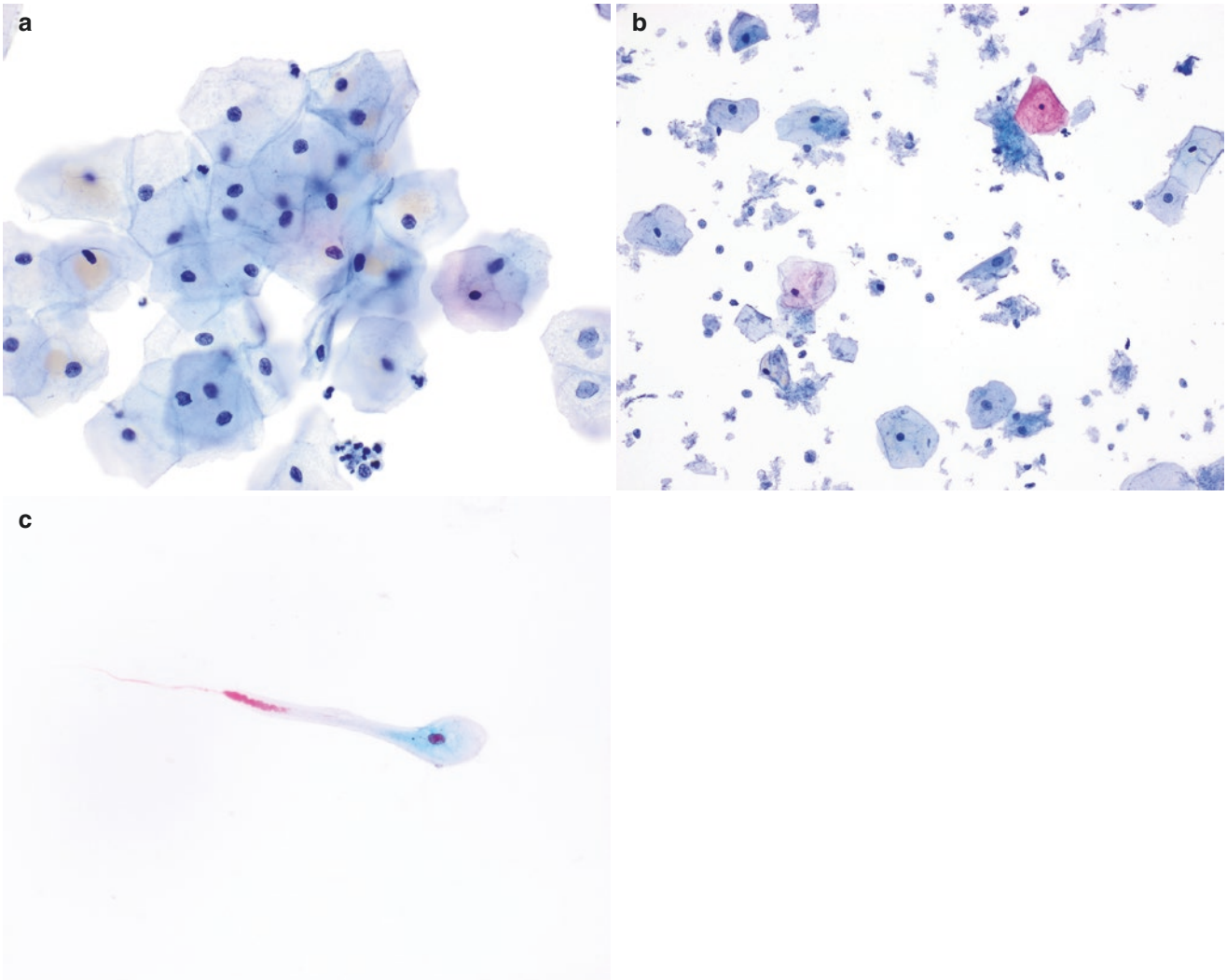

Fig. 9.4 (**a**) Navicular cells are glycogenated intermediate squamous cells. Glycogen imparts a clear to yellow appearance to the cytoplasm around nuclei, and should not be mistaken for koilocytes. (**b**) Cytolysis occurs when lactobacilli lyse the cytoplasm of navicular cells. Naked nuclei are abundant, and lactobacilli are seen on the surface of adjacent intact squamous cells. (**c**) Squamous cell with Herxheimer spiral, a coil-shaped intracytoplasmic keratin fibril. Cervical Pap, ThinPrep preparation, 20× (**b**) and 40× magnification (**a**, **c**)

the cytoplasm of spindle-shaped squamous cells (Fig. 9.4c). These spirals may be associated with benign metaplastic cells or associated with radiation-induced change, but can also be encountered in tadpole-shaped squamous cells in keratinizing dysplasia or squamous cell carcinoma [5]. The presence of these spirals can help differentiate spindle-shaped squamous cells from smooth muscle cells or fibroblasts.

Squamous cell atrophy can be a physiological or pathological process, ultimately related to a decreased estrogenic state. Atrophic smears are typical in postmenopausal patients and in the postpartum period. In Pap tests demonstrating atrophy, parabasal cells predominate, but basal cells may also be present and should not be mistaken for HSIL [6, 7]. Though parabasal and basal cells have high nuclear to cytoplasmic ratios, their nuclei are small (10 uM) with evenly distributed chromatin (Fig. 9.5). Pseudo-keratosis, marked by polygonal squamous cells with dense cytoplasm and small degenerated central nuclei, is commonly identified in both atrophic smears and other relatively high progesterone states (e.g., post-pregnancy).

Parakeratosis and hyperkeratosis are reactive, protective conditions that may be seen in both benign and malignant processes [1, 2]. Thickening (plaques) of the squamous epithelium occurs as a result of chronic irritation (e.g., uterine prolapse), and consequentially keratotic squamous cells from the mucosal surface can be sampled during a Pap test. On Pap tests, these keratinized cells are typically intensely orangeophilic. Two forms of keratosis exist: hyperkeratosis and parakeratosis. Hyperkeratosis is marked by plaques of anucleate superficial squamous cells (Fig. 9.6a). Parakeratosis is marked by keratinizing squamous cells that have dense

cytoplasm and small, pyknotic nuclei (Fig. 9.6b). Often, parakeratotic cells take on a spindled, elongated shape in comparison to the typical polygonal shape of squamous cells. In most cases, parakeratosis and hyperkeratosis are associated with benign and reactive processes, but careful examination is necessary when keratoses are present, as such protective processes may also result from dysplastic and malignant conditions. Contaminating squamous cells from the vulva or skin can mimic keratosis. Pseudo-keratosis can be seen with high progesterone states (e.g., postpartum) and atrophy and is characterized by orangeophilic degenerated glandular cells with pyknotic nuclei.

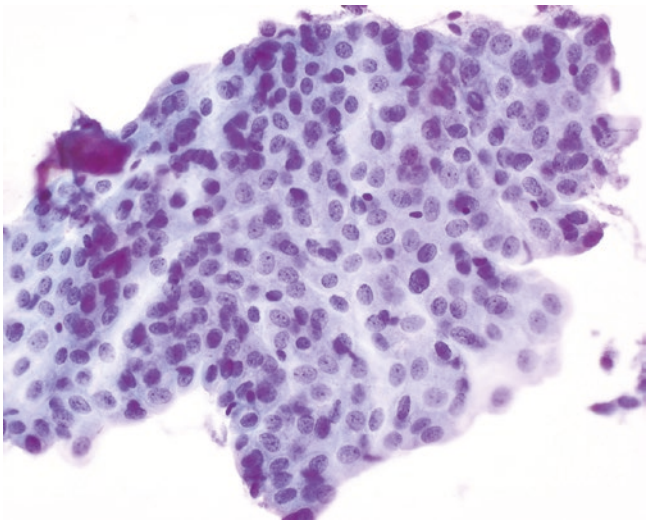

Fig. 9.5 Tightly cohesive group of parabasal-type squamous cells in a patient with atrophy. Cervical Pap, ThinPrep preparation, 40× magnification

Transitional cell metaplasia is less common than squamous metaplasia, but it is not infrequently encountered on Pap tests. Like atrophy, it may be encountered in postmenopausal patients. It is also commonly seen in patients receiving exogenous testosterone therapy (e.g. female-to-male transgender patients) and in patients who have received partial agonist estrogen therapy (e.g., Tamoxifen) [8]. Transitional cell metaplasia exhibits cohesive sheets of squamous cells resembling squamous metaplastic cells (Fig. 9.7a). Nuclei from transitional cell metaplastic cells have smooth borders, fine chromatin, and a distinctive longitudinal nuclear groove that helps distinguish these cells from squamous metaplasia. Small parabasal-type cells ("small cell change") are often present in conjunction with transitional cell metaplasia (Fig. 9.7b).

Reactive/reparative change in squamous cells is important to recognize, as they represent benign changes that morphologically overlap with invasive carcinoma. In fact, under regulations from the Clinical Laboratory Improvement Amendments (CLIA) of 1988 in the United States, all Pap tests screened as negative with reactive or reparative changes must be reviewed by a pathologist due to this morphologic overlap. However, reparative changes are not premalignant. They occur in association with typical causes of inflammation and irritation, such as infections, physical or chemical irritation, and intrauterine devices, although in many cases, an etiology is not clear.

Reactive and reparative changes are characterized by cohesive sheets of nonoverlapping squamous cells that may have a streaming appearance [6, 7] (Fig. 9.8). Nuclear enlargement is

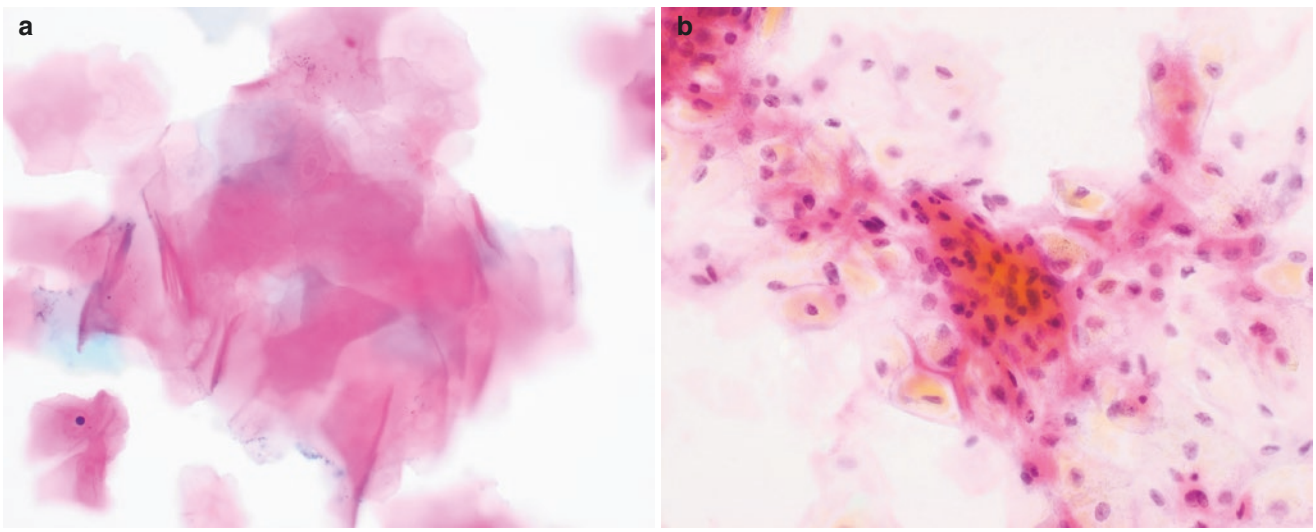

Fig. 9.6 (**a**) Hyperkeratosis in this Pap test appears as anucleated superficial squamous cells, often in association with occasional nucleated forms (bottom left). (**b**) Parakeratosis is marked by squamous cells with dense, keratin-rich cytoplasm and dark, elongated nuclei. Cervical Pap, ThinPrep preparation, 50× magnification (**a**). Cervical Pap, alcohol-fixed smear preparation, Papanicolaou stain, 50× magnification (**b**)

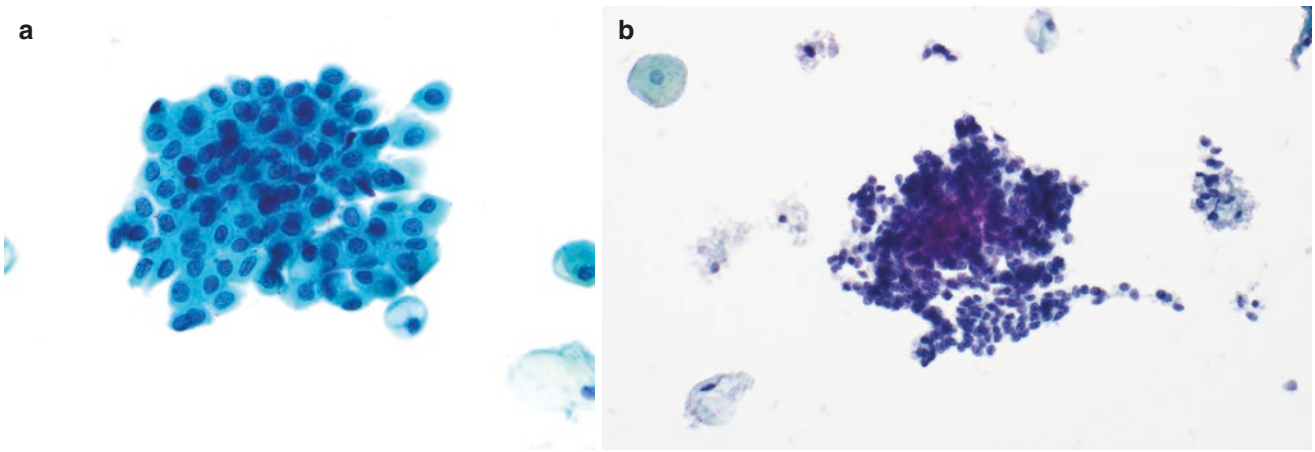

Fig. 9.7 (**a**) Transitional cell metaplasia, present as cohesive group resembling squamous metaplastic epithelium. Nuclei are round to elongated with longitudinal grooves. (**b**) Small cell change is shown in a patient receiving Tamoxifen. These basal-like epithelial cells have nuclei that occupy nearly the entire cell diameter. However, nuclear size has not increased and chromatin is bland. Cervical Pap, SurePath preparation, 50× magnification (**a**). ThinPrep preparation, 50× magnification (**b**)

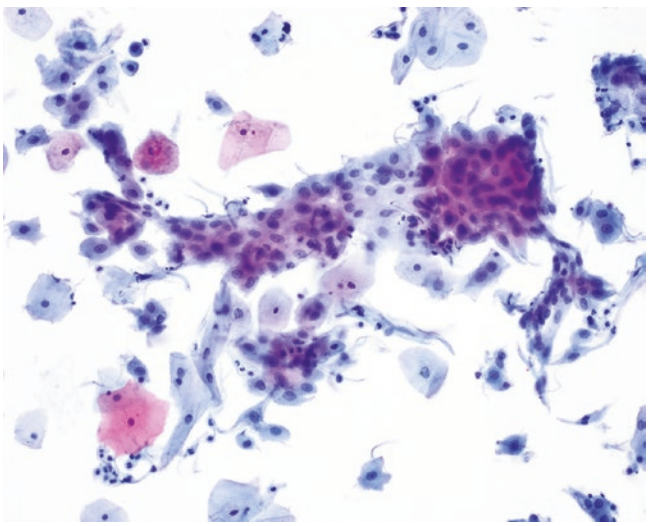

Fig. 9.8 Reactive changes in squamous cells include mild nuclear enlargement and central nucleoli. Note that the nuclear membranes are smooth, and chromatin is pale and open. Cervical Pap, ThinPrep preparation, 40× magnification

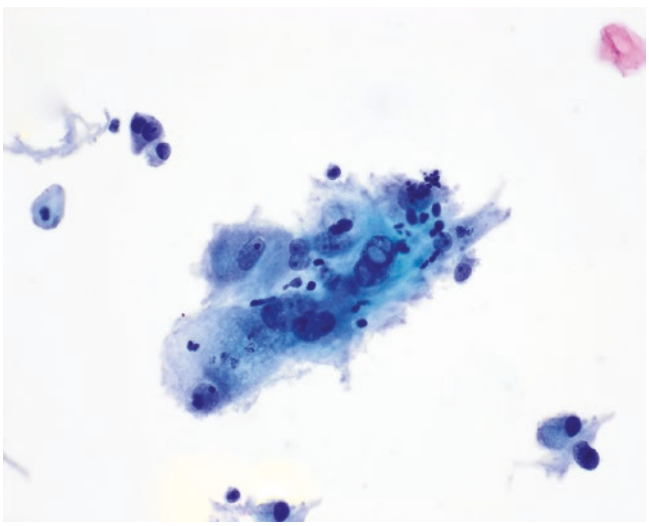

Fig. 9.9 Radiation change in squamous cells, exhibiting increased nuclear size but low nuclear to cytoplasmic ratios. Characteristic smudgy chromatin is notable. Cervical Pap, ThinPrep preparation, 60× magnification

often present, but nuclear membranes are typically smooth and chromatin is euchromatic to mildly hyperchromatic. Multinucleation may be seen, but no koilocytic changes are present. The cytoplasm of reactive squamous cells can range from dense and metaplastic to larger more mature forms, the latter of which may display polychromatic cytoplasm that imparts a "moth-eaten" appearance. Perinuclear halos, a thin rim of cytoplasmic clearing around the nucleus, can be seen. In contrast to koilocytosis, the cleared area is smaller and nuclear changes of dysplasia are absent.

Reactive and reparative changes can show different backgrounds and cytologic appearances depending on the underlying cause [1, 6, 7]. Bacterial vaginosis, trichomonas infection, and herpes virus infection are associated with polymorphous leukocytic (acute) inflammation. A lymphocytic background, with polymorphous lymphocytes and tingible body macrophages (follicular cervicitis), can be seen in chlamydial infections and other reactive inflammatory conditions. Radiation change includes markedly increased cell size with preserved nuclear to cytoplasmic ratios, anisonucleosis, multinucleation, and degenerated "smudgy" chromatin (Fig. 9.9). Nucleoli can be prominent and multiple. Cytoplasm is abundant, frequently vacuolated, and polychromatic.

Endocervix

The surface epithelium of the endocervix is composed of glandular cells with columnar morphology, which are approximately twice as tall as wide (Fig. 9.10) [1, 7]. When present in groups, depending on the direction of their long axis, they display either honeycomb (en face) or picket-fence arrangements (long axis visible). En face endocervical cells show evenly spaced nuclei (Fig. 9.11a). The nuclei, which are slightly larger than intermediate squamous cell nuclei, are basally located, which becomes apparent in picket-fence arrangements (Fig. 9.11b). Like benign squamous cells, endocervical cells have even chromatin distribution and smooth, round nuclear borders. Multinucleated endocervical cells are sometimes seen. Nucleoli are more commonly visible than in squamous cells. The cytoplasm is better appreciated in picket-fence arranged cells, where moderately abundant granular or vacuolated apical cytoplasm is appreciated. The cytoplasm appears less abundant in honeycomb cell arrangements.

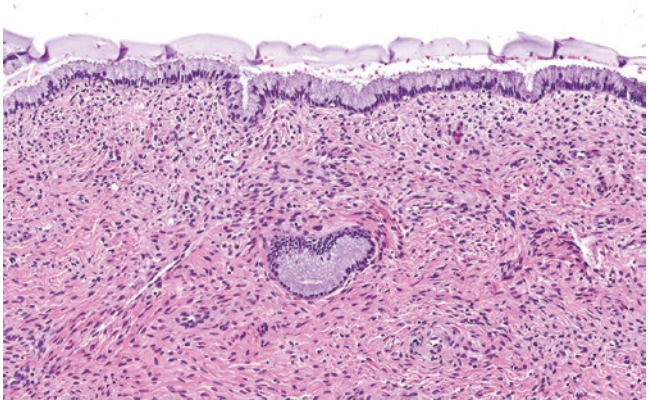

Fig. 9.10 Normal endocervical mucosa composed of a single layer of surface columnar epithelium. Nuclei are basally located and uniform. An endocervical gland is also present in the superficial cervical stroma. Cervical biopsy, hematoxylin & eosin, 20× magnification

Tubal metaplasia is a common finding in the Pap test, with endocervical cells undergoing metaplastic change to ciliated epithelium [9]. The apical surface of the cells contains terminal bars with attached cilia (Fig. 9.12). The basally located nuclei may be slightly enlarged with prominent nucleoli, which can be mistaken for atypical endocervical cells on a Pap test when cilia and terminal bars are obscured from view.

Reactive change is also commonly encountered in endocervical glandular cells. As with squamous cells, they may be associated with a variety of inflammatory or directly irritating factors. Streaming of reactive endocervical cells can give a whorled appearance to the endocervical cell groups. Significant nuclear enlargement of up to twice the size of nonreactive endocervical epithelium is common, and nucleoli can become more prominent. However, nuclear membranes remain smooth and chromatin is evenly distributed (Fig. 9.13). Of note, mitoses can be encountered in benign reparative change. As with squamous cells, the background may include various inflammatory elements [6, 7].

Cytoplasmic vacuolization can be encountered in reactive endocervical cells, particularly when associated with an intrauterine device. Such vacuoles may be quite large, occupying most of the visible cytoplasm, in some cases displacing the nucleus and imparting a signet ring appearance. Endocervical polyps can show reactive and degenerative changes in endocervical cells, including reactive nuclear

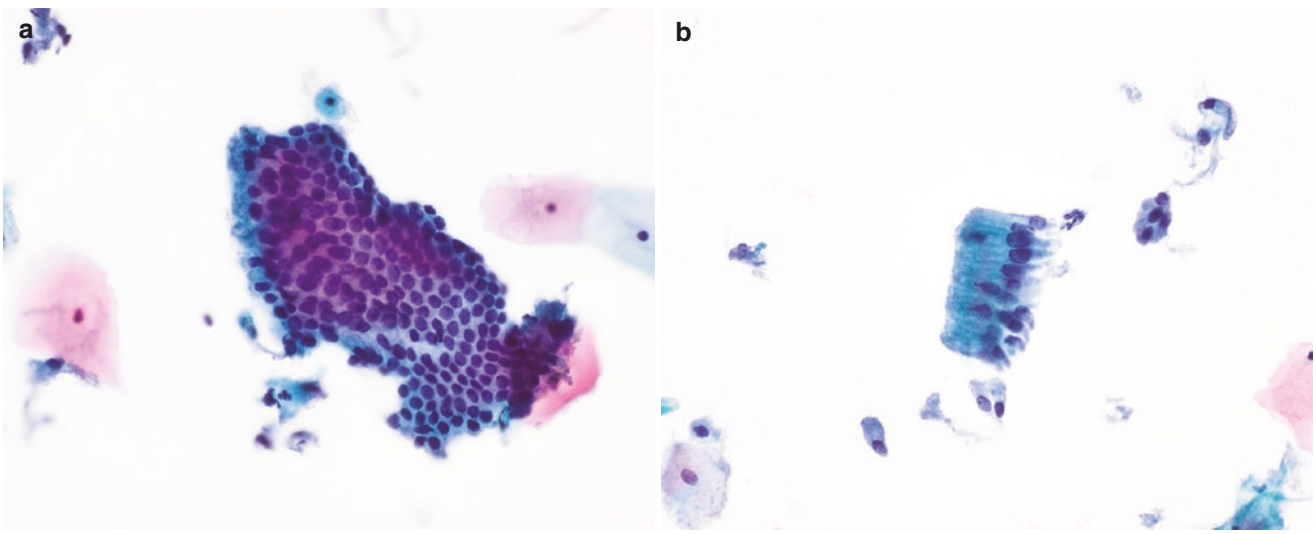

Fig. 9.11 (**a**) Endocervical cells shown in honeycomb arrangement and (**b**) "picket-fence" arrangement, with even nuclear size and shape throughout. Cervical Pap, ThinPrep preparation, 40× magnification (**a**, **b**)

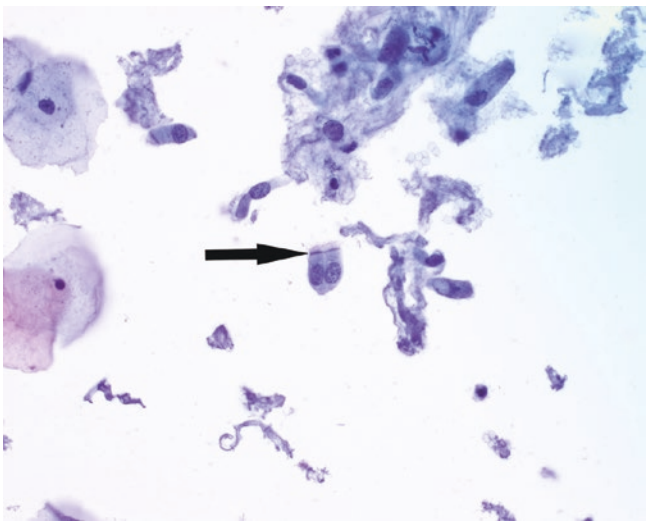

Fig. 9.12 Tubal metaplasia in endocervical cells is shown in the center of the image, with a visible apical terminal bar and attached cilia (arrow). Cervical Pap, ThinPrep preparation, 40× magnification

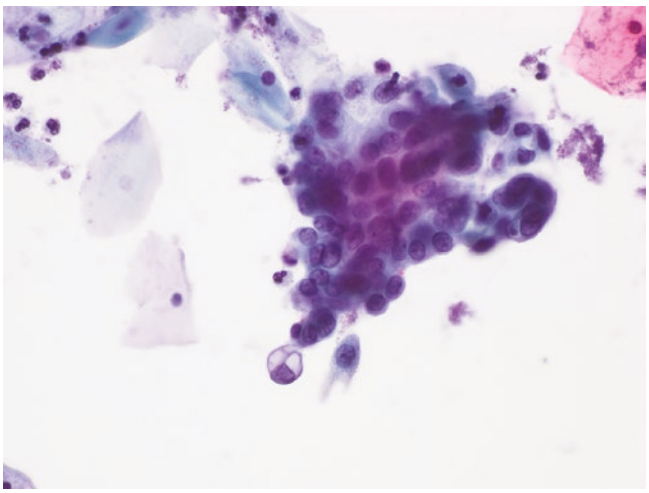

Fig. 9.13 Endocervical cells with reactive change in a patient with an intrauterine device. Mild nuclear enlargement and nucleoli are visible. Note the single vacuolated cell. Cervical Pap, ThinPrep preparation, 50× magnification

change and cytoplasmic vacuolization which can resemble signet ring cells.

Although glandular cells seen on a Pap test are primarily of endocervical origin, benign glandular cells resembling endocervical epithelium can occasionally be seen in post-hysterectomy patients (Fig. 9.14). These may represent vaginal adenosis or glandular rests in vaginal mucosa [1].

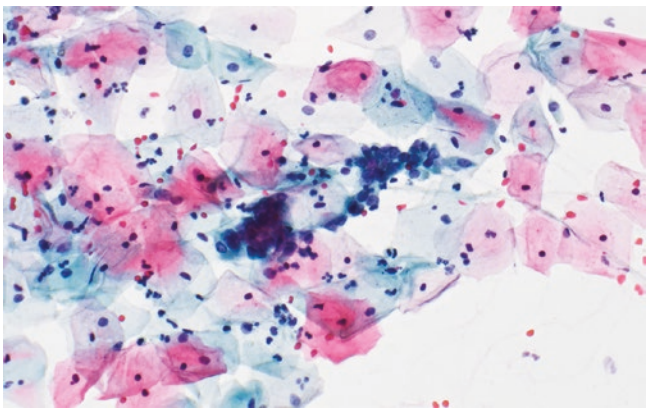

Fig. 9.14 Vaginal adenosis in a patient status-post-hysterectomy. Benign glandular cells in the center of this image, resembling endocervical glands, can be encountered in vaginal Pap tests. Vaginal Pap, ThinPrep preparation, 40× magnification

Endometrium

Normal endometrial glands are present in the proliferative phase during the first half of the menstrual cycle and the secretory phase in the second half (Fig. 9.15a, b). Proliferative-phase endometrium is more commonly encountered on Pap tests. Endometrial glandular cells are identified in 2–3% of Pap test cytology specimens, and they may be acquired either as a result of normal shedding during the menstrual cycle or direct sampling of the lower uterine segment [10]. Diagnostic endometrial cytology sampling is also occasionally performed [11].

Endometrial cells are most commonly encountered in reproductive-aged women during the first half of the menstrual cycle. Endometrial sampling during days 1–5 of the menstrual cycle typically reveals small clusters of endometrial glandular cells in a background of blood and cellular debris. Later in the cycle, on days 6–10, the Pap test commonly shows an "exodus" pattern, with cellular clusters composed of a central portion of endometrial stromal cells surrounded by benign endometrial glandular cells. Cytoplasmic vacuolization may be seen in endometrial glandular cells during exodus, as well as histiocytic inflammation.

Exfoliated endometrial cells are usually present in packed, three-dimensional clusters with scant cytoplasm (Fig. 9.16). Normal endometrial glandular cells are very small and are about a third the size of endocervical cells and comparable to basal squamous cells [10]. Their nucleus occupies nearly the entire cytoplasmic diameter. However, these nuclei are small, approximately the size of an intermediate squamous cell

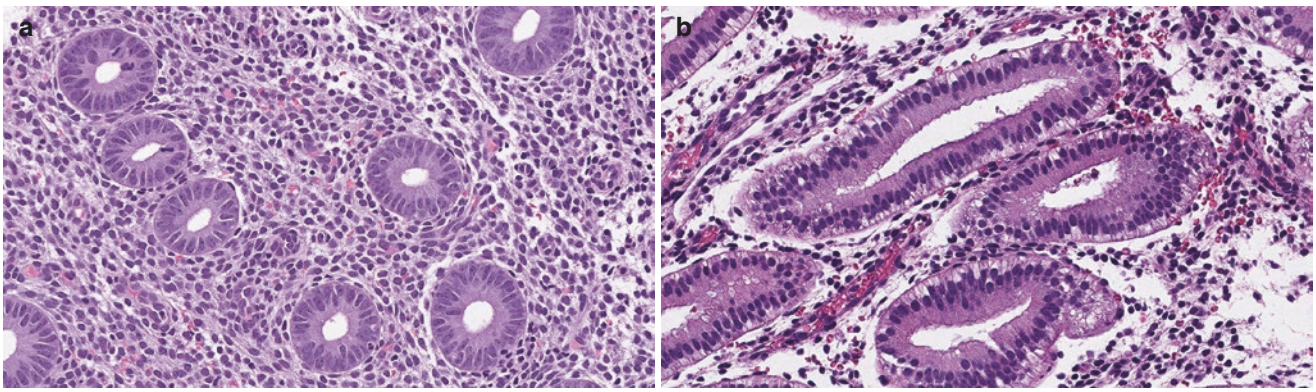

Fig. 9.15 Normal endometrial glands in (**a**) proliferative phase have a tubular appearance with frequent mitotic figures while (**b**) secretory glands have more abundant cytoplasm with secretory vacuoles, and mitoses are absent. Endometrial biopsy, hematoxylin & eosin, 40× magnification (**a**, **b**)

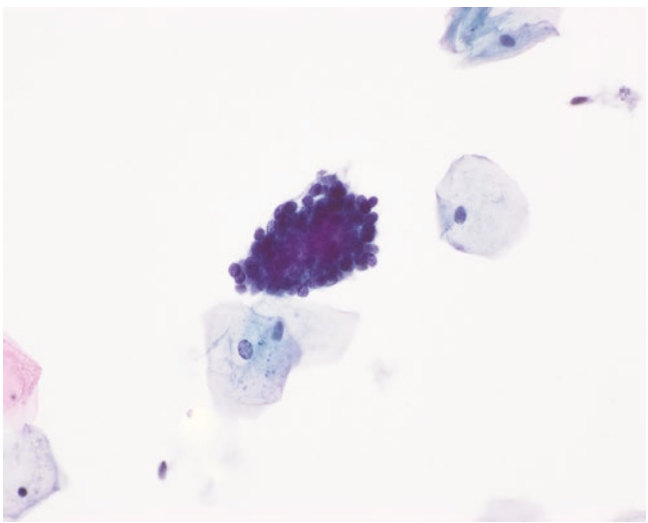

Fig. 9.16 Exfoliated endometrial cells. Small clusters of endometrial glandular cells are shown. These cells are tightly cohesive, with very scant cytoplasm and nuclei that are of the size of adjacent intermediate squamous cells. Cervical Pap, ThinPrep preparation, 40× magnification

nucleus (7–8 uM). Single cell necrosis (karyorrhexis) is often evident, but mitoses are absent. Endometrial stromal cells are less commonly encountered on a Pap test, but have a similar appearance to glandular cells and are present in tightly cohesive clusters. The nuclear density of benign endometrial stroma is quite high, and the nuclei are often compressed and somewhat elongated or spindled. When present, endometrial stroma is often surrounded by endometrial glandular tissue. Endometrial stromal cells can resemble histiocytes and may also mimic the appearance of HSIL.

Although endometrial cells are considered an unremarkable Pap test finding in younger women during the first half of the menstrual cycle, the presence of endometrial cells in women 45 years of age or older should be reported according to the Bethesda System (third edition) guidelines. This is due to the presumed increased risk of endometrial hyperplasia and endometrial carcinoma when endometrial cells are identified in perimenopausal and postmenopausal patients, even in the absence of cellular atypia.

Direct sampling of the endometrium occurs when high sampling of the endocervical canal results in abrasion of the endometrium in the lower uterine segment (LUS). It occurs most frequently in Pap tests obtained from patients who have had prior excisional cervical procedures. In contrast to exfoliated endometrial cells, directly sampled endometrium has no increased association with endometrial hyperplasia or neoplasia on a Pap test, and is not considered a reportable finding [12].

Whereas shed endometrial cells are often present in small, three-dimensional groups, directly sampled endometrial fragments are larger and two dimensional (Fig. 9.17). The fragments are tubular shaped and may be branched [12]. In the proliferative phase, directly sampled endometrium shows endometrial glandular cells that are tightly packed with scant cytoplasm and indistinct cell borders. Nucleoli are inconspicuous, and mitoses may be encountered. Endometrial stromal cells can sometimes be seen at the edges of cell groups. Secretory endometrium appears similar to proliferative endometrium, but the cytoplasm of endometrial cells is often more abundant and vacuolated, and mitoses are not identified. Atrophic endometrium appears similar to proliferative endometrium, although decreased nuclear density may be encountered, and mitoses are absent.

Pregnancy/progesterone-related changes seen in endometrial glandular and stromal cells can occasionally appear in Pap test cytology [13]. Prominent decidualization of endo-

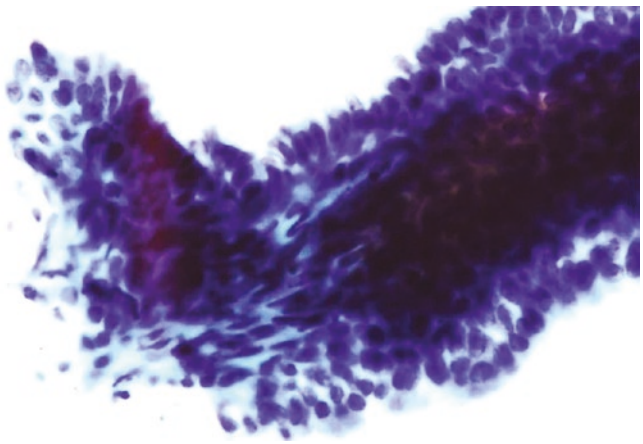

Fig. 9.17 Branching and folding sheets of directly sampled lower uterine segment endometrium are shown. Cervical Pap, SurePath preparation, 40× magnification

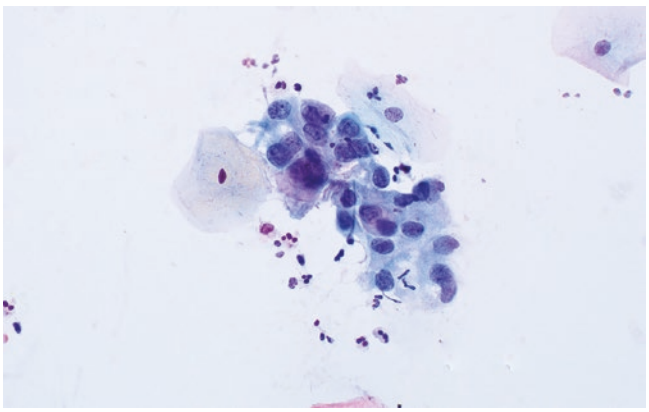

Fig. 9.18 Glandular cells with Arias-Stella reaction in a peripartum patient. Note the marked nuclear enlargement and chromatin irregularity seen in this physiological, pregnancy-related change. Cervical Pap, ThinPrep preparation, 50× magnification

metrial and cervical stroma occurs late in pregnancy and in the postpartum period. Like endometrial cells, the stromal cells have abundant granular cytoplasm, well-defined and distinct cell borders, and a central, round nucleus with a prominent nucleolus. They can appear singly or in clusters in a Pap test. Arias-Stella reaction is a prominent glandular change that may occur in endometrial and endocervical mucosa associated with pregnancy. Cytologically, this resembles clear cell carcinoma, so clinical history and recognition of this change is important. Glandular cells with Arias-Stella reaction show severe nuclear atypia, marked enlargement, hyperchromasia, and vesicular chromatin, with vacuolated clear to eosinophilic cytoplasm (Fig. 9.18). Syncytiotrophoblasts, the multinucleated form of placental trophoblastic cells, are occasionally encountered. Their cytoplasm is dense to coarsely granular, and often there is a "tail" of cytoplasm at one end. The nuclei are bland with distinct nucleoli and can be difficult to distinguish from histiocytic nuclei.

Endometriosis is defined by the presence of ectopic endometrial tissue, and it is occasionally encountered in a Pap test and in pelvic washing cytology [14]. It is classically diagnosed by the presence of at least two of the following: endometrial glands, endometrial stroma, and hemosiderin-laden macrophages. It can occur anywhere in the gynecologic tract, including the cervix. Endometriosis can also form mass lesions which may be targeted by fine needle aspiration (FNA) biopsy. Endometrial glands and hemosiderin-laden macrophages tend to predominate in FNA preparations, although intact endometrial glandular and stromal tissue is sometimes seen (Fig. 9.19).

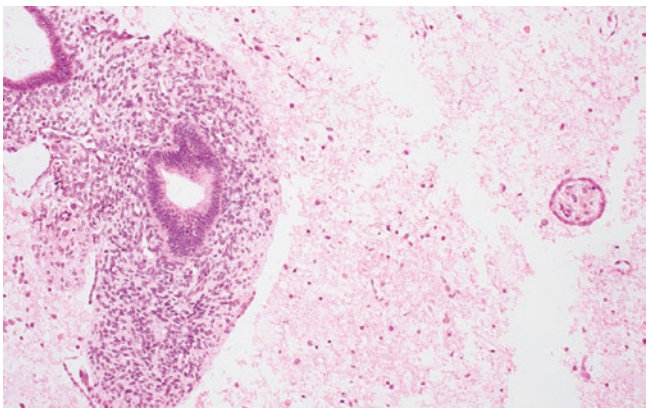

Fig. 9.19 Intact fragments of endometrial-type glands and stroma in a patient with endometriosis, with epithelium and associated hemosiderin-laden macrophages noted on the right side. Pelvic washing, cell block, hematoxylin & eosin, 40× magnification

Inflammatory Elements

Pap tests may contain histiocytes that appear singly and in loose aggregates of cells with moderately abundant cytoplasm, which can range from being foamy, granular to dense [1]. These macrophages may contain hemosiderin, as well as other cellular and acellular debris. The shape of their nuclei ranges from bean-shaped to round, and their chromatin is characteristically bland with a finely granular appearance. Histiocytes are commonly encountered in Pap tests during exodus (days 6–10) and are considered a normal finding during the perimenstrual period. They are also commonly encountered in patients with prior cervical procedures, and

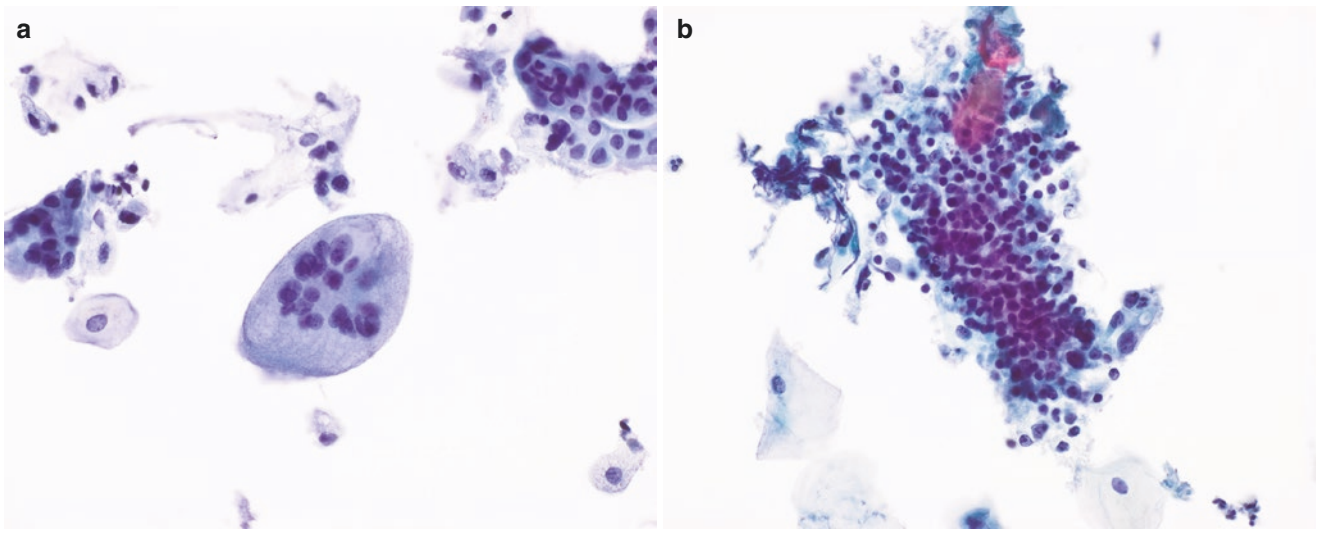

Fig. 9.20 (**a**) Multinucleated giant cell is shown in a patient who has undergone prior instrumentation. (**b**) Follicular cervicitis is shown marked by the presence of many polymorphous lymphocytes. Cervical Pap, ThinPrep preparation, 40× (**a**) and 50× (**b**) magnification

when a foreign body (e.g., intrauterine device) is present. In postmenopausal patients, foamy histiocytes or hemosiderin-laden histiocytes may be associated with endometrial carcinoma, and in this clinical setting should thus prompt careful examination for associated endometrial cells or other cellular glandular abnormalities.

Multinucleated giant cell forms of histiocytes can be seen in patients with prior pelvic surgery or radiation history, and may also be encountered in the postpartum period and in postmenopausal patients. Multinucleated giant cells have cytoplasm similar to that of associated mononuclear histiocytes, and their nuclei are likewise bland and uniform (Fig. 9.20a).

Polymorphonuclear leukocytes (neutrophils) and lymphocytes are the most commonly encountered inflammatory cells seen in Pap tests [1, 15]. Neutrophils are slightly larger (~10 uM in diameter), with multilobed nuclei and scant pale cytoplasm. They are the predominant infiltrate of acute inflammation and can be associated with many benign and malignant conditions, even obscuring underlying abnormal cells. In many cases, no obvious cause for acute inflammation is present, although bacterial vaginosis and atrophic vaginitis are common etiologies. Lymphocytes are slightly smaller (around 8 uM in diameter) and have unilobed, round nuclei that occupy the bulk of the cell diameter. A thin rim of dense cytoplasm is present. In cervical samples, small lymphocytes tend to predominate, with pyknotic nuclei. However, in follicular cervicitis, when germinal centers form within cervical epithelium, polymorphous lymphocytosis is seen (Fig. 9.20b). Small lymphoid cells are intermixed with larger, more immature cells that can display more vesicular chromatin. In such cases, tingible body macrophages can also be evident. Although classically associated with chlamydial infection, many cases of follicular cervicitis are associated with prior instrumentation or are idiopathic in nature.

Common Microorganisms

A number of microbial organisms are commonly encountered in routine Pap tests, including normal vaginal flora, opportunistic organisms, and pathogenic infectious organisms. A focused approach to the most commonly seen microbial elements is described here.

Lactobacilli (previously called Doderleïn bacilli) are facultative anaerobic, Gram-positive bacterial rods that are part of the normal vaginal flora [1]. They maintain the acidic vaginal pH through lactic acid production. They appear as thin, rod-shaped bacilli on the surface of squamous cells and in the background. They induce cytolysis of intermediate cells (Fig. 9.4b), releasing glycogen which allows for production of lactic acid and maintenance of the vaginal pH. As a result, naked nuclei and fragments of cytoplasm from intermediate squamous cells are frequently seen in combination with lactobacilli in a Pap test.

Bacterial vaginosis is a polymicrobial infectious state caused by an overgrowth of anaerobic bacteria, with *Gardnerella vaginalis* being the most common microorganism [15]. In contrast to the thin rod shape of lactobacilli, Gardnerella are coccobacilli. When present, these coccobacilli often coat the surface of squamous cells, imparting the classic "clue cell" appearance seen on Pap tests (Fig. 9.21a). Clumps of coccobacilli can also be seen in the background. Squamous cells often show associated reactive change, and associated acute inflammation is often present.

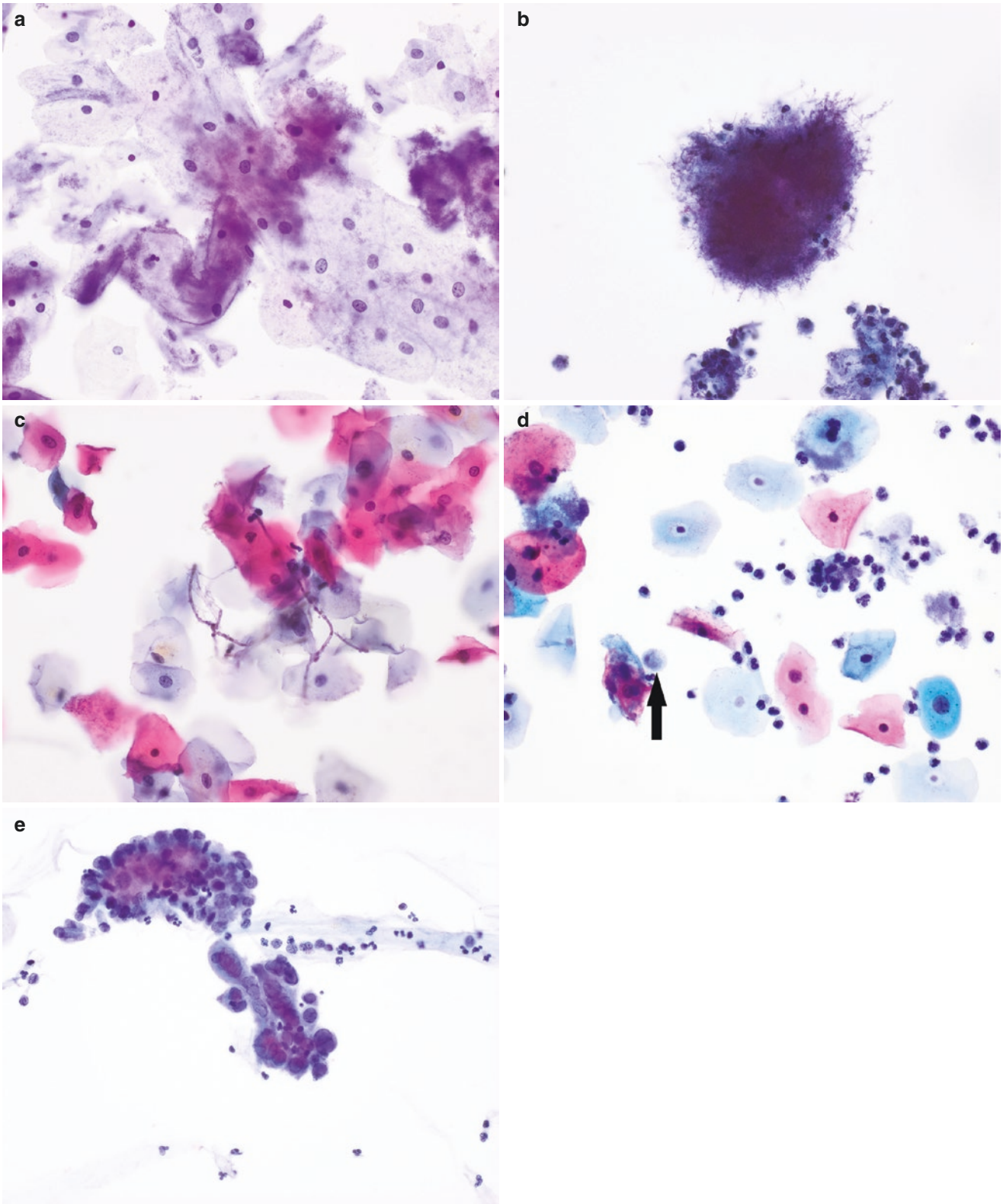

Fig. 9.21 (**a**) Bacterial vaginosis. Squamous cells are coated with coccobacilli, imparting a "shaggy" appearance to the cytoplasm. (**b**) Actinomyces presenting as a tangle of filamentous bacteria. (**c**) Branching pseudohyphae of *Candida* spp. (**d**) Trichomonas organism (arrow) appears as a small ovoid cell with a tiny, pale nucleus that may be hard to visualize. Note the reactive perinuclear clearing in adjacent squamous cells and background associated neutrophils. (**e**) Cytopathic effect of herpes simplex virus (HSV). The nuclei of infected epithelial cells appear glassy, with marginated chromatin and frequent multinucleation. Cervical Pap, ThinPrep preparation, 40× magnification (**a**–**e**)

Actinomyces are Gram-positive filamentous bacteria commonly present in the Pap test of patients with intrauterine devices, and infections are often asymptomatic [1, 15]. Actinomyces presents as dense balls of radiating filamentous bacteria, giving a "fluffy ball" or "dust bunny" appearance (Fig. 9.21b). Macrophages and neutrophils may be seen in the background, along with reactive epithelial change.

Candida subspecies are also frequently encountered in Pap tests. In many cases, Candida infections are asymptomatic and may be associated with varying degrees of acute inflammation and reactive squamous cell change. Candida on Pap tests presents as round to oval budding yeasts (~5 uM) with pseudohyphae (Fig. 9.21c). Candida also tends to "skewer" squamous cells, creating a characteristic "shish kabob" appearance [1].

Trichomonas vaginalis is a common parasitic sexually transmitted infection, which may be asymptomatic or associated with vaginal discharge [1, 15]. Trichomonads are small oval to pear-shaped organisms, 15–30 uM in size, which may be present singly or in small aggregates. Their cytoplasm is pale gray, with red granules occasionally visible. Nuclei are eccentrically located, pale-staining, and small, approximately a quarter the size of an intermediate squamous cell nucleus (Fig. 9.21d). They have a single flagellum which is not typically visible on Pap tests. Acute inflammation is typically abundant, and collections of neutrophils ("poly balls") are often present. Reactive changes in squamous cells include a small perinuclear clearing of cytoplasm ("trich halos") that should not be mistaken for koilocytosis. Leptothrix, a long Gram-positive bacterium (several times longer than lactobacilli), is often seen in the background, and its presence almost always indicates trichomonas infection.

Chlamydia trachomatis is the most common sexually transmitted infection [1]. Chlamydia are obligate intracellular Gram-negative bacteria. Changes associated with chlamydia on a Pap test are often nonspecific and include follicular cervicitis. Intracellular inclusion bodies ("aggregate bodies") in squamous or endocervical cells can be seen in some cases. These are large clear intracytoplasmic vacuoles that can resemble mucin at scanning power, within which small elementary bodies or larger reticulate bodies may be seen.

Herpes simplex virus is another common sexually transmitted infection [1, 15]. Infected epithelial cells commonly display multinucleation, nuclear molding, and chromatin margination (Fig. 9.21e). Acute inflammation is typically abundant.

Miscellaneous Cellular and Acellular Elements

A number of miscellaneous structures and acellular or foreign substances are often identified in Pap tests and/or abdominopelvic washings at the time of gynecologic surgery. Recognition of these elements is important to avoid confusion with infection or neoplasms.

Mucin is normally produced by endocervical glandular cells and is often collected at the time of Pap test acquisition [1]. Mucin is more commonly encountered on conventional smears, as LBC removes most noncellular elements. However, abundant mucin material can be seen on LBC slides; Curschmann spirals, identical to those seen in respiratory specimens, can sometimes be encountered (Fig. 9.22a). With high estrogen states (e.g., prior to ovulation, during pregnancy) cervical mucus can form a fern-like pattern (fern-ing) on a slide. This finding is only noticeable on conventional Pap smear slides.

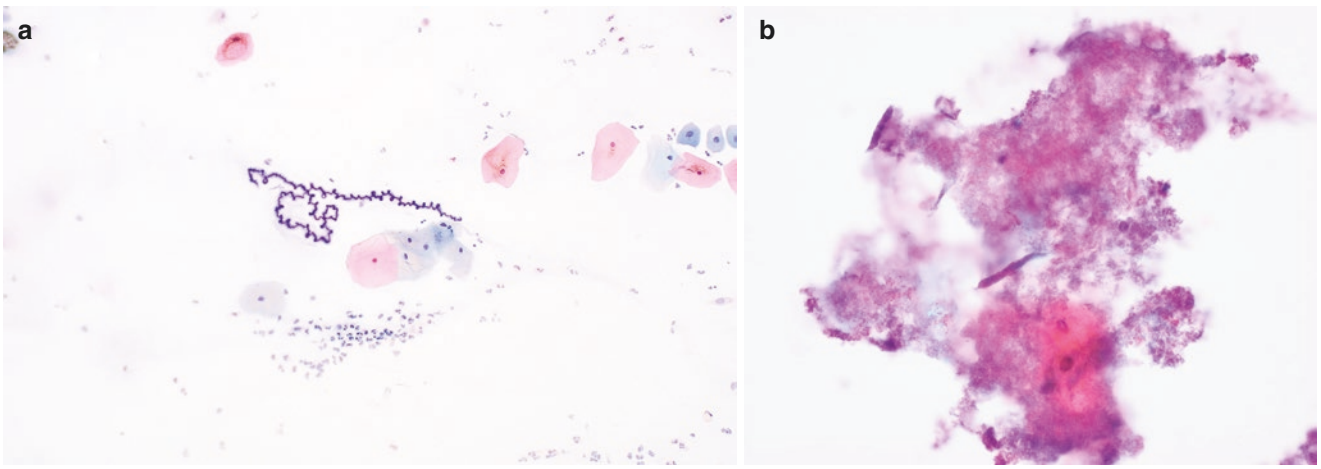

Fig. 9.22 (**a**) Curschmann spirals are shown comprised of twisted strands of mucin material. (**b**) Grainy lubricant material shown obscuring squamous cells from view. Cervical Pap, alcohol-fixed smear preparation, Papanicolaou stain, 20× magnification (**a**). Cervical Pap, ThinPrep preparation, 40× magnification (**b**)

Like mucin, lubricant gel material often used on instruments used to perform a Pap test is largely removed in LBC preparations [16]. However, amorphous "blobs" of lubricant material can occasionally make their way through the filtration process. When overly abundant, this contaminating material may obscure the visibility of squamous cells (Fig. 9.22b).

Psammoma bodies are laminated calcifications formed from the degeneration of cellular elements. They are rarely present on Pap tests but are not infrequent in abdominopelvic washings. They are associated with a range of nonneoplastic, benign, and malignant conditions including endosalpingiosis, the presence of intrauterine devices, and a range of serous neoplasms from benign to high-grade malignancy [17].

Cockleburs may be encountered in Pap tests, often in association with pregnancy. They are radiating arrays of club-shaped orange crystalline bodies surrounded by histiocytes. They may mimic actinomycosis.

Collagen balls are commonly identified in abdominopelvic washings, but rarely in spontaneous effusions [17]. They may also be occasionally seen in Pap test cytology. Collagen balls are three-dimensional collections of dense hyalinized matrix material surrounded by benign mesothelial cells with indistinct cell borders. The nuclei of involved cells may become crowded, but they are small and ovoid to flattened in shape without atypia.

Pollen and other plant material (e.g., *Alternaria* fungus) can occasionally be seen as a contaminant in Pap test cytology specimens, which can be identified by their thick refractile cell walls. Sperm can also sometimes be seen in postcoital Pap tests. Mature sperm have small pale nuclei, scant cytoplasm, and a single long flagellum at one end.

Fallopian Tubes

The fallopian tubes are not routinely sampled by FNA or directed brushing sampling. However, fallopian tube cellular elements may be encountered in numerous cytology preparations including the Pap test, either from direct exfoliation or in patients with fallopian tube prolapse. Fallopian tube epithelium may also be encountered in pelvic washing cytology at the time of gynecologic surgery, as well as at the frozen section bench in touch and smear preparations.

The fallopian tubes are lined by a single layer of columnar to cuboidal epithelium (Fig. 9.23). Classically, three epithelial cell types are described: ciliated cells, secretory cells, and intercalated ("peg") cells. Ciliated cells are the most abundant, particularly in the distal end of the tube. They are typically columnar in shape, with a terminal bar at the apical end to which fine cilia are attached. Secretory cells are more numerous in the proximal fallopian tube. Secretory cells appear similar to ciliated cells, but lack terminal bars and cilia, and may display foamy cytoplasm. The existence of smaller intercalated cells is controversial, and they are not routinely identified in cytology preparations.

Whether directly sampled or identified through passive exfoliation, fallopian tube epithelial cells may be present singly, in clusters, or in large sheets (Fig. 9.24) [17]. When in sheets, they tend to form honeycomb monolayers similar to other benign glandular epithelium. Ciliated cells are usually columnar, with a basally located, round nucleus and apical terminal bar. Ciliary "tufts" (detached fragments of apical cytoplasm from ciliated cells called ciliocytophthoria) can also be identified in Pap tests and pelvic washing specimens. Secretory cells are also columnar, and sometimes contain finely vacuolated cytoplasm. Clusters of benign fallopian tube epithelium can show moderate anisonucleosis and nuclear pleomorphism. However, they lack mitotic figures, and the presence of cilia indicates their benign nature.

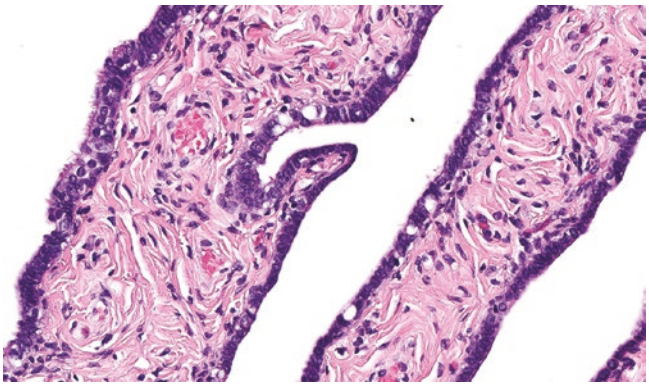

Fig. 9.23 Fimbriated end of the fallopian tube lined by single layers of ciliated columnar epithelium. Fallopian tube resection, hematoxylin & eosin, 40× magnification

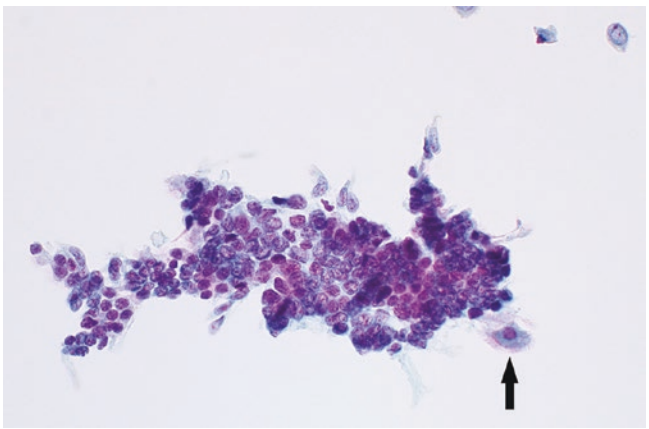

Fig. 9.24 Fallopian tube epithelium is shown in two-dimensional sheets. Nuclei are round and uniform, and occasional ciliated forms can be seen (arrow). Cervical Pap, ThinPrep preparation, 50× magnification

Endosalpingiosis is defined by the presence of ectopic, benign fallopian tube-like epithelial deposits outside the fallopian tube. This can be encountered in pelvic washings and Pap tests. Cytologically, the epithelium is indistinguishable from cells of the benign fallopian tube lining [17]. Occasionally, this process may be associated with hemosiderin-laden macrophages.

Ovaries

Like the fallopian tube, directed cytologic sampling of the ovary is uncommonly performed. However, cells of ovarian origin can rarely be seen in pelvic washings and Pap tests. In addition, FNA is occasionally performed for ovarian cysts and masses [18].

The primary cells of the ovarian follicle are the granulosa cells, which surround the maturing Graafian follicles (Fig. 9.25). Follicle cyst fluid may sometimes be sampled in patients of reproductive age. Granulosa cells are small, round cells with central round nuclei and a small but distinct rim of cytoplasm, which appear singly and in loose sheets on cytology preparations (Fig. 9.26). Their chromatin is coarsely granular, without distinct nucleoli, and occasional nuclear grooves may be present. Mitotic figures may also occur. Theca cells, the outer lining cells of the follicle, are less commonly encountered in cytologic preparations. They have more abundant, vacuolated cytoplasm than granulosa cells, with eccentrically located nuclei.

The functional corpus luteum is composed of luteinized granulosa cells, which are distinct from the nonluteinized granulosa cells of the follicle. They have more abundant granular cytoplasm, which may be vacuolated. Nuclei are eccentric, with prominent nucleoli. Corpus luteal cysts can grow several centimeters in size, and like follicle cysts, their fluid is occasionally sampled by FNA.

The ovarian surface is lined by a layer of simple cuboidal epithelial cells. When sampled by FNA, ovarian surface epithelium is present in tight sheets of bland, evenly spaced cells resembling mesothelium. Nuclei are round to oval and pale. Reactive change, including pleomorphism and prominent nucleoli, may occur in the setting of chronic irritation (e.g., from surface adhesions). Ovarian stroma may occasionally also be encountered on FNA. Stromal cells are spindle-shaped, with elongated nuclei, and are typically present in tightly cohesive groups. They may resemble a spindle cell neoplasm. However, their nuclei are uniform in shape and staining.

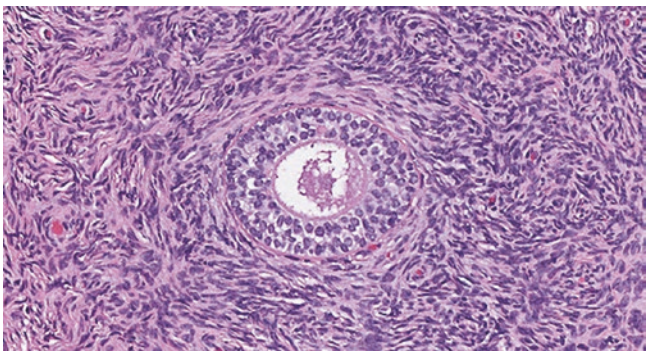

Fig. 9.25 An ovarian follicle, lined by granulosa cells, surrounded by ovarian spindle cell stroma. Ovary resection, hematoxylin & eosin, 40× magnification

Fig. 9.26 A loose sheet of granulosa cells is shown from ovarian follicle cyst fluid, exhibiting central round nuclei and scant granular cytoplasm. Ovarian cyst fluid, cell block, hematoxylin & eosin, 20× magnification

References

1. Kurtycz DFI, Staats PN, Young NA, Bibbo M, Colgan TJ, Prey MU, Nayar R. Non-neoplastic findings. In: Nayar R, Wilbur D, editors. The Bethesda system for reporting cervical cytology. Cham: Springer; 2015. p. 29–89.
2. Hoda RS, Loukeris K, Abdul-Karim FW. Gynecologic cytology on conventional and liquid-based preparations: a comprehensive review of similarities and differences. Diagn Cytopathol. 2013;41(3):257–78.
3. Crothers BA, Booth CN, Darragh TM, Zhao C, Souers RJ, Thomas N, Moriarty AT. False-positive Papanicolaou (PAP) test rates in the College of American Pathologists PAP education and PAP proficiency test programs: evaluation of false-positive responses of high-grade squamous intraepithelial lesion or cancer to a negative reference diagnosis. Arch Pathol Lab Med. 2014;138(5):613–9.
4. Morrison C, Prokorym P, Piquero C, Wakely PE, Nuovo GJ. Oral contraceptive pills are associated with artifacts in ThinPrep Pap smears that mimic low-grade squamous intraepithelial lesions. Cancer. 2003;99:75–82.
5. Kanahara T, Hirokawa M. Herxheimer spiral in cervico-vaginal smears. J Jpn Soc Clin Cytol. 1999;38(6):623–4.
6. Torous VF, Pitman MB. Interpretation pitfalls and malignant mimics in cervical cytology. J Am Soc Cytopathol. 2021;10(2):115–27.
7. Samedi VG, Bocklage T. Female reproductive system cytology. In: Pitfalls in diagnostic cytopathology with key differentiating cytologic features. Essentials in cytopathology, vol. 27. Cham: Springer; 2016. p. 43–81.

8. Williams MPA, Kukkar V, Stemmer MN, Khurana KK. Cytomorphologic findings of cervical Pap smears from female-to-male transgender patients on testosterone therapy. Cancer Cytopathol. 2020;128(7):491–8.
9. Novotony DB, Maygarden SJ, Johnson DE, Frable WJ. Tubal metaplasia. A frequent potential pitfall in the cytologic diagnosis of endocervical glandular dysplasia on cervical smears. Acta Cytol. 1992;36:1–10.
10. Cibas ES, Chelmow D, Waxman AG, Moriarty AT. Endometrial cells: the how and when of reporting. In: Nayar R, Wilbur D, editors. The Bethesda system for reporting cervical cytology. Cham: Springer; 2015. p. 91–102.
11. Munakata S. Diagnostic value of endometrial cytology and related technology. Diagn Cytopathol. 2022;50(7):363–6. https://doi.org/10.1002/dc.24956.
12. De Peralta-Venturino MN, Purslow MJ, Kini SR. Endometrial cells of the "lower uterine segment" (LUS) in cervical smears obtained by endocervical brushings: a source of potential diagnostic pitfall. Diagn Cytopathol. 1995;12(3):263–71.
13. Chhieng DC, Elgert P, Cangiarella JF, Cohen JM. Significance of AGUS Pap smears in pregnant and postpartum women. Acta Cytol. 2001;45(3):294–9.
14. Barkan GA, Naylor B, Gattuso P, Küllü S, Galan K, Wojcik EM. Morphologic features of endometriosis in various types of cytologic specimens. Diagn Cytopathol. 2013;41(11):936–42.
15. Pantanowitz L, Austin RM, Michelow P. Gynecological infections. In: Cytopathology of infectious diseases. Essentials in cytopathology, vol. 17. New York: Springer; 2011. p. 85–102.
16. Birdsong GG, Davey DD. Specimen adequacy. In: Nayar R, Wilbur D, editors. The Bethesda system for reporting cervical cytology. Cham: Springer; 2015. p. 1–28.
17. Selvaggi SM. Diagnostic pitfalls of peritoneal washing cytology and the role of cell blocks in their diagnosis. Diagn Cytopathol. 2003;28(6):335–41.
18. Martínez-Onsurbe P, Ruiz Villaespesa A, Sanz Anquela JM, Valenzuela Ruiz PL. Aspiration cytology of 147 adnexal cysts with histologic correlation. Acta Cytol. 2001;45(6):941–7.

Male Reproductive System

10

Madelyn Lew, L. Priya Kunju, and Liron Pantanowitz

Prostate Gland

The prostate is a walnut-sized accessory gland within the male pelvis that is situated at the base of the bladder and lies just anterior to the rectum [1]. The prostatic urethra passes through the central aspect of the prostate and provides a conduit from which urine from the bladder and semen from the ejaculatory ducts exit through the penile urethra to the external environment. It is composed of two major components—glands and fibromuscular stroma. The glandular component is predominantly composed of prostatic acini. These acini are responsible for the creation of a slightly alkaline fluid that is subsequently carried through the prostatic ducts to combine with sperm from the ejaculatory ducts and fluid from the seminal vesicles in the prostatic urethra. This combination of fluids ultimately forms semen. Within the semen, the prostatic fluid serves as a protective barrier for spermatozoa as they enter the slightly acidic environment of the vaginal tract during intercourse, prolonging their survival and protecting their genetic material. The fibromuscular stroma forms the supporting framework for the prostatic glands and predominantly consists of smooth muscle, vessels, lymphatics, and nerve branches. While most of the muscle fibers of the stroma is smooth muscle, skeletal muscle fibers from the urogenital diaphragm also extend into the apical and anterior aspects of the prostate. The overall muscle-rich stroma facilitates rapid expulsion of prostatic fluid during ejaculation. There is no histologically distinct "prostate capsule" surrounding the prostate gland. Instead, Denonvilliers fascia covers the posterior aspect of the prostate and seminal vesicles as a sheath between the prostate and rectum. Despite the lack of a well-defined capsule, the prostate has well-defined edges at the posterior and lateral aspects, except at the most apical and basal parts of the prostate.

On histologic examination, the glandular component of the prostate consists of a branching network of prostatic acini, ductules, and ducts. On higher power evaluation, prostatic acini are composed of two cell types—basal cells and acinar cells. Benign acinar cells are cuboidal to columnar cells with round basally oriented nuclei, granular chromatin distribution, smooth nuclear contours, indistinct nucleoli, and moderately abundant amounts of lightly eosinophilic to clear cytoplasm (Fig. 10.1a). These cells secrete the aforementioned slightly alkaline and proteinaceous prostatic fluid, which can become lamellated concretions within the acinar lumina, called corpora amylacea (Fig. 10.1b). Occasionally, these acinar cells display yellow-brown fine intracytoplasmic lipofuscin granules. Basal cells underlie the acinar cells and are typically characterized by small nuclei, variable nuclear grooves, and scant cytoplasm (Fig. 10.1a). The glandular elements can become atrophic with age and in inflammatory processes, which histologically manifests as a loss of cytoplasm of the acinar cells (Fig. 10.1c). Partially to fully atrophic glands may appear to have crowded, distorted, and disorganized basaloid cells and can also display mild nuclear enlargement with distinct nucleoli, thereby mimicking the appearance of prostatic adenocarcinoma. However, a lobular architecture is typically maintained, and patchy basal cell distribution may still be appreciated with p63 and/or high molecular weight keratin (e.g., 34betaE12) immunostains.

The fluid from prostatic acini coalesces into prostatic ductules and ducts. The cytomorphology of these ductules and ducts is similar to that of the acini, and often cannot be easily differentiated on histologic sections without a longitudinal section that highlights the long axis of the ductules and ducts. The fluid eventually deposits into the prostatic urethra, which along with the adjacent periurethral glands, is lined by the same urothelial mucosa seen in the urinary bladder and ureters. As highlighted in Chap. 8 (Urinary Tract), urothe-

M. Lew (✉) · L. P. Kunju
Department of Pathology, University of Michigan,
Ann Arbor, MI, USA
e-mail: lewm@med.umich.edu; lkunju@med.umich.edu

L. Pantanowitz
Department of Pathology, Michigan Medicine,
Ann Arbor, MI, USA
e-mail: lironp@med.umich.edu

M. Lew et al. (eds.), *Normal Cytology*, https://doi.org/10.1007/978-3-031-20336-7_10

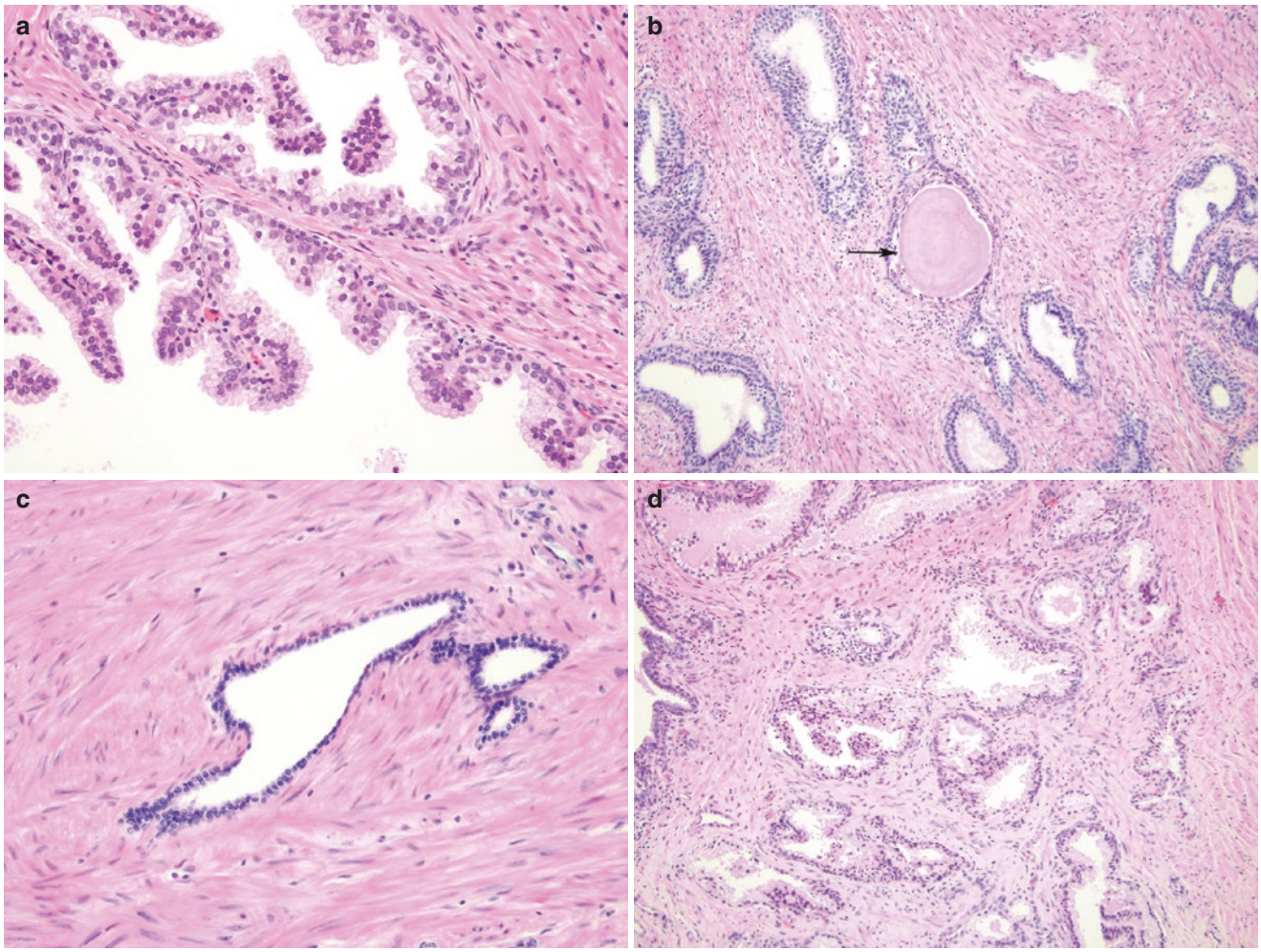

Fig. 10.1 (**a**) Prostate histology highlighting normal prostatic acini. Each normal acinus is lined by a bilayer of cells. The luminal or acinar cells are characterized by basally oriented round nuclei with smooth nuclear contours, granular chromatin distribution, and moderate to abundant amounts of lightly eosinophilic to clear cytoplasm. Oriented perpendicularly to the acinar cells are the underlying basal cells. The basal cells are ovoid and have slightly coarser chromatin distribution and scant cytoplasm. (**b**) The prostatic fluid secreted into lumina of prostatic acini can become lamellated concretions (black arrow) called corpora amylacea. (**c**) Acinar cells in atrophic prostatic glands have a notable loss of cytoplasm. (**d**) Fibromuscular prostatic stroma between glands contains delicate vessels. Prostate resection, hematoxylin & eosin, 10× (**d**) 20× magnification (**a**–**c**)

lium is composed of three main cell types—basal cells, intermediate urothelial cells, and superficial cells.

The supporting fibromuscular stroma of the prostate gland ranges from loosely woven, like that seen in the more peripheral zone of the prostate, to more compact, such as that seen in the central and transition zones (Fig. 10.1d). Embedded within this stroma at the anterior aspect of the prostate are skeletal muscle fibers.

Given the widespread use of image-guided core biopsies of the prostate, fine needle aspiration (FNA) has become increasingly less common in the evaluation of prostate abnormalities. However, prostatic FNA still remains an economical and convenient option when core biopsies may not be feasible or available. Studies have highlighted FNA as a reasonably sensitive, specific, and diagnostically accurate modality for the diagnosis of prostatic adenocarcinoma [2–4]. Cytologic preparations of the prostate in younger men are typically more cellular and composed mostly of acinar cells arranged in small groups or in a single cell dispersion pattern (Fig. 10.2a). The short columnar acinar cells are characterized by small to moderately abundant amounts of granular to vacuolated cytoplasm (if not stripped from the nucleus) that contain round nuclei with smooth nuclear contours. When found in groups, the acinar cells typically display uniformity in cell size and are well spaced with minimal nuclear crowding or overlap (Fig. 10.2b). Occasionally, intracytoplasmic pigment granules of lipofuscin may be seen, which appear dark blue to purple on air-dried smear preparations and yellow-brown on alcohol-fixed Papanicolaou-stained smear preparations (Fig. 10.2c). The degree of cellularity and cyto-

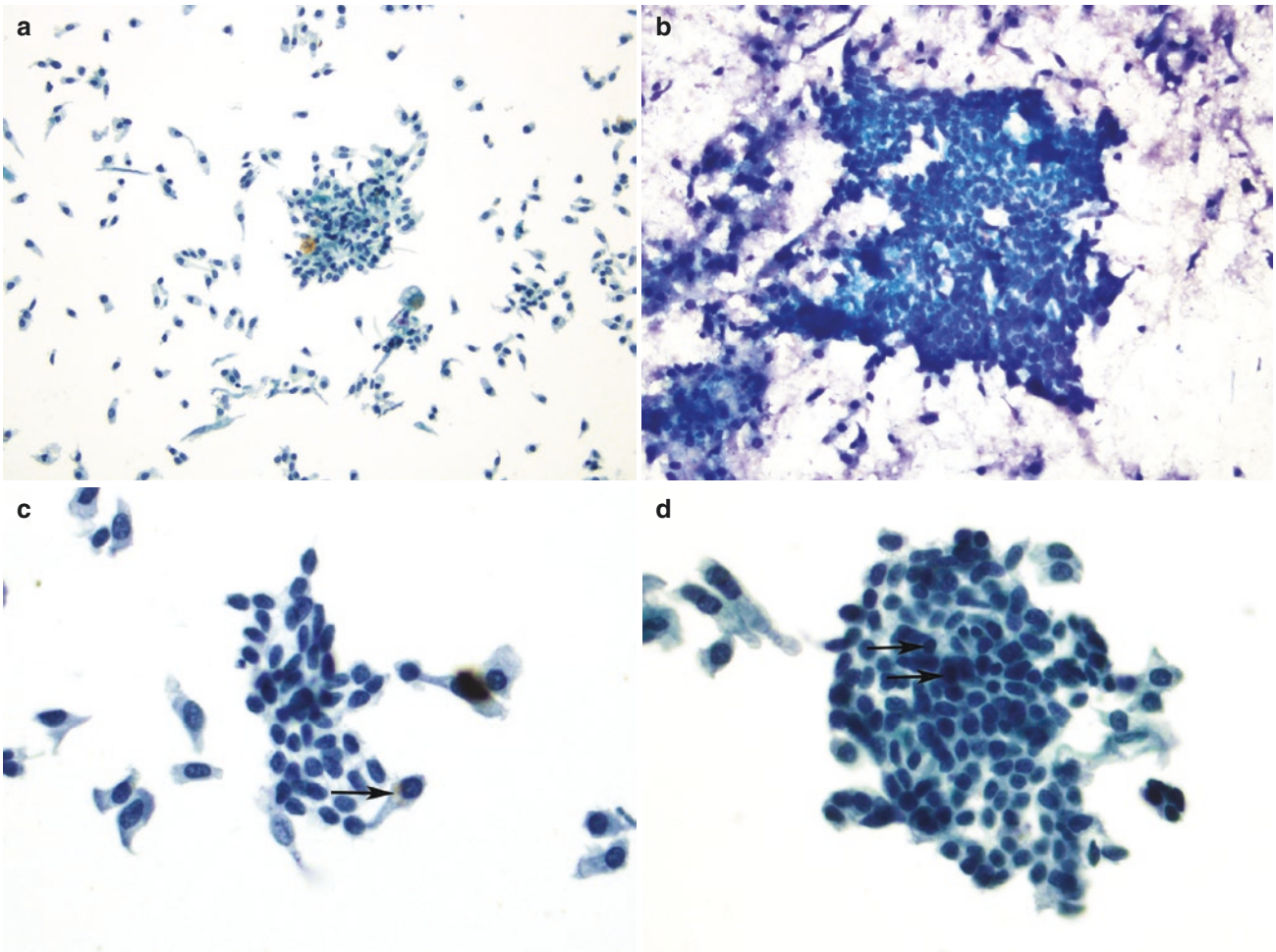

Fig. 10.2 (**a**, **b**) Normal prostate acinar cells arranged singly and in sheets. The acinar cells display uniformity in cell and nuclear size with low nuclear:cytoplasmic ratios, even granular chromatin distribution, round nuclei, and smooth nuclear contours. (**c**) Occasionally, fine yellow-brown intracytoplasmic pigment granules from lipofuscin (black arrow) can be identified within acinar cells. (**d**) Basal cells (black arrows) can be seen in a separate plane of focus from the underlying sheet of acinar cells. These basal cells have scant cytoplasm and ovoid, dark nuclei. Prostate, ThinPrep preparation, 10× magnification (**a**). Prostate, air-dried smear preparation, Diff-Quik, 20× magnification (**b**). Prostate, alcohol-fixed smear preparation, Papanicolaou stain, 20× magnification (**c**, **d**)

plasm within the acinar cells can be variable depending on the age of the patient as well as the presence of concurrent inflammatory, fibrotic, or hyperplastic changes. In hyperplastic conditions, cellular aspirates consisting of acinar cells in large flat sheets as well as crowded, papillary-like arrangements can be encountered.

Basal cells can be seen intimately admixed with groups of benign acinar cells and are identified as small cells with scant amounts of cytoplasm, ovoid nuclei, and smooth to slightly irregular nuclear contours. In cell groups of acinar cells, the basal cells can sometimes be better appreciated in another plane of focus from the acinar cells (Fig. 10.2d). Corpora amylacea may also be identified on cytologic preparations as extracellular spherules or angulated structures with radial striations and/or concentric laminations. Occasionally, urothelial cells can be appreciated when incidentally sampling the prostatic urethra. In such cases, all of the different cell types of the urothelium may be appreciated such as basal cells, intermediate urothelial cells, and superficial cells, which are described in detail in Chap. 8 (Urinary Tract). Urothelium lining prostatic urethra can undergo squamous metaplasia, occasionally giving rise to the presence of squamous cells in prostatic aspirates.

While stromal elements are not typically appreciated in FNA samples from the prostate, they may occasionally be present when regions of stromal hyperplasia are sampled. Stromal cells have small to moderately abundant amounts of dense cytoplasm, display elongated to spindled nuclei, and may be arranged singly or in loosely cohesive cell clusters.

Common sources of contamination with prostatic aspirate specimens include glandular and stromal tissue from the rectum, as the needle traverses through the rectum to gain access

to the prostatic parenchyma. Glandular cells derived from rectal mucosa can be arranged singly or in sheets, strips, or crowded clusters and are characterized by basally oriented round nuclei with smooth nuclear contours and moderate to abundant amounts of delicate cytoplasm. Sampling from the other nearby normal anatomic structures (e.g., ganglion cells, seminal vesicle) may result in misinterpretation of malignancy. Ganglion cells are very large cells with enlarged nuclei and prominent nucleoli. Sampling from the seminal vesicle may also be problematic, as the epithelial cells from this site tend to exhibit large, hyperchromatic, and irregularly contoured nuclei with variably prominent nucleoli (Fig. 10.3a–c) [5]. However, as detailed below, the presence of coarse yellow-brown cytoplasmic granules of lipofuscin within these seminal vesicle cells may be helpful in appropriately mitigating concern.

Well-differentiated prostatic adenocarcinoma can mimic the appearance of bland acinar cells at scanning magnification (5–10×). However, on higher power evaluation, malignant cell groups will tend to show higher degrees of nuclear atypia, nuclear crowding, and mild size variation. Basal cells will be absent from these malignant cell groups [2]. The absence of basal cells can be highlighted by PIN-4 cocktail, a combination of p63 (nuclear expression in basal cells), high molecular weight keratin (cytoplasmic expression in basal cells), and AMACR/p504s (variable cytoplas-

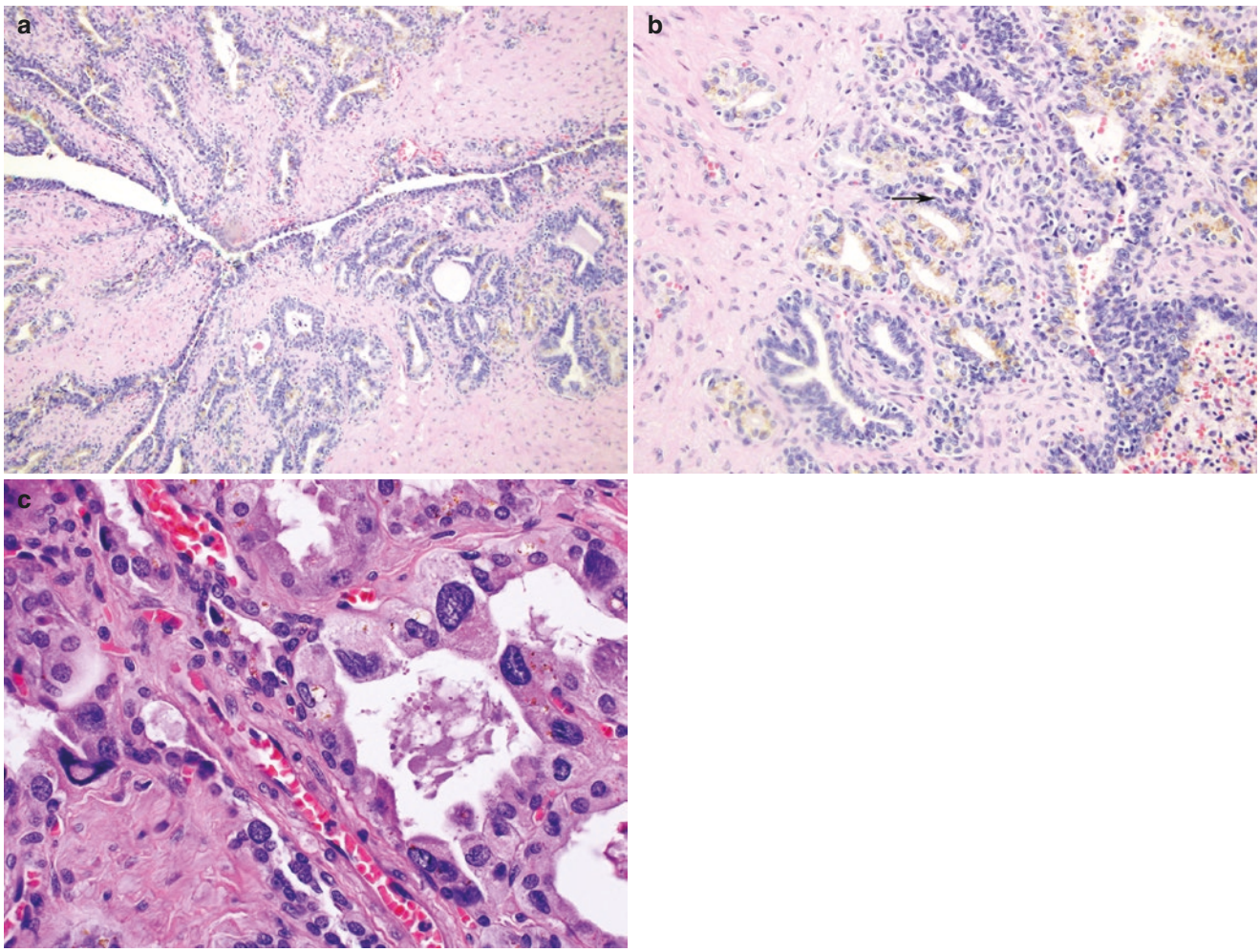

Fig. 10.3 (**a**) The epithelium of the seminal vesicle is arranged into a complex undulating and outpouching pattern of glands supported by surrounding smooth muscle. (**b**) The luminal low cuboidal to columnar cells show nuclei with variable shapes and sizes. Yellow-brown coarse cytoplasmic granules of lipofuscin are readily evident in these cells. Basal cells (black arrow) can be seen underlying the luminal cells. (**c**) Seminal vesicle epithelium is shown with large, hyperchromatic nuclei exhibiting degenerative atypia. Seminal vesicle, hematoxylin & eosin, 10× (**a**), 20× (**c**), and 40× (**b**) magnification

mic expression in malignant as well as a subset of benign prostatic acinar cells) immunohistochemical markers. Additionally, the nuclei of neoplastic acinar cells are larger, imparting a higher nuclear: cytoplasmic ratio. Most characteristically, with prostatic adenocarcinoma there should be distinct nucleoli in a significant proportion of these cells. However, scattered small nucleoli can also be identified in benign conditions, such as atrophy. In these challenging cases, the atrophic acinar cells will show substantial loss of cytoplasm. Other inflammatory and reactive conditions, such as granulomatous prostatitis, may induce reactive atypia characterized by the presence of distinct nucleoli, often raising concern for a malignant process. A background of associated neutrophils, lymphocytes, plasma cells, multinucleated giant cells, and/or granulomas may be helpful in this setting [5].

Seminal Vesicles

The seminal vesicles are paired tan-brown, coiled, pouch-like glands located at the posterolateral base of the prostate gland, base of the urinary bladder, and anterior to Denonvilliers retroprostatic fascia. They produce fluid that is important for sperm motility and ultimately becomes an important constituent of semen.

On low-power histologic examination, one can appreciate the undulations and outpouchings of the secretory epithelium of the seminal vesicle (Fig. 10.3a), which subsequently become the straight, tubular excretory duct. Each excretory duct joins the ampulla of the ipsilateral vasa deferentia to form the intraprostatic ejaculatory duct, which traverses through the prostate gland before entering the prostatic urethra at a junction called the verumontanum. The utricle, which is a vestigial Müllerian structure, is a central depression in the verumontanum. On high-power histologic evaluation, the seminal vesicle mucosa is bilayered, similar to that of the prostatic acini and ducts. The luminal cells are composed of cuboidal to columnar epithelial cells with apical microvilli. These cells are characterized by variably sized nuclei, coarse chromatin distribution, and moderately abundant amounts of clear to lightly eosinophilic cytoplasm. Characteristically, coarse yellow-brown cytoplasmic pigment granules representing lipofuscin can be found within these cells (Fig. 10.3b). These lipofuscin granules are often first identified during puberty, and their quantity continues to increase with age. Some of these epithelial cells may show markedly enlarged and hyperchromatic nuclei with prominent nucleoli or degenerative atypia (Fig. 10.3c). Underlying these columnar cells are basal cells with ovoid nuclei and scant cytoplasm. The supporting connective tissue of the seminal vesicle smooth muscle wall is composed of an inner thick circular layer and an outer thin longitudinal layer.

The seminal vesicle is not typically a target for fine needle aspiration, although there have been reports of its potential utility in sperm retrieval in patients with obstructive azoospermia [6, 7]. However, familiarity with normal elements from the seminal vesicle gland is important in reducing misinterpretation as malignant cells in the evaluation of aspirates intended to be procured from the bladder, prostate [8], peri-rectal lymph nodes and nearby soft tissue [9]. Rarely, urine cytology specimens from men can contain seminal vesicle elements. On cytologic assessment, seminal vesicle epithelial cells show variable nuclear shapes and sizes and are arranged singly as well as in variably crowded sheets (Fig. 10.4a). As mentioned previously, while some of these epithelial cells will show bland, round nuclei with smooth nuclear contours and even chromatin distribution, others can look quite bizarre with markedly enlarged nuclei (Fig. 10.4b), coarse chromatin distribution, and prominent nucleoli. It is unclear how seminal vesicle cells obtain such bizarre morphology, but it has been postulated that endocrine influences may contribute to this appearance [10]. While these features may initially be alarming, it is critical not to mistake this degenerative type of nuclear atypia as a feature of malignancy. It is helpful to carefully search for coarse pigment granules of lipofuscin characteristic of seminal vesicle epithelial cells in the moderate to abundant amounts of granular to vacuolated cytoplasm. Importantly, although lipofuscin pigment is more abundant and coarser in seminal vesicle epithelium, it is not specific as it may be seen in epithelial cells of the prostate, vas deferens, and ejaculatory ducts. On Diff-Quik-stained preparations, these granules will appear dark blue-green (Fig. 10.4b) and on Papanicolaou-stained preparations, they will appear yellow-brown (Fig. 10.4c). In addition to the coarse granularity of lipofuscin, other background elements may point to the possibility of seminal vesicle sampling, including the presence of mature sperm (Fig. 10.4a) and dense seminal vesicle secretion material (Fig. 10.4a–c) that can resemble cracked "parched earth."

As the morphology of seminal vesicle cells may raise concern for malignancy, immunohistochemistry on cell block material may be helpful. PAX-2 and PAX-8 show nuclear expression in seminal vesicle epithelium and are typically negative in prostatic acini (although there can be rare reactivity in prostatic acini from the central zone) and

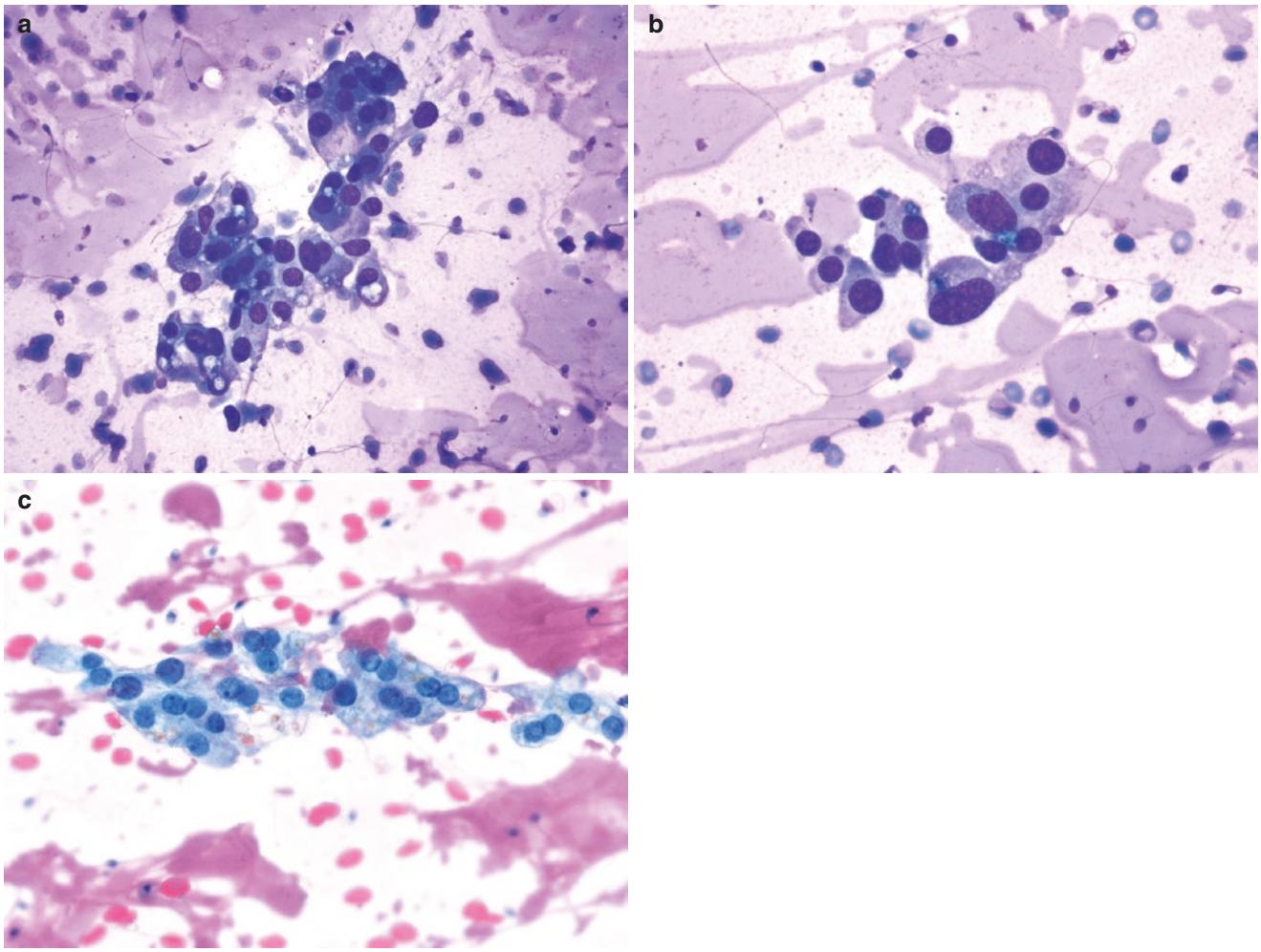

Fig. 10.4 (**a**) Seminal vesicle epithelial cells are shown arranged in a cell cluster displaying variation in nuclear size and shape. The cytoplasm varies from granular to vacuolated. Note the scattered mature sperm and dense seminal vesicle secretion material in the background. (**b**) Lipofuscin can be seen as coarse dark blue granules within the cytoplasm of these cells on Diff-Quik-stained preparations. Note the abundant background dense proteinaceous material. (**c**) In this Papanicolaou-stained preparation, lipofuscin can be seen as yellow-brown cytoplasmic granules. Distinct nucleoli can also be appreciated, as well as pink, dense secretory material in the background. Seminal vesicle, air-dried smear preparation, Diff-Quik, 40× (**a**) and 60× (**b**) magnification. Seminal vesicle, alcohol-fixed smear preparation, Papanicolaou stain, 60× magnification (**c**)

prostatic adenocarcinoma [11–13]. Conversely, NKX3.1 shows nuclear expression in prostatic acinar cells and prostatic adenocarcinoma but is negative in seminal vesicles. It is important to note that other prostatic markers such has PSA and PSAP can be positive in both seminal vesicles and prostatic acini. However, AMACR (also known as p504S), which is positive in the majority of prostatic adenocarcinomas, is absent in seminal vesicle acini. As mentioned previously, epithelial cells from the seminal vesicle may be inadvertently sampled in a targeted bladder aspirate or, rarely, in urine cytology specimens, which brings up the differential of urothelial carcinoma. While urothelial carcinoma is known to show expression for GATA-3, both the secretory and basal cells of the seminal vesicle are also positive for GATA-3 [14]. Additionally, p63 and high molecular weight cytokeratin, while positive in urothelial carcinoma and negative in prostate adenocarcinoma, also highlight the basal cells in normal seminal vesicle acini.

Testis

The testes are paired oval-shaped organs contained within the scrotal sac, located posterior to the penis, with a primary function in spermatogenesis and testosterone production. Each testis (or testicle) is covered by a thick capsule (Fig. 10.5a), which is subdivided into three main components. The inner most portion is the thick, fibrous tunica albuginea, which underlies the tunica vaginalis. The tunica vaginalis is a thin, sac-like structure composed of basement membrane

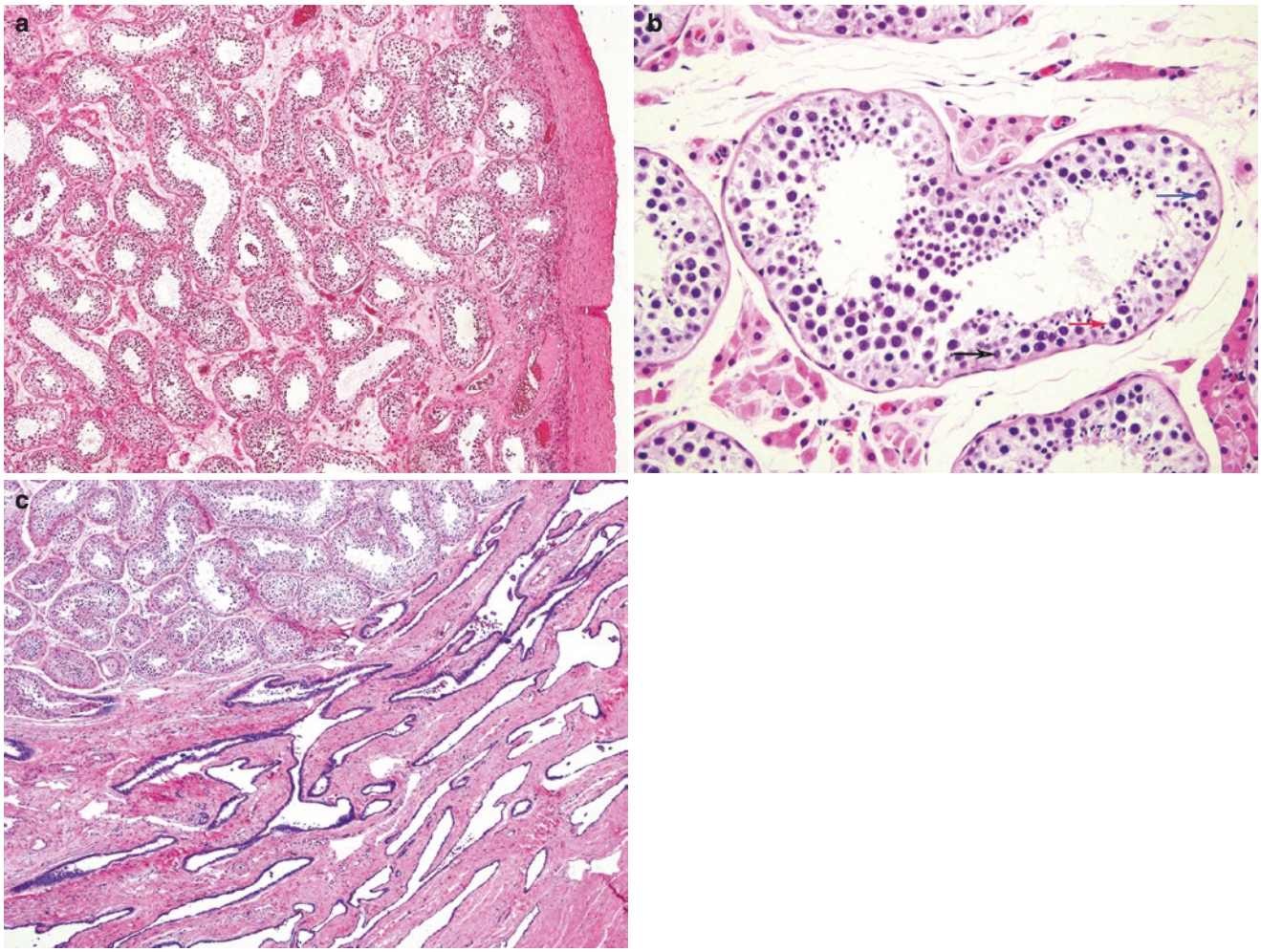

Fig. 10.5 (**a**) A thick fibrous tunica albuginea covers the testicular parenchyma, mostly composed of seminiferous tubules. Each seminiferous tubule is bound by a basement membrane and underlying connective tissue. (**b**) Seminiferous tubule showing a mix of germ cells undergoing maturation to spermatids. Spermatogonia (red arrow) are basally located with large, round nuclei, distinct nucleoli, and small amounts of cytoplasm. Primary spermatocytes (blue arrow) have a bead-like quality to their chromatin distribution. Sertoli cells (black arrow) are highlighted by their prominent nucleoli. Spermatids are apically located and notable for having small, round nuclei with condensed chromatin. In the interstitium between the seminiferous tubules are clusters of eosinophilic Leydig cells. (**c**) The rete testes in the bottom portion of this image form an anastomosing network of irregularly shaped tubules lined by low cuboidal to attenuated epithelium at the hilar aspect of the testis. Testis resection, hematoxylin & eosin, 5× (**a**), 10× (**c**), and 20× (**b**) magnification

material lined by mesothelial cells and has two layers—a visceral layer that covers the surface of the tunica albuginea and the parietal layer, which covers the internal spermatic fascia. Superficial to the internal spermatic fascia is the dartos muscle, which functions to expand and contract the overlying skin in order to regulate testicular temperature and promote spermatogenesis.

On histology, fibrous bands extending from the tunica albuginea become septa that divide the testicular parenchyma into many lobules, each of which largely consists of 1–4 seminiferous tubules arranged in a convoluted loop. On histologic evaluation, several cross sections of the seminiferous tubules can be seen in testicular parenchyma, each measuring approximately 150–250 μm in diameter. These tubules contain Sertoli cells and germ cells at various levels of maturation, including spermatogonia, primary and secondary spermatocytes, spermatids, and spermatozoa (Fig. 10.5b). At the periphery of the tubules, there is a basement membrane with underlying connective tissue comprised of fibroblasts and myoid cells, which outlines the boundary of each cross section. Sertoli cells are columnar cells with abundant amounts of lightly eosinophilic cytoplasm and basally oriented nuclei that have smooth to slightly irregular nuclear contours, even chromatin distribution, and a characteristic prominent nucleolus. The base of the Sertoli cell adheres to the basement membrane of the tubule. In a normal testis with spermatogenesis, Sertoli cells comprise approximately 10–15% of seminiferous tubule cellularity [15]. Germ cells

take on a varied morphologic appearance depending on their level of maturity. The immature and undifferentiated spermatogonia are located in the more basal aspect of the tubule and are characterized by large, round nuclei, smooth nuclear contours, 1–2 distinct nucleoli, and small amounts of cytoplasm. The chromatin appearance varies and may be dark or light depending on the specific type of spermatogonia. Some spermatogonia will develop into primary spermatocytes, characterized by distinctive alterations in chromatin distribution which confers a beaded look to the nucleus. Maturation of the primary spermatocytes is accompanied by movement toward the luminal aspect of the seminiferous tubule. After the first round of meiosis in spermatogenesis, these primary spermatocytes become secondary spermatocytes with smaller nuclei and finely granular chromatin distribution. After a second round of meiosis, secondary spermatocytes become spermatids, which are noted by their dark, round to ovoid nuclei and more apical presence within the seminiferous tubule. As they further mature into spermatozoa, the nuclei become increasingly ovoid to spindle shaped with progressive loss of cytoplasm. In the interstitium of the testis between seminiferous tubules, Leydig cells can be found. These cells produce testicular androgens and are characterized by round nuclei with prominent nucleoli and abundant amounts of eosinophilic cytoplasm (Fig. 10.5b). Reinke crystalloids can be found as elongated dense, eosinophilic structures within Leydig cell cytoplasm. While the exact origin and nature of these crystals is unclear, they have been postulated to represent aggregated protein products, possibly related to aging [16].

The spermatozoa-containing fluid of the seminiferous tubules moves toward the hilum of the testis that collects into a branching network of irregularly shaped ductules called the rete testes (Fig. 10.5c). The rete testes are lined by low columnar to attenuated epithelial cells with round to elongated nuclei, variably irregular nuclear contours, granular chromatin distribution, and small to moderate amounts of cytoplasm. Spermatozoa move from this anastomosing network through the ductuli efferentia, then into the epididymis and vas deferens. The fluid within the vas deferens joins with that in the excretory duct of the seminal vesicle to form the ejaculatory duct, which traverses through the prostate to enter the prostatic urethra at the verumontanum.

Currently, aspiration of the testis for evaluation of palpable masses is uncommon, but similar to the seminal vesicle, its utility has been reported in the evaluation of male infertility [17–19]. In cytology specimens, germ cells at various levels of maturation can be identified (Fig. 10.6a). While subclassification of spermatogonia is not always feasible on cytology, they can be identified by their round to ovoid centrally placed nuclei that harbor distinct nucleoli. Spermatocytes have variable appearances depending on their stage of maturation. While some may have similar features to spermatogonia, the most recognizable can be characterized by clumped to bead-like chromatin distribution (Fig. 10.6a). Spermatids can be identified by their small, round nuclei interspersed with other germ cell elements. As they undergo their morphologic transformation into spermatozoa, the presence of a small, round nucleus and tail at one end can be identified (Fig. 10.6b). Sertoli cells also have prominent nucleoli, but they often show more abundant amounts of delicate to vacuolated cytoplasm and less clearly defined cell borders than spermatogonia (Fig. 10.6c). Sertoli cells may contain fine spindle-shaped Charcot-Böttcher crystalloids. Occasionally, Leydig cells with abundant densely granular cytoplasm, centrally placed round nuclei, and prominent nucleoli can be identified. Leydig cells can show binucleation and multinucleation as well as contain elongated rod-like Reinke crystals. On Diff-Quik-stained preparations, these crystals are unstained but are red-orange on Papanicolaou-stained preparations.

While morphologic assessment is frequently sufficient for evaluation of male infertility specimens, immunohistochemistry may be used in rare circumstances. Adult germ cells show weak, focal expression of SALL 4 and lack OCT 4 and CD117 staining, while Sertoli cells commonly demonstrate AR expression. Leydig cells are usually strongly and diffusely positive with calretinin. The epididymis shows CK7 and PAX8 expression and is negative for ER, PR, calretinin, and WT-1 [20].

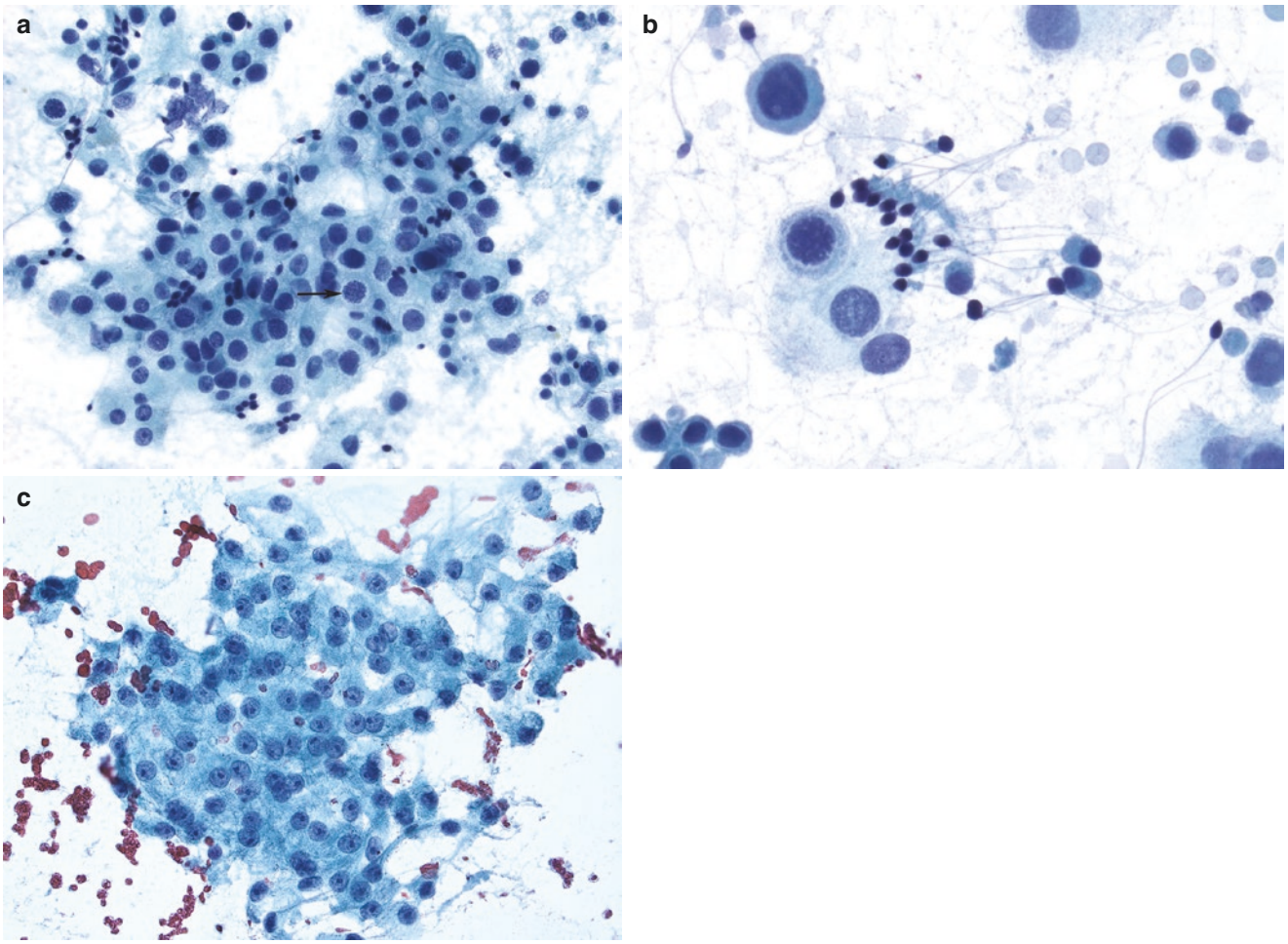

Fig. 10.6 (**a**) Mix of germ cells including spermatogonia with distinct nucleoli, spermatocytes (black arrow) with clumped chromatin, spermatids, and spermatozoa. (**b**) Spermatozoa have small dark nuclei and a characteristic flagellum (tail). (**c**) Sertoli cells have prominent nucleoli with moderate amounts of delicate granular to vacuolated cytoplasm and can be found in large clusters without spermatogonia in sterile males with germ cell aplasia. Testis, alcohol-fixed touch preparation, Papanicolaou stain, 40× (**a**, **c**) and 60× (**b**) magnification

References

1. Young B, O'Dowd G, Woodford P. Wheater's functional histology: a text a colour atlas. 6th ed. Philadelphia: Elsevier; 2013.
2. Maksem JA, Berner A, Bedrossian C. Fine needle aspiration of the prostate gland. Diagn Cytopathol. 2007;35(12):778–85.
3. Saleh AFM, Rahman AJE, Salam MA, Islam F. Role of fine needle aspiration cytology (FNAC) in the diagnosis of prostatic lesions with histologic correlation. Bangladesh Med Res Counc Bull. 2005;31(3):95–103.
4. Polito M, Albert R, Muzzonigro G, Bladi A, Diambrini M, Vecchi A. Fine needle aspiration biopsy of the prostate gland: our experience concerning 101 cases with histological follow-up. Prostate. 1990;17(2):85–94.
5. Perez-Guillermo M, Acosta-Ortega J, Garcia-Solano J. Pitfalls and infrequent findings in fine-needle aspiration of the prostate gland. Diagn Cytopathol. 2005;33(2):126–37.
6. Cerruto MA, Novella G, Zechhini Antoniolli S, Zattoni F. Use of transperineal fine needle aspiration of seminal vesicles to retrieve sperm in a man with obstructive azoospermia. Fertil Steril. 2006;86(6):1764.
7. Boehlen D, Schmid HP. Novel use of fine needle aspiration of seminal vesicles for sperm retrieval in infertile men. Urology. 2005;66(4):880.
8. Koivuniemi A, Tyrrko J. Seminal vesicle epithelium in fine-needle aspiration biopsies of the prostate as a pitfall in the cytologic diagnosis of carcinoma. Acta Cytol. 1976;20(2):116–9.
9. Satturwar S, Monaco SE, Xing J, Brand RE, Pantanowitz. Bizarre benign cells in peri-rectal endoscopic ultrasound-guided fine-needle aspiration due to seminal vesicle sampling. Diagn Cytopathol. 2020;48(6):586–8.
10. Kuo T, Gomez LG. Monstrous epithelial cells in human epididymis and seminal vesicles: a pseudomalignant change. Am J Surg Pathol. 1981;5(5):483–90.
11. Quick CM, Gokden N, Sangio AR, Brooks JD, McKenney JK. The distribution of PAX-2 immunoreactivity in the prostate gland, seminal vesicle, and ejaculatory duct: comparison with prostatic adenocarcinoma and discussion of prostatic zonal embryogenesis. Hum Pathol. 2010;41(8):1145–9.
12. Tong GX, Memeo L, Colarossi C, Hamele-Bena D, Magi-Galluzzi C, Zhou M, Lagana SM, Harik L, Oliver-Krasinski JM, Mansukhani M, Falcone L, Hibshoosh H, O'Toole K. PAX8 and PAX2 immu-

nostaining facilitates the diagnosis of primary epithelial neoplasms of the male genital tract. Am J Surg Pathol. 2011;35(10):1473–83.
13. Ortiz-Rey JA, Juaneda-Benavides L, Peteiro-Cancelo Á, de María CG, Tejado BS, Tardío-Baigés A. Another application of PAX8: to confirm the presence of seminal vesicle epithelium in prostate needle biopsies. Appl Immunohistochem Mol Morphol. 2015;23(2):161–2.
14. Ortiz-Rey JA, Chantada-de la Fuente D, Peteiro-Cancelo MA, Gomez-deMaria C, San Miguel-Fraile MP. Usefulness of GATA-3 as a marker of seminal epithelium in prostate biopsies. Actas Urol Esp. 2017;41(9):577–83.
15. Trainer TD. Histology of the normal testis. Am J Surg Pathol. 1987;11(10):797–809.
16. Nagano T, Ohtsuki I. Reinvestigation of the fine structure of Reinke's crystal in the human testicular interstitial cell. J Cell Boil. 1971;51(1):148–61.
17. Yildiz-Aktas IZ, Monaco SE, Khalbuss WE, Parwani AV, Jaffe TM, Pantanowitz. Testicular touch preparation cytology in the evaluation of male infertility. Cytojournal. 2011;8:24.
18. Cito G, Coccia ME, Sessa F, Cocci A, Verrienti P, Picone R, Fucci R, Criscuoli L, Serni S, Carini M, Natali A. Testicular fine-needle aspiration for sperm retrieval in azoospermia: a small step toward the technical standardization. World J Mens Health. 2019;37(1):55–67.
19. Jashani K, Gundawar R, Kavishwar V, Parameshwar V. Fine-needle aspiration cytology of the testes for classification of azoospermia and its value in the assessment of male infertility. Acta Cytol. 2020;64(3):216–33.
20. Magers MJ, Udager AM, Chinnaiyan AM, French D, Myers JL, Jentzen JM, McHugh JB, Heider A, Mehra R. Comprehensive immunophenotypic characterization of adult and fetal testes, the excretory duct system, and testicular and epididymal appendages. Appl Immunohistochem Mol Morphol. 2016;24(7):e50–68.

Breast

11

Judy Pang

Core needle biopsy (CNB) in the evaluation of breast abnormalities has largely replaced fine needle aspiration (FNA) in some practices in the United States given its higher diagnostic accuracy. CNB also has the additional advantage of being able to differentiate between in situ and invasive carcinoma. In many practices, FNA and CNB are performed in different clinical settings, with FNA preferentially used when there is a low suspicion of malignancy or for cystic lesions [1]. FNA is also used when the targeted lesion is not amenable to CNB (i.e., small size or posterior location against the chest wall). Although CNB is preferred in the United States, FNA is not infrequently utilized for evaluating breast abnormalities in other countries. For these reasons, recognizing normal breast elements and their potential mimickers of malignancy on cytology remains important.

The breast is a highly modified apocrine sweat gland that rests on the anterior chest wall overlying the pectoralis major and minor muscle. Breast tissue may extend to the sternum, clavicle, and axilla (tail of Spence). Its size varies with the patient's body shape and size, as well as hormonal status. The breast undergoes continuous changes in response to menarche, pregnancy, lactation, and menopause as it is a target of various hormones that regulate development and physiologic function. This results in a broad range of what is encountered in normal breast histology.

The breast is comprised of large ducts and terminal ductal lobular units (TDLU), the morphological and functional unit of the breast gland, arranged as segments or lobes of the breast, admixed with varying amounts of fat. It typically contains 15–20 segments or lobes that contain the major duct systems which empty at the nipple. From superficial (nipple) to deep (parenchyma), the duct system ramifies as follows: collecting duct, lactiferous sinus, lactiferous duct (segmental duct), major duct (subsegmental duct), terminal duct, and terminal ductal lobular unit (TDLU). TDLUs comprise a lobule, which is a cluster of 10–100 sac-like acini and a terminal duct (Fig. 11.1). The majority of breast lesions, benign and malignant, arise from the TDLU [2, 3].

Two types of epithelial cells are present in the breast: luminal or ductal cells and myoepithelial cells. The luminal cells express GATA3, ER, and PR while the myoepithelial cells express p63, smooth muscle myosin, and calponin. The luminal cells form the innermost layer lining ducts and acini (Fig. 11.2a). Luminal cells in the TDLU may undergo lactational change and produce milk while those in the larger ducts do not. Luminal cells are relatively monotonous cuboidal to columnar cells and have a moderate amount of eosinophilic cytoplasm with small, round to oval nuclei and inconspicuous nucleoli. Metaplastic change may occur and can be a result of injury, hormonal influences, or unknown factors. Apocrine metaplasia, characterized by an increased amount of granular to vacuolated cytoplasm and prominent nucleoli, is commonly seen (Fig. 11.2b) and can be fre-

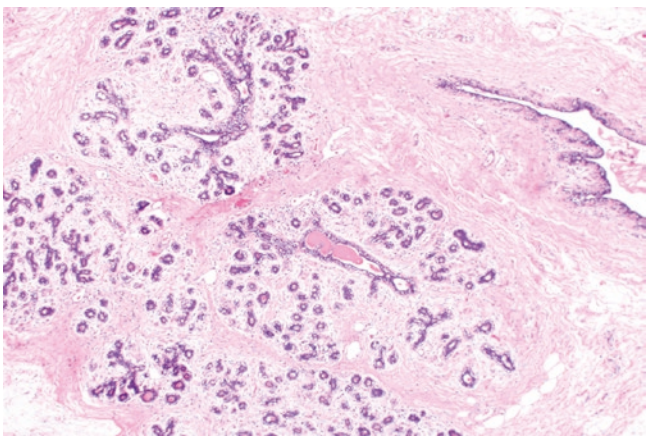

Fig. 11.1 Breast resection showing normal adult breast lobules. This terminal ductal lobular unit (TDLU) is composed of many acini connected to a terminal duct shown draining into an extralobular duct. The acini are surrounded by loose connective tissue, the intralobular stroma. This contrasts with the interlobular stroma composed of dense fibroconnective tissue. Hematoxylin & eosin, 4× magnification

J. Pang (✉)
Department of Pathology, University of Michigan–Ann Arbor, Ann Arbor, MI, USA
e-mail: jcpang@med.umich.edu

M. Lew et al. (eds.), *Normal Cytology*, https://doi.org/10.1007/978-3-031-20336-7_11

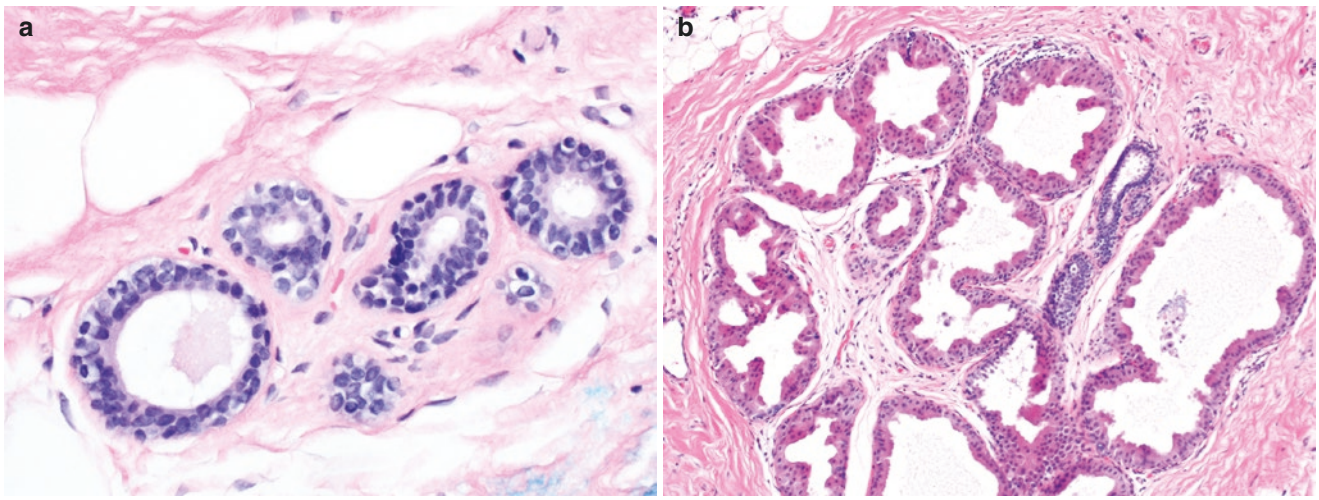

Fig. 11.2 (**a**) The two types of epithelial cells are well demonstrated in this breast biopsy: inner luminal cells with cuboidal epithelium and outer myoepithelial cells with small round nuclei and clear cytoplasm. (**b**) Apocrine metaplasia with abundant granular cytoplasm is seen in this breast biopsy. Hematoxylin & eosin, 40× (**a**) and 10× (**b**) magnification

quently observed in cysts and papillomas. Squamous metaplasia can result in response to injury or inflammation. Other changes include clear cell change and columnar cell change. Myoepithelial cells form the outermost layer between luminal cells and basement membrane and serve to help produce and maintain the basement membrane, aid in luminal cell polarity, inhibit angiogenesis, and facilitate lactation via contraction and expulsion of luminal contents. Myoepithelial cells are frequently flattened with small round nuclei and often have abundant clear cytoplasm that may mimic lobular neoplasia. Immunostains for myoepithelial cells including p63, smooth muscle myosin, and calponin can be helpful in these scenarios. Sometimes myoepithelial cells can show myoid features with dense, eosinophilic cytoplasm and may be spindled in shape. In the male breast there are branching ducts without lobules.

In cytology specimens, benign ductal cells can be seen in flat two-dimensional sheets, tubules, branching patterns, and microacinar formations and may show mild to moderate crowding and overlapping which could represent benign usual ductal hyperplasia. Single dispersed intact epithelial cells are rare, except in benign conditions such as apocrine metaplasia and fibroadenomas. Benign ductal cells are relatively uniform, although they can be variable in benign proliferative conditions such as usual ductal hyperplasia and fibroadenoma. Benign ductal cells usually have a single round to oval nucleus with smooth nuclear membranes, but binucleate forms can be encountered. The average size of the nucleus is approximately 1.5 times the diameter of a red blood cell. Nucleoli are often single and inconspicuous. Cytoplasm is typically scant with variable degrees of apocrine change (Fig. 11.3a, b). Apocrine cells arranged singly, in sheets, or papillary structures display diffuse, finely granular cytoplasm, prominent nucleoli, and well-defined cell boundaries that can be seen in fibrocystic change as well as benign lesions of the breast including fibroadenomas and papillomas (Fig. 11.3c–e). In cystic lesions, apocrine cells along with foam cells, or foamy macrophages predominate. In lactational change, ductules of the TDLU become hyperplastic with prominent cytoplasmic vacuolization and luminal secretions (Fig. 11.4a). In cytology specimens, these lactational cells are uniform with abundant delicate and wispy granular or finely vacuolated cytoplasm and have prominent nucleoli in a proteinaceous background (Fig. 11.4b). Although monolayer sheets predominate, the increased proportion of single cells, occasional crowded clusters, and prominent nucleoli can be a pitfall for malignancy (Fig. 11.4c). Intracytoplasmic lumina (targetoid mucin vacuoles) are abnormal and are typically associated with malignancy. The presence of myoepithelial cells in an aspirate is indicative of a benign process, but does not entirely exclude a malignancy. Myoepithelial cells frequently lose their cytoplasm in aspirates and thus are noticeable as naked bipolar nuclei reminiscent of sesame seeds. Myoepithelial cells can be scattered in the background or attached to groups of ductal cells oftentimes slightly in a different plane of focus above a sheet of ductal cells [4–8] (Fig. 11.5).

The composition of breast stroma is dependent on age, menstrual status, pregnancy history, and lactation. It is composed of varying amounts of fibrous connective tissue and adipose tissue. The interlobular stroma accounts for the majority of the breast volume. The cellular components include fibroblasts, myofibroblasts, adipocytes, and vessels (blood and lymphatic). Occasionally, large, hyperchromatic multinucleated stromal cells can be encountered and may be due to degenerative changes. The intralobular stroma sur-

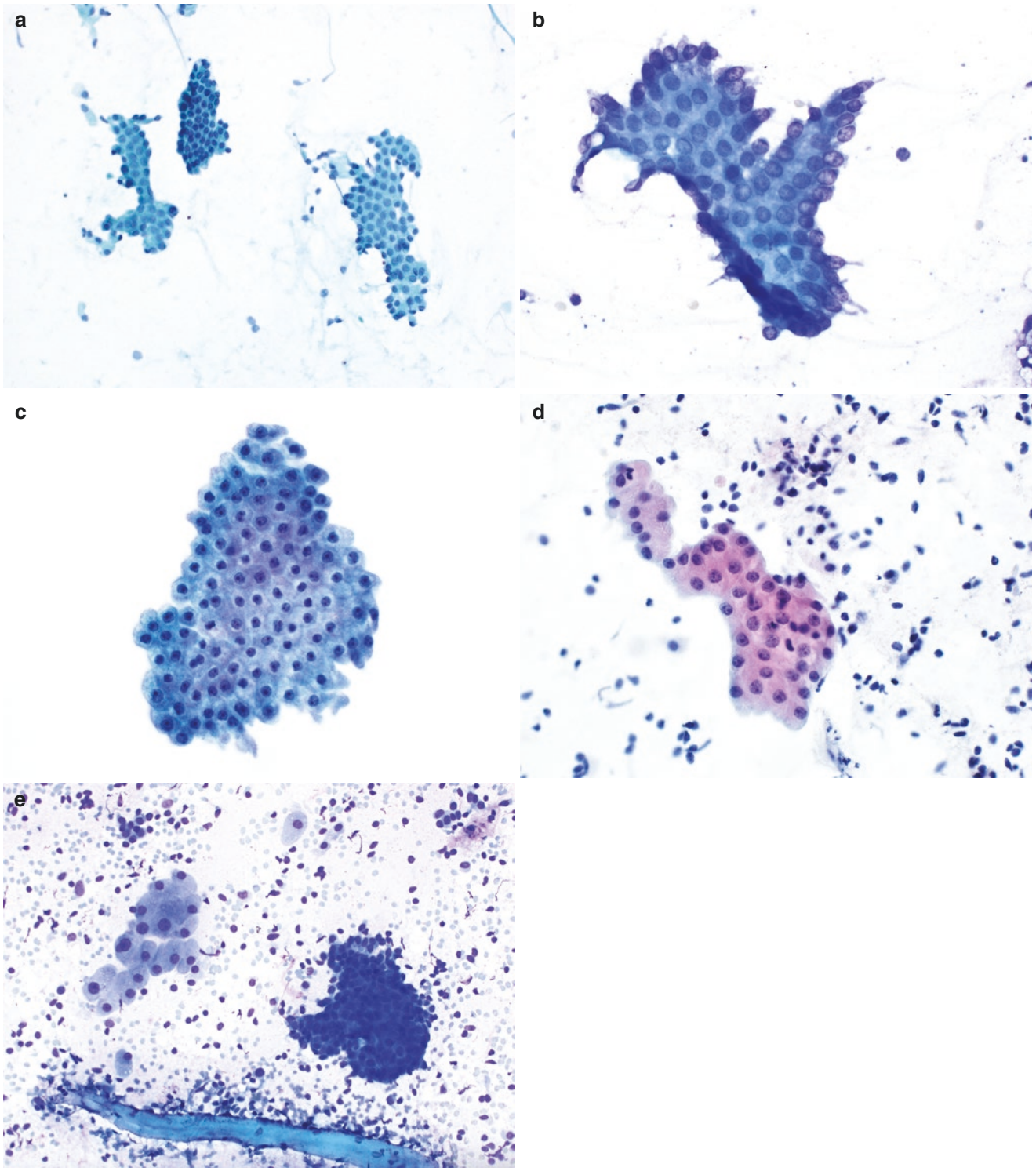

Fig. 11.3 (**a**, **b**) Fine needle aspirate of breast with normal ductal cells forming cohesive flat two-dimensional sheets. Their nuclei are round to oval with small inconspicuous nucleoli and the cytoplasm is scant. (**c**, **d**) Apocrine cells have abundant diffuse granular cytoplasm and prominent nucleoli. (**e**) Apocrine cells are seen in this aspirate of a fibroadenoma to the left of the image with stripped myoepithelial cells in the background. Breast, fine needle aspiration. Alcohol-fixed smear preparation, Papanicolaou stain, 20× magnification (**a**, **d**), air-dried smear preparation, Diff-Quik, 40× (**b**) and 20× (**e**) magnification, ThinPrep preparation 40× magnification (**c**)

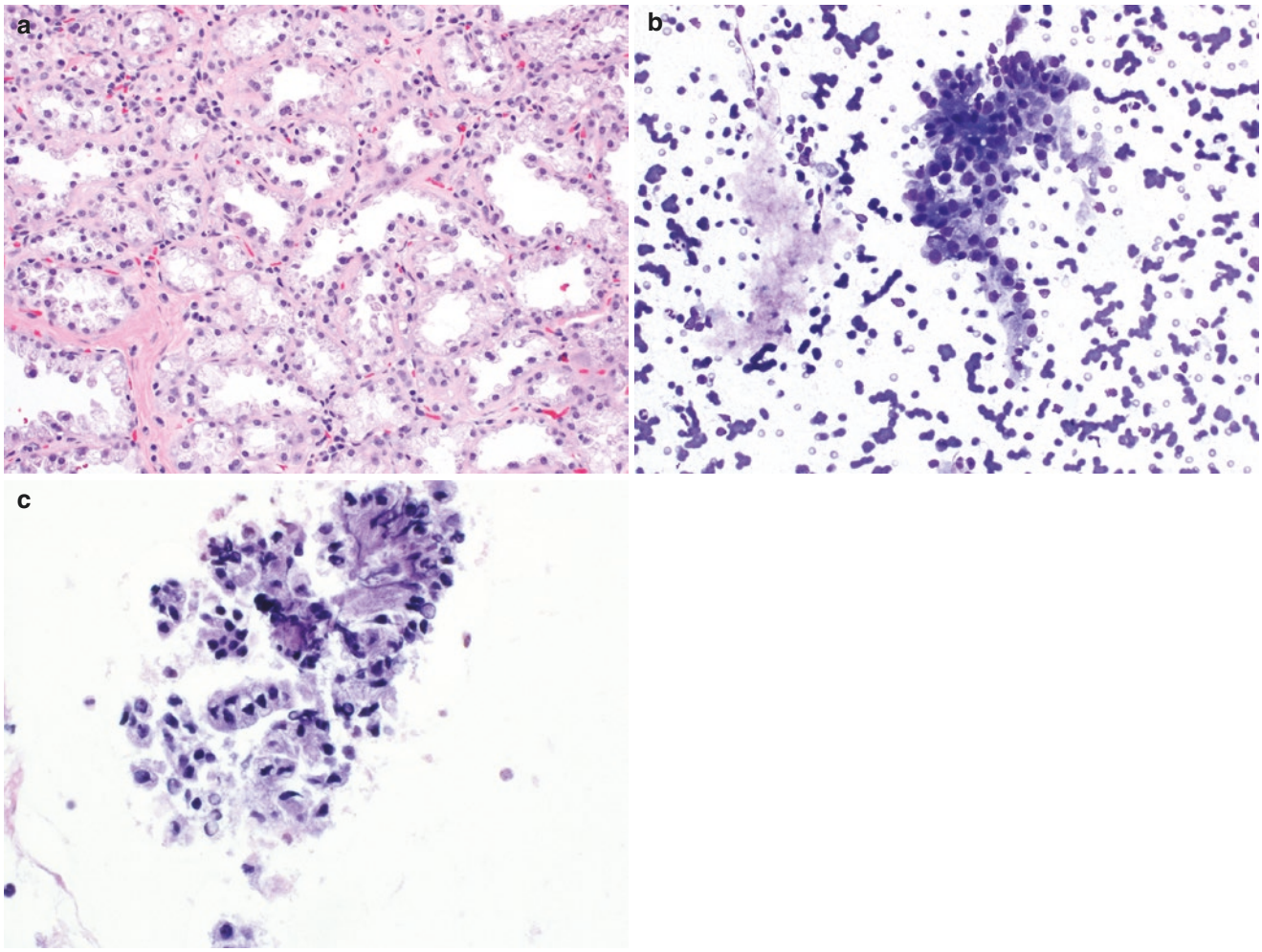

Fig. 11.4 (**a**) Breast biopsy with lactational change showing prominent cytoplasmic vacuolization and prominent nucleoli. (**b**) Fine needle aspirate of a breast with lactational change demonstrating a monolayered sheet of ductal cells with delicate wispy and finely vacuolated cytoplasm in a proteinaceous background. (**c**) Crowded cluster of ductal cells with occasional prominent nucleoli and areas showing more dyscohesion of cells can mimic malignancy. Associated proteinaceous debris could be mistaken for necrosis. Breast biopsy, Hematoxylin & eosin, 20× magnification (**a**). Breast FNA, air-dried smear preparation, Diff-Quik, 20× magnification (**b**), Cell block, hematoxylin & eosin, 40× magnification (**c**)

rounds and supports the acini of the TDLU. They appear looser and more cellular than the interlobular stroma and can have a myxoid appearance (Fig. 11.1). Scattered lymphocytes and plasma cells are often present. Any of these elements can be sampled in fine needle aspiration biopsies [2, 3]. The breast also contains scattered intramammary lymph nodes.

The nipple-areola complex is supported by a subdermal layer of smooth muscle. Around 10–15 major lactiferous duct orifices open on the surface of the nipple. The nipple is covered by pigmented squamous epithelium. Toker cells are a normal epidermal component best highlighted with a cytokeratin 7 immunohistochemical stain, which are recognized as bland single cells with clear or pale cytoplasm near the nipple orifices. Ducts dilate to form lactiferous sinuses beneath the nipple. The basement membrane of the ducts is continuous with the basement membrane of the skin and surrounds the entire ductal lobular system, separating the epithelial cells from the stroma. Keratin producing squamous cells of the epidermis extends into major ducts for 1–2 mm. Cytology specimens obtained from the nipple are typically exfoliative from a nipple discharge. Nipple discharge can be expressed by massaging the breast toward the nipple and then collecting the secretion by touching it with a glass slide. Foamy macrophages are the most commonly observed cells in nipple discharge specimens, but ductal cells and apocrine cells are sometimes present. Benign squamous cells including anucleate squamous cells are also commonly seen in these specimens, sometimes accompanied by inflammatory cells (Fig. 11.6). In many cases, however, nipple secretions

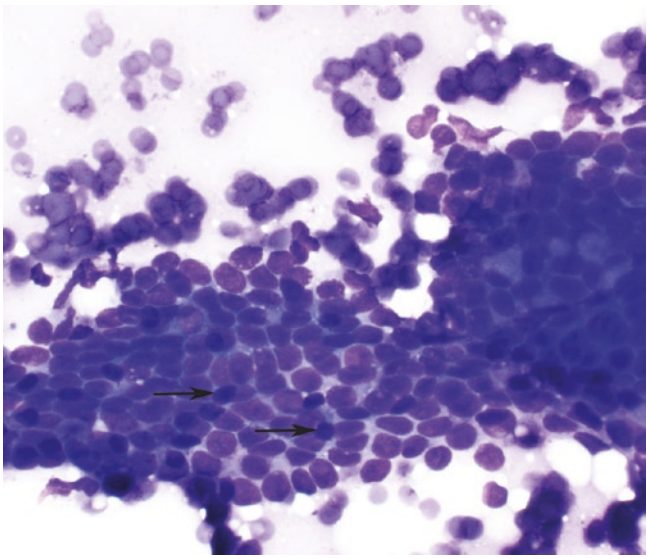

Fig. 11.5 Attached myoepithelial cells can be seen 1/2 plane above a flat sheet of ductal cells. Air-dried smear preparation, Diff-Quik, 40× magnification

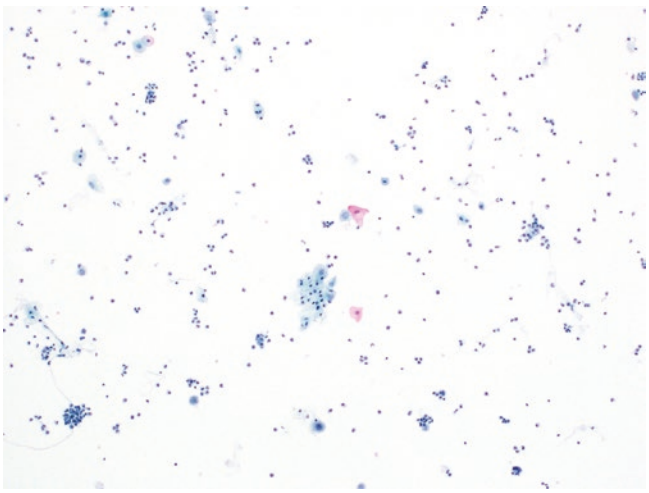

Fig. 11.6 Nipple discharge consisting of scattered squamous cells, foamy macrophages, and mixed acute inflammatory cells. ThinPrep, preparation, 10× magnification

are completely acellular. Ductal lavage using a microcatheter to cannulate individual breast ducts can hence be employed to help evaluate nipple discharges. This procedure is time consuming and relatively expensive with a low sensitivity and thus not utilized frequently [5].

References

1. VanderLaan PA. Fine-needle aspiration and core needle biopsy; an update on 2 common minimally invasive tissue sampling modalities. Cancer Cytopathol. 2016;124:862–70.
2. Pinamonti M, Zanconati F. Breast cytopathology. Assessing the value of FNAC in the diagnosis of breast lesions. Monogr Clin Cytol. 2018;24:20–4.
3. Guinebretiere JM, Menet E, Tardivon A, Cherel P, Vanel D. Normal and pathological breast, the histological basis. Eur J Radiol. 2005;54:6–14.
4. Samedi VG, Bocklage T. Chapter 1: breast cytology. In: Siddiqui M, editor. Pitfalls in diagnostic cytopathology with key differentiating cytologic features, essentials in cytopathology, vol. 27. Cham: Springer; 2016. p. 1–41.
5. Demay RM. Chapter 14: breast. In: Demay RM, editor. The art and science of cytopathology. Superficial aspiration cytology. 2nd ed. Chicago: American Society for Clinical Pathology Press; 2012. p. 1052–79.
6. Saad RS, Silverman JF. Chapter 25: breast. In: Bibbo M, Wilbur D, editors. Comprehensive cytopathology. 3rd ed. Amsterdam: Elsevier; 2008. p. 713–32, 760-762.
7. Ducatman BS, Wang HH. Chapter 9: breast. In: Cibas ES, Ducatman BS, editors. Cytology diagnostic principles and clinical correlates. 4th ed. Amsterdam: Elsevier; 2014. p. 233–45.
8. Sharma M, Gupta A, Kaul R. Cytological evaluation of breast masses during pregnancy and lactation: a retrospective analysis. Glob J Reprod Med. 2017;2:555594. https://doi.org/10.19080/GJORM.2017.02.555594.

Musculoskeletal System (Bone, Cartilage, Muscle, Soft Tissue) and Skin

12

Richard L. Cantley and Liron Pantanowitz

Adipose Tissue

Normal white adipose tissue is abundantly present subcutaneously and in surrounding organs. Fatty infiltration, lipomatosis, or lipomatous hypertrophy can also occur within certain organs (e.g., heart, pancreas, muscle, lymph nodes). Normal adipose tissue is present as sheets of cells with abundant, univacuolar cytoplasm with occasional interspersed thin blood vessels (Fig. 12.1). When sampled at the time of fine needle aspiration (FNA), fatty tissue tends to be hypocellular and present in cytology preparations as small cohesive clusters of large adipocytes [1–3]. Single cells are rare or absent. Benign adipocytes have abundant and univacuolated cytoplasm due to a large lipid vacuole, and small eccentrically located dark nuclei (Fig. 12.2). When viewed en face, the nucleus of an adipocyte is oval-shaped, but when seen from the side it may appear crescent-shaped. Intranuclear inclusions may be observed (Lochkern nucleus). Small capillaries are often visible traversing the clusters of adipocytes on smear cytology. If adipose tissue is aggressively aspirated and manipulated when preparing cytology slides, the adipocytes may be damaged, resulting in oily droplets in certain fixatives and on smeared slides. Remnant cell membranes can form lipid micelles that appear as clear round "holes" surrounded by proteinaceous material and blood on stained slides.

Differentiating normal adipose tissue from sampling of a circumscribed lipoma usually requires clinical and/or radiographic correlation, as mature adipose tissue and benign lipomas have very similar morphology [2, 3]. Single adipocytic cells and multivacuolated cytoplasm have been more commonly described in lipoma, but differentiating cytomorphologic factors are not well-established. Adipocytes demonstrate S100 immunoreactivity.

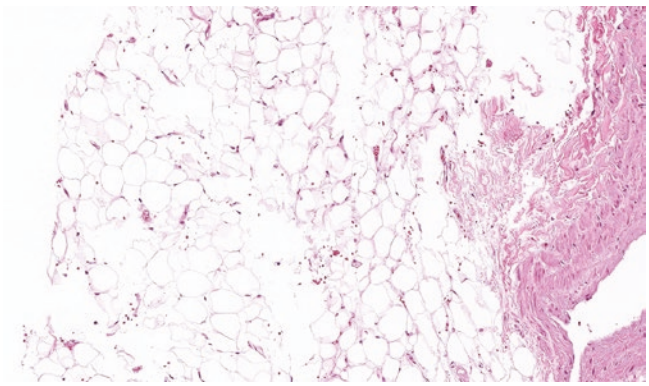

Fig. 12.1 Normal cohesive group of adipocytes with abundant univacuolar cytoplasm. Fibroadipose tissue, hematoxylin & eosin, 20× magnification

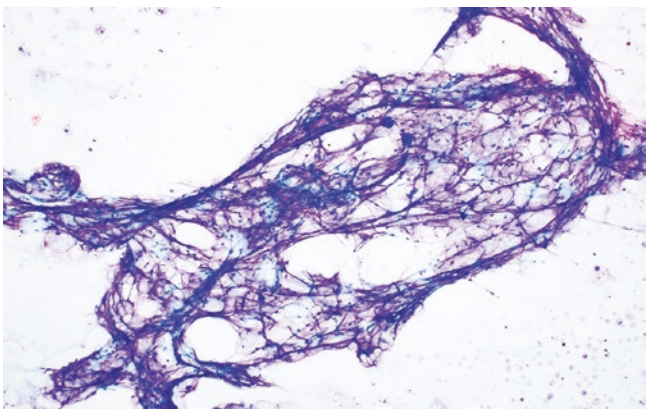

Fig. 12.2 Large cluster of normal adipocytes, exhibiting abundant pale, univacuolar cytoplasm, with traversing slender capillaries. Soft tissue, air-dried smear preparation, Diff-Quik, 10× magnification

Adipose tissue can undergo reactive and degenerative change in response to trauma, infection, prior biopsy, or previous surgical procedure [2–4]. In such situations, increased

R. L. Cantley (✉)
Department of Pathology, University of Michigan, Ann Arbor, MI, USA
e-mail: rcantley@med.umich.edu

L. Pantanowitz
Department of Pathology, Michigan Medicine, Ann Arbor, MI, USA
e-mail: lironp@med.umich.edu

M. Lew et al. (eds.), *Normal Cytology*, https://doi.org/10.1007/978-3-031-20336-7_12

vascularity and proliferation of fibroblasts may be seen. Histiocytic inflammation, including multinucleated giant cells, can be present. Fat necrosis, which can occur following trauma, can present as a palpable mass in the breast or other fatty locations. Degenerative changes associated with fat necrosis include adipocytes that are smaller and have fine, multivacuolated cytoplasm present in an oily and granular background with foamy macrophages, inflammatory cells, and giant cells (Fig. 12.3).

Abdominal fat pad FNA is often performed in the workup of suspected systemic amyloidosis [5]. With special histochemical stains such as Congo red or fluorescent stains, amyloid material when present can be identified most prominently around the walls of intervening blood vessels, but also between adipocytes. Special stains for amyloid protein can be performed directly on air-dried smears or cell block material (Fig. 12.4).

Brown fat is distinctive adipose tissue involved in thermoregulation. When it forms a mass lesion, it is referred to as a hibernoma. Brown fat is often present in the mediastinum and retroperitoneum, as well as the soft tissue of the posterior neck and shoulders. The adipocytes of brown fat are smaller than those of white fat. The cytoplasm is multivacuolated rather than univacuolated, and eosinophilic mitochondrial granules are prominent and impart its characteristic red-brown color on hematoxylin and eosin stain (Fig. 12.5). Traversing capillaries

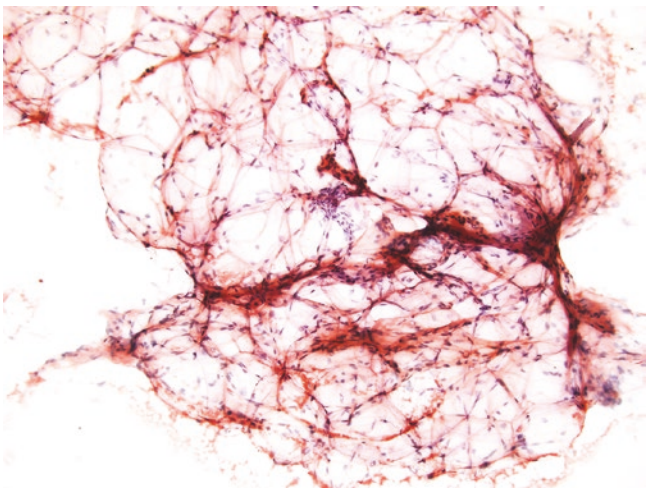

Fig. 12.4 Benign adipose tissue from an abdominal fat pad and is negative for amyloid protein on this Congo red stain. Abdominal fat pad, air-dried smear preparation, Congo red stain, 10× magnification

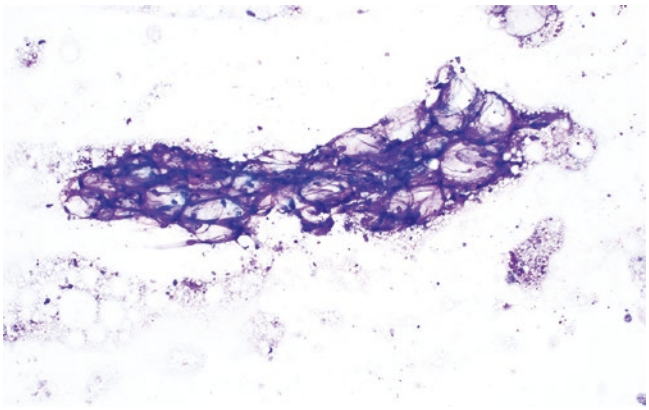

Fig. 12.3 Fat necrosis. A cluster of adipocytes is shown with degenerated, multivacuolated cytoplasm. Note that the background shows scant inflammatory cells and lipid deposits from ruptured adipocytes. Soft tissue nodule, air-dried smear preparation, Diff-Quik, 10× magnification

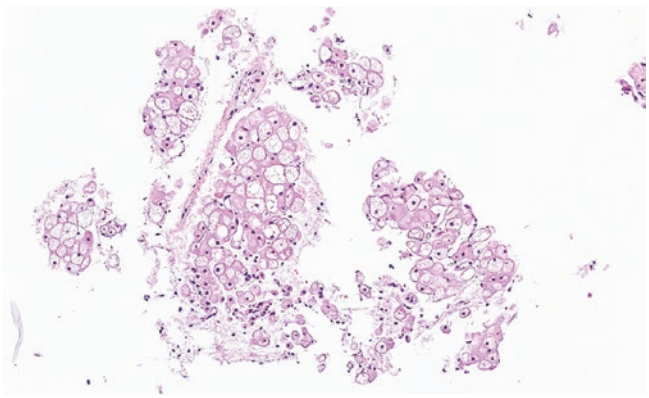

Fig. 12.5 In contrast to white fat, brown fat adipocytes are smaller with distinct cell borders, multivacuolated cytoplasm, and prominent eosinophilic mitochondrial granules. Peri-adrenal gland, cell block, hematoxylin & eosin, 20× magnification

are more prominent than in white fat. Brown fat demonstrates both S100 and CD31 immunoreactivity [6].

Striated Muscle

Skeletal muscles are composed of fascicles of parallel muscle fibers that insert onto bones via tendons (Fig. 12.6). In cytology samples, skeletal muscle presents as dense striated fibers with multiple small, dark, flat myocyte nuclei typically aligned along the subsarcolemmal periphery [2, 3]. These fibers stain strongly eosinophilic on hematoxylin and eosin (H&E), are amphophilic on Papanicolaou stain, and appear deep blue on modified Giemsa stains including Diff-Quik (DQ) (Fig. 12.7a, b). Striations may not always be seen. Fiber typing (dark type 1 and pale type 2 fibers) requires histochemical stains. Regenerating or degenerated skeletal muscle fibers can take on a multinucleated appearance ("bag of nuclei"). Regenerative skeletal muscle nuclei can also show reactive changes, including moderate nuclear enlargement and prominent nucleoli.

Cardiac muscle is also striated, but these muscle fibers are shorter, do not run as tightly parallel as skeletal muscle fibers, and exhibit branching [2, 3, 7] (Fig. 12.8a, b). Intercalated discs can sometimes be seen between cardiac myocytes, which appear as clear spaces. Cardiac myocytes have small, slightly eccentric nuclei, morphologically similar to those seen in skeletal muscle, that may be more centrally placed. One may find perinuclear lipofuscin pigment.

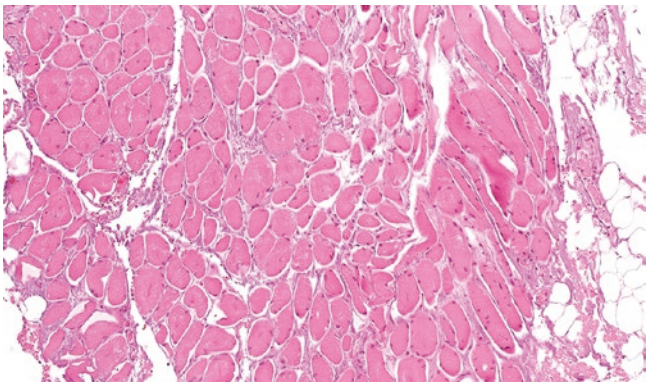

Fig. 12.6 Striated skeletal muscle fibers, seen in cross section, with peripherally located nuclei. Skeletal muscle, hematoxylin & eosin, 20× magnification

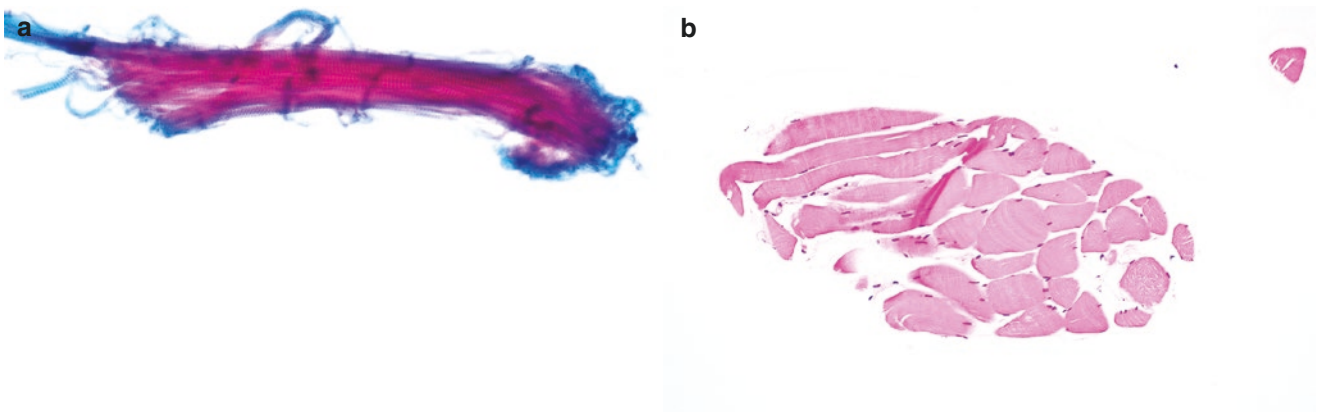

Fig. 12.7 (**a**) Nonbranching fragment of skeletal muscle fibers containing parallel cross striations, and myocytes with spindled nuclei and indistinct cell borders. (**b**) On cell block preparation, cross sections of muscle fibers reveal central eosinophilic fibers and peripheral small nuclei. Soft tissue, alcohol-fixed smear preparation, Papanicolaou stain, 60× magnification (**a**). Soft tissue, cell block, hematoxylin & eosin, 20× magnification (**b**)

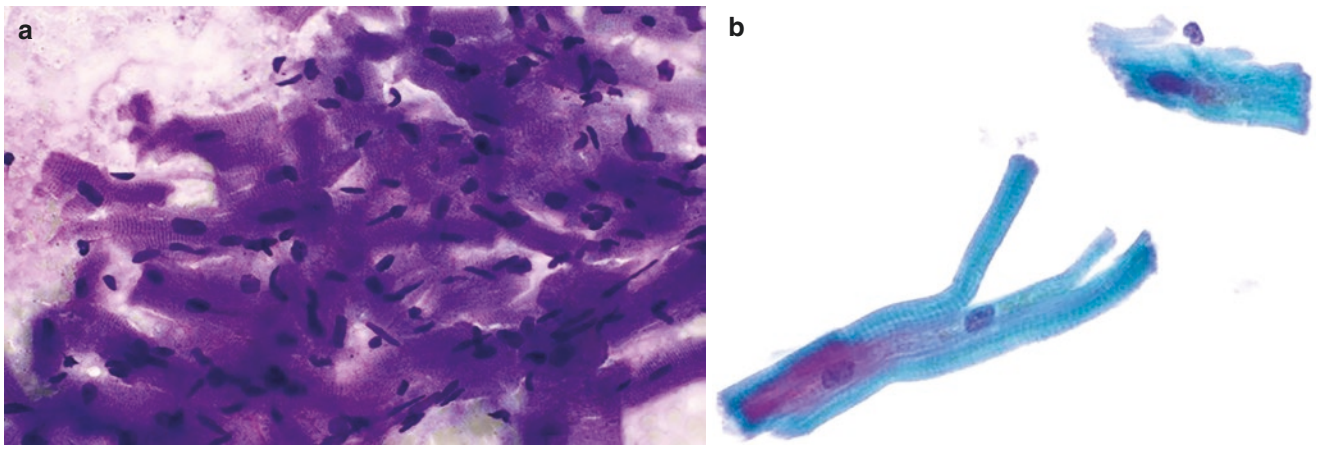

Fig. 12.8 (**a**) Cardiac muscle, exhibiting rectangular branching of fibers. Intercalated discs create greater separation between myocytes compared to those seen in skeletal muscle. (**b**) Branching of cardiac myocytes can be appreciated. Heart, air-dried smear preparation, Diff-Quik, 50× magnification (**a**). Heart, alcohol-fixed smear preparation, Papanicolaou stain, 50× magnification (**b**)

Fibrous Connective Tissue

Mesenchymal stroma and fascia are fibrous tissues composed of fibroblasts and extracellular matrix material, including collagen and ground substance. Dense fibrous connective tissue contains abundant collagen and elastin, and it makes up the strong connective tissue of the tendons, ligaments, and fascia (Figs. 12.9 and 12.10). Loose fibrous connective tissue contains little collagen and looser, pale-staining ground substance. It is found surrounding and supporting organs and blood vessels [7].

Fibroblasts are the principal cell of connective tissue, and they can be sampled from essentially any body site [2, 3, 7]. They produce the matrix materials of connective tissue, including collagen and ground substance, and are found embedded within the connective tissue they produce. Fibroblasts range in shape and appearance. They are present more abundantly in dense connective tissue, where they take on a spindled appearance embedded between collagen fibers (Fig. 12.11). In loose connective tissue, fibroblasts are less abundant, and they take on a polygonal or stellate shape. In both types of connective tissue, these cells have delicate cytoplasm and the nuclei of fibroblasts have bland even chromatin and absent or inconspicuous nucleoli. Naked fibroblast nuclei can sometimes be found in vigorous fine needle aspiration smears.

Myxoid change is a common degenerative process of connective tissue, in which the matrix material takes on an amorphous, granular amphophilic to mucoid appearance. It is associated with degenerative changes in mesenchymal elements of nonneoplastic, benign, and malignant entities.

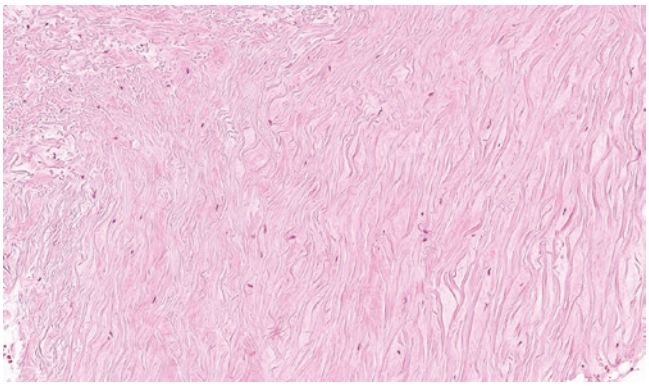

Fig. 12.9 Dense collagenous stroma of fascia with scattered fibroblastic cells. Fascia, hematoxylin & eosin, 20× magnification

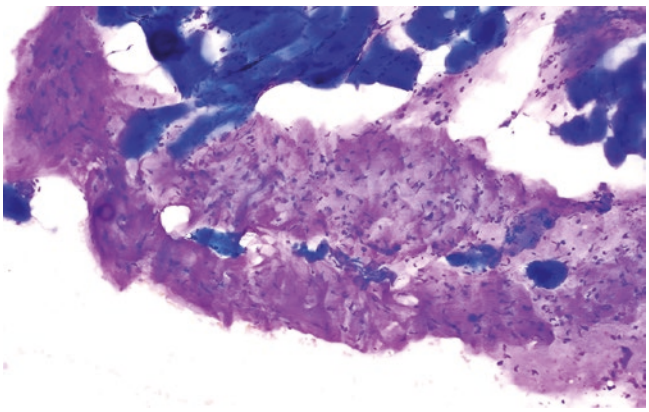

Fig. 12.10 Pink collagenous stroma containing embedded fibroblasts in soft tissue associated with blue-staining skeletal muscle. Fascia, air-dried smear preparation, Diff-Quik, 10× magnification

Reactive cellular changes in connective tissue are common following an injury or procedural intervention. In such circumstances, reactive (versus resting) fibroblasts show variation in size and shape, from spindled to polygonal to stellate, often with angulated cytoplasmic extensions [4, 8]. Variation in nuclear size and shape is common, as are reactive-type nucleoli (Fig. 12.12). Reactive fibroblasts may be binucleated. Loose but cohesive clusters of reactive fibroblasts without obvious associated stroma can be seen, which can mimic neoplastic processes.

Myofibroblasts are cells of uncertain origin with features of both normal fibroblasts and smooth muscle cells [9]. In reactive soft tissue conditions, they likely represent modified fibroblasts, and are not always readily distinguishable from reactive fibroblasts. Myofibroblasts are most often spindle shaped, have ill-defined eosinophilic cytoplasm that is paler than smooth muscle cells, and contain wavy or plump, rounded nuclei with small nucleoli. In contrast to fibroblasts, myofibroblasts express markers of smooth muscle differentiation, such as alpha-smooth muscle actin.

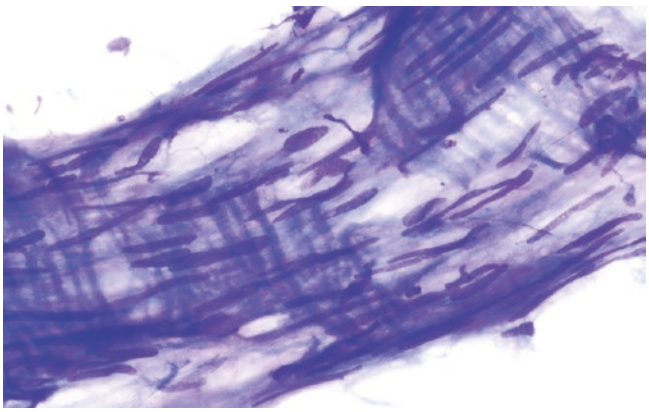

Fig. 12.11 Densely cellular connective tissue from fascia, with spindle-shaped fibroblast nuclei running in parallel rows. Fascia, air-dried smear preparation, Diff-Quik, 60× magnification

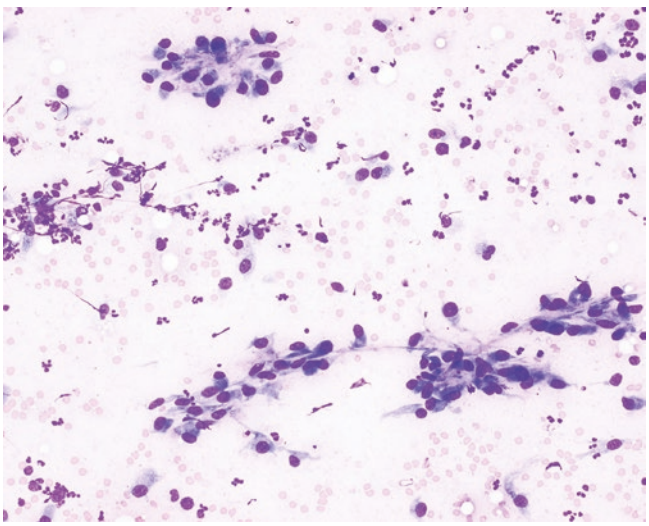

Fig. 12.12 Reactive fibroblasts are present as single cells and in small groups, with round nuclei, occasional nucleoli, and angulated cytoplasmic borders. The background also contains scattered neutrophils. Post-surgical site, air-dried smear preparation, Diff-Quik, 20× magnification

Bone

Bones vary in shape and include tubular and flat bones. Tubular bones are anatomically subdivided into epiphysis (articular edge), metaphysis, and diaphysis (shaft). Bone tissue is composed of ossified (mineralized) organic matrix (e.g., collagen), inorganic minerals (calcium hydroxyapatite), and cellular elements including osteoblasts, osteoclasts, and marrow elements. Lamellar bone is mature, highly organized, and ossified bone that makes up the dense compact (cortical) outer structural bone and spongy cancellous (trabecular) bone of the marrow cavity (Fig. 12.13). Woven bone is immature bone found in fetal development and bone healing, which is the foundation on which lamellar bone forms. It is weaker and more flexible, with disorganized collagen and less mineralization than lamellar bone. In lamellar bone, the collagen is deposited with a parallel pattern. The outer surface of bone is lined by thin fibrous periosteum and the inner medullary surface is lined by endosteum. Bone formation and remodeling (e.g., endochondral or intramembranous ossification) is best appreciated in histopathology sections [2, 3].

Bone material may be present in a number of cytology specimens, especially for primary and secondary bone lesions that are targeted for computed tomography (CT)-guided FNA. In addition, contaminating fragments of bone can be obtained during aspiration of lesions adjacent to bone and in cerebrospinal fluid specimens (Fig. 12.14a, b). They often appear as acellular fragments of amorphous calcified

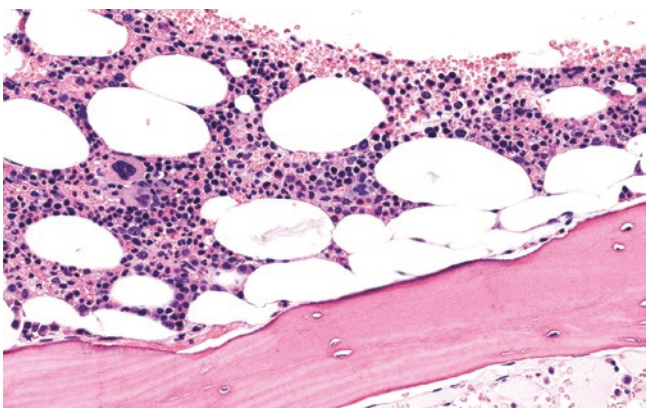

Fig. 12.13 Trilineage bone marrow elements and bony trabeculae of normal spongy bone. Bone, hematoxylin & eosin, 40× magnification

material. These bone fragments often cause air bubbles to form under glass slide coverslips. Decalcification of bone specimens can impair cellular preservation.

Normal cellular elements of bone encountered in cytology samples must not be misinterpreted as atypical or malignant [10]. Osteoblasts are uniform, round to polygonal cells with abundant cytoplasm and typically have eccentric nuclei which may show perinuclear hofs due to their Golgi apparatus (Fig. 12.15a). They can thus mimic plasma cells. They are usually found as single cells. However, when they present in sheets and clusters, they can resemble epithelium. However, osteoblast nuclei are ovoid and regular, have open chromatin with distinct nucleoli, and they lack the three dimensionality of metastatic carcinoma. Osteoblasts that become embedded within bone matrix become osteocytes and are located within a lacunar space. These are infrequently seen in FNA samples because they are hard to reach with aspiration. Osteoclasts are cells of histiocytic origin involved in bone reabsorption. They typically appear as single, large (40–100 uM in diameter), multinucleated giant cells similar to those seen in foreign body giant cell reactions (Fig. 12.15b). Their nuclei (often 4–20 in number, but can reach up to 100) are scattered throughout the cytoplasm, which is abundant and often granular or vacuolated. These nuclei are ovoid with regular nuclear membranes and euchromatin. Nucleoli may range from being indistinct to prominent.

Bone marrow cellular elements can also be encountered in cytology specimens, including all three lines of blood cell precursors: erythropoietic, myelopoietic, and megakaryocytic [10] (Fig. 12.16a, b). Megakaryocytes are large cells

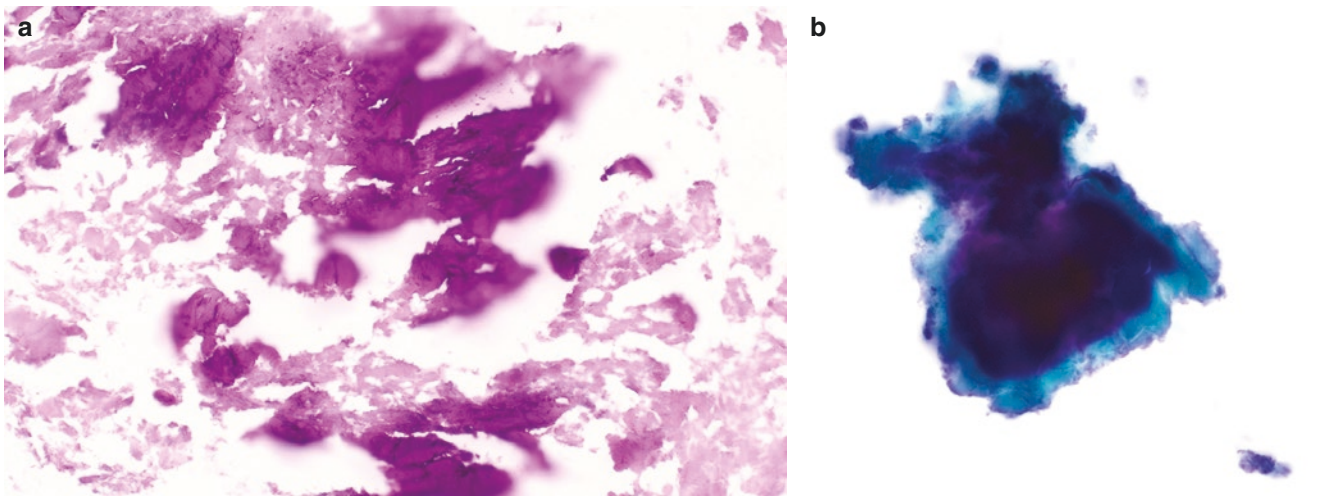

Fig. 12.14 Amorphous, calcified bone matrix material. Bone, air-dried smear preparation, Diff-Quik, 40× magnification (**a**). Bone, alcohol-fixed smear preparation, Papanicolaou stain, 60× magnification (**b**)

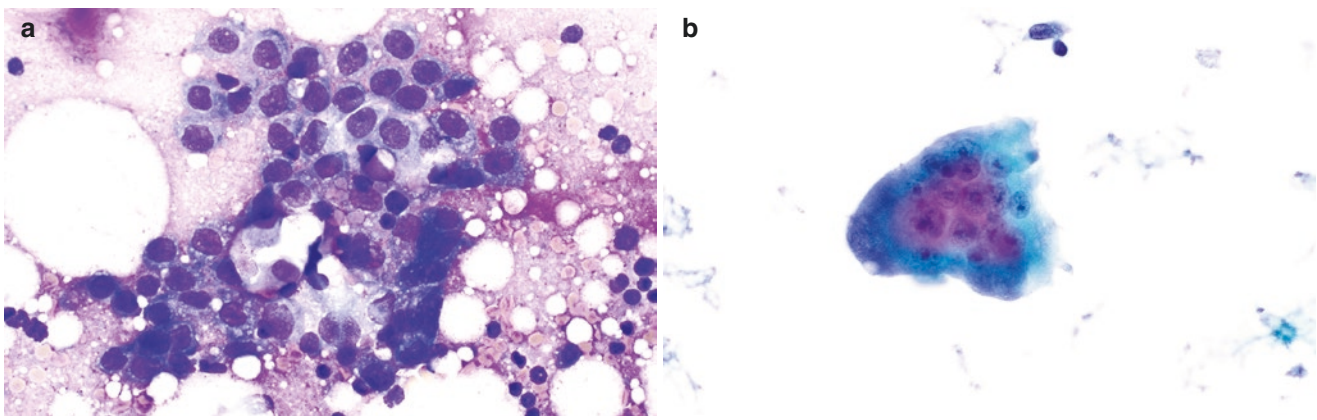

Fig. 12.15 (**a**) Osteoblasts forming epithelioid clustering. The cells are polygonal with uniform round nuclei, round central nucleoli, and smooth nuclear membranes. (**b**) An osteoclast is shown which appears as a multinucleated giant cell containing many ovoid, bland nuclei. Bone, air-dried smear preparation, Diff-Quik, 60× magnification (**a**). Bone, alcohol-fixed smear preparation, Papanicolaou stain, 60× magnification (**b**)

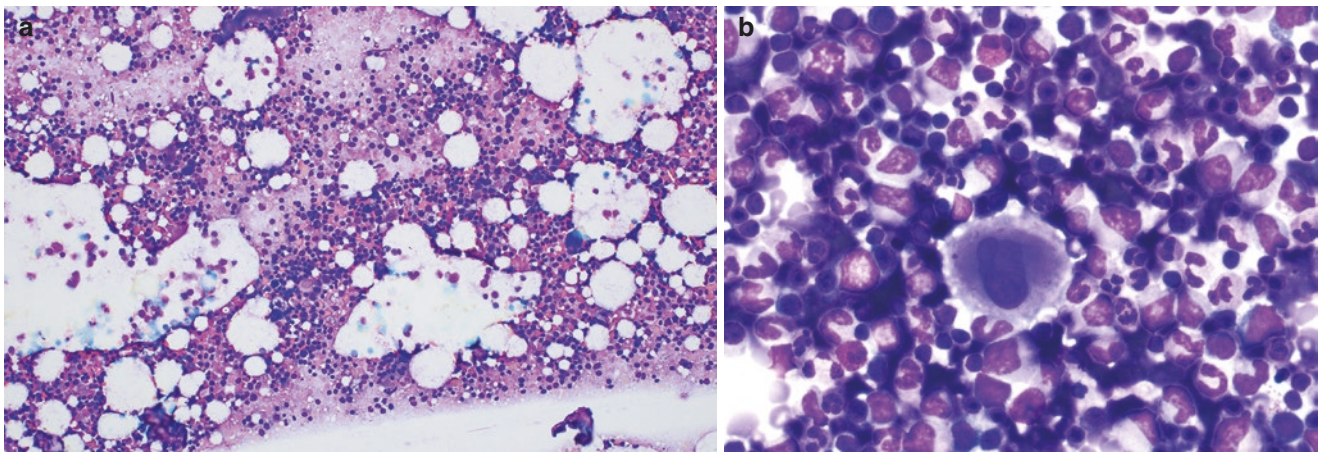

Fig. 12.16 Bone marrow elements. (**a**) Adipocytes are shown admixed with hematopoietic bone marrow elements. (**b**) Normal trilineage elements are present including a central megakaryocyte with a large lobated nucleus, and numerous erythroid and myeloid elements. Bone marrow, air-dried smear preparation, Diff-Quik, 20× (**a**) and 60× (**b**) magnification

with abundant amphophilic, granular cytoplasm, and multilobated nuclei. Their chromatin is dense and nucleoli are usually absent. The multilobation and dark staining of the nuclei can be mistaken for the nuclear changes of malignant cells such as metastatic carcinoma. However, normal megakaryocytes are always present singly in the background of other marrow elements while carcinoma cells often present in crowded clusters. Erythroid precursors appear as small, lymphocyte-sized cells with round eccentric nuclei and condensed to pyknotic chromatin. Myeloid precursors have a range of appearances, from larger cells with unilobed, pale nuclei to smaller cells with band-like or lobated nuclei.

Cartilage

Cartilage is composed of its primary cellular elements (chondrocytes) embedded within an acellular matrix (Fig. 12.17). Chondrocytes appear as large polygonal cells, often with angular edges (Fig. 12.18). Their cytoplasm is lightly basophilic, and their nuclei are typically pyknotic and degenerated [2, 3, 10].

There are three types of cartilage: hyaline, elastic, and fibrocartilage. Hyaline cartilage is the most abundant form in the body, and it is the most commonly encountered form seen in cytology preparations. Hyaline cartilage is found at the tip of the nose, around the trachea, and at joints. So named because of its glassy appearance, hyaline cartilage is predominantly made of collagen fibers. The collagen matrix appears as homogenously dense but amphophilic matrix material with embedded chondrocytes (Fig. 12.19). Hyaline cartilage can be encountered by needle contamination in transbronchial FNA and cerebrospinal fluid samples, as well as sampling of bone and soft tissue lesions.

Elastic cartilage is less strong but more flexible than hyaline cartilage. Its matrix contains an abundance of elastin fibers and relatively less collagen than hyaline cartilage, but the histologic appearance is otherwise similar to hyaline cartilage. Elastic cartilage is found in the external ear and the larynx. Fibrocartilage is the strongest and most dense cartilage. It is found in the transition points between hyaline cartilage and tendons or ligaments, and its histologic features often resemble a transition between hyaline cartilage and dense fibrous connective tissue.

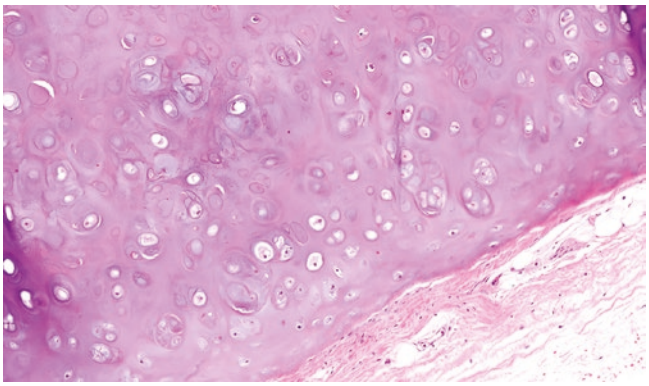

Fig. 12.17 Hyaline cartilage from the bronchial wall, composed of homogeneous amphophilic matrix material with embedded chondrocytes. Bronchus, hematoxylin & eosin, 40× magnification

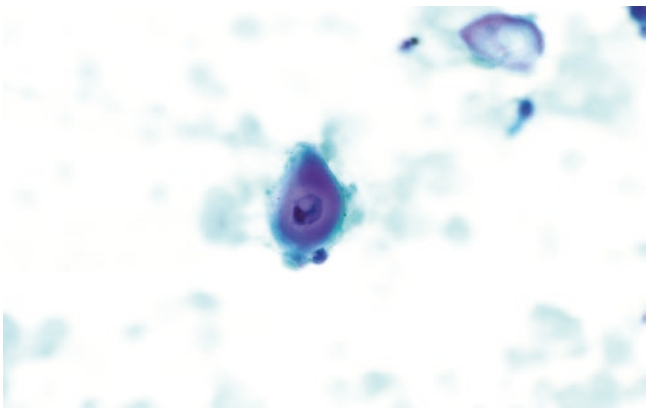

Fig. 12.18 A single benign chondrocyte is shown with moderate pale cytoplasm, pyknotic nucleus, and surrounding chondroid matrix material. Cerebrospinal fluid, ThinPrep preparation, 60× magnification

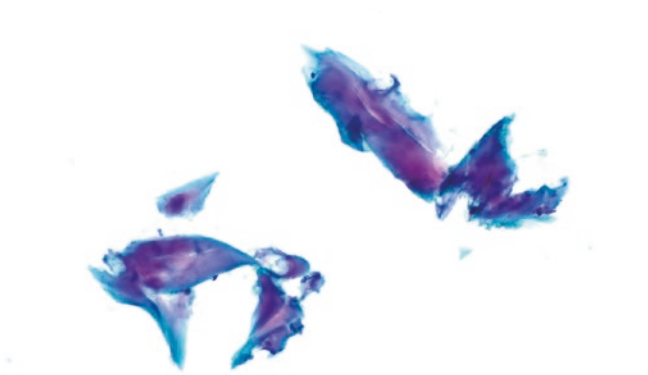

Fig. 12.19 Fragments of hyaline cartilage from the bronchial wall, collected during endobronchial fine needle aspiration of a lung nodule, containing scant embedded chondrocytes with small pyknotic nuclei. Endobronchial fine needle aspiration, alcohol-fixed smear preparation, Papanicolaou stain, 20× magnification

Synovium

The joints of the skeletal system typically include hyaline cartilage covering the articular surfaces of bones, ligaments formed mainly by collagen, and synovium. The temporomandibular, sternoclavicular, and intervertebral joints are instead covered by fibrocartilage. The joint capsule includes three layers: outer fibrous layer, subsynovium, and inner synovial lining [11, 12]. The synovial lining is composed of synoviocytes, which include type A cells (histiocyte-like) and type B cells (fibroblast-like) (Fig. 12.20). The type A cells have a phagocytic function while the type B cells produce hyaluronic acid. Synovial cells can be obtained during aspiration of lesions involving or adjacent to joints. On aspiration cytology, they present as clusters of bland, fibroblastic cells (Fig. 12.21). Macrophages and other inflammatory cells can also be obtained on sampling of joint fluid. The subsynovium is comprised of fibrovascular tissue with variable fat, nerves, and scattered histiocytes.

Arthrocentesis of joint fluid for cytology examination and synovial fluid analysis is often undertaken in patients with a joint effusion or inflammation. Normal synovial fluid is usually clear and viscous, and should not clot in a tube. It functions as a lubricant and supplies nutrients to the articular cartilage. The volume of this fluid is usually minimal in the normal state, even for large joints. When there is inflammation, this volume increases, along with the number of inflammatory cells. Normal synovial fluid contains very few cells. Polarized microscopic examination of normal synovial fluid should not identify crystal deposition, as occurs with crystal-induced arthropathy (e.g., gout and pseudogout).

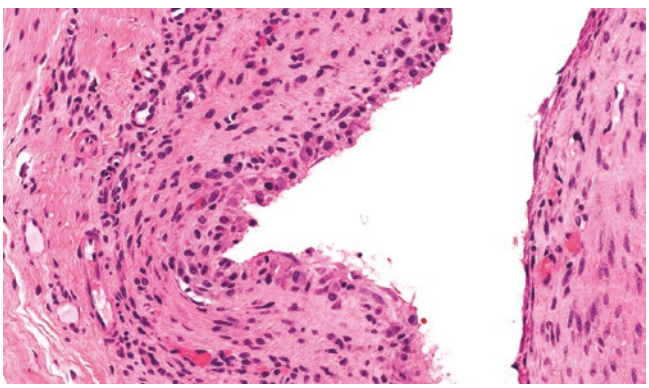

Fig. 12.20 Synovium composed of an inner lining of histiocyte-like and fibroblast-like cells within a fibrous wall. Synovium, hematoxylin & eosin, 40× magnification

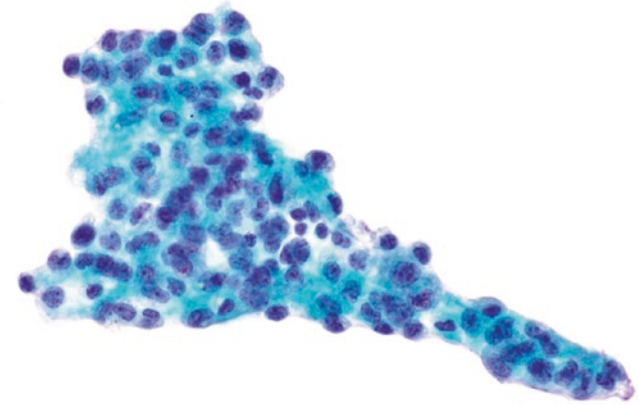

Fig. 12.21 Cluster of bland, fibroblastic synovial cells. Nuclei are ovoid and contain euchromatin. Joint fluid, alcohol-fixed smear preparation, Papanicolaou stain, 60× magnification

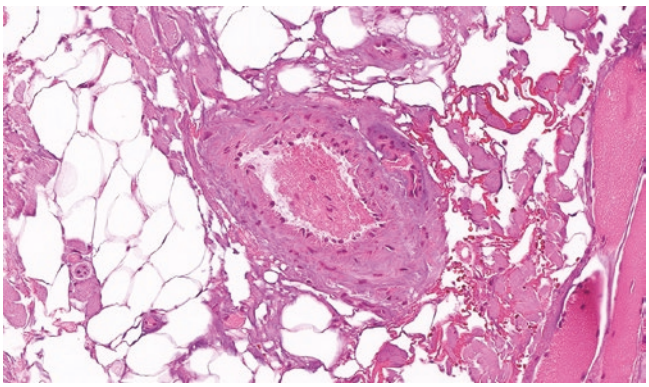

Fig. 12.22 Muscular artery lined by a low cuboidal layer of endothelium surrounded by smooth muscle. Soft tissue, hematoxylin & eosin, 20× magnification

Blood Vessels

Fragments of blood vessels and endothelial cells are frequently present in FNA samples at a variety of sites [2, 3, 7]. Small capillaries are commonly collected at aspiration, particularly in highly vascular sites such as the endocrine organs. Capillaries, arterioles, and venules present as thin, branching structures containing endothelial cells, the nuclei of which usually present in a "single file" appearance along the vascular structure. Larger arterial vessels are lined by inner endothelium surrounded by smooth muscle (Fig. 12.22).

Endothelial cells can show a range of appearances on aspiration cytology (Fig. 12.23). Nonreactive endothelium most commonly presents as clusters of small, elongated cells with flat nuclei. Reactive changes can occur, such as in the setting of inflammation and/or angiogenesis, resulting in nuclear enlargement, rounding of nuclei, and prominent nucleoli. Normal endothelium usually does not have mitotic figures. Endothelial cells are immunoreactive for CD34, CD31, and ERG.

Large and medium-sized arteries include both elastic and muscular types. Elastic arteries are the large arteries of the cardiopulmonary system (i.e., aorta and pulmonary arteries). These vessels have thin walls relative to the size of their lumen. The wall of elastic arteries contains abundant collagen and elastin fibers, and relatively scant smooth muscle myocytes, which are embedded within the fibrous stroma of the vessel wall. Elastic arteries may occasionally be sampled on aspiration of mediastinal and central lung lesions. Muscular arteries include the medium- and large-sized arteries which arise and draw blood from elastic arteries (Fig. 12.24a, b). They are of smaller caliber, and their wall is composed of a greater density of smooth muscle myocytes and relatively less fiber material. Veins are also lined by endothelial cells. They have thinner walls than arteries, with abundant collagen and few smooth muscle myocytes within their vessel wall.

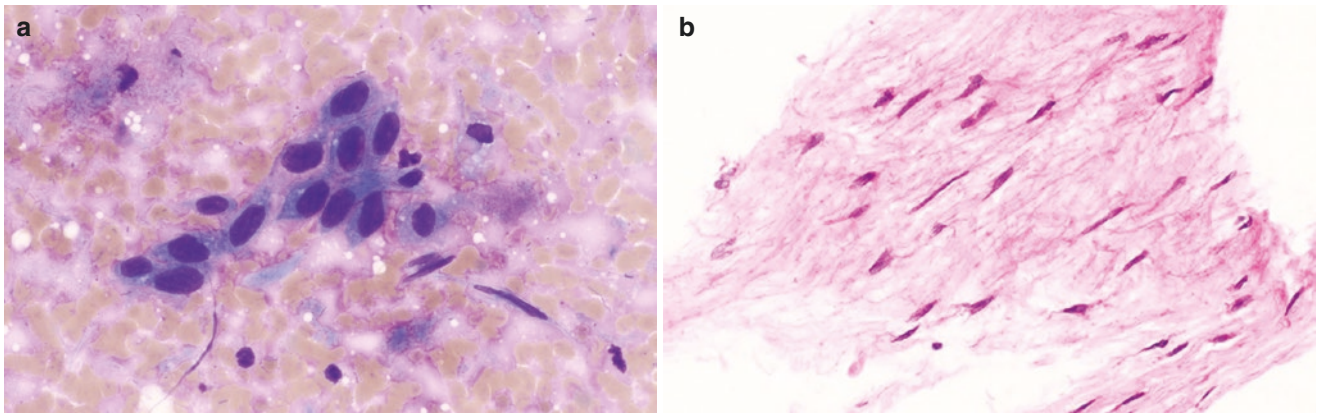

Fig. 12.23 Endothelial cells from the aortic lining. (**a**) Endothelial cells are ovoid to elongated, with bland, ovoid nuclei. (**b**) The wall of the aortic contains single smooth muscle myocytes embedded in collagen and elastin material. Aorta, air-dried smear preparation, Diff-Quik, 60× magnification (**a**). Aorta, cell block, hematoxylin & eosin, 40× magnification (**b**)

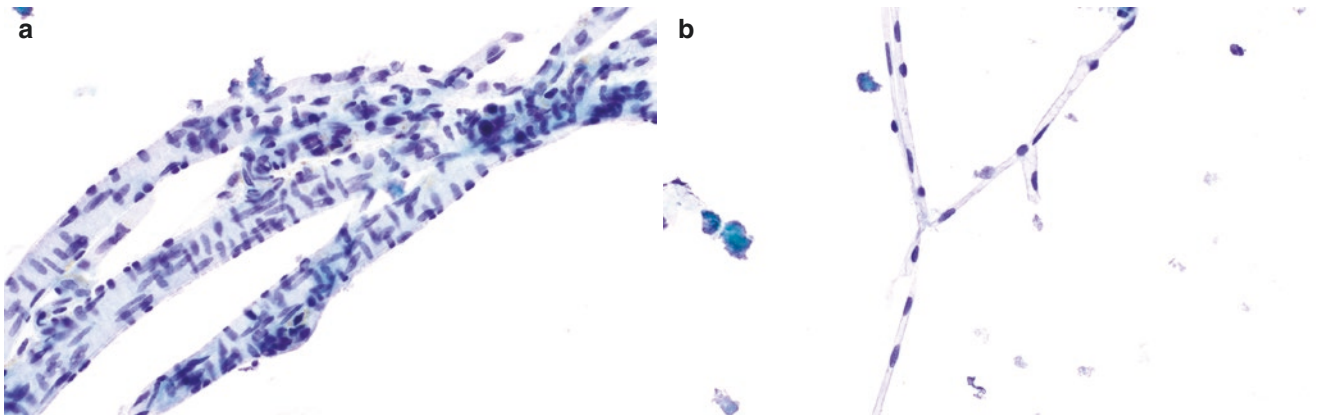

Fig. 12.24 (**a**) Medium-sized muscular arteries have a greater density of myocyte nuclei than elastic arteries, while (**b**) capillaries appear as thin, branching structures with single-file endothelial nuclei and no smooth muscle. Soft tissue, alcohol-fixed smear preparation, Papanicolaou stain, 40× (**a**) and 20× magnification (**b**)

Skin

The skin is composed of the outer epidermis and the underlying dermis, separated by a basement membrane [2, 13, 14] (Fig. 12.25). The epidermis contains a superficial layer of keratin, with a mid-portion composed of several layers of keratinocytes (squamous cells), and basal cells near the basement membrane admixed with fewer melanocytes and Langerhans cells.

Keratin, anucleated squamous cells, and occasional mature, nucleated superficial squamous cells are typically the most abundant elements seen on skin scraping specimens (Fig. 12.26). These outer epidermal elements are also commonly a minor contaminating component of percutaneous FNA at any site.

The dermis is composed of similar mesenchymal elements as seen elsewhere in the soft tissues of the body. As a connective tissue layer, the dermis is composed of fibroblasts and abundant collagen, as well as elastin fibers. Adipocytes, macrophages, mast cells, blood vessels, and nerves may also be present.

The dermis also contains skin appendages that connect to the surface skin and hair follicles [13, 14]. Eccrine sweat glands, found essentially on all body surfaces, are tortuous ductal structures lined by stratified, cuboidal epithelial cells with scant to moderate cytoplasm. Apocrine sweat glands, which are associated with hair follicles, are ductal structures

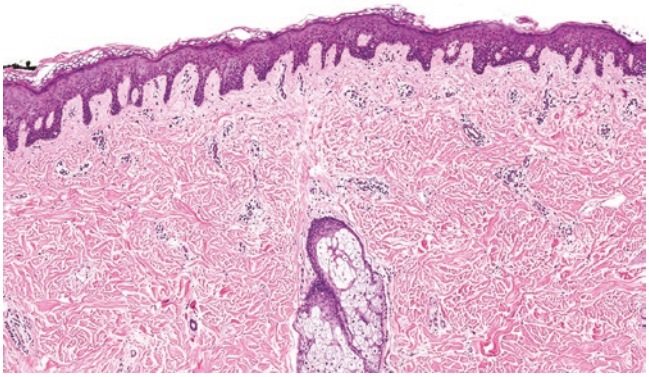

Fig. 12.25 Normal skin with a surface layer of keratinocytes and underlying dermis with embedded sebaceous gland. Skin, hematoxylin & eosin, 4× magnification

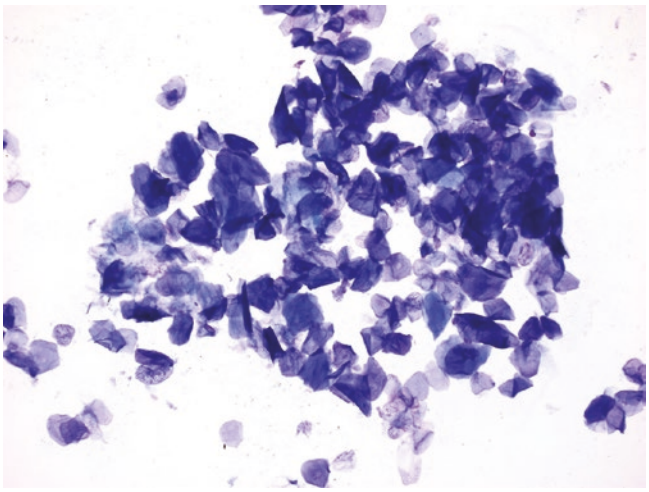

Fig. 12.26 When superficial skin is sampled, anucleated surface squamous cells predominate, with occasional mature nucleated squamous cells seen. Skin scraping, air-dried smear preparation, Diff-Quik, 20× magnification

lined by a single layer of apocrine-type epithelium, which is columnar epithelium marked by abundant eosinophilic cytoplasm and conspicuous nucleoli. Sebaceous glands (Fig. 12.25), which are found both at the skin surface and at hair follicles, are acinar glands filled with large, round sebaceous cells marked by abundant vacuolated cytoplasm (Fig. 12.27a, b).

Hair follicles may be occasionally sampled on superficial FNA, particularly from the scalp, axillary, or inguinal areas. They are tubular structures extending from the dermis and opening onto the skin surface. The hair follicle is composed of multiple layers of keratocytes surrounding a central hair shaft. Melanin pigment is frequently seen, particularly at the base of the hair bulb within the inner keratinocytes. Hair follicle material appears as tightly cohesive epithelial structures composed of keratinocytes with variable amounts of melanin pigment.

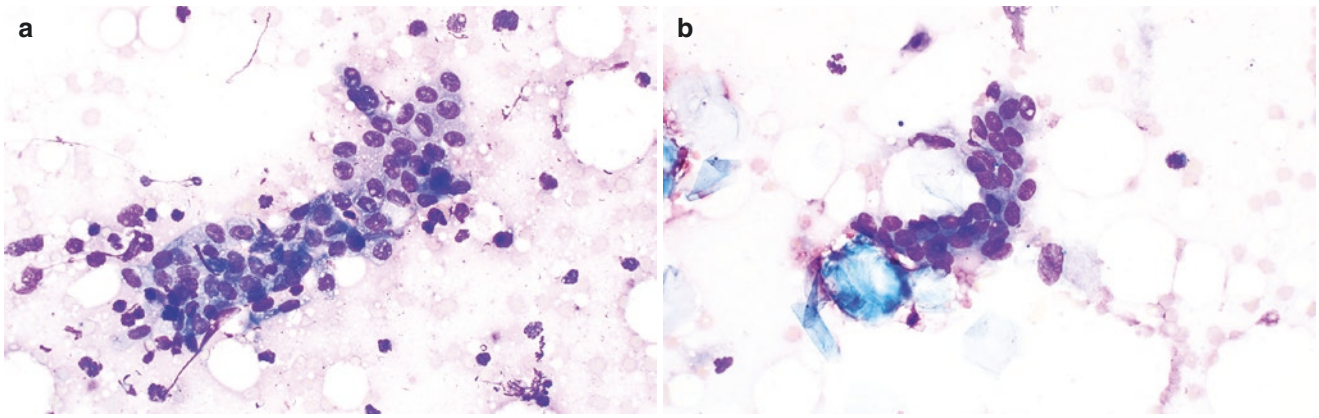

Fig. 12.27 Sebaceous glandular cells (**a**) exhibit abundant multivacuolated cytoplasm, ovoid nuclei, and distinct nucleoli, whereas eccrine sweat glands (**b**) are lined by basaloid, cuboidal cells with scant cytoplasm lacking vacuoles. Cutaneous fine needle aspiration, air-dried smear preparation, Diff-Quik, 50× magnification (**a**, **b**)

References

1. Winckler G. Characteristics of the vacuolar nucleus of the fat cell in man. Z Anat Entwicklungsgesch. 1960;122:241–6.
2. Demay RM. Soft tissue, bone, and skin. In: The art and science of cytopathology, superficial aspiration cytology. Chicago: American Society for Clinical Pathology; 2012. p. 635–750.
3. DeMay RM. Soft tissue & bone. In: The book of cells: a breviary of cytopathology. Chicago: American Society for Clinical Pathology; 2016. p. 282–318.
4. James LP. Cytopathology of mesenchymal repair. Diagn Cytopathol. 1985;1(2):91–104.
5. Ansari-Lari MA, Ali SZ. Fine-needle aspiration of abdominal fat pad for amyloid detection: a clinically useful test? Diagn Cytopathol. 2004;30(3):178–81.
6. Lemos MM, Kindblom LG, Meis-Kindblom JM, Remotti F, Ryd W, Gunterberg B, Willén H. Fine-needle aspiration characteristics of hibernoma. Cancer. 2001;93(3):206–10.
7. Raso DS. Connective tissue. In: Herzberg AJ, Raso DS, Silverman JF, editors. Color atlas of normal cytology. New York: Churchill Livingstone; 1999. p. 34–7.
8. Åkerman M. Reactive cellular changes in soft tissue. In: Goerttler K, Feichter GE, Witte S, editors. New Frontiers in cytology. Berlin: Springer; 1988. p. 302–5.
9. Menzel T, Fletcher CD. The emerging role of myofibroblasts in soft tissue neoplasia. Am J Clin Pathol. 1997;107(1):2–5.
10. Samedi VG, Bocklage T. Bone and soft tissue cytology. In: Pitfalls in diagnostic cytopathology with key differentiating cytologic features. Essentials in cytopathology, vol. 27. Cham: Springer; 2016. p. 201–39.
11. Ostovic KT, Kaic G, Ostovic I, Skoro M, Novak NP, Morovic-Vergles J. The importance of urgent cytological examination of synovial fluids in differentiation inflammatory and non-inflammatory joint diseases. Coll Antropol. 2010;34(1):145–52.
12. Freemont AJ. Microscopic analysis of synovial fluid – the perfect diagnostic test? Ann Rheum Dis. 1996;55(10):695–7.
13. Sheaff MT, Singh N. Skin cytology. In: Cytopathology. London: Springer; 2013. p. 453–66.
14. Durdu M. Cytological definitions. In: Cutaneous cytology and tzanck smear test. Cham: Springer; 2019. p. 27–61.

Body Cavities (Mesothelium, Synovium)

13

Judy Pang

Mesothelium

The space between the body wall and viscera is termed coelom. There are three major body cavities: thorax, pericardium, and abdomen. Mesothelium, which is derived from the mesoderm, extends as a monolayer over the entire surface of these body cavities, which are designated as pleural, pericardial, and peritoneal surfaces, respectively. The serous membrane that envelops the internal organs is referred to as the visceral layer of mesothelium while the serous membrane that lines the body cavity wall is termed the parietal layer of mesothelium. The pleura, pericardium, and peritoneum share common embryology, physiology, histology, and cytology and are indistinguishable by microscopy alone [1].

Serous membranes consist of a single flat layer of mesothelial cells. However, when irritated, they can become plump and cuboidal. This layer of mesothelial cells is supported by connective tissue that is rich in capillaries and lymphatics (Fig. 13.1). The parietal layer is continuous with the visceral layer forming a potential space.

Serous membranes produce a clear fluid. This fluid is produced by filtration of blood plasma through semipermeable endothelium of capillaries, most of which are normally resorbed by the venous system (80–90%), with the remaining resorbed by the lymphatics. The amount of fluid in the body cavity space is dependent on this balance of fluid formation and resorption. Formation is affected by hydrostatic pressure in the capillaries (determined by the heart and sodium retention), plasma oncotic pressure (primarily albumin), and capillary permeability. Capillaries and venules take up water, electrolytes, and small molecules whereas the lymphatics can additionally take up proteins and particulate matter in the resorption process. Typically, the small space between the parietal and visceral layers allows for a minimal amount of serous fluid (approximately 7–16 ml) that keeps the surfaces moist and acts as a lubricant, facilitating gliding of membranes over each other with each breath, heartbeat, or peristaltic contraction. Surface microvilli on mesothelial cells have glycocalyx rich in sialic acid and secrete glycosaminoglycans, particularly hyaluronic acid [1–4].

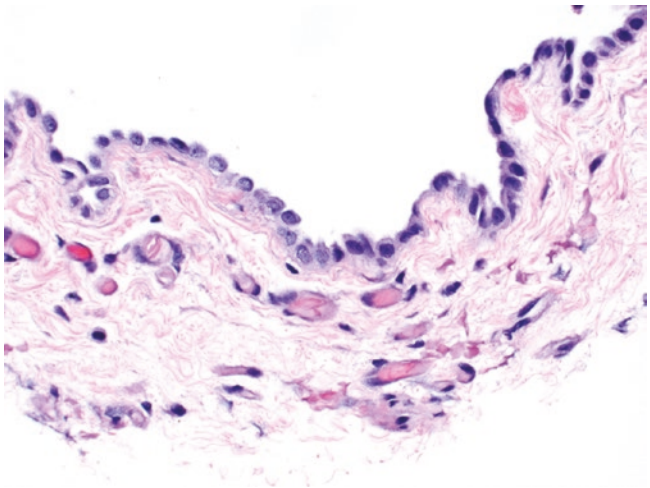

Fig. 13.1 Fragment of mesothelium with plump and cuboidal mesothelial cells supported by connective tissue rich in capillaries and lymphatics. Lung biopsy, hematoxylin & eosin, 40× magnification

Effusions can be benign or malignant but are always pathologic and can be subclassified as transudates or exudates. Transudates are typically benign and are secondary to mechanical factors, whereas exudates can be malignant or benign and are a result of damage to the serous membranes. Effusions are sampled by insertion of a needle into the body cavity (thoracentesis, pericardiocentesis, paracentesis). Fresh specimens are preferred with an optimal volume of 75 ml of fluid for cytological evaluation [5] and can be refrigerated at 4 degrees Celsius for several days if needed before processing with good cellular preservation. There are various slide preparations available for specimen processing, including direct smears, cytocentrifuge (cytospin) preparations, liquid-based preparations, and cell blocks. Utilizing more

J. Pang (✉)
Department of Pathology, University of Michigan–Ann Arbor, Ann Arbor, MI, USA
e-mail: jcpang@med.umich.edu

M. Lew et al. (eds.), *Normal Cytology*, https://doi.org/10.1007/978-3-031-20336-7_13

than one preparation method improves sensitivity for the detection of malignancy [1, 2].

Transudates are typically clear, pale, or yellow in appearance and are defined by a low protein content (<3.0 g/dL) and specific gravity (<1.015). Common clinical settings in which transudates are encountered include congestive heart failure, cirrhosis, renal failure, pulmonary embolism, peritoneal dialysis, and nephrotic syndrome. While most transudates are associated with benign conditions, 5% have been reported to be due to malignant processes [1–4]. On cytology, transudates are hypocellular (<500/ul). The cellular constituents are mostly made up of mesothelial cells, and occasional inflammatory cells including macrophages. Cellularity and the types of inflammatory cells present depend on the inciting stimulus and duration of the effusion. Cell counts may increase in chronic processes. Mesothelial cells typically occur singly or in small clusters, are bland in appearance, and often show varying degrees of degeneration and reactive changes. The background is typically clean.

Exudates resemble unfiltered plasma and are usually related to irritation of the serous membrane and mesothelium with damaged blood vessels resulting in increased permeability. This is frequently due to inflammation or malignancy. Grossly, exudates are usually cloudy, yellow, or bloody and have a high protein content (>3 g/dL) and specific gravity (>1.015). Lactate dehydrogenase (LDH) is usually >20 U/dL, and the ratio of fluid LDH to serum LDH is >0.6. LDH correlates with increased cellularity and is usually elevated in malignant effusions. On cytology, exudates are typically hypercellular. Mesothelial cells are numerous, presenting singly or in small clusters. Reactive changes are common including variable cell shape, size, enlarged nuclei, prominent nucleoli, and cytoplasmic vacuolization. Taken together with the high cellularity, this constellation of findings can mimic malignancy [1–4].

Mesothelial cells average about 20–25 μm in diameter (10–30 μm), but cellular enlargement is common and multinucleated forms can occasionally be encountered (Fig. 13.2). Nuclear/cytoplasmic (N/C) ratio is relatively constant, but small cells with high N/C ratios and large cells with low N/C ratios are not infrequently encountered. The nucleus is typically round to ovoid but can be bean shaped, like those seen in macrophages. The nuclear membrane is well defined and usually smooth but can be folded or convoluted, especially in peritoneal/pelvic washings (Fig. 13.3). Chromatin is typically fine but can be coarser with reactive changes. The nucleoli can range from small and inconspicuous to large and prominent in reactive cells, but multiple or macronucleoli should raise concern for malignancy. Rare intranuclear cytoplasmic invaginations can be seen in benign effusions. Mitotic figures are uncommon, but can be seen in benign effusions. Numerous mitoses or atypical mitotic figures are more indicative of malignancy. The cytoplasm has a two-toned appearance with a densely granular cytoplasm in the central component (endoplasm) due to perinuclear accumulation of filaments and a pale ectoplasmic rim. Differential staining of the endoplasm (eosinophilic to orangeophilic) and the ectoplasm (basophilic to cyanophilic) is characteristic and sometimes occurs with the Pap stain. Occasionally, hemosiderin or lipofuscin pigment can be present. Cytoplasmic vacuoles are common and are degenerative or reactive in nature. A large degenerative vacuole can displace the nucleus to the edge of the cell, mimicking signet ring adenocarcinoma. Degenerative vacuoles are empty in appearance (clear and glassy) since they only contain water

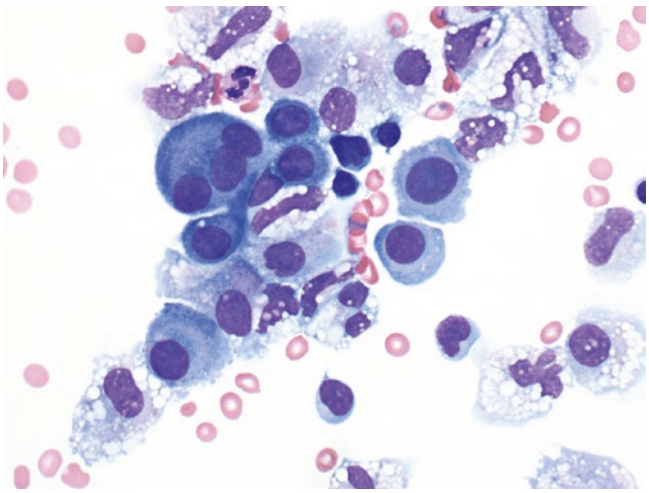

Fig. 13.2 Ascites fluid with a large multinucleated mesothelial cell and admixed smaller mesothelial cells with round nuclei, dense cytoplasm, and cytoplasmic blebs. Foamy macrophages, lymphocytes, and neutrophils are also seen. Cytospin preparation, Giemsa, 60× magnification

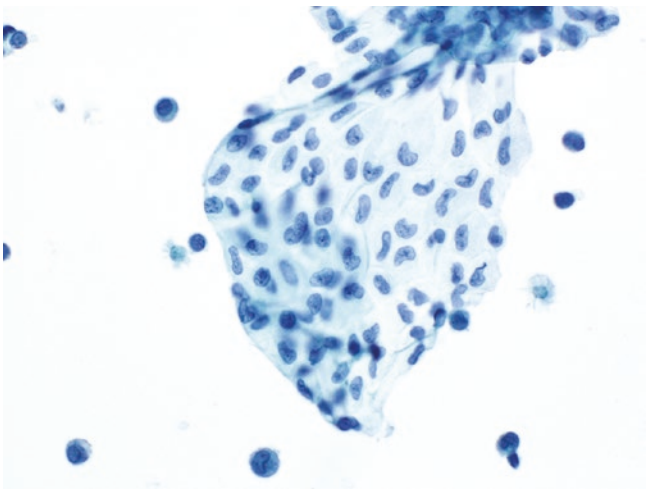

Fig. 13.3 Pelvic washing with a sheet of mesothelial cells demonstrating convoluted nuclear membranes. The background contains scattered lymphocytes and histiocytes. ThinPrep preparation, 40× magnification

and electrolytes (hydropic degeneration) in contrast to mucin vacuoles of adenocarcinoma (Fig. 13.4). Other cytoplasmic inclusions that can occur in mesothelial cells include lipid vacuoles (small and located near the nucleus) and glycogen (large and located in the periphery) [1, 2, 4].

Mesothelial cells exfoliate predominantly as single cells and small groups. Large groups are unusual, and when present, should raise the possibility of malignancy (i.e., adenocarcinoma, mesothelioma). Mosaic-like sheets are characteristic in peritoneal/pelvic washings obtained intraoperatively (Fig. 13.5a, b) and as contaminants in various fine needle aspiration procedures [6]. "Windows," or clear spaces between adjacent cells, are characteristic of mesothelial cells (Fig. 13.6). Cell molding (where one cell makes an impression on the adjacent cell) and hugging (where two cytoplasmic arms embrace an adjacent cell) can also be seen. In contrast to the well-demarcated cell boundaries of epithelial cells, mesothelial cells have a "lacy skirt" at the cell's edge due to their long, slender apical microvilli (Fig. 13.7). These trap mesenchymal mucin (rich in hyaluronic acid) to facilitate surface lubrication and also increase the surface area for fluid absorption [7]. Prominent microvilli can sometimes mimic cilia. Blebs, blunt rounded cytoplasmic projections, are nonspecific degenerative changes.

Collagen balls are hyaline bodies with smooth or lobulated outlines that are covered with mesothelium (Fig. 13.8)

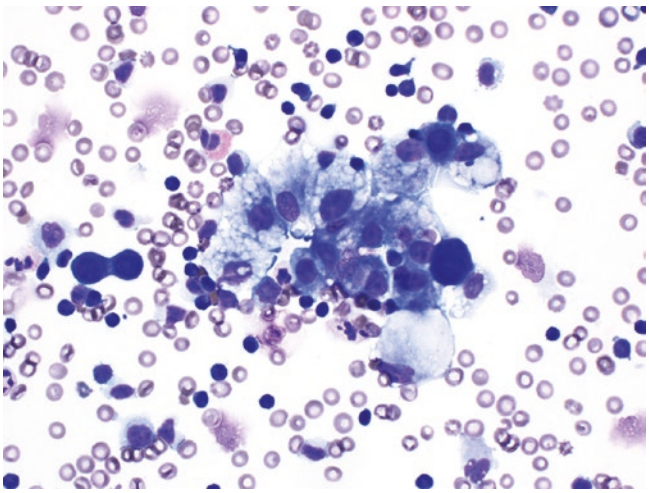

Fig. 13.4 Pleural fluid with variably sized mesothelial cells. Cytoplasmic vacuolization is seen making differentiation from histiocytes difficult. Some of the vacuoles displace the nucleus to the side imparting a signet ring cell morphology. Air-dried smear preparation, Diff-Quik, 40× magnification

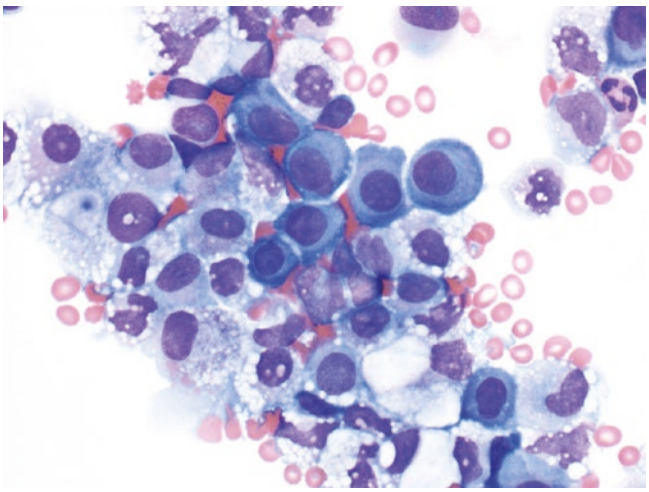

Fig. 13.6 Ascites fluid with characteristic "windows" between adjacent mesothelial cells admixed with vacuolated histiocytes. Cytospin preparation, Giemsa, 60× magnification

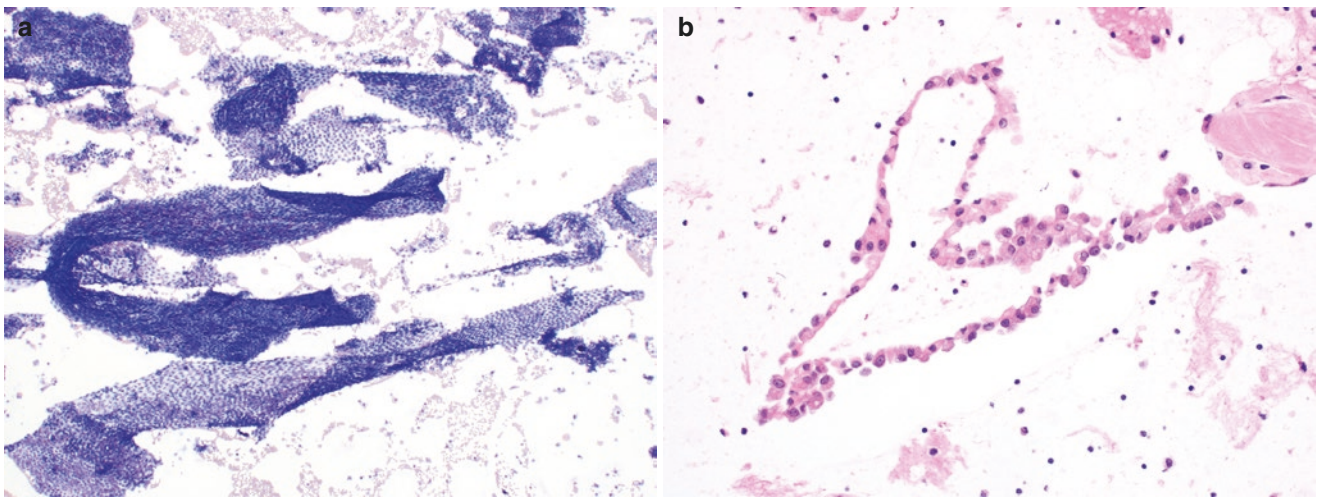

Fig. 13.5 Pelvic washing with (**a**) numerous convoluted mosaic-like sheets of mesothelial cells which (**b**) on cell block section is seen as an intact strip (so-called "string of pearls"). Air-dried smear preparation, Diff-Quik, 4× magnification (**a**), Cell block, hematoxylin & eosin, 20× magnification (**b**)

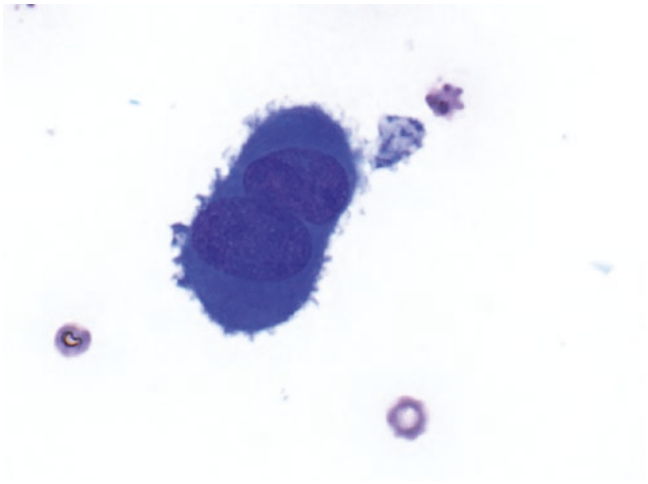

Fig. 13.7 Pleural fluid with binucleated mesothelial cell demonstrating a lacy skirt secondary to surface microvilli. Air-dried smear preparation, Diff-Quik, 60× magnification

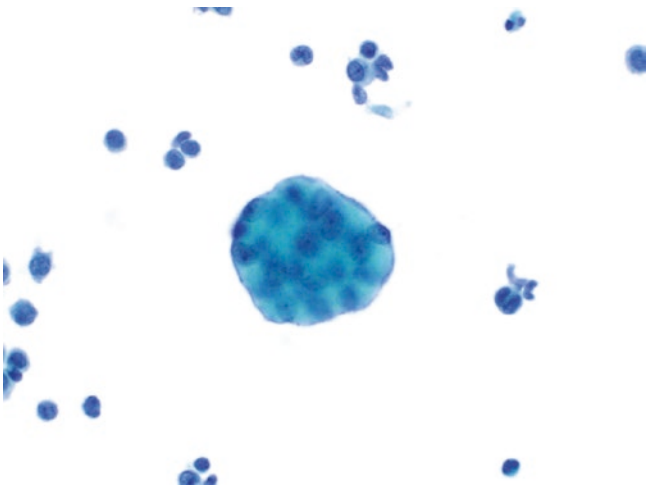

Fig. 13.8 Collagen ball in a pelvic washing showing the classic three-dimensional structure with a dense, aqua hyaline matrix core covered by bland mesothelial cells. ThinPrep preparation, 60× magnification

[8]. They are observed in peritoneal/pelvic washings performed during a surgical procedure and represent detached fragments of serosa and underlying stroma which then round up to produce balls. Their three-dimensional, spheroidal nature can sometimes be misinterpreted as adenocarcinoma to the inexperienced eye. Other potential pitfalls in washings include benign elements such as endosalpingiosis and endometriosis. Psammoma bodies, concentrically laminated calcified structures, are not always diagnostic of malignancy and are not uncommonly seen in washings in the setting of mesothelial hyperplasia [3, 6]. Ciliocytophthoria, which are detached ciliary tufts derived from ciliated tubal epithelium, may sometimes be encountered in peritoneal fluid samples.

The search for a foreign cell population in a fluid is oftentimes straightforward in the evaluation of a malignant effusion, especially in the setting of a known clinical history of malignancy. However, not infrequently, the significant overlap in cytomorphology of exuberant reactive changes in mesothelial cells or histiocytes and malignant cells (i.e., adenocarcinoma, mesothelioma) can result in misdiagnoses in a hypercellular fluid. In conjunction with clinical and radiologic correlation, ancillary immunohistochemistry (IHC) is crucial in the differentiation of reactive mesothelial cells from malignant epithelial cells, especially if the malignant cells are morphologically bland and/or low in quantity. Since no single marker can accurately differentiate between these two, it is important to utilize a panel of epithelial and mesothelial markers to enhance diagnostic accuracy. Epithelial membrane antigen (EMA) is helpful as it is typically negative in benign effusions, but shows membranous/cytoplasmic staining in carcinomas and mesotheliomas [9]. Ber-Ep4 and MOC-31 along with Claudin-4 are useful additions to IHC panels for effusion specimens as they are typically negative in benign mesothelial cells but are positive in metastatic carcinoma cells [10]. Mesothelial origin can be confirmed with markers such as calretinin, D2-40, WT-1 for mesothelial origin. Additional site-specific IHC should be performed in an attempt to determine the site of origin once it is determined that the effusion contains a metastatic carcinoma. IHC can also be helpful when the malignant cells comprise a minority of the cell population and can be missed on cytomorphology alone. This can occur with such entities as metastatic signet ring cell carcinoma and lobular carcinoma of the breast.

Inadvertent "pick-ups" from the needle while sampling effusions can sometimes result in miscellaneous cell types including lung, liver, muscle, cartilage, skin with appendages, fibroadipose tissue, or gastrointestinal cells. Benign squamous cells can occasionally be encountered in the setting of a ruptured dermoid cyst, fistula, or squamous metaplasia of the mesothelium (which is extremely rare).

Synovium

Body cavities and joint spaces share some similarities. Synovium is composed of two to three layers of synoviocytes which overlie loose connective tissue consisting of fat, collagen, and blood vessels. Synoviocytes are similar to mesothelial cells, growing as layers that surround fluid-filled spaces. They are relatively indistinct, appearing as flattened

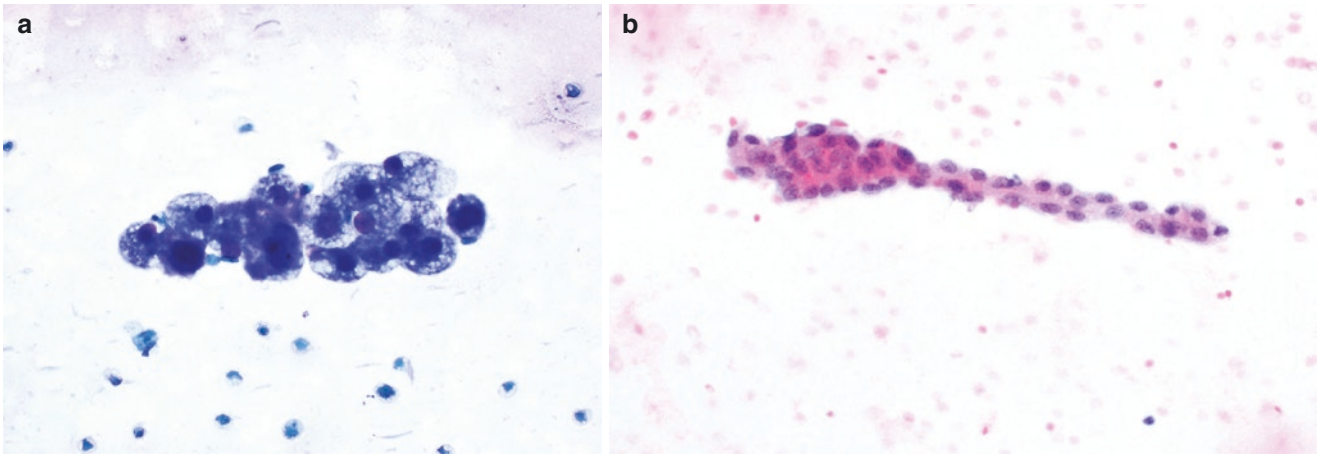

Fig. 13.9 Synovial cells with round to oval nuclei, fine chromatin, and abundant vacuolated cytoplasm. Air-dried smear preparation, Diff-Quik, 40× magnification (**a**), alcohol-fixed smear preparation, Papanicolaou stain, 20× (**b**) magnification

cells with oval dark-staining nuclei. When synovial cells react to injury, they achieve a more rounded epithelioid morphology. The supportive connective tissue beneath the surface synoviocytes varies in composition depending on the anatomic site. Large joints, which contain folds of synovium, typically have a well-developed vascular network and abundant mature adipose tissue. Deep to this is the dense supporting fibrous joint capsule. In tendon sheaths, the supportive connective tissue network is scant and the synovial cells closely approximate the fibrous layer of the tendon sheath or tendon [1, 11–13].

Synovial fluid is formed by ultrafiltration of the plasma and acts as a lubricant for joints while also providing nutrients to the articular cartilage. Synoviocytes add mesenchymal mucins, particularly hyaluronic acid. As in other body cavities, only a small amount of fluid is normally present in the joint space and an increased amount, or an effusion, indicates a pathologic process. Synovial fluid should be anticoagulated (heparin or liquid EDTA) for cytologic examination to prevent clotting and should be examined fresh, ideally within 24–48 h after collection [1, 13].

Normal synovial fluid is clear, straw-colored, and highly viscous. Synovial cells are normally present but sparse. Increased numbers can occur in noninflammatory arthropathies. In cytology specimens, synoviocytes morphologically resemble mesothelial cells. They have round to oval nuclei, fine chromatin, and abundant cytoplasm, which when vacuolated can make differentiating them from histiocytes (macrophages) difficult (Fig. 13.9a, b). Inflammatory cells are normally scant, consisting mostly of monocytes and histiocytes. A few mature lymphocytes and rare neutrophils are also normally present [1, 13]. On immunohistochemistry, synoviocytes focally stain for CD68 but are negative for cytokeratin and desmin (in contrast to mesothelial cells).

References

1. DeMay RM. Chapter 3. Fluids. In: DeMay RM, editor. The art & science of cytopathology. Exfoliative cytology. 2nd ed. Chicago: American Society for Clinical Pathology Press; 2012. p. 268–89, 338-341.
2. Naylor B. Chapter 19. Pleural, peritoneal, and pericardial effusions. In: Bibbo M, Wilbur D, editors. Comprehensive cytopathology. 3rd ed. Amsterdam: Elsevier; 2008. p. 515–35.
3. Samedi VG, Bocklage T. Chapter 10: body cavity fluids. In: Siddiqui M, editor. Pitfalls in diagnostic cytopathology with key differentiating cytologic features, essentials in cytopathology, vol. 27. Springer: Cham; 2016. p. 183–93.
4. Cibas ES. Chapter 4. Pleural pericardial, and peritoneal fluids. In: Cibas ES, Ducatman BS, editors. Cytology diagnostic principles and clinical correlates. 4th ed. Amsterdam: Elsevier; 2014. p. 127–31.
5. Rooper LM, Ali SZ, Olson MT. A minimum volume of 75 ml is needed to ensure adequacy in a pleural effusion: a retrospective analysis of 2540 cases. Cancer Cytopathol. 2014;122(9):657–65.
6. Cibas ES. Chapter 5. Peritoneal washings. In: Cibas ES, Ducatman BS, editors. Cytology diagnostic principles and clinical correlates. 4th ed. Amsterdam: Elsevier; 2014. p. 155–60.
7. Mutsaers SE. The mesothelial cell. Int J Biochem Cell Biol. 2004;36(1):9–16.
8. Wojcik EM, Naylor B. "Collagen balls" in peritoneal washings. Prevalence, morphology, origin and significance. Acta Cytol. 1992;36(4):466–70.
9. Hasteh F, Lin GY, Weidner N, Michael CW. The use of immunohistochemistry to distinguish reactive mesothelial cells from malignant mesothelioma in cytologic effusions. Cancer Cytopathol. 2010;118(2):90–6.
10. Vojtek M, Walsh MD, Papadimos DF, Shield PW. Claudin-4 immunohistochemistry is a useful pan-carcinoma marker for serous effusion specimens. Cytopathology. 2019;30:614–9.
11. O'Connell JX. Pathology of the synovium. Am J Clin Pathol. 2000;114:773–84.
12. Smith MD. The normal synovium. Open Rheumatol J. 2011;5:100–6.
13. Mundt LA, Shanahan K. Chapter 11. Synovial fluid. In: Mundt LA, editor. Graff's textbook of routine urinalysis and body fluids. 2nd ed. Philadelphia: Lippincott Williams & Wilkins; 2011. p. 253–60.

Central Nervous System, Peripheral Nervous System, and Eye

14

Yelena Fudym, Sandra Camelo-Piragua, and Liron Pantanowitz

Central Nervous System

The central nervous system (CNS) is composed of the cerebrum, cerebellum, brainstem, spinal cord, pineal gland, and pituitary gland; as well as its coverings (meninges) and linings (ventricles and choroid plexus). The parenchyma of the cerebrum, cerebellum, brainstem, and spinal cord are composed of gray and white matter with different architectural layering and organization depending on their function and phylogenetic evolution. Herein we describe the major cytologic components of the CNS from its coverings, and parenchyma to its linings.

Cytologic analysis of the CNS is often done by examining the cerebral spinal fluid (CSF) which can be sampled via lumbar puncture (LP) or collected from the cisterna magna at the base of the brain, an implanted Ommaya reservoir (brain pouch), or directly from the ventricles [1]. CSF should normally contain very few cells (less than 5 cells/mm^3), except in newborns where it may be more cellular. However, it is not uncommon to find blood contamination and occasional chronic inflammatory cells such as mature lymphocytes and larger monocytes [2]. Rarely, CSF may also contain benign choroid plexus cells, ependymal cells, meningothelial cells, small brain tissue fragments, isolated neurons, and germinal matrix. When present, these normal elements are usually very scant. If a misguided LP procedure accidentally samples the vertebral body or intervertebral disc, such a CSF sample may be contaminated by bone marrow cells and scant chondrocytes [3].

Y. Fudym
Department of Pathology and Laboratory Medicine, Akron Children's Hospital, Akron, OH, USA
e-mail: yelenaf@med.umich.edu

S. Camelo-Piragua
Department of Pathology and Clinical Laboratories, Michigan Medicine, Ann Arbor, MI, USA
e-mail: sandraca@med.umich.edu

L. Pantanowitz (✉)
Department of Pathology, Michigan Medicine, Ann Arbor, MI, USA
e-mail: lironp@med.umich.edu

Meninges

The meninges are composed of the pachymeninges (dura mater) and the leptomeninges. The dura is a thick, fibrous membrane adhered to the calvarium. Cytology preparations of the dura show stromal collagen and fibroblasts. Its layers split to form the sinuses through which venous blood is drained from the brain. The leptomeninges are composed of arachnoid and pia mater and lie over the surface of the brain (Fig. 14.1), carrying vital vasculature in the subarachnoid space that provides a supportive suspension network for the delicate brain parenchyma and allows for transit of cerebrospinal fluid. The subarachnoid space is devoid of cells in its

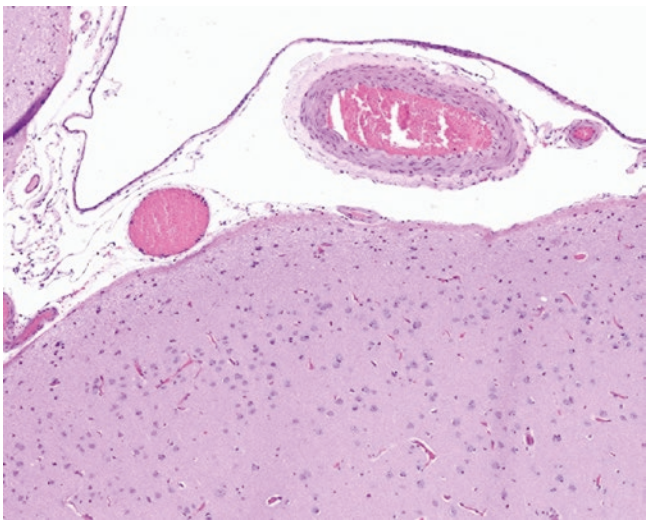

Fig. 14.1 Leptomeninges overlying the cerebral cortex. A thin layer of arachnoid cells is seen at the top of the image. In the subarachnoid space, blood vessels and cobweb-like arachnoid cells connect with the pia mater, which is firmly adhered to the cortex. Histology, hematoxylin & eosin, 5× magnification

M. Lew et al. (eds.), *Normal Cytology*, https://doi.org/10.1007/978-3-031-20336-7_14

normal state. The arachnoid meningothelial cells have syncytial-like cytoplasm due to their tight intracellular junctions. Therefore, cellular borders are not evident on histologic or cytologic preparations. Meningothelial (meningeal) cells have abundant eosinophilic cytoplasm and occasional intranuclear inclusions and pseudoinclusions. They often form whorls and can be associated with psammomatous calcifications (Fig. 14.2). These features are preserved in meningothelial hyperplasia and meningioma [4, 5]. Meningothelial cells can occasionally be seen in CSF and frequently in intraoperative consultation (IOC) smear preparations. When smeared or squashed, the cytoplasm of meningothelial cells will characteristically billow out, resembling flowing curtains or a flag waving in the breeze, and their cell membrane edges will curl (Fig. 14.3) [6]. The Papanicolaou (Pap) stain allows for greater visualization of the cell's open nuclear chromatin (Fig. 14.4). There may be occasional longitudinal nuclear grooves present. On Diff-Quik stain, the nuclei appear larger due to slide preparation (compared to other stains) and the pseudoinclusions can sometimes be more evident (Fig. 14.5). The abundant syncytial cytoplasm is well appreciated in all stains. One pitfall to be aware of is the presence of leptomeningeal melanocytes, commonly seen on the ventral aspect of the upper spinal cord and brainstem in patients with dark skin complexion (Fig. 14.6). Primary melanocytic proliferations can rarely arise from these cells. Finally, meningothelial nests can also be seen in the ventricular system, particularly in the core connective tissue of the choroid plexus. Meningothelial cells are positive for progesterone receptor, somatostatin receptor 2 (SSTR2), and weakly positive for epithelial membrane antigen (EMA). Cytokeratins, S-100, and glial fibrillary associated protein (GFAP) should be negative.

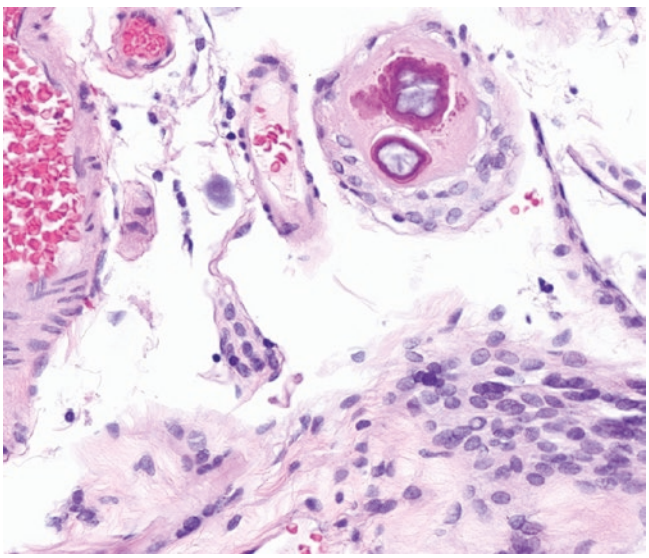

Fig. 14.2 Meningothelial cells have a syncytial pattern of growth with no defined cellular borders. There are occasional nuclear inclusions and whorling created by cells wrapping around each other. They can sometimes be associated with psammomatous calcifications. Histology, hematoxylin & eosin, 25× magnification

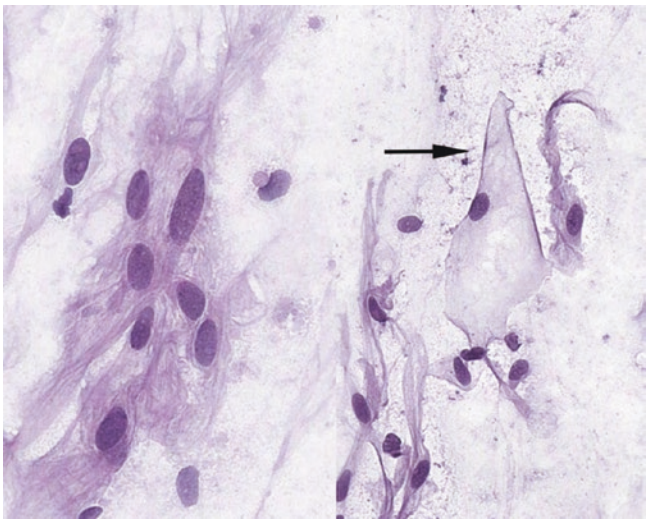

Fig. 14.3 Meningothelial cells have abundant cytoplasm. Some of these cells (arrow) show typical billowing with curled cytoplasmic edges. The nuclei are oval with smooth nuclear borders and fine chromatin. Nucleoli are not evident. Alcohol-fixed smear preparation, hematoxylin & eosin, 40× magnification

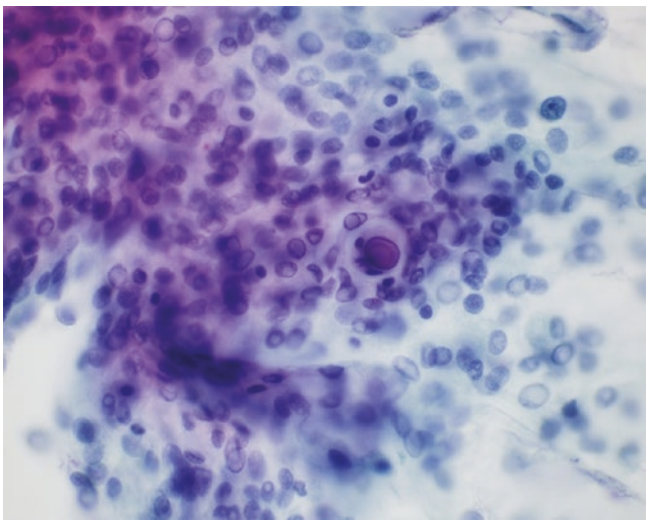

Fig. 14.4 Smear showing numerous meningothelial cells. They have oval to round nuclei with open chromatin and intranuclear inclusions. Note the concentric psammoma body in the middle of the image. Alcohol-fixed smear preparation, Papanicolaou stain, 40× magnification

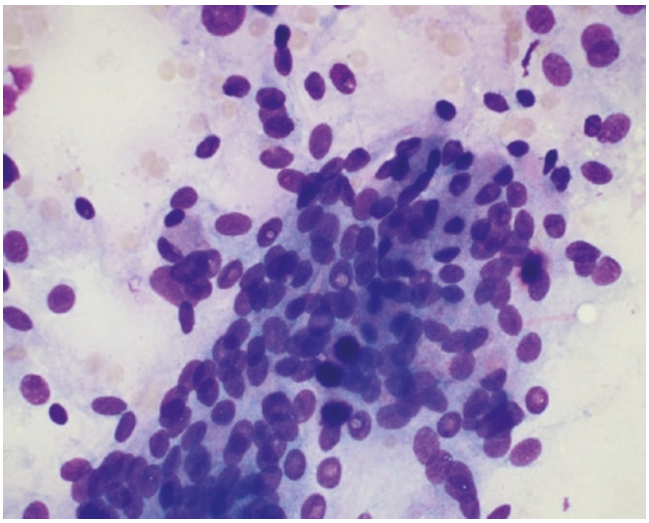

Fig. 14.5 Syncytial pattern of meningeal cells showing a faintly whorled architecture. The larger nuclei are attributed to air drying artifact. The nuclei are otherwise characterized by smooth contours, finely granular chromatin, and intranuclear inclusions. Air-dried smear preparation, Diff-Quik, 60× magnification

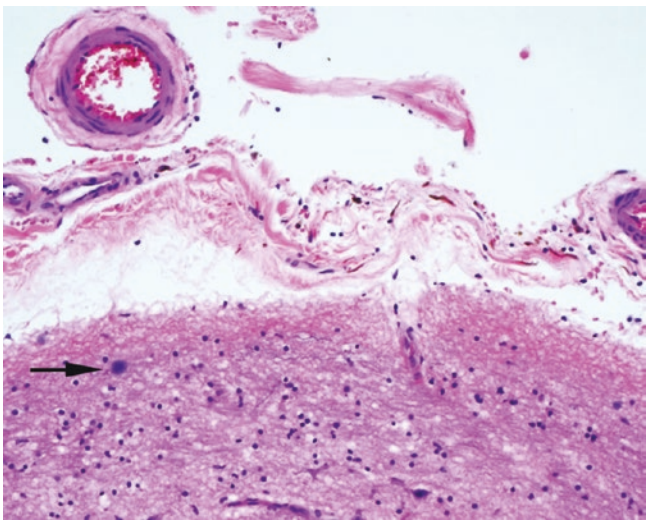

Fig. 14.6 Melanin is present inside arachnoid meningothelial cells, completely filling their cytoplasm and conferring an elongated dendritic shape to the cells. Note the corpora amylacea in the subpial region as a spherical, basophilic refractile body (arrow). Histology, hematoxylin & eosin, 40× magnification

Brain Parenchyma: Neurons, Astrocytes, and Oligodendrocytes

The brain can be divided into three main portions: the cerebrum, cerebellum, and brainstem. Brain parenchyma is composed of two primary layers: gray matter and white matter. Gray matter is richly inhabited by neurons which are variably organized in layers depending on the region such as in the neocortex, limbic system, and cerebellum. Neurons can also be aggregated into groups called nuclei (e.g., deep gray nuclei of the cerebrum, cerebellar nuclei, or brainstem nuclei). In addition to neurons, the gray matter also has glial cells (nonneuronal cells that provide a supportive framework for neurons and are important in metabolic homeostasis of the microenvironment), most of which are astrocytes. White matter is a bundle of packed myelinated axons, mostly composed of glial cells such as oligodendrocytes and astrocytes. In the cerebrum and cerebellum, the gray matter is the outer most layer, whereas in the spinal cord the gray matter is centrally placed, surrounded by descending and ascending white matter tracts. The germinal matrix refers to a region of the developing brain that gives rise to neuronal and glial cells of the gray matter (Fig. 14.7). When detected in CSF of neonates or premature infants, germinal matrix cells can mimic blasts or small blue cell tumors (e.g., medulloblastoma, lymphoma) [7]. These immature cells have scant cytoplasm with a high nuclear:cytoplasmic ratio, nuclei with indentations, and fine, evenly dispersed chromatin and small nucleoli. They tend to form groups, can show nuclear molding, and, because they are often seen in the context of hemorrhage, tend to be associated with hemosiderin-laden macrophages. The germinal matrix disappears by the end of the first year of life.

Neurons have a wide array of morphologic appearances ranging from massive motor neurons (e.g., Betz cells in the motor cortex or motor neurons of the spinal cord) or large Purkinje cell neurons of the cerebellum to small granular neurons of the hippocampus and cerebellum (Figs. 14.8, 14.9, 14.10, and 14.11). The large pyramidal cells are triangular in shape, have large round nuclei with prominent

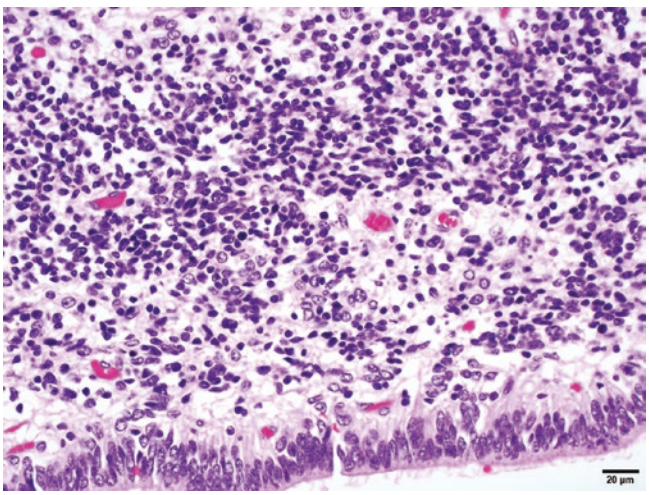

Fig. 14.7 Subependymal densely cellular germinal matrix from a 28-week fetus composed of immature neural precursor cells. Ependymal cells which are tall, columnar, ciliated cells (bottom of image) line the ventricles. The fragile, thin-walled vessels are the source of hemorrhage in some preterm neonates. Histology, hematoxylin & eosin, 20× magnification

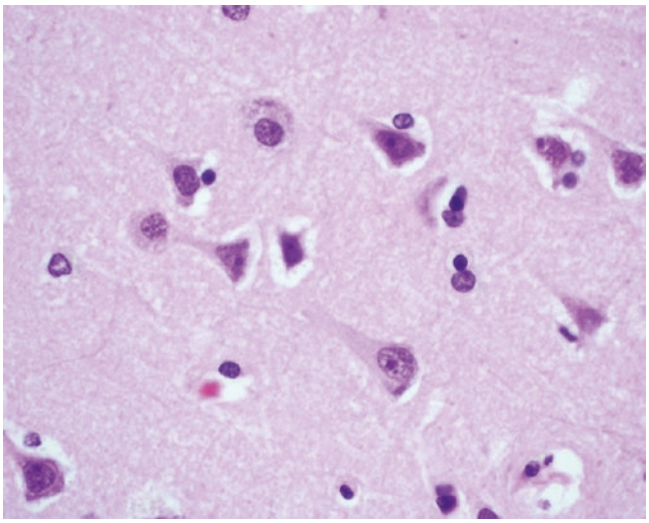

Fig. 14.8 Neocortex showing large pyramidal neurons with ample eosinophilic cytoplasm, large round nuclei, and prominent nucleoli. Note the fluffy, glial fibrillary background. Histology, hematoxylin & eosin, 40× magnification

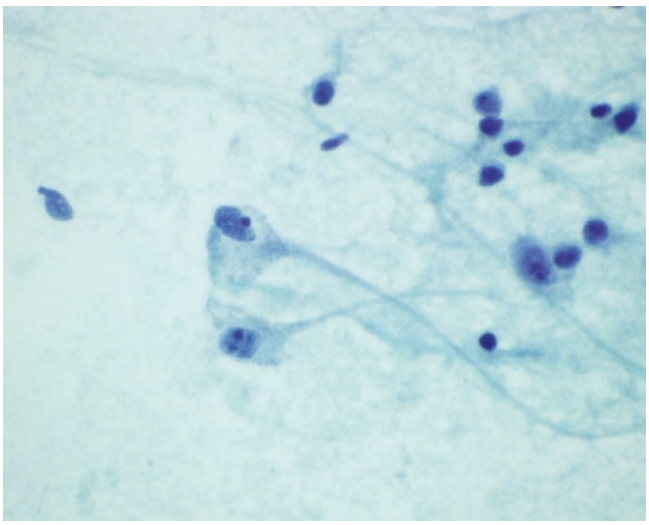

Fig. 14.9 Neocortex smear showing two entangled large pyramidal neurons with moderate cytoplasm, oval nuclei, distinct nucleoli, and long axons. The nuclei of the neurons are larger than those of the scattered surrounding glial cells. Alcohol-fixed smear preparation, Papanicolaou stain, 60× magnification

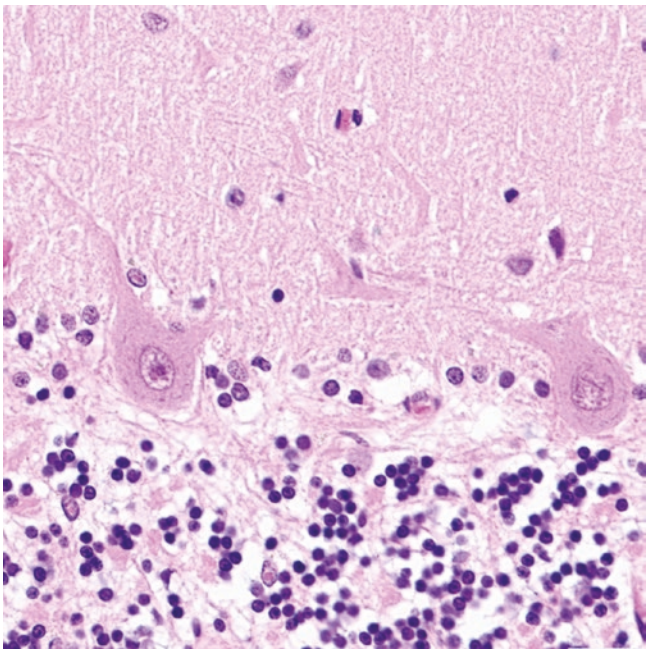

Fig. 14.10 Cerebellar cortex showing large Purkinje cells with prominent dendrites. Located in the lower aspect of the image are small internal granular neurons that contain minimal cytoplasm and small, round nuclei with salt-and-pepper chromatin. Histology, hematoxylin & eosin, 40× magnification

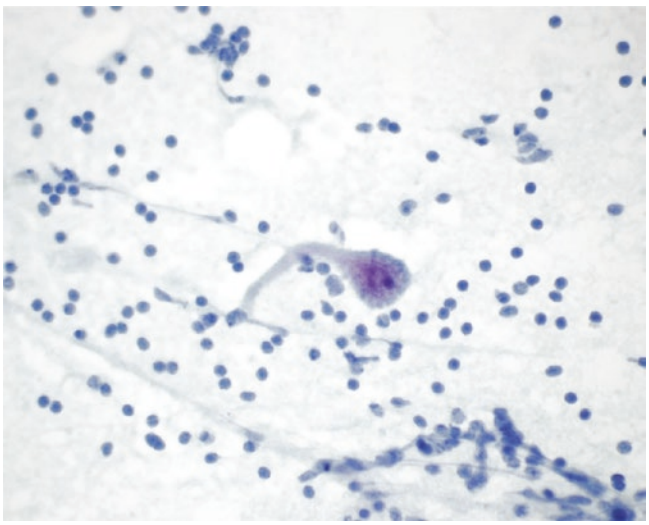

Fig. 14.11 Smear of the cerebellar cortex showing a large Purkinje cell with a large tapering axon. The nucleus is large, filling most of the neuronal body, with a distinct nucleolus. In the background, there are numerous small round internal granular neurons stripped of cytoplasm and comprised largely of bare nuclei with homogenous chromatin. Alcohol-fixed smear preparation, Papanicolaou stain, 60× magnification

nucleoli, and abundant cytoplasm and Nissl substance at the periphery. Nissl substance is a basophilic neuronal pigment composed of RNA and proteins in the rough endoplasmic reticulum; its quantity varies depending on the type of neuron. In some instances, the axon and dendrites can be identified. The smaller granular neurons have high nuclear:cytoplasmic ratios, round nuclei with speckled, salt-and-pepper chromatin and discrete nucleoli. The main pitfalls, particularly in the cerebellum given the abundance of granular neurons, are to mistake them for lymphocytes or a small round blue cell tumor [6]. However, mature granular neurons lack anaplasia and are mitotically inactive. Their salt-and-pepper chromatin pattern differs from the more condensed chromatin distribution seen in lymphocytes.

Some specialized neurons, often of catecholaminergic origin, harbor neuromelanin, most commonly seen in the substantia nigra of the midbrain or locus ceruleus in the ventral pons (Figs. 14.12 and 14.13). CSF samples may sometimes contain fragments of brain tissue (Fig. 14.14). This usually occurs when CSF is aspirated during neurosurgery directly from a ventricle and the needle traverses brain parenchyma, or when a ventricular shunt is in place, which may disturb and shed small fragments of brain components.

Astrocytes are diffusely present throughout the CNS and have several functions. They form the tight junction of the blood-brain barrier, contribute to neuronal health through monitoring of ion and water homeostasis, and are responsible for scar formation. Astrocytes have oval nuclei with smooth nuclear contours and open chromatin. In their quiescent state, cytoplasmic processes are difficult to appreciate; however, when they become reactive due to injury or a nearby lesion, their multiple large slender processes become evident forming the star shape for which they are named. Occasionally, reactive astrocytes can also become binucleated and this should not be interpreted as a sign of malignancy [5].

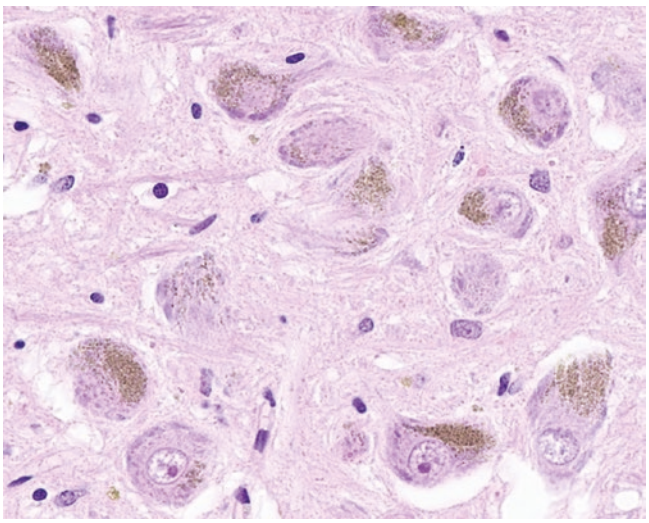

Fig. 14.12 Midbrain showing large neurons of the substantia nigra with prominent intracytoplasmic neuromelanin granules. Histology, hematoxylin & eosin, 40× magnification

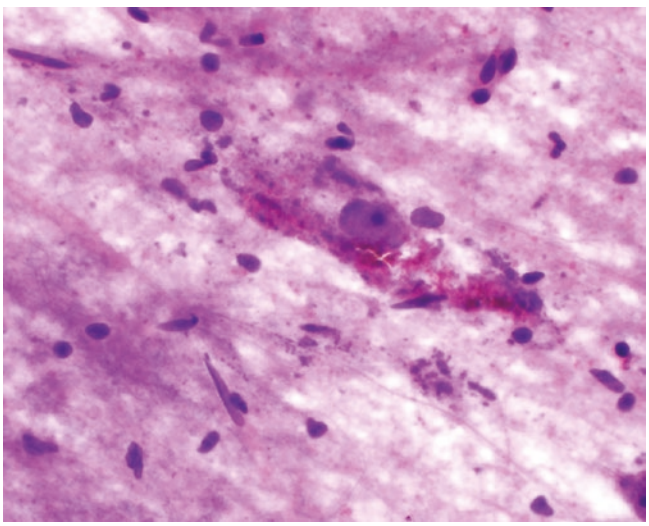

Fig. 14.13 Smear preparation of the midbrain showing a large nigral neuron with intracytoplasmic granular neuromelanin. Alcohol-fixed smear preparation, hematoxylin & eosin, 60× magnification

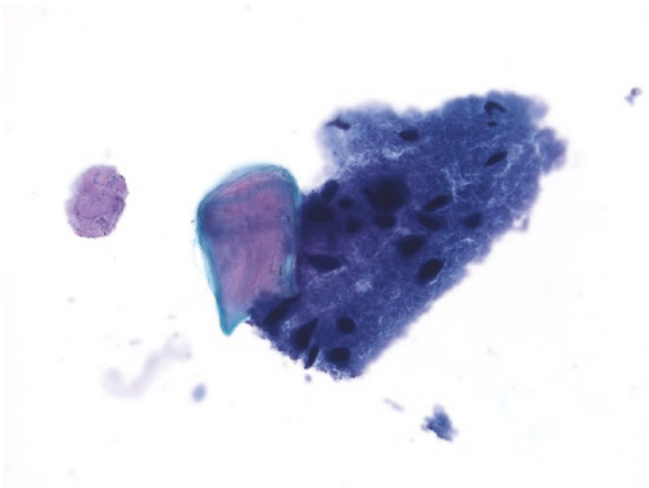

Fig. 14.14 Fragment of normal brain tissue detected in CSF. The fibrillary tissue contains benign glial cell nuclei. ThinPrep preparation, 40× magnification

Corpora amylacea (15–30 μm in diameter) are polyglucosan aggregates produced by astrocytes, commonly seen in the subpial and subependymal regions (Fig. 14.6). They are basophilic, spherical bodies with concentric rings and have a glassy, refractile quality. They are PAS-positive and should not be confused with fungal organisms. They are often seen in association with increased age, neurodegeneration, or chronic injury.

Oligodendrocytes are responsible for the myelination of the CNS. They are seen in highest density in white matter. One oligodendrocyte myelinates multiple segments of several axons. Oligodendrocytes have small, rounded nuclei with dense chromatin. In formalin-fixed paraffin-embedded tissue, the cytoplasm is clear and gives the appearance of a "fried egg." This halo of perinuclear clearing is an artifact of formalin fixation and is absent from cytologic preparations or unfixed histologic sections taken for IOC. Oligodendrocytes have short and fewer glial processes compared to astrocytes; however, their monotonous evenly rounded nuclei are very helpful to recognize in cytologic preparations [1].

Microglia are specialized macrophages of the brain that come from the bone marrow and are not glial in origin despite their name. They are generally inconspicuous in normal, healthy brains and may appear as infrequent comma-shaped nuclei with minimal cytoplasm.

The role of cytologic preparations in IOC is to identify the type of cells involved in a disease process. The normal smear has a pattern of sand on a beach being shaped by waves into a tidal-sine pattern on low power (Figs. 14.15, 14.16, 14.17, 14.18, and 14.19). The intraparenchymal structures: neurons, axons and glial cells which would typically be seen in IOC cytologic preparations should rarely, if ever, be seen in CSF specimens, except for in patients who have intraventricular catheters, which can irritate the brain parenchyma and lead to shedding of neuroglial tissue [2]. In cell block material, glial cells can be highlighted with GFAP, Olig 2, and S-100. Neurons are positive for NeuN and synaptophysin. Axons are best visualized with neurofilament. It is important to also note that glial cells will cross-react with cytokeratin AE1/AE3; therefore, when excluding an epithelial lesion in the brain, CAM5.2 is a better alternative.

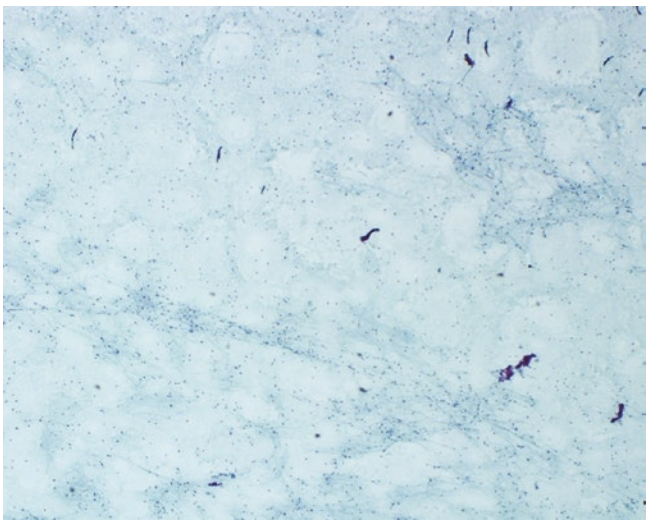

Fig. 14.15 Smear of normal brain parenchyma at low power has a characteristic "tidal waves over a sandy beach" or "checkerboard" pattern. Alcohol-fixed smear preparation, Papanicolaou stain, 4× magnification

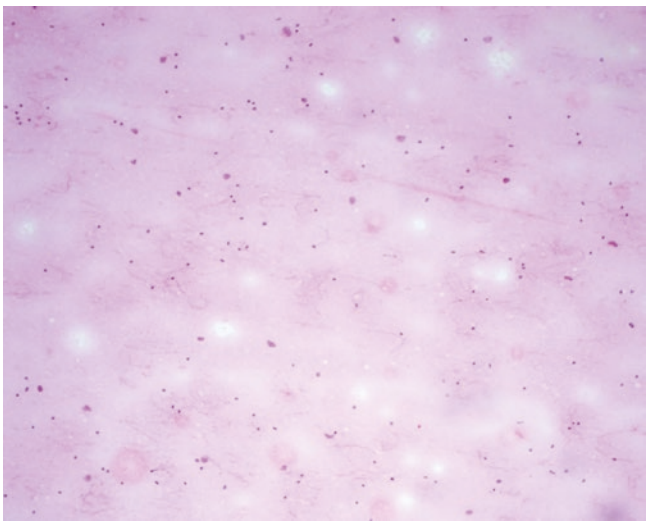

Fig. 14.16 Smear of normal brain parenchyma. The sample is hypocellular and composed mostly of abundant fluffy eosinophilic neuropil ("cotton-candy" appearance) with scant dispersed cells. Alcohol-fixed smear preparation, hematoxylin & eosin, 10× magnification

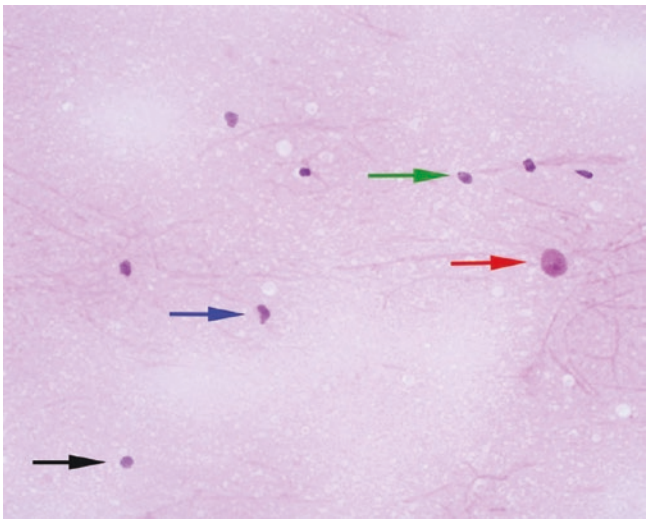

Fig. 14.17 Smear of normal cortex. Oligodendrocyte with a round nucleus (black arrow). Comma-shaped microglial cell with mildly irregular nucleus (blue arrow). Quiescent astrocyte without prominent cytoplasm or processes. The nucleus is oval with smooth nuclear contours and open chromatin (green arrow). Neuron with a large round nucleus and prominent nucleolus (red arrow). Alcohol-fixed smear preparation, hematoxylin & eosin, 40× magnification

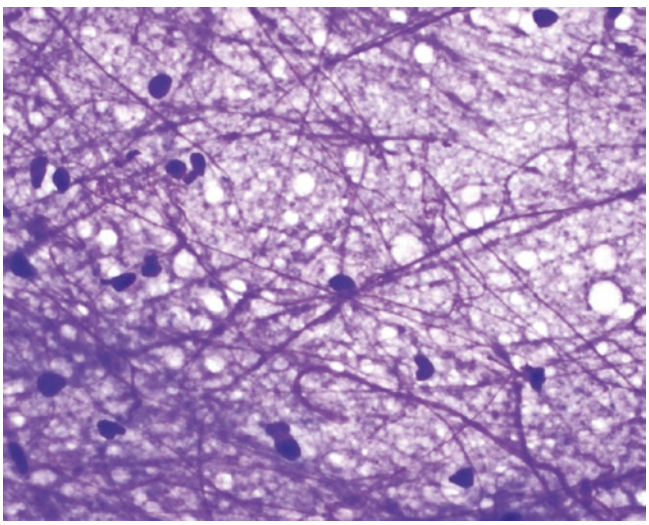

Fig. 14.18 Smear of brain parenchyma with reactive astrocytes containing multiple long, slender glial processes that form a tangled meshwork of strands. The white vacuoles represent myelin. Air-dried smear preparation, Diff-Quik, 60× magnification

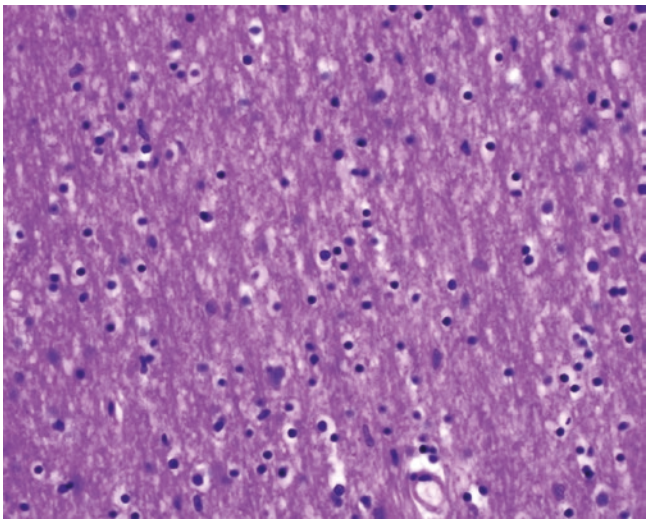

Fig. 14.19 White matter tract showing parallel axons (pink lines) surrounded by monotonous round oligodendrocytes with clear cytoplasmic halos ("fried eggs"), only seen in formalin-fixed histological sections. Histology, hematoxylin & eosin, 40× magnification

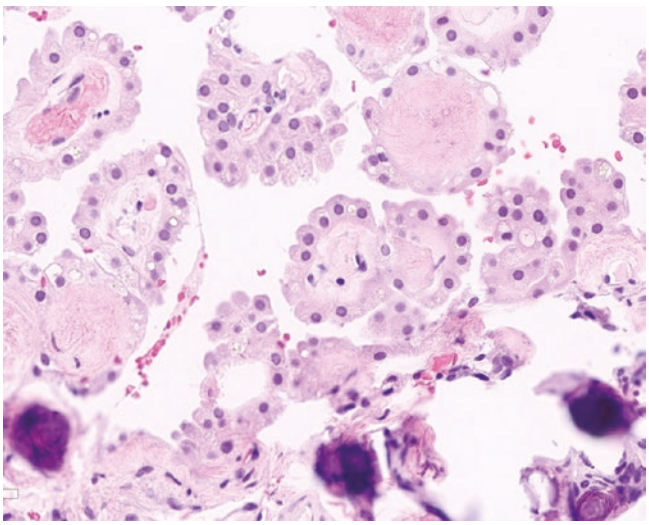

Fig. 14.20 Choroid plexus showing fibrovascular papillary structures, lined by a single layer of low cuboidal epithelium with round nuclei and intracytoplasmic vacuoles. Note the psammomatous calcifications at the bottom of the image. Some of the cells (top left corner) have lipofuscin content. Histology, hematoxylin & eosin, 20× magnification

Ventricular Lining (Choroid Plexus and Ependymal Cells)

CSF is produced by the choroid plexus and circulated by ependymal cells. The choroid plexus is located bilaterally in the body, atrium, and temporal horns of the lateral ventricles and in the roof and lateral angles of the fourth ventricle and can extend outwards through the foramina of Luschka. The ependymal cells form a single cell layer lining the ventricles of the brain and spinal central canal. Together, they play an important role in ion and fluid homeostasis. The choroid plexus also forms part of the blood-CSF barrier, which helps separate blood from the CSF.

The choroid plexus is a highly vascular structure with long papillary fronds lined by low cuboidal epithelium (modified ependymal cells) with abundant clear, bubbly cytoplasm, arranged in a cobblestone pattern (Fig. 14.20). These cells have cilia, as well as surface microvilli and ridges to help with CSF absorption, which forms a prominent brush border. Focal, small meningothelial (arachnoid) nests are present within the fibrovascular core that, with age, calcify forming psammoma bodies. In infants and young children, there is abundant intracytoplasmic glycogen content, whereas in older individuals, an increase of lipofuscin content can be seen instead. Cytologically, the cells of the choroid plexus have small round, eccentric nuclei with dense chromatin and abundant cytoplasm that is occasionally frothy or foamy. They form groups of polygonal cells (Figs. 14.21 and 14.22) [8]. Cells of low-grade choroid plexus neoplasms have nearly identical cytology to those of normal choroid plexus cells. However, increased mitotic activity may be suggestive of a neoplastic process, as it should be exceedingly low in normal tissue (<2/10 HPF). Choroid plexus carcinoma exhibits a higher degree of cytologic atypia which should not be seen in normal choroid plexus [5, 7, 9].

Ependymal cells form a low columnar epithelial lining of the ventricles and central canal of the spinal cord. They can be identified by abundant clear to eosinophilic cytoplasm, round to oval nuclei, open chromatin, and variably distinct nucleoli (Figs. 14.23 and 14.24). They are often ciliated, which helps with movement of the CSF, and can occasionally show binucleation. When the ventricular lining is injured, ependymal cells become denuded and exfoliate into CSF, where they tend to aggregate in groups (Figs. 14.25 and 14.26) potentially mimicking the appearance of metastatic carcinoma. Identification of cilia is very helpful in differentiating these cells from metastatic carcinoma. The abundant cytoplasm can also help distinguish these cells from lymphoma, which tends to have scant amounts of cytoplasm. However, this differentiation may be more difficult in preparations that may create frequent naked nuclei (e.g., cytospins). Additionally, leukemic blasts pose a unique challenge in CSF as they can appear similar to ependymal cells. Pale nuclei or cytoplasmic granules can help delineate hematolymphoid blasts.

It is often difficult to distinguish between ependymal and choroid plexus cells in CSF; therefore, when encountered in clinical practice, these cells are usually referred to as ependymal/choroidal cells [8]. In cell block preparations, ependymal cells can be shown by immunohistochemistry to be positive for GFAP, have focal perinuclear dot positivity with EMA, and are negative for cytokeratins. On the other hand,

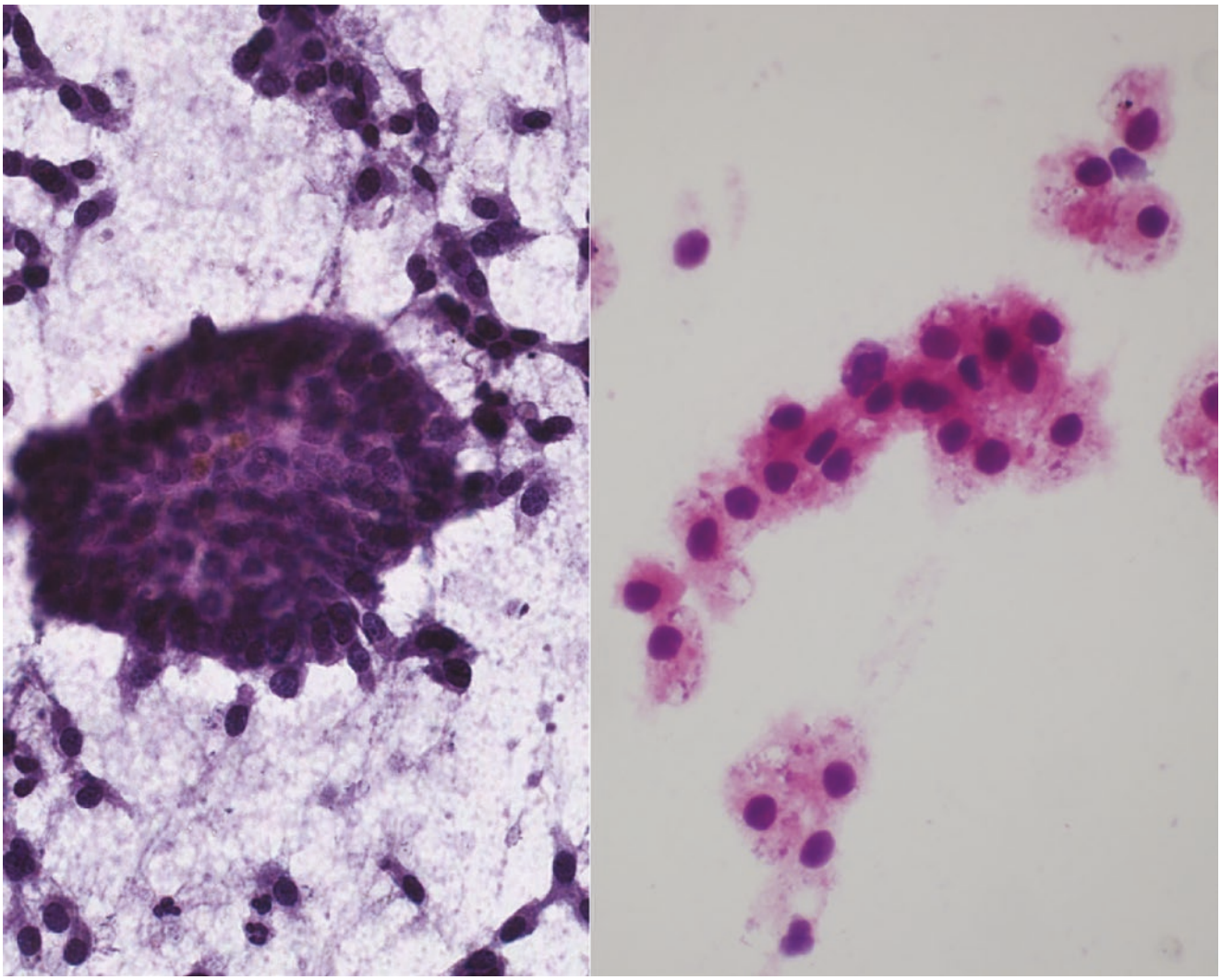

Fig. 14.21 Smear preparations of choroid plexus. (Left) Cluster of cohesive epithelial cells forming a papillary structure. The cells have regular round nuclei and focal intracytoplasmic lipofuscin pigment. (Right) Flat group of choroid plexus cells with fluffy, granular, and vacuolated cytoplasm. The clear vacuoles contain glycogen. Alcohol-fixed smear preparation, hematoxylin & eosin, 40× magnification

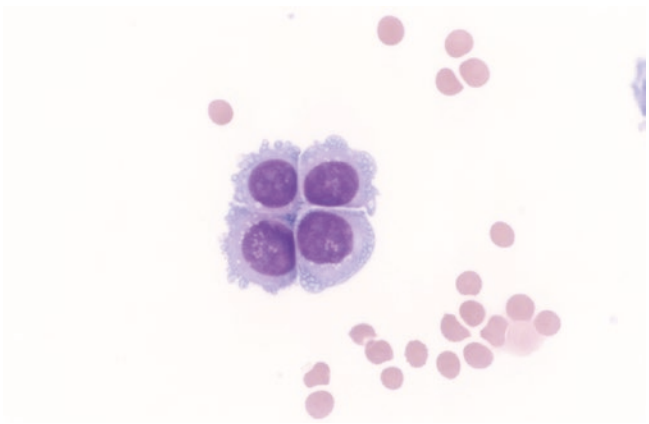

Fig. 14.22 Cluster of choroidal cells exfoliated into CSF. These cuboidal cells have round nuclei with uniform, fine chromatin and moderate amounts of vacuolated cytoplasm. Villi, which are frond-like processes, help increase their surface area. Cytospin preparation, Diff-Quik, 40× magnification

choroid plexus epithelium shows focal expression with GFAP, but does express several cytokeratins, S-100, vimentin, transthyretin (pre-albumin), and the potassium channel Kir7.1

Pituitary Gland

The pituitary gland is a bilobed structure situated beneath the frontal lobe, under the optic chiasm and tucked into the sella turcica.

The anterior pituitary originates embryologically from the oral ectoderm. It is also called the adenohypophysis and secretes six hormones, each from a specialized cell type: growth hormone, luteinizing hormone, follicle-stimulating hormone, prolactin, adrenocorticotropic hormone, and thyroid-stimulating hormone. The cells are admixed and

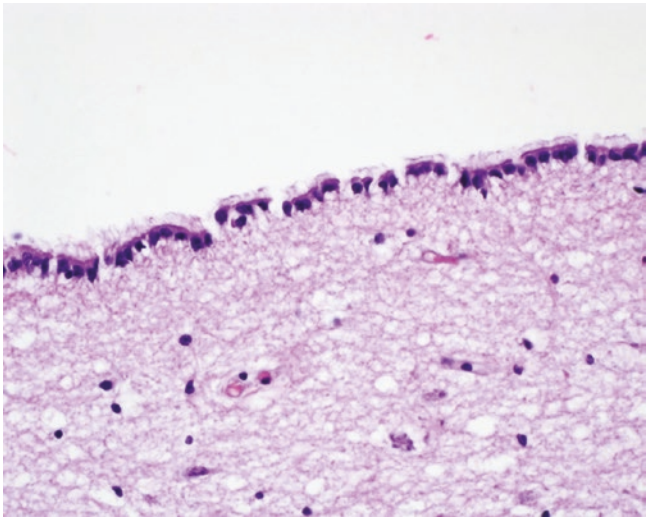

Fig. 14.23 Histologic section of the third ventricle, showing a single layer of low cuboidal epithelium of ependymal cells with basaloid nuclei. Note the surface cilia. Histology, hematoxylin & eosin, 40× magnification

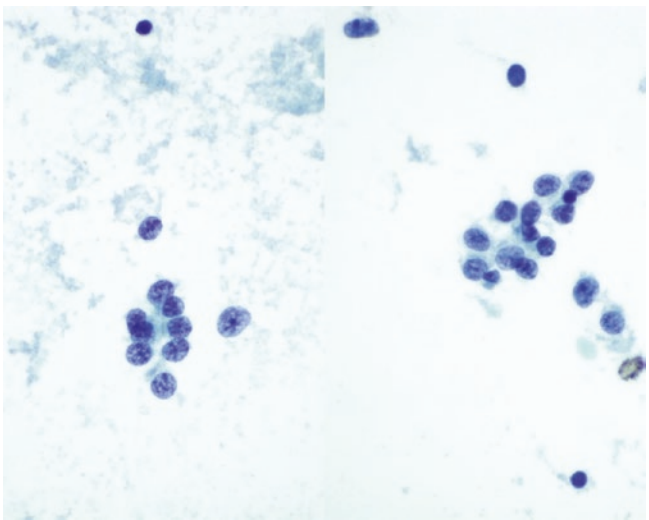

Fig. 14.24 Smear preparation of the periventricular region. Clusters of ependymal cells are shown with round nuclei and delicate cytoplasm that is easily disrupted during slide preparation. Alcohol-fixed smear preparation, Papanicolaou stain, 40× magnification

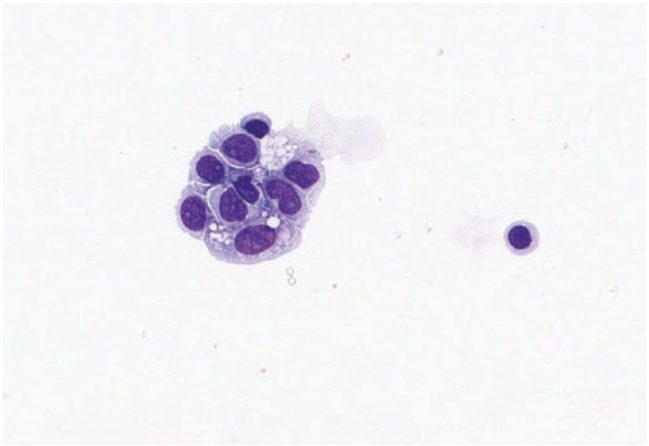

Fig. 14.25 Cluster of ependymal cells in a CSF sample. The cells have round to oval nuclei with uniform chromatin, moderate cytoplasm with focal clear vacuoles, and knobby cytoplasmic borders. A mature lymphocyte is shown to the right for size comparison. Cytospin preparation, Diff-Quik, 40× magnification

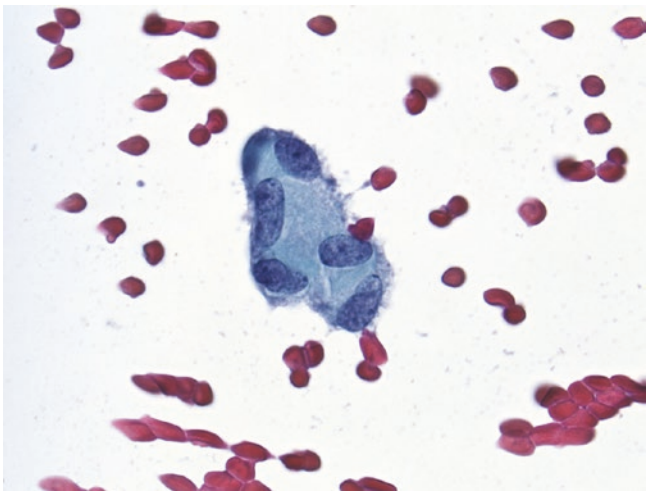

Fig. 14.26 Ependymal cells in CSF. The fuzzy outer edge on these cells is due to cilia, most easily identified in children. These cilia help distinguish ependymal cells from choroid plexus cells. Cytospin preparation, Papanicolaou stain, 60× magnification

arranged in acinar structures tightly held together by a reticular network (Fig. 14.27). A touch or smear preparation can be invaluable during intraoperative consultations to determine if a sellar mass represents a pituitary adenoma. The extensive reticular network in a normal pituitary gland prevents many of the cells from being released and smeared on the slide, resulting in a relatively hypocellular smear preparation with neuroendocrine cells. In contrast, in an adenoma, the loss of acinar architecture and the clonal proliferation of cells allow for a cellular smear [5, 7, 10]. Anterior pituitary cells have rounded, often eccentric nuclei, salt-and-pepper chromatin, and abundant cytoplasm (Fig. 14.28). They may have variably sized nuclei. The cytoplasm on hematoxylin and eosin staining can be acidophilic, basophilic, or chromophobe. Frequently, granules are seen within the cytoplasm owing to the secretory role of the cells.

The posterior lobe of the pituitary gland, or the neurohypophysis, is derived from the forebrain and is composed mostly of neural tissue (Fig. 14.29) [11]. It stores and secretes vasopressin and oxytocin. It is very unlikely that the posterior pituitary would be sampled for cytologic preparations such as an FNA, but this lobe may be sampled during IOC

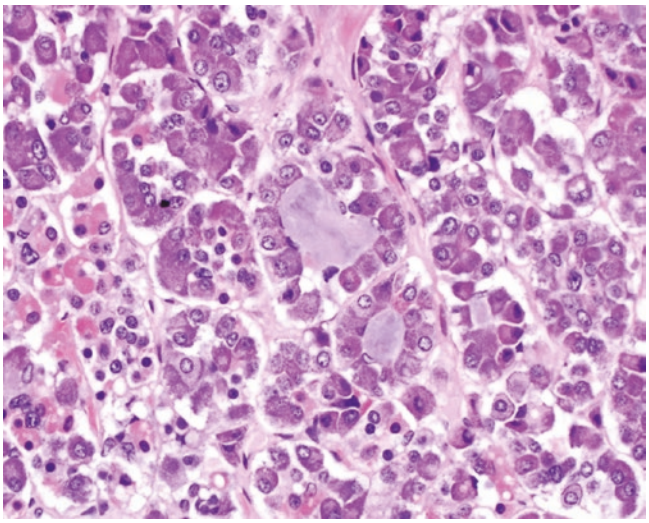

Fig. 14.27 Anterior pituitary demonstrating acinar architecture. Each acinus is populated by a mix of acidophilic, basophilic, and chromophobe cells. Some acini show intraluminal secretions. The nuclei are round with salt-and-pepper chromatin and prominent small nucleoli. Their cytoplasm is granular. Histology, hematoxylin & eosin, 40× magnification

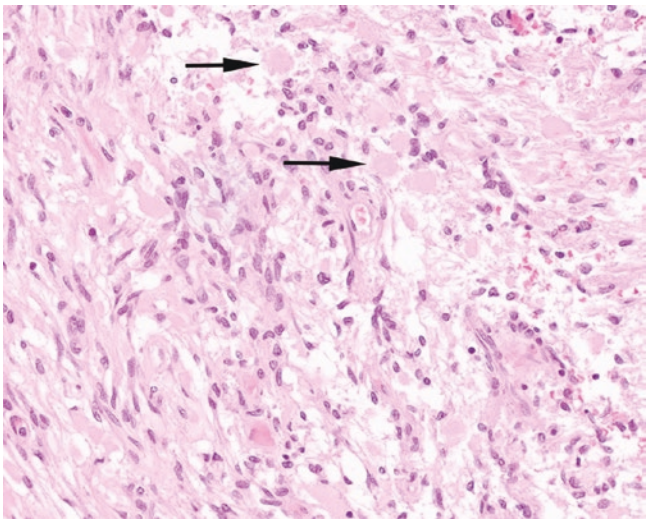

Fig. 14.29 Pituicytes of the posterior pituitary are shown arranged in a fascicular pattern of growth with oval to spindled nuclei present in a background similar to brain parenchyma. Of note, the posterior pituitary has characteristic pink axonal swellings (arrows), named Herring bodies, which represent intra-axonal transport of oxytocin and vasopressin granules. Histology, hematoxylin & eosin, 40× magnification

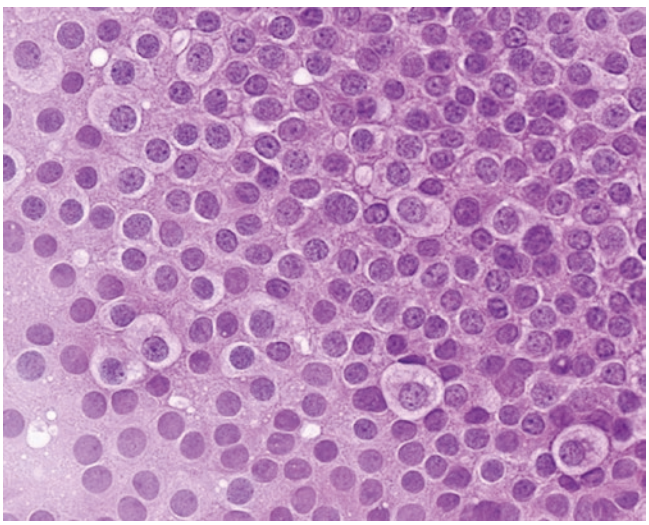

Fig. 14.28 Anterior pituitary showing discohesive cells with ample granular cytoplasm. Like any neuroendocrine organ, there can be some nuclear size variation. The nuclei all show salt-and-pepper chromatin and have small prominent nucleoli. Alcohol-fixed smear preparation, hematoxylin & eosin, 60× magnification

for evaluation of a pituitary lesion. A cytologic preparation of the posterior pituitary looks much like any neural portion of the brain [7, 10].

One may encounter fragments of pituitary on needle biopsies of sinonasal or suprasellar tumors using endonasal approaches. The cells of the adenohypophysis are positive for synaptophysin, specific pituitary hormones and transcription factors (SF1, PIT1, TPIT) important in lineage differentiation, and are variably positive for cytokeratins, particularly Cam5.2. The cells of the neurohypophysis are diffusely positive for S-100 and TTF-1.

Pineal Gland

The pineal gland is a neurosecretory gland situated in the posterior midline of the brain, attached by a stalk from the posterior third ventricle. The ventral part of the stalk is lined by ependymal cells. The rest of the gland is surrounded by meningothelial cells. This gland secretes melatonin and contributes to circadian rhythm regulation.

Histologically, the pineal gland is composed of neuroendocrine cells called pinealocytes, arranged in glandular structures embedded within a loose fibrillary glial network (Figs. 14.30 and 14.31) [12, 13]. Pinealocytes are small and round with minimal cytoplasm and exhibit the typical salt-and-pepper chromatin of a neuroendocrine cell. The presence of corpora arenacea, which calcifies in a lobular manner after puberty, can often be seen when the gland is sampled. Focal melanin pigment can also be seen in some of the pinealocytes. Cytological preparations will most often be made during an IOC setting and will often show small, round neuronal like cells admixed with reactive astrocytes and, occa-

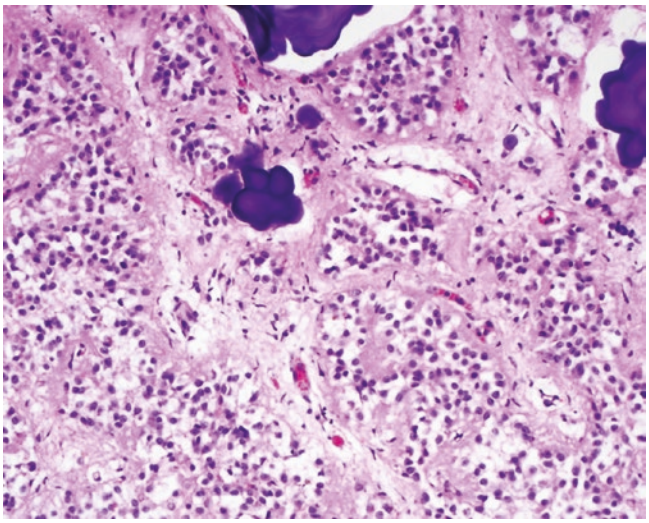

Fig. 14.30 Pineal gland showing small, round to oval neuroendocrine cells, vaguely forming glandular structures, embedded in a fibrillary glial eosinophilic background. Mineralization (top) is common with increasing age. Histology, hematoxylin & eosin, 40× magnification

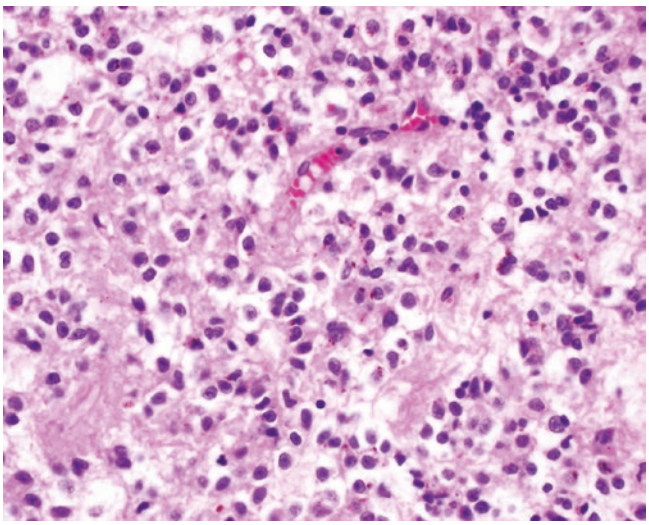

Fig. 14.31 Pinealocytes have small round to oval nuclei with speckled chromatin. Some of these cells have melanin pigment. Histology, hematoxylin & eosin, 40× magnification

sionally, ependymal lining cells (Fig. 14.32). In older patients, smears may be less cellular and contain more microcalcifications. In pineocytomas, rosettes (spoke-wheel arrangement of cells surrounding a central space) may be formed. Pinealocytes are positive for synaptophysin and neurofilament. Rare admixed glial cells will be positive for GFAP and S100, though pinealocytes themselves are negative [12].

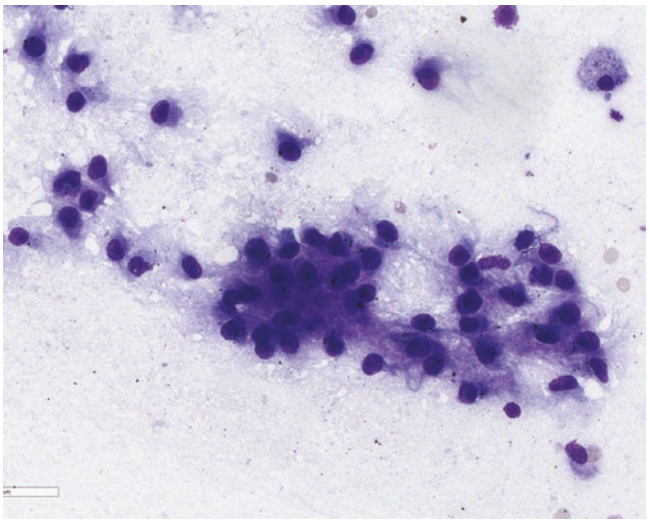

Fig. 14.32 Pinealocytes with round nuclei and abundant cytoplasm. Air-dried smear preparation, Diff-Quik, 60× magnification

Peripheral Nervous System

Ganglia

A ganglion is a collection of neural bodies located outside the CNS. Sensory ganglia are located at the dorsal roots of the spinal nerves and some cranial nerve roots (e.g., trigeminal ganglion). Dorsal root ganglia (DRG) lie in the intervertebral foramina bilaterally along the length of the spine. Motor (autonomic) ganglia are located in a row along the vertebral column (paravertebral and prevertebral ganglia) or are associated with visceral organs (terminal ganglia). Terminal ganglia located below the head and neck are often found within the wall of an organ and are referred to as a plexus (e.g., enteric plexus). The celiac (solar) plexus surrounds the roots of the celiac trunk, superior mesenteric and renal arteries and is made up of ganglia that supply nerves to abdominal viscera. Ganglia may occasionally be inadvertently sampled; for example, when a paraspinal mass is targeted, or when the celiac plexus is mistaken for a peri-pancreatic lymph node during an endoscopic ultrasound-guided FNA.

Histologically, ganglia are nodules of densely packed neurons with large cell bodies (perikaryon), abundant optically dense and coarsely granular cytoplasm, large nuclei, and prominent nucleoli surrounded by small ovoid satellite cells supported in minimal fibrous tissue (Fig. 14.33) [14, 15]. Similar to neurons anywhere else in the CNS, Nissl substance or lipofuscin can be seen as pigmented material in the cytoplasm. Cytologic preparations from ganglia are gener-

ally hypocellular due to its fibrous network but can reveal large neuron bodies and scattered satellite cells (Figs. 14.34 and 14.35) [14, 15]. Also, like neurons elsewhere in the nervous system, these are positive for S100 [15].

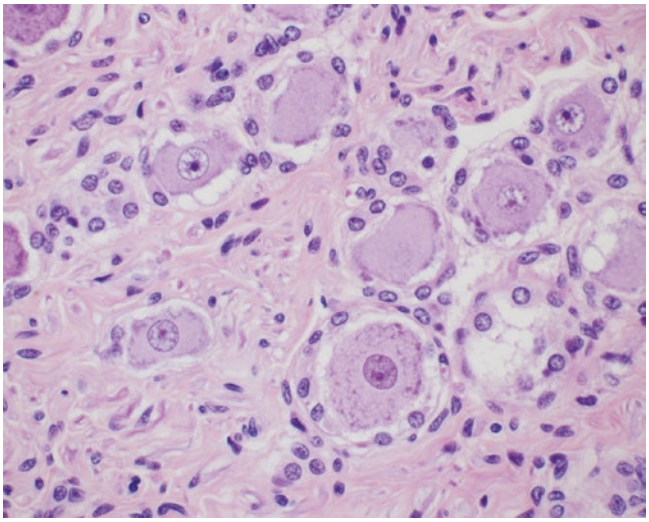

Fig. 14.33 Dorsal root ganglion showing large neuronal bodies with round nuclei, prominent nucleoli, and vacuolated cytoplasm with peripheral Nissl substance. The ganglion cells are surrounded by small ovoid satellite cells, and interspersed between are myelinated axons. Histology, hematoxylin & eosin, 60× magnification

Peripheral Nerves

Normal peripheral nerves are rarely sampled in cytologic preparations but can be encountered during IOC of spine or limb surgeries or neoplasms of the peripheral nerve/soft tissue. FNA of a peripheral nerve is painful. The peripheral

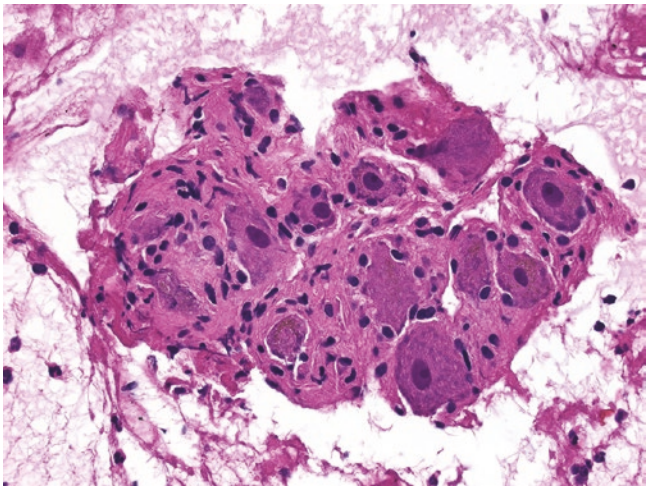

Fig. 14.35 FNA of the mesenteric plexus showing large neuronal cell bodies embedded within motor nerve fibers. Cell block, hematoxylin & eosin, 20× magnification

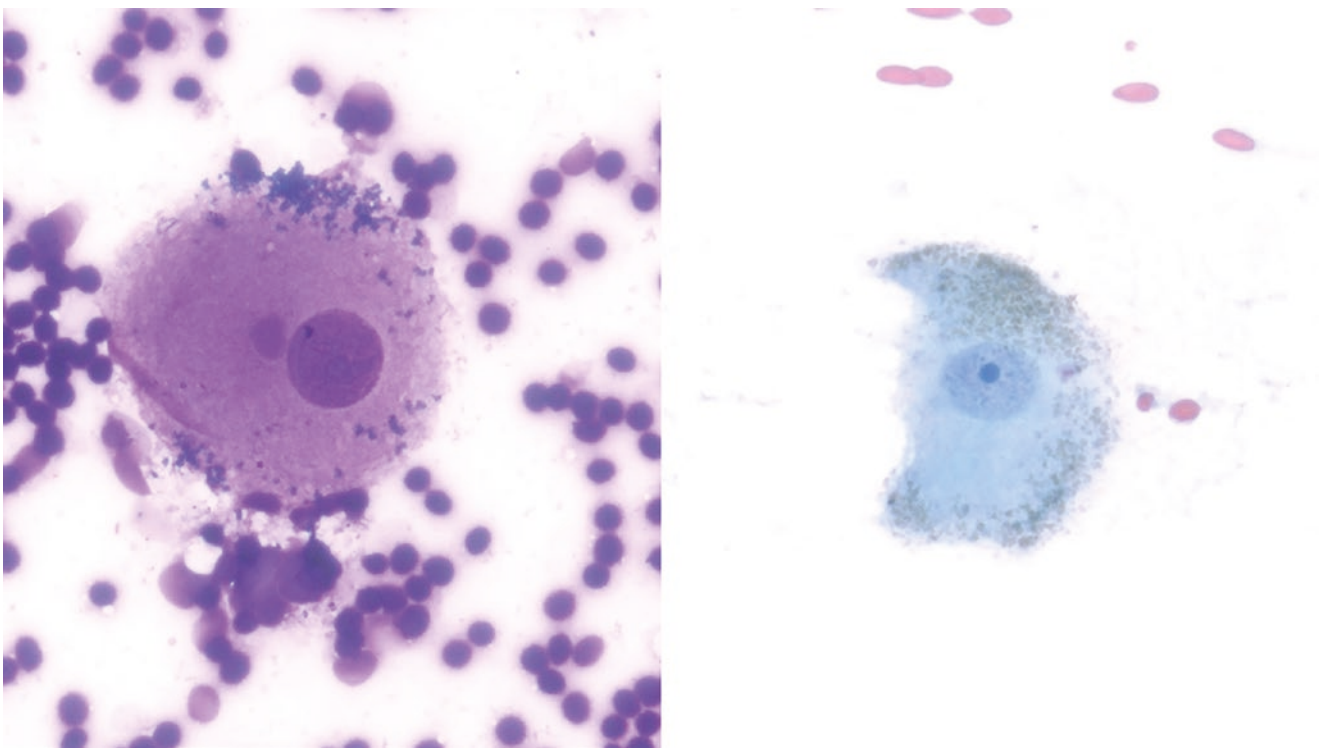

Fig. 14.34 FNA showing single nerve cell body with granular Nissl substance in the peripheral cytoplasm, large round nucleus and prominent nucleolus. Air-dried smear preparation, Diff-Quik, 60× magnification (left) (also highlights the smaller round to ovoid satellite cells). Alcohol-fixed smear preparation, Papanicolaou stain, 60× magnification (right)

nerve is covered by perineurium, which is a modified extension of the meninges. The perineurium stains for EMA and GLUT1. The nerve fascicles carry myelinated and unmyelinated afferent or efferent fibers from or to the spinal cord, positive for neurofilament. Schwann cells stain with S-100 and SOX-10. Tumors of the peripheral nerve include neurofibromas, schwannomas, and malignant peripheral nerve sheath tumors (MPNST). Neurofibroma infiltrates the nerve fascicles and has a mix of perineurial and endoneurial elements. On the other hand, schwannoma is a tumor with clonal proliferation of Schwann cells only, which pushes the axons aside and is well-circumscribed with a defined capsule. MPNST may show nuclear atypia, mitotic activity, hypercellularity, and may or may not have necrosis.

Smear preparations of both cranial and peripheral nerves are generally hypocellular as the dense fibrous tissue associated with these nerves tends not to aspirate easily or shed many cells (Fig. 14.36). Cytology preparations usually demonstrate cohesive fragments of collagenous-type stroma within which several spindled to wavy nuclei of Schwann cells are embedded [16]. These cells have indistinct cytoplasm, wavy dark nuclei with a tapered or hooked end, uniform chromatin, and inconspicuous nucleoli. Occasionally, scant bare single Schwann cell nuclei may be seen in the background. Myelin has a fibrillary texture and appears light green with a Pap stain or blue-purple with a Diff-Quik stain. Axon tangles may fail to stain and hence will appear translucent. Mast cells can be seen in these samples, but other inflammatory cells should be absent. Fat may be present in aspirates from surrounding fibroadipose tissue. However, lipid droplets (micelles) may sometimes also be encountered, which are believed to be derived from disrupted myelin.

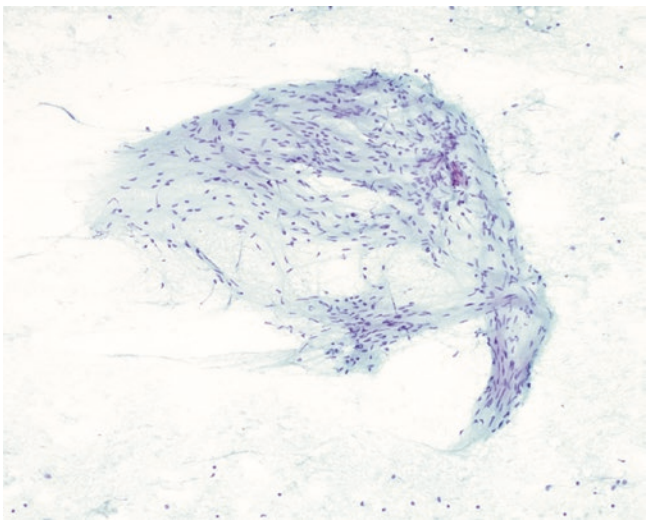

Fig. 14.36 Fragment of normal peripheral nerve comprised of cohesive Schwann cells with uniform spindle nuclei embedded within extracellular matrix associated with myelin and axons. Alcohol-fixed smear preparation, Papanicolaou stain, 10× magnification

Eye

The human eyeball (globe) is protected within the bony orbit. The eyelids contain striated muscle (orbicularis oculi) and eccrine glands, apocrine glands (of Moll), and sebaceous (Meibomian) glands, as well as hair follicles. The lacrimal gland is located in the superior-temporal aspect of the orbit. The orbital cavity may also contain fat, nerves, and ganglia. Six extraocular muscles are attached to the white outer sclera of the eye to aid in eye movement.

The eye has three main layers: outer transparent cornea (anterior) and opaque white sclera (posterior), middle uvea (uveal tract), and inner retina. The uvea includes the iris, ciliary body, and choroid. The anterior eye surface (bulbar lining) and inner eyelids (palpebral lining) are covered by the conjunctiva. The white sclera, which extends from the cornea posteriorly to the optic nerve, is rigid and helps protect the eye. The anterior clear, dome-shaped cornea helps transmit and focus light entering the eye. Between the cornea and iris is the anterior chamber filled with clear aqueous fluid, which is maintained at constant pressure to help keep the eye inflated. If intraocular pressure is too high (e.g., glaucoma) vision can be impaired. Behind this anterior chamber lies the colored part of the eye called the iris (diaphragm) and its central dark opening, the pupil. Muscles in the iris regulate the amount of light entering the eye. The space between the iris and lens is called the posterior chamber, which is also filled with aqueous fluid. The transparent biconvex lens is situated directly behind the pupil and, by changing shape, helps focus light onto the retina. The ciliary body is a muscle-containing structure behind the iris that holds the lens in place and helps it focus. The epithelial lining of the ciliary body is responsible for aqueous fluid production. The vitreous cavity, located between the lens and back of the eye, contains clear gelatinous material called the vitreous fluid. The retina lining the back of the eye is made up of photoreceptors (rods and cones) that convert light into electrical signals to be transmitted via the optic nerve to the brain. Between the retina (inner layer) and sclera (outer layer) is the pigmented vascular choroid layer.

Cytologists may encounter several types of cytology samples from the eye [17]. Surface epithelial samples (scrapes, direct smears, swabs, or brushings) of the conjunctiva or cornea may be collected to detect infections (e.g., viral conjunctivitis, acanthamoeba keratitis in contact lens wearers, trachoma caused by the bacteria *Chlamydia trachomatis*) or screen for premalignant lesions (e.g., squamous dysplasia) and malignancy (e.g., squamous cell carcinoma). These samples may be directly applied to glass slides or submitted in a

liquid-based fixative. Conjunctival impression cytology (CIC) is minimally invasive, convenient, and cost-effective to perform but may rarely cause subconjunctival cyst formation [18]. Fine needle aspiration (FNA) may be performed to procure intraocular fluid from the anterior or posterior chambers, or target a specific mass within or around the eyeball [19]. Traumatic complications of FNA (e.g., bleeding, infection, lens damage) are infrequent and typically minor in severity [20]. Vitrectomy surgery may also be performed to remove vitreous fluid (washing), for diagnostic and therapeutic purposes. FNA specimens may yield a diagnosis of intraocular inflammation/infection (e.g., uveitis), hemorrhage from retinal vessels, or malignancy (e.g., lymphoma, melanoma, retinoblastoma) [21, 22]. Uveal melanoma is the most common primary intraocular malignancy in adults. In order to render a correct cytologic diagnosis it is important to appreciate the normal cytomorphology of the eye. Any component of the eye may be incidentally sampled.

The bulbar conjunctiva is nonkeratinized stratified squamous epithelium, whereas the tarsal conjunctiva is a thin mucous membrane composed of 2–5 layers of cuboidal to columnar epithelium that rests on a basal lamina (Fig. 14.37). Cytology specimens of the conjunctiva usually show large cohesive clusters (Fig. 14.38) and occasionally singly dispersed epithelial cells (Fig. 14.39) with abundant cytoplasm, oval nuclei with finely granular chromatin, and variably visible nucleoli [23]. Individual cell boundaries are typically easy to appreciate within these sheets. Goblet (mucus) cells contribute to tear production and are characterized by clear, mucin-filled apical vacuoles and eccentrically compressed nuclei (Figs. 14.39 and 14.40). Goblet cells are most numerous in the lower eyelid and near the medial canthus of the eye (caruncle and semilunar folds). Individuals with dry eyes may have diminished goblet cells. The presence of keratin-

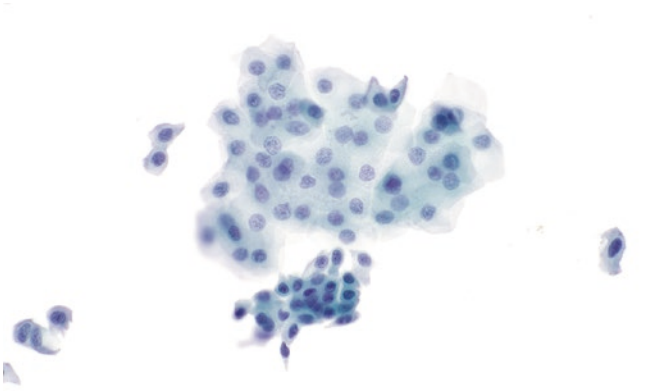

Fig. 14.38 Conjunctival scrape preparation showing cohesive clusters of bland squamous epithelium. The lower cell group contains mostly basal cells. ThinPrep preparation, 40× magnification

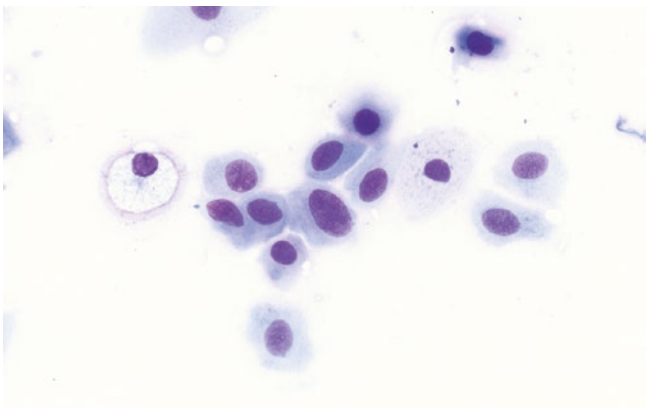

Fig. 14.39 Conjunctival scrape preparation showing individual polygonal squamous cells with mild nuclear variation. This scraping also contains a few goblet cells with clear intracytoplasmic mucin. Air-dried smear preparation, Diff-Quik, 60× magnification

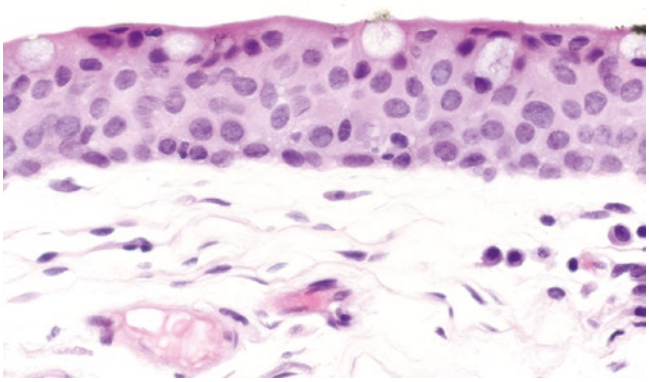

Fig. 14.37 Conjunctiva showing nonkeratinized stratified squamous epithelium with interspersed goblet cells filled with clear mucin. The underlying stroma normally contains scant mononuclear chronic inflammatory cells. Histology, hematoxylin & eosin, 60× magnification

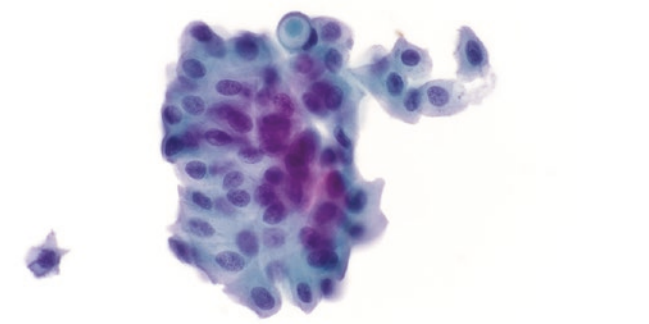

Fig. 14.40 Conjunctival scrape showing a cohesive cluster of bland squamous epithelium. Note the single distended goblet cell (top of the image) with a mucin vacuole and eccentrically compressed nucleus. ThinPrep preparation, 60× magnification

ized squamous epithelium in a conjunctival cytology sample is abnormal, unless the caruncle or eyelid was accidentally sampled [24]. The conjunctiva may also contain basal melanocytes, accessory lacrimal glands, Langerhans dendritic cells, and rarely intraepithelial lymphocytes, plasma cells, and mast cells. Small lymphoid follicles may sometimes be encountered.

The cornea consists of the following layers (from outside to inside) (Fig. 14.41): outer epithelium (stratified, nonkeratinizing squamous cells about 5–7 layers thick), basement membrane, Bowman layer (8–14 microns), stroma (dense connective tissue with scant fibroblast-like keratocytes and collagen layers), Descemet membrane (10–12 microns), and "endothelium" (single flat layer of S100-positive cells). The cornea's epithelial layer merges with the conjunctiva at the limbus. The cornea is typically avascular and lacks inflammatory cells. Contact lens irritation may cause abrasions, epithelial thinning, and edema. Smear preparations obtained from normal cornea show cohesive sheets of nonkeratinizing squamous epithelium (Fig. 14.42). These cells are of intermediate size and contain round to oval nuclei with uniform chromatin. It is abnormal to find keratinized cells in corneal smears [24]. In normal cornea, only the basal cells have mitoses.

Melanin pigment is frequently seen in the eye (Fig. 14.43). Melanin pigment can be seen as fine intracytoplasmic granules or contained within melanosomes, which are intracellular organelles unique to pigmented cells of the skin and eye that may be oval, elliptical (cigar-shaped), or spindle in shape. On Diff-Quik stains, melanin appears deep blue-green to black, while on Pap stains, it appears brown to black, and with hematoxylin & eosin, it is brown. Application of Fontana-Masson special stain highlights melanin in black. In contrast, hemosiderin is more coarsely granular (Fig. 14.44). Pigmentation with melanin may be seen in the iris (epithe-

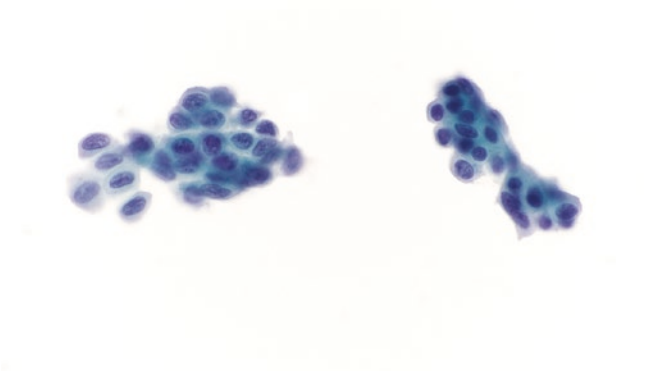

Fig. 14.42 Corneal scrape showing cohesive clusters of nonkeratinizing squamous epithelium. These polygonal cells have round nuclei, occasional nuclear membrane grooves, and evenly distributed chromatin. ThinPrep preparation, 60× magnification

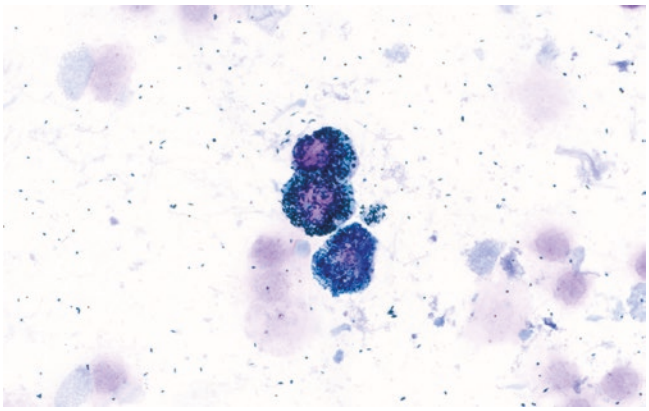

Fig. 14.43 FNA showing several cells from the retinal pigment epithelium (RPE) with elliptical melanosomes. Melanosomes are also loosely scattered in the background. Air-dried smear preparation, Diff-Quik, 60× magnification

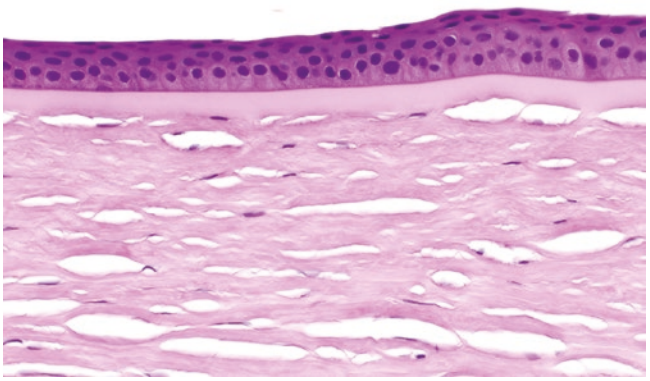

Fig. 14.41 Cornea showing stratified squamous epithelium overlying a glassy Bowman layer. The underlying avascular collagenous stroma has scant fibroblasts and characteristic clefts. Histology, hematoxylin & eosin, 40× magnification

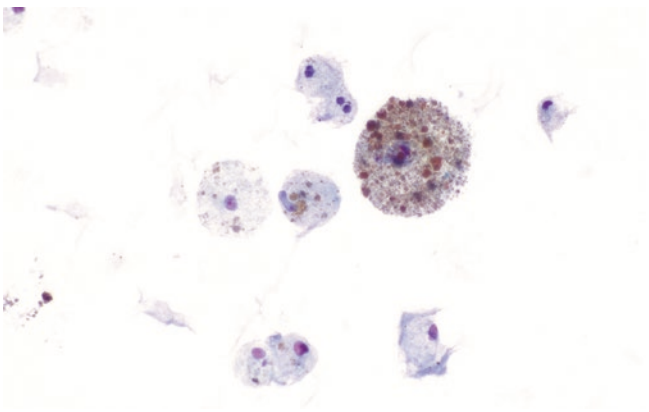

Fig. 14.44 FNA from the anterior chamber showing hemosiderin-laden macrophages due to hyphema (bleeding). ThinPrep preparation, 60× magnification

lium and stroma), ciliary body (outer epithelial layer), and retina. The amount of melanin present in the iris affects eye color. The choroid may also contain focal aggregates of uveal melanocytes (choroidal nevi) [25]. Free melanin granules can often be seen in the background of normal cytology specimens [26]. It is important not to overdiagnose cytology samples with melanoma due to the mere presence of melanin. Identification of large epithelioid or spindle malignant cells with overt atypia and prominent macronucleoli is indicative of melanoma.

The iris is composed of multiple layers: anterior border, stroma, muscular layer, and posteriorly two pigmented epithelial layers (Fig. 14.45). On cytologic preparations, cells from the iris are usually heavily pigmented, making it difficult to appreciate any cellular details (Figs. 14.46 and 14.47).

The ciliary body, which extends from the iris to the choroid, contains the ciliary processes, ciliary muscle, and epithelium (Fig. 14.48). The epithelial lining includes an inner nonpigmented epithelial layer and an outer pigmented epithelial layer that rests on a basal lamina (Figs. 14.49, 14.50, 14.51, and 14.52). The pigmented ciliary layer is continuous with the retinal pigment epithelium (RPE). The choroid is richly vascularized and, on its inner aspect, is lined by RPE (Fig. 14.53). The stroma of the choroid contains vessels, numerous pigmented melanocytes, some smooth muscle, and occasional inflammatory cells (lymphocytes, monocytes, and mast cells). Sampling the choroid can yield collagenous stroma embedded with any of these components (Fig. 14.54).

The retina is composed of photoreceptors (rods and cones), neurons, and glial (Müller) cells. The layers of the retina (from outside in) are stratified (Fig. 14.55) as follows: photoreceptors (neurosensory retina) resting on an external

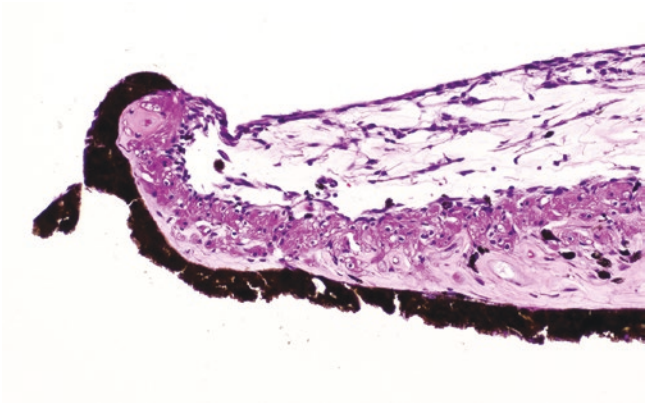

Fig. 14.45 This section of iris shows a heavily pigmented posterior epithelial lining extending around the tip of the pupil (left). The anterior surface has no cellular lining. Note the sphincter (smooth) muscle within the stroma. The color of this iris was blue, attributed to a lack of stromal melanocytes. Individuals with brown eyes have abundant stromal melanocytes. Histology, hematoxylin & eosin, 20× magnification

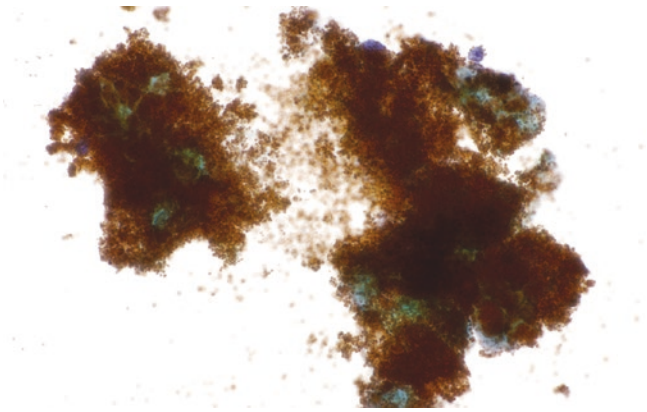

Fig. 14.47 FNA of the iris showing epithelium that is so densely packed with melanin that the underlying nucleus is completely obscured. ThinPrep preparation, 60× magnification

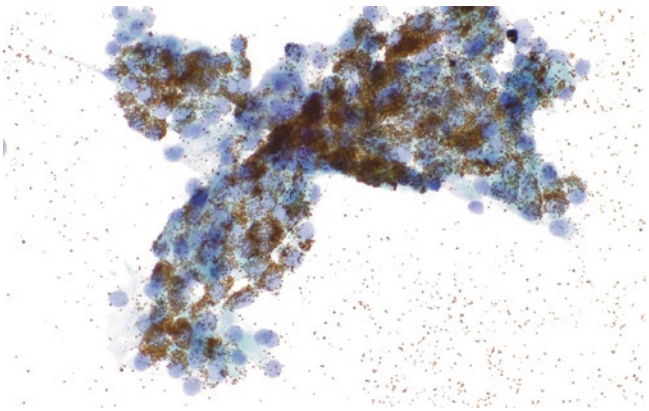

Fig. 14.46 FNA of the iris showing a group of epithelial cells containing fine granules of melanin pigment. ThinPrep preparation, 40× magnification

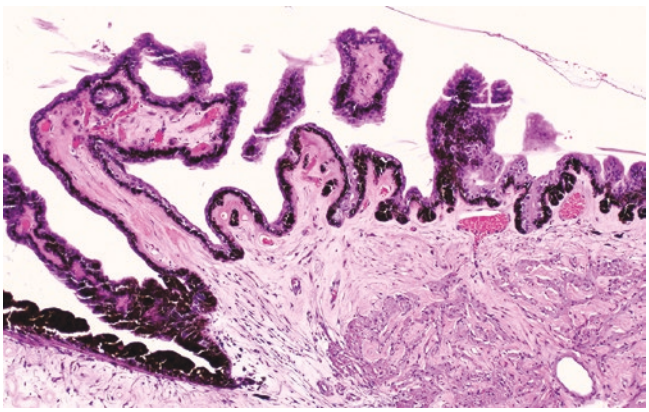

Fig. 14.48 Ciliary body showing bilayered epithelium overlying papillary folds. Note the smooth muscle at the bottom right of the image. Histology, hematoxylin & eosin, 10× magnification

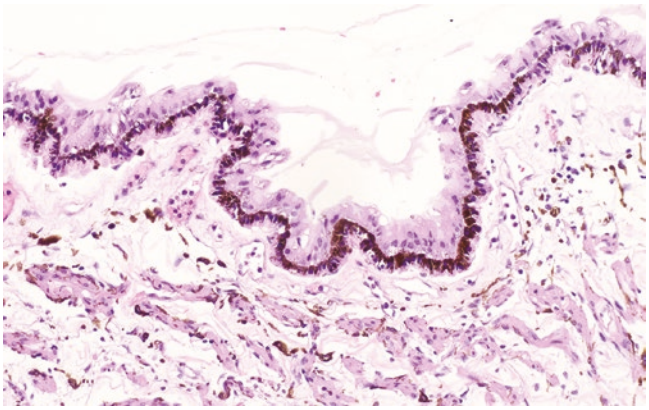

Fig. 14.49 Ciliary epithelium showing an inner nonpigmented epithelial layer facing aqueous fluid of the posterior chamber, and outer pigmented epithelial layer adjacent to the stroma. Histology, hematoxylin & eosin, 20× magnification

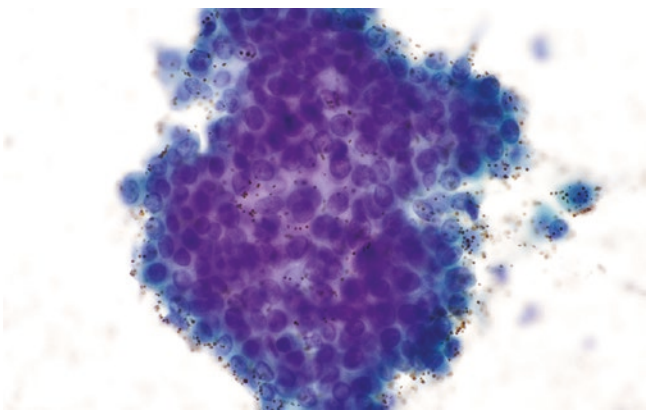

Fig. 14.50 FNA of the ciliary body showing a cluster of bland epithelium and scant brown pigmented granules. Alcohol-fixed smear preparation, Papanicolaou stain, 60× magnification

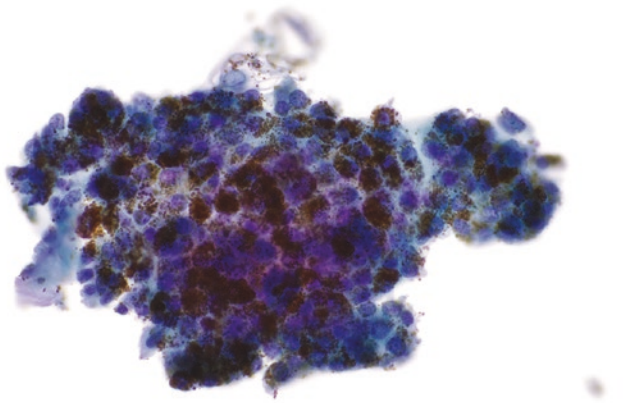

Fig. 14.51 FNA of the ciliary body showing a cluster of pigmented epithelial cells. ThinPrep preparation, 40× magnification

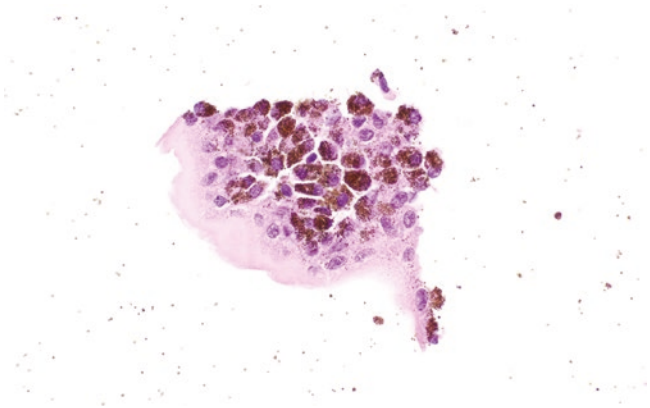

Fig. 14.52 FNA showing mostly pigmented epithelium from the ciliary body. The basal lamina (bottom) underlying the epithelium is thickened in this patient, which is usually a finding seen with diabetes mellitus. Cell block, hematoxylin & eosin, 40× magnification

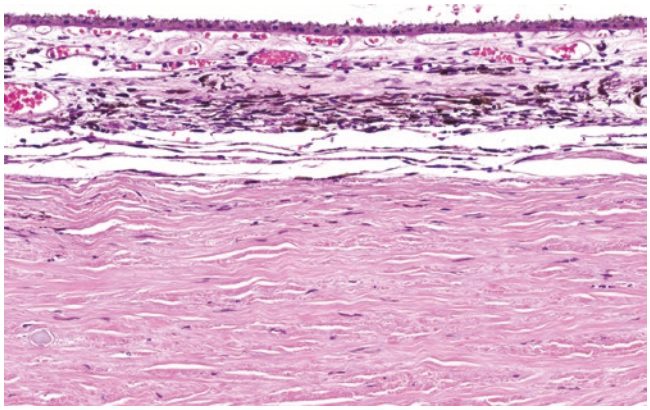

Fig. 14.53 Vascularized choroid is shown above the collagenous sclera. Note the thin layer (top) or retinal pigment epithelium and numerous pigmented melanocytes within the choroidal stroma. Histology, hematoxylin & eosin, 40× magnification

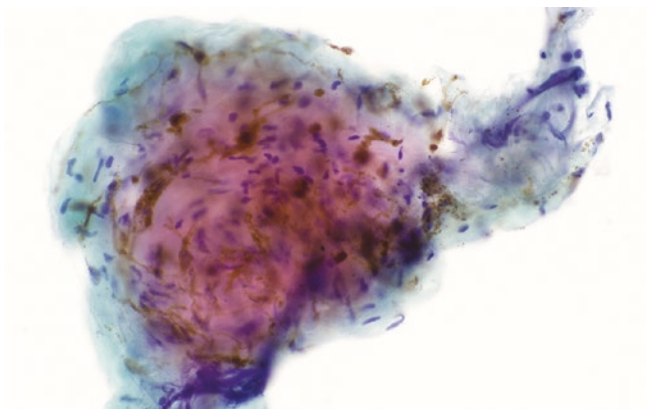

Fig. 14.54 FNA of choroid showing myxocollagenous stroma containing scattered spindled fibroblasts and spindled melanophages. ThinPrep preparation, 40× magnification

Fig. 14.55 Neurosensory retina organized into multiple layers. 1 = nerve fiber layer, 2 = ganglion cell layer, 3 = inner plexiform layer, 4 = inner nuclear layer, 5 = outer plexiform layer, 6 = outer nuclear layer, 7 = photoreceptors. The arrow depicts the path of light from the anterior eye toward the outer optic nerve. Histology, hematoxylin & eosin, 20× magnification

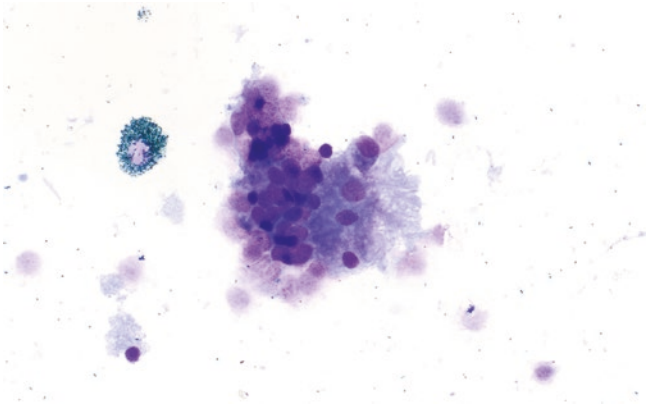

Fig. 14.56 FNA of the retina showing a portion of the nuclear layer (left) and plexiform (right) cell process layer. A single pigmented cell (left) from the RPE is also present. Air-dried smear preparation, Diff-Quik, 40× magnification

limiting membrane, outer nuclear layer, outer plexiform layer, inner nuclear layer, ganglion cell layer, nerve fiber layer, and inner limiting membrane. The anterior edge in direct contact with the vitreous fluid is serrated (ora serrata). Posteriorly, the rods (cylindrical) and cones (conical and longer) are positioned close to the RPE, which is a monolayer of cells containing intracytoplasmic melanosomes. The rods have small dark nuclei while cones have larger and lighter nuclei [26]. The nuclear layer is comprised of various neuron and glial cell types. By immunohistochemistry, neurons are synaptophysin and NeuN positive and glial cells stain with GFAP [27]. The plexiform layers are formed by cell processes, axons, and dendrites. In FNA samples that include the RPE there will be small sheets of polygonal cells. These polygonal cells have abundant cytoplasm, round nuclei, granular chromatin, and a single nucleolus. They also contain many pigment granules that tend to be more elliptical than round or spindle-shaped. FNA samples from other regions of the retina may contain various segments showing neurosensory elements, as well as nuclear or plexiform layers (Figs. 14.56, 14.57, and 14.58). Aspirated fragments from the nuclear layer are characterized by small dark nuclei, often arranged with their processes (neuropil) at one edge. FNA samples may also contain single nuclei stripped of cytoplasm. The crowded nuclei of the normal retina can mimic retinoblastoma. However, in retinoblastoma, FNA samples are usually hypercellular with potential rosettes of tumor cells and numerous mitoses and necrosis are common. The retina can also contain lipofuscin pigment and corpora amylacea. It is important to report the presence of normal retina in an FNA sample, as it may raise concern for retinal detachment.

The lens is avascular and enveloped by a PAS+ capsule (Fig. 14.59). It is lined anteriorly by a single layer of cuboidal

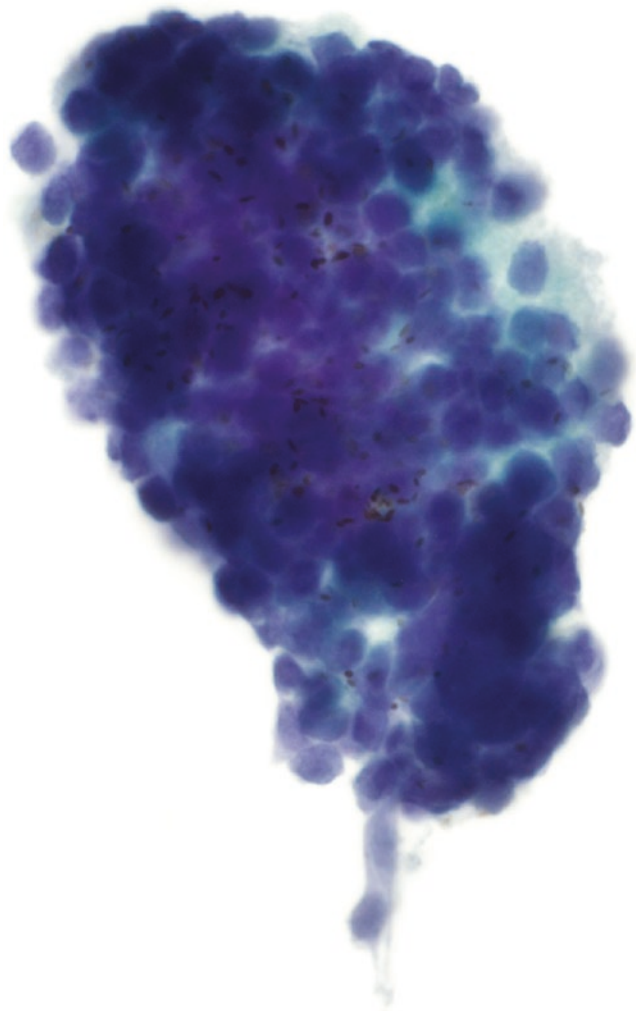

Fig. 14.57 FNA of the retina showing a cohesive group of uniform cells without cytoplasm, and small round nuclei containing dark, evenly distributed chromatin. ThinPrep preparation, 60× magnification

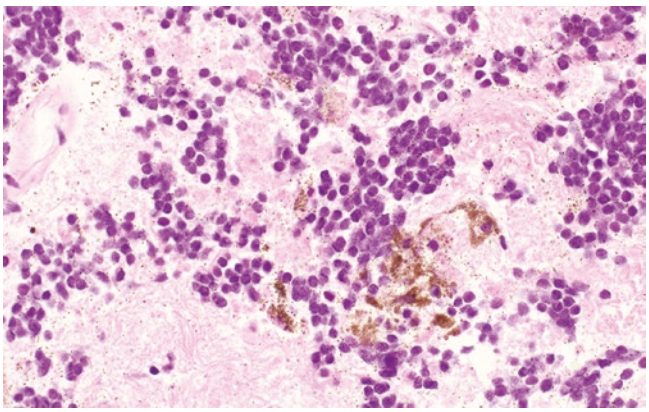

Fig. 14.58 FNA of the retina showing predominantly the nuclear layer and scattered melanin pigment. Cell block, hematoxylin & eosin, 40× magnification

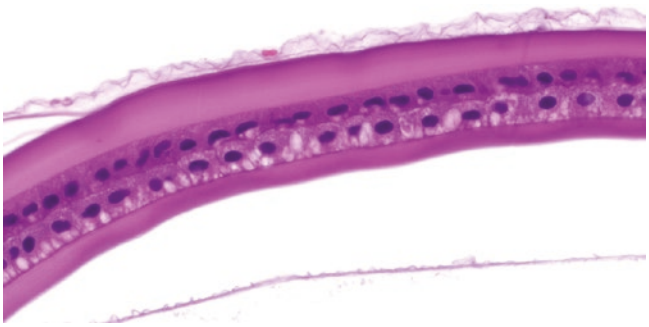

Fig. 14.59 Fragment of crystalline lens is shown, each with an acellular capsule overlying a cuboidal epithelial cell layer. Histology, hematoxylin & eosin stain, 60× magnification

epithelial cells, but posteriorly has no epithelial lining. In FNA samples that contain lens material one may find crystalline fragments (light green with Pap stain), translucent portions of the capsule, and occasional cells with lacy cytoplasm and pyknotic central nuclei.

The aqueous liquid (humor) contains mostly water and is similar to plasma but contains less protein and glucose. Vitreous liquid (humor) is avascular and contains gel-like material (protein, hyaluronic acid, water, collagen) and hyalocytes (vitreous cells) (Figs. 14.60 and 14.61). The presence of inflammatory cells is abnormal [24]. FNA samples may contain hyalocytes which are benign spindle or stellate cells with oval nuclei embedded within vitreous fluid. They have macrophage-like characteristics and are believed to be blood-borne CD34+ mesenchymal cells (fibrocytes) that produce collagen and play an important role in chronic inflammation and wound repair [28]. When recruited into tissue they differentiate into fibroblasts. By immunohistochemistry, hyalocytes are positive for LCA (CD45), CD34, S-100, CD64, and CD11a but are negative for CD68, cytokeratin, and GFAP [29].

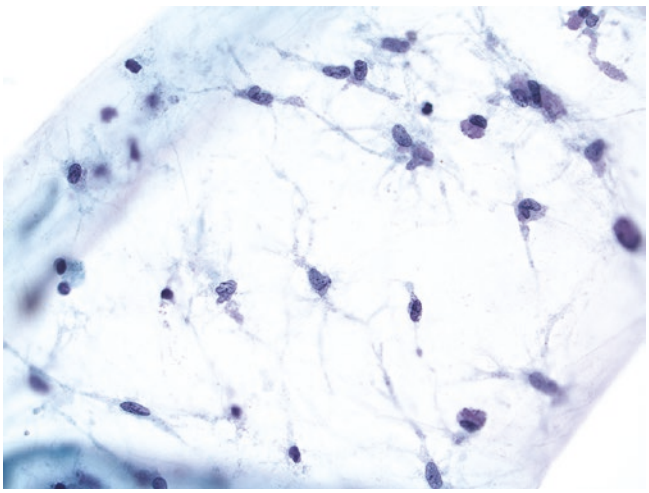

Fig. 14.60 FNA of vitreous fluid showing numerous hyalocytes embedded within gelatinous fluid. ThinPrep preparation, 40× magnification

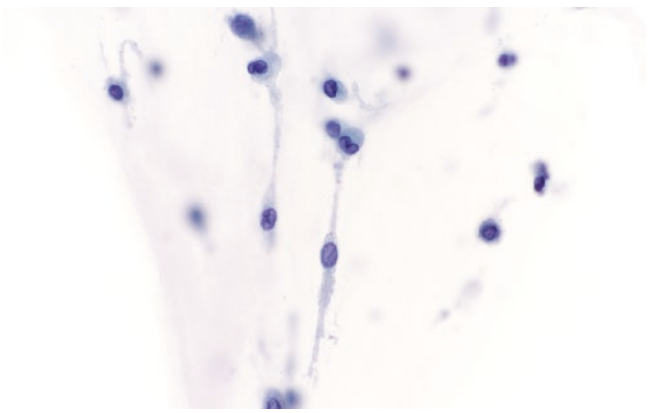

Fig. 14.61 FNA showing hyalocytes with spindled cytoplasmic processes and oval or reniform nuclei with fine granular chromatin. ThinPrep preparation, 60× magnification

With aging the cornea flattens and has attrition of endothelial cells, the lens may develop cataracts causing cloudy vision, the ciliary body becomes collagenized, the sclera may calcify, vitreous becomes more liquid, retinal vessels become hyalinized, Bruch's membrane thickens, and there may be other minor changes [30].

References

1. Cibas ES. Cerebrospinal fluid. In: Cibas ES, Ducatman BS, editors. Cytology diagnostic principles and clinical correlates. 5th ed. Philadelphia: Elsevier; 2021. p. 188–213.
2. Guseo A. Classification of cells in the cerebrospinal fluid. A review. Eur Neurol. 1977;15:169–76.
3. Mathios AJ, Nielsen SL, Barrett D, King EB. Cerebrospinal fluid cytomorphology identification of benign cells originating in the central nervous system. Acta Cytol. 1977;21:403–12.

4. Nguyen GK, Johnson ES, Mielke BW. Cytology of meningiomas and neurilemomas in crush preparations. A useful adjunct to frozen section diagnosis. Acta Cytol. 1988;32:362–6.
5. Burger PC. Smears and frozen sections in surgical neuropathology: a manual. 1st ed. Baltimore: PB Medical Publishing; 2009.
6. Burger PC, Scheithauer BW. Tumors of the central nervous system. In: Atlas of tumor pathology armed forces institute of pathology series 4. Washington: ARP Press; 2007.
7. Jaffey PB, Varma SK, DeMay RM, McLucas EJ, Campbell GA. Blast-like cells in the cerebrospinal fluid of young infants. Further characterization of clinical setting, morphology, and origin. Am J Clin Pathol. 1996;105:544.
8. De Reuck J, Vanderdonckt P. Choroid plexus and ependymal cells in CSF cytology. Clin Neurol Neurosurg. 1986;88:177–9.
9. Jimenez-Heffernan JA, Alvarez F, Muñoz-Hernández P, Bárcena C, Azorin D, Bernal I, Pérez-Campos A. Cytologic features of ventricular tumors of the central nervous system: a review with emphasis on Diff-Quik stained smears. Acta Cytol. 2021;65:111–22.
10. Lacruz CR, Catalina-Fernández I, Bardales RH, Pimentel J, López-Presa D, Sáenz-Santamaría J. Intraoperative consultation on pediatric central nervous system tumors by squash cytology. Cancer Cytopathol. 2015;123:331–46.
11. Hagel C, Buslei R, Buchfelder M, Fahlbusch R, Bergmann M, Giese A, Flitsch J, Lüdecke DK, Glatzel M, Saeger W. Immunoprofiling of glial tumours of the neurohypophysis suggests a common pituicytic origin of neoplastic cells. Pituitary. 2017;20:211–7.
12. Jiménez-Heffernan JA, Bárcena C, Agra C, Asunción A. Cytologic features of the normal pineal gland of adults. Diagn Cytopathol. 2015;43(8):642–5.
13. Murro D, Alsadi A, Nag S, Arvanitis L, Gattuso P. Cytologic features of the normal pineal gland on squash preparations. Diagn Cytopathol. 2014;42:939–43.
14. Collins BT, Warrick J. Endoscopic ultrasound fine needle aspiration biopsy of celiac ganglia. Acta Cytol. 2012;56:495–500.
15. ElGabry EA, Monaco SE, Pantanowitz L. Frequency and characterization of celiac ganglia diagnosed on fine-needle aspiration. Cytojournal. 2015;12:4.
16. Raso DS. Peripheral nerve. In: Herzberg AJ, Raso DS, Silverman JF, editors. Color atlas of normal cytology. New York: Churchill Livingstone; 1999. p. 457–64.
17. Laver NMV. Ocular cytology: diagnostic features and ongoing practices. Cancer Cytopathol. 2021;129:419–31.
18. Gillian WDH. Conjunctival impression cytology: a review. S Afr Optom. 2008;67:136–41.
19. Midena E, Segato T, Piermarocchi S, Boccato P. Fine needle aspiration biopsy in ophthalmology. Surv Ophthalmol. 1985;29:410–22.
20. Shields CL, Manquez ME, Ehya H, Mashayekhi A, Danzig CJ, Shields JA. Fine-needle aspiration biopsy of iris tumors in 100 consecutive cases: technique and complications. Ophthalmology. 2006;113:2080–6.
21. Liu K, Klintworth GK, Dodd LG. Cytologic findings in vitreous fluids. Analysis of 74 specimens. Acta Cytol. 1999;43:201–6.
22. Boulagnon C, Ducasse A, Patey M, Diebold MD, Arndt C. Cytopathology of vitreous humor samples in routine practice. Acta Cytol. 2016;60:65–73.
23. Nolan GR, Hirst LW, Wright RG, Bancroft BJ. Application of impression cytology to the diagnosis of conjunctival neoplasms. Diagn Cytopathol. 1994;11:246–9.
24. Sudha A. Anatomy, physiology, histology and normal cytology of eye. J Cytol. 2007;24:16–9.
25. Chien JL, Sioufi K, Surakiatchanukul T, Shields JA, Shields CL. Choroidal nevus: a review of prevalence, features, genetics, risks, and outcomes. Curr Opin Ophthalmol. 2017;28(3):228–37.
26. Herzberg AJ. Eye. In: Herzberg AJ, Raso DS, Silverman JF, editors. Color atlas of normal cytology. New York: Churchill Livingstone; 1999. p. 450–6.
27. Proia AD, Cummiings TJ. Eye and ocular adnexa. In: Mills SE, editor. Histology for pathologists. 5th ed. Philadelphia: Wolters Kluwer; 2002. p. 335–6.
28. Zhang F, Liu K, Zhao H, He Y. The emerging role of fibrocytes in ocular disorders. Stem Cell Res Ther. 2018;9:105.
29. Lazarus HS, Hageman GS. In situ characterization of the human hyalocyte. Arch Ophthalmol. 1994;112:1356–62.
30. Grossniklaus HE, Nickerson JM, Edelhauser HF, Bergman LA, Berglin L. Anatomic alterations in aging and age-related diseases of the eye. Invest Ophthalmol Vis Sci. 2013;54:23–7.

Index

M. Lew et al. (eds.), *Normal Cytology*, https://doi.org/10.1007/978-3-031-20336-7